

CARDIFF UNIVERSITY

**Novel approaches to the development of
PMMA bone cement**

by
Wayne Nishio Ayre

A thesis submitted in partial fulfilment for
the degree of Doctor of Philosophy

Institute of Medical Engineering and Medical Physics
School of Engineering and School of Pharmacy and Pharmaceutical Sciences

2013

Abstract

With an ageing population on the increase, there is a growing need for more effective treatments to enhance the quality of life of patients. Biomaterials employed in such treatments are therefore required to last longer and function more effectively. A biomaterial of particular interest is polymethyl methacrylate (PMMA) bone cement, which is widely employed in joint replacement surgery. Although this replacement procedure reduces pain and restores joint function, it is associated with a failure rate of approximately 10% after 15 years usually as a consequence of cement functional deterioration. Failure usually requires a complicated revision surgery, which is a burden on both the patient and health care services. This study has therefore applied novel interdisciplinary approaches to the design of PMMA bone cements in an effort to reduce failure in cemented joint replacements.

Failure of PMMA bone cements has been previously linked to agglomerations of the radiopacifier employed, which create stress concentrations and initiate cracks. A model cement was therefore developed, with compositional, mechanical, fatigue and rheological properties similar to commercial cements, which enabled two novel radiopacifiers to be tested (anatase TiO_2 and yttria-stabilised ZrO_2). Regardless of the material employed, agglomerations of the radiopacifiers were found to be a significant problem. Silane treating the radiopacifiers enhanced their dispersion, improving the mechanical and fatigue properties of the cement. Furthermore, anatase TiO_2 and silane-treated anatase TiO_2 were found to induce hydroxylapatite mineralisation *in vitro* and enhance the adhesion of MC3T3-E1 osteoblast precursor cells on the surface of the cement. The silane treatment however, was found to decrease the rate of osteoblast proliferation.

Ageing effects and moisture uptake in PMMA bone cements were also examined as cement is known to fail predominantly after long periods of use. Ageing cements in isotonic fluid resulted in a maximum moisture uptake of approximately 2%w/w, which was found to induce structural changes over time and caused degradation in the mechanical properties of the cement, potentially contributing to cement failure.

A major obstacle with joint replacements is the likelihood of post-operative infections. In an attempt to prevent this, many commercial cements incorporate large amounts of powdered antibiotic to achieve a local therapeutic release. The powdered antibiotic was found to be poorly dispersed and resulted in an uncontrolled initial release from surface agglomerations within the first 6 hours, with potentially sub-inhibitory resistance-inducing levels thereafter. Furthermore, only a small percentage (2-9%) of the antibiotic was released, the commercial cements demonstrated poor bacterial inhibition and incorporating powdered antibiotics was detrimental to the mechanical and fatigue performance of the cement. To overcome these limitations a novel delivery system was developed based on drug-entrapped liposome vesicles. A block co-polymer coating was applied to phospholipid liposomes (100nm diameter) to achieve a uniform dispersion in a commercial bone cement (Palacos R). When antibiotic-loaded liposomes (gentamicin sulphate) were dispersed in the cement, greater levels of antibiotic were released in a more prolonged manner, with enhanced antimicrobial, mechanical, fracture toughness and fatigue properties.

Techniques from a variety of disciplines were employed in this study and this inter-disciplinary approach has allowed many features of PMMA bone cement to be investigated. The experiments have offered an insight into cement failure while novel techniques and formulations have been developed, which have the potential to reduce failure and infection in cemented implants and may have wider application in a variety of biomaterials.

Declaration of Authorship

This work has not been previously accepted in substance for any degree and is not concurrently submitted in candidature for any degree.

Signed.....(Wayne Nishio Ayre)

Date.....

STATEMENT 1

This thesis is being submitted in partial fulfilment of the requirements for the degree of PhD.

Signed.....(Wayne Nishio Ayre)

Date.....

STATEMENT 2

This thesis is the result of my own independant work/investigation, except where otherwise stated. Other sources are acknowledged by explicit references.

Signed.....(Wayne Nishio Ayre)

Date.....

STATEMENT 3

I hereby give consent for my thesis, if accepted, to be available for photocopying and for inter-library loan, and for the title and summary to be made available to outside organisationst.

Signed.....(Wayne Nishio Ayre)

Date.....

STATEMENT 4: PREVIOUSLY APPROVED BAR ON ACCESS

I hereby give consent for my thesis, if accepted, to be available for photocopying and for inter-library loan **after expiry of a bar on access previously approved by the Graduate Development Committee.**

Signed.....(Wayne Nishio Ayre)

Date.....

I dedicate this to my parents, my family and my friends who have always lovingly supported me.

Acknowledgements

I would like to acknowledge and thank the following people for all their help, support and guidance over the course of my postgraduate study. Without their collaboration and contributions this research project would not have been possible.

Firstly I would like to express a great deal of gratitude to all my supervisors: Prof. Sam L. Evans, Prof. Stephen P. Denyer and Dr. Cathy A. Holt for giving me the opportunity to carry out this research. A great deal of thanks is owed to Prof. Evans whose knowledge and experience has provided invaluable guidance, assistance and advice. I would like to thank Prof. Denyer for all his patience, time, supervision and for inspiring me to pursue a career as an academic researcher. I owe sincere and earnest thankfulness to Dr. Holt who supervised my undergraduate project as well as my postgraduate research and whose encouragement and support has helped me over the years.

Dr. James C. Birchall has been a tremendous help with the liposomal work and therefore I would like to extend my gratitude for all the advice and input and for making me feel welcome at the School of Pharmacy. I would also like to show appreciation to my colleagues at the School of Pharmacy for their assistance and know-how. It gives me great pleasure in acknowledging the support and help of the following people within the School of Medicine. Dr. Bronwen Evans and Mrs. Carole Elford for taking the time to assist and advise me with biological related testing; Ms. Nicole Scully for teaching me the basics of cell culture and for all her time, help and patience; and Dr. Mari Nowell for her help with X-ray imaging. I would also like to express my gratitude to the technical staff at the School of Engineering for providing expertise and help with equipment used in this study. I would like to thank Dr. Panagiota Manti for her tutorials and assistance in using FTIR spectroscopy equipment and Mrs. Wendy Rowe from the School of Dentistry for the SEM images.

I am thankful to Arthritis Research UK (ARUK) for supporting this research. Without the funding, expertise and help from the centre, this project would not be possible.

Finally I would like to thank my family, friends and colleagues for always supporting and encouraging me throughout the course of my education. In particular I owe my deepest gratitude to my loving parents, Izaura and Robert Ayre for raising me with the utmost patience and for all the years they have endured with me. I would like to thank my girlfriend for putting up with my moodiness, my dogs for listening to my woes and my friends back in Lagos, who to this day do not fully understand what a PhD is.

Contents

Contents	i
List of Figures	vii
List of Tables	xi
List of abbreviations	xiii
Nomenclature	xvii
1 Introduction	1
1.1 Ageing population	1
1.2 Clinical conditions	2
1.3 Biomaterials	3
1.4 Cemented and cementless joint replacements	4
1.5 Revision surgery	6
1.6 Background on PMMA bone cements	8
1.6.1 History of bone cements	8
1.6.2 Poly(methyl methacrylate)	9
1.6.3 Implant technique	14
1.6.4 Surgical complications	17
1.6.5 Failure rates	19
1.6.6 Failure of PMMA bone cement	22
1.6.7 Novel Formulations	38
1.6.8 Drug delivery systems and antibiotics	48
1.7 Test methods	51
1.7.1 Test parameters	51
1.7.2 Standard tests	52
1.7.3 Alternative tests	53
2 General Methods	55
2.1 Mixing bone cements	55
2.2 Setting properties	56
2.3 Mechanical properties	57
2.3.1 Compressive strength	57
2.3.2 Bending modulus and strength	58

2.4	Fracture toughness tests	59
2.5	Fatigue testing	60
2.6	Vickers hardness tests	63
2.7	Glass transition temperature	64
2.8	Scanning electron microscopy	65
2.9	Statistical analysis	65
3	Mechanical properties of commercial cements and the development of a standardised model of cement	67
3.1	Introduction	67
3.1.1	Failure modes and toughening in polymers	68
3.1.2	Fracture mechanics theory	72
3.2	Methods	74
3.2.1	Materials	74
3.2.2	Mechanical testing	75
3.2.3	Setting properties	75
3.2.4	Fracture toughness	75
3.2.5	Fatigue testing	75
3.2.6	SEM images	75
3.3	Results	76
3.3.1	Setting properties	76
3.3.2	Mechanical properties	77
3.3.3	Fracture toughness	78
3.3.4	Fatigue	78
3.3.5	SEM images	79
3.4	Discussion	81
3.5	Conclusions	85
4	Development of novel radiopacifiers	87
4.1	Introduction	87
4.1.1	Radiopacifiers as functional fillers	87
4.1.2	Barium sulphate	88
4.1.3	Zirconium dioxide	88
4.1.4	Titanium dioxide	89
4.1.5	X-ray imaging	90
4.1.6	Thermal conductivity and heat transfer	92
4.2	Methods	93
4.2.1	Materials	93
4.2.2	Particle Sizing	93
4.2.3	Mechanical testing	94
4.2.4	Setting properties	95
4.2.5	Fracture toughness	95
4.2.6	Fatigue testing	95
4.2.7	SEM images	95

4.2.8	X-ray imaging	95
4.3	Results	96
4.3.1	Particle size	96
4.3.2	Setting properties	97
4.3.3	Mechanical properties	97
4.3.4	Fatigue	101
4.3.5	SEM	102
4.3.6	Radiopacity	103
4.4	Discussion	104
4.5	Conclusions	107
5	Improving radiopacifier dispersion and adhesion	109
5.1	Introduction	109
5.2	Methods	112
5.2.1	Materials	112
5.2.2	Silane treatment	112
5.2.3	FTIR of treated radiopacifiers	113
5.2.4	Setting properties	113
5.2.5	Mechanical testing	114
5.2.6	Fracture toughness	114
5.2.7	Fatigue	114
5.2.8	SEM images	114
5.3	Results	114
5.3.1	FTIR analysis of treated radiopacifiers	114
5.3.2	Setting properties	116
5.3.3	Mechanical testing	117
5.3.4	Fracture toughness	119
5.3.5	Fatigue	119
5.3.6	Scanning electron microscopy	121
5.4	Discussion	122
5.5	Conclusions	125
6	Biocompatibility and osseointegration of PMMA bone cements	127
6.1	Introduction	127
6.1.1	Bone growth	128
6.2	Methods	132
6.2.1	Surface energy determinations	132
6.2.2	Hydroxylapatite growth	134
6.2.3	MC3T3-E1 cell culture	135
6.2.4	Osteoblast adhesion	135
6.2.5	Osteoblast proliferation	136
6.3	Results	137
6.3.1	Surface Energy	137
6.3.2	Hydroxylapatite growth	138

6.3.3	Osteoblast adhesion	144
6.3.4	Osteoblast proliferation	147
6.4	Discussion	148
6.5	Conclusions	152
7	Mechanical and structural changes in commercial bone cements due to ageing and moisture uptake	155
7.1	Introduction	155
7.1.1	Diffusion in polymers	156
7.2	Methods	158
7.2.1	Materials	158
7.2.2	Ageing conditions	158
7.2.3	Moisture uptake and mechanical testing	158
7.2.4	Mathematical modelling	159
7.2.5	Fracture toughness	159
7.2.6	Fatigue testing	159
7.2.7	Scanning electron microscopy	160
7.2.8	Vickers hardness	160
7.2.9	Glass transition temperature	160
7.2.10	Structural changes	160
7.3	Results	161
7.3.1	Moisture uptake	161
7.3.2	Mathematical modelling	162
7.3.3	Mechanical properties	164
7.3.4	Fracture toughness	164
7.3.5	Fatigue testing	166
7.3.6	SEM images	168
7.3.7	Vickers hardness	168
7.3.8	Glass transition temperature	168
7.3.9	Structural changes	170
7.4	Discussion	172
7.5	Conclusions	179
8	Commercially available antibiotic-loaded cements	181
8.1	Introduction	181
8.1.1	Antibiotics	181
8.2	Methods	184
8.2.1	Materials	184
8.2.2	Antibiotic release	184
8.2.3	Mathematical modelling	186
8.2.4	Agar diffusion assay	188
8.2.5	Mechanical properties	188
8.2.6	Fracture toughness	189
8.2.7	Fatigue testing	189

8.2.8	SEM images	189
8.2.9	Vickers hardness	189
8.2.10	Glass transition temperature	190
8.3	Results	190
8.3.1	Antibiotic release	190
8.3.2	Mathematical modelling	194
8.3.3	Agar diffusion assay	196
8.3.4	Mechanical properties	199
8.3.5	Fracture toughness	201
8.3.6	Fatigue testing	202
8.3.7	SEM images	204
8.3.8	Vickers hardness	212
8.3.9	Glass transition temperature	213
8.4	Discussion	213
8.5	Conclusions	219
9	Incorporating a liposomal drug delivery system	221
9.1	Introduction	221
9.1.1	Liposomes	221
9.1.2	Preparation of liposomes	228
9.1.3	Liposomes in PMMA bone cements	230
9.1.4	Surfactants	230
9.2	Methods	237
9.2.1	Materials	237
9.2.2	Liposome preparation	237
9.2.3	Liposome diameter	238
9.2.4	Sedimentation rate	239
9.2.5	Transmission electron microscopy	239
9.2.6	Temperature stability tests	240
9.2.7	Fluorescence microscopy	241
9.3	Results	241
9.3.1	Liposome diameter	241
9.3.2	Sedimentation rate	243
9.3.3	Transmission electron microscopy	244
9.3.4	Temperature stability tests	245
9.3.5	Fluorescence microscopy	246
9.4	Discussion	247
9.5	Conclusions	254
10	Release characteristics of liposomal bone cements and their mechanical, fatigue and structural properties	257
10.1	Introduction	257
10.2	Methods	258
10.2.1	Materials	258

CONTENTS

10.2.2	Liposome preparation	258
10.2.3	Antibiotic release	259
10.2.4	Mathematical modelling	259
10.2.5	Agar diffusion assay	260
10.2.6	Mechanical testing	260
10.2.7	Fracture toughness	260
10.2.8	Fatigue testing	260
10.2.9	SEM images	261
10.2.10	Vickers hardness	261
10.2.11	Glass transition temperature	261
10.2.12	Structural changes	261
10.3	Results	262
10.3.1	Antibiotic release	262
10.3.2	Mathematical modelling	265
10.3.3	Agar diffusion	268
10.3.4	Mechanical properties	270
10.3.5	Fracture toughness	272
10.3.6	Fatigue testing	272
10.3.7	SEM images	275
10.3.8	Vickers hardness	281
10.3.9	Glass transition temperature	282
10.3.10	Structural changes	283
10.4	Discussion	284
10.5	Conclusions	292
11	Discussion	295
12	Conclusions and further work	305
12.1	Conclusions	305
12.2	Further work	308
	References	311

List of Figures

1.1	Osteoarthritis of the knee joint ⁴	2
1.2	Cemented total hip replacements	5
1.3	Methyl methacrylate monomer	9
1.4	Poly(methyl methacrylate) polymer	9
1.5	Benzoyloxide radical formation	11
1.6	Primary free radical formation	12
1.7	Free radical propagation	12
1.8	Free radical termination by combination	13
1.9	Free radical termination by disproportionation	13
1.10	Typical cement gun system ³⁷	15
1.11	Recommended setting times at 23°C for commercially available cements	16
1.12	Common hip fractures in untoward intra-operative incidents ⁴⁸	19
1.13	Scanning electron microscopy image of a pore in PMMA bone cement	24
1.14	SEM of a BaSO ₄ agglomeration in PMMA bone cement ²⁴	27
1.15	X-ray of iodine-based bone cements ¹⁷⁰	43
2.1	ISO5833 and ISO13586 tests	57
2.2	CT fatigue testing samples	61
2.3	Stress (σ) and strain (ϵ) during a dynamic mechanical analysis	64
3.1	Crack propagation modes ²⁶⁵	68
3.2	Crack blunting mechanisms in polymers ^{266–268}	69
3.3	Craze formation. (a) Side view of the craze tip; (b)-(d) sections through the midline of the craze showing the craze advance by meniscus instability ²⁷⁰	70
3.4	Characteristic crack propagation results	73
3.5	Setting profiles of commercial bone cements and the model cement	76
3.6	Crack propagation of commercial bone cements and the model cement	79
3.7	SEM images of the fracture surfaces of fatigue samples for (a-b) Palacos R, (c-d) Cemex and (e-f) the model cement	80
3.8	SEM images of the powder morphologies of (a-b) Palacos R and (c-d) Cemex	81
4.1	Crystal structures of ZrO ₂	89
4.2	Attenuation spectra for Barium, Titanium, Zirconium and PMMA	90
4.3	Absorption spectra for Barium, Titanium, Zirconium and PMMA	91
4.4	Particle size of BaSO ₄ , TiO ₂ and ZrO ₂ in water	96
4.5	Average compressive strength	98

LIST OF FIGURES

4.6	Average flexural properties	99
4.7	Average fracture toughness	100
4.8	Fatigue results for commercial, model and novel cements	101
4.9	Void formation around agglomerations of radiopacifiers	102
4.10	Surface roughness of fractures	103
4.11	Mean grey values of X-ray images	103
5.1	Silane structure	109
5.2	Hydrolytic deposition of silanes	110
5.3	Methacryloxypropyl trimethoxysilane	111
5.4	FTIR of silane-treated radiopacifiers using KBr discs	115
5.5	Average compressive strength	117
5.6	Average bending properties	118
5.7	Average fracture toughness	119
5.8	Fatigue test results	120
5.9	SEM images of fracture surfaces	122
6.1	Structure of bone and its remodelling process	129
6.2	Contact angle technique to measure surface energy or the hydrophobic/hydrophilic properties of a material	130
6.3	Contact angle measurements	133
6.4	XRD spectra of the model cement samples stored in SBF over time	139
6.5	XRD spectra of TiO ₂ samples stored in SBF over time	139
6.6	XRD spectra of silane TiO ₂ samples stored in SBF over time	140
6.7	XRD spectra of ZrO ₂ samples stored in SBF over time	140
6.8	XRD spectra of silane ZrO ₂ samples stored in SBF over time	141
6.9	SEM images of the surface of samples stored in SBF for 1 week	143
6.10	SEM images of the surface of samples stored in SBF for 4 weeks	143
6.11	SEM images of the TiO ₂ and Silane TiO ₂ samples after storage in SBF for 6 weeks	144
6.12	Osteoblast adhesion	144
6.13	Stained MC3T3-E1 cells on the surface of the radiolucent cement	145
6.14	Stained MC3T3-E1 cells on the surface of the model cement	146
6.15	Stained MC3T3-E1 cells on the surface of the TiO ₂ cement	146
6.16	Stained MC3T3-E1 cells on the surface of the silane TiO ₂ cement	146
6.17	Stained MC3T3-E1 cells on the surface of the ZrO ₂ cement	146
6.18	Stained MC3T3-E1 cells on the surface of the silane ZrO ₂ cement	147
6.19	Osteoblast proliferation	147
7.1	Moisture uptake over time for Cemex and Palacos R in Ringer's solution and in air	161
7.2	Moisture uptake data and model data for (a) Cemex and (b) Palacos R over time in Ringer's solution	162

LIST OF FIGURES

7.3	Changes in mechanical properties of Cemex and Palacos R over time in Ringer's solution and in air	165
7.4	Fatigue results for (a) Cemex and (b) Palacos R over time in Ringer's solution and air	167
7.5	SEM images of the fracture surfaces of (a-b) Cemex aged in air, (c-d) Cemex aged in Ringer's solution, (e-f) Palacos R aged in air and (g-h) Palacos R aged in Ringer's solution	169
7.6	FTIR spectra using ATR of Cemex and Palacos R after ageing in air for 24 hours and Ringer's solution for 60 days	171
7.7	FTIR spectra using KBr discs of Cemex and Palacos R after ageing in air for 24 hours and Ringer's solution for 60 days	171
7.8	Hydrolysis of ester groups in (a) MMA and (b) PMMA	176
8.1	Calibration curve for the PHT assay of gentamicin sulphate	190
8.2	Cumulative antibiotic release from Cemex Genta, CMW Smartset GHV and Palacos R+G bone cement	192
8.3	Cumulative percentage release from Cemex Genta, CMW Smartset GHV and Palacos R+G bone cement	193
8.4	Antibiotic release models for (a) Cemex Genta, (b) CMW Smartset and (c) Palacos R+G	197
8.5	Average zones of inhibition for commercially available cements	198
8.6	Zones of inhibition for (a-c) 10µg discs, (d-f) Cemex, (g-i) Cemex Genta, (j-l) Palacos R, (m-o) Palacos R+G and (p-r) CMW	199
8.7	Fatigue results from commercially available antibiotic-loaded and unloaded bone cements	202
8.8	Fatigue results from commercially available antibiotic-loaded bone cements before and after ageing in Ringer's at 37°C in Ringer's solution	203
8.9	Fracture surfaces of fatigue samples aged in air and Ringer's solution for (a-d) Cemex and (e-h) Cemex Genta	205
8.10	Fracture surfaces of fatigue samples aged in air and Ringer's solution for (a-d) Palacos R, (e-h) Palacos R+G	206
8.11	Fracture surfaces of fatigue samples aged in air and Ringer's solution for (a-d) CMW Smartset GHV	207
8.12	Surfaces of antibiotic release samples at 0 hours and after 1440 hours (60 days) in Ringer's solution for (a-d) Cemex and (e-h) Cemex Genta	208
8.13	Surfaces of antibiotic release samples at 0 hours and after 1440 hours (60 days) in Ringer's solution for (a-d) Palacos R and (e-h) Palacos R+G	209
8.14	Surfaces of antibiotic release samples at (a-b) 0 hours and (c-d) after 1440 hours (60 days) in Ringer's solution for CMW Smartset GHV	210
8.15	SEM images of the powder component of (a) Cemex, (b) Cemex Genta, (c) Palacos R, (d) Palacos R+G and (e) (c) CMW Smartset GHV	211
9.1	Liposome vesicle	222
9.2	Phospholipid structure	223

LIST OF FIGURES

9.3	Lamellar structures	224
9.4	Classification of liposome preparation methods (FRV - Freeze/rehydrated vesicles)	229
9.5	Surfactant structure	231
9.6	Different stabilization systems ³⁹⁸	232
9.7	Pluronic structure	233
9.8	Liposome-Pluronic structure	236
9.9	Sedimentation rate of liposomes with different Pluronics in MMA	243
9.10	TEM images of PC:C liposomes in (a) water, (b) water with L61, (c) MMA and (d) MMA with L61 (Bar=1 μ m)	244
9.11	TEM of dispersed liposomes with L61 in MMA (Bar=2 μ m)	245
9.12	Fluorescent microscopy images of liposomes (a) in water, (b) in Palacos R, (c) in Palacos R with L31, (d) in Palacos R with L43 and (e) in Palacos R with L61	246
10.1	Cumulative gentamicin sulphate release from commercial cements and liposomal Palacos R samples	263
10.2	Cumulative percentage release of gentamicin sulphate from commercial cements and liposomal Palacos R samples	264
10.3	Antibiotic release models for liposomal Palacos R with (a) L31, (b) L43 and (c) L61	266
10.4	Average zones of inhibition for Palacos R+G and the liposomal Palacos R cements	269
10.5	Zones of inhibition for the (a-c) 10 μ g discs, (d-f) Palacos R+G and the liposomal Palacos R cements with L31 (g-i), L43 (j-l) and L61 (m-o) Pluronics	269
10.6	Fatigue results from commercial and liposomal Palacos R bone cement after storage in air	273
10.7	Fatigue results from commercial and liposomal bone cement after storage in Ringer's solution at 37 $^{\circ}$ C in Ringer's solution	273
10.8	Fracture surfaces of fatigue samples aged in air and Ringer's solution for (a-d) Palacos R and (e-h) Palacos R+G	276
10.9	Fracture surfaces of fatigue samples aged in air and Ringer's solution for (a-d) liposomal Palacos R with L31 and (e-h) L43	277
10.10	Fracture surfaces of fatigue samples aged in (a-b) air and (c-d) Ringer's solution for liposomal Palacos R with L61	278
10.11	Surfaces of antibiotic release samples after 0 and 1440 hours (60 days) in Ringer's solution for (a-d) Palacos R and (e-h) Palacos R+G	279
10.12	Surfaces of antibiotic release samples after 0 and 1440 hours (60 days) in Ringer's solution for (a-d) liposomal Palacos R with L31 and (e-h) L43	280
10.13	Surfaces of antibiotic release samples after (a-b) 0 hours and (c-d) 1440 hours (60 days) in Ringer's solution for liposomal Palacos R with L61	281
10.14	FTIR spectrum of Palacos R, Palacos R+G and liposomal Palacos R using ATR	284

List of Tables

1.1	Composition of commercially available PMMA bone cements	10
1.2	ISO5833 Requirements for acrylic resin cements	52
3.1	Composition of the model cement and the commercial cements used	74
3.2	Setting properties of commercial bone cements and the model cement	76
3.3	Mechanical properties and fracture toughness of commercial and model cements	77
3.4	Fatigue constants of commercial and model cements	78
4.1	Transmitted intensity values at varying energy levels	92
4.2	Thermal conductivity and expansion of radiopacifier materials	93
4.3	Composition of tested bone cements	94
4.4	Setting properties of commercial bone cements, the model cement, radiolucent cement and the cement with novel radiopacifiers	97
4.5	Fatigue constants of commercial, model and novel cements	102
5.1	Setting properties of commercial bone cements, the model cement, radiolucent cement and the cement with untreated and silane-treated novel radiopacifiers	116
5.2	Fatigue constants of commercial, model and novel silane-treated cements	121
6.1	Surface energies of different materials	131
6.2	Interfacial tensions of test liquids	134
6.3	Experimental surface energies	138
7.1	Mathematical modelling of diffusion types to moisture uptake results for Cemex	163
7.2	Mathematical modelling of diffusion types to moisture uptake results for Palacos R	163
7.3	Fracture toughness of Cemex and Palacos R cements before and after ageing in Ringer's for 60 days	164
7.4	Fatigue test constants of Cemex and Palacos R cements before and after ageing in Ringer's for 60 days	166
7.5	Vickers hardness of Cemex and Palacos R cements before and after ageing in Ringer's for 60 days	168
7.6	T_g of Cemex and Palacos R cements before and after ageing in Ringer's for 60 days	168

LIST OF TABLES

8.1	Composition of gentamicin containing bone cements	185
8.2	Mathematical modelling of antibiotic release for Cemex Genta, CMW Smart-set and Palacos R+G	194
8.3	Mathematical modelling of antibiotic release for Cemex Genta, CMW Smart-set and Palacos R+G using the additional coefficient	195
8.4	Mechanical properties of commercially available cements before and after ageing in Ringer's for 60 days	200
8.5	Fracture toughness of commercially available cements before and after ageing in Ringer's for 60 days	201
8.6	Fatigue test constants of commercially available cements before and after ageing in Ringer's for 60 days	204
8.7	Vickers hardness of commercially available cements before and after ageing in Ringer's for 60 days	212
8.8	T_g of commercially available cements before and after ageing in Ringer's for 60 days	213
9.1	Naturally occurring phospholipids	225
9.2	Classification of surfactants	232
9.3	Structure of different Pluronics	234
9.4	HLB values and their application	235
9.5	HLB values for component groups	236
9.6	Particle size of liposomes with Pluronics in MMA	242
9.7	Particle size of liposomes before and after heating in a wet and dry state	246
10.1	Mathematical modelling of antibiotic release for liposomal Palacos R	267
10.2	Mathematical modelling of antibiotic release for liposomal Palacos R samples using the additional coefficient	268
10.3	Mechanical properties of commercial and liposomal Palacos R bone cements before and after storage in Ringer's solution for 60 days	270
10.4	Fracture toughness of commercial and liposomal bone cements before and after storage in Ringer's solution for 60 days	272
10.5	Fatigue test constants of commercial and liposomal Palacos R bone cement before and after storage in Ringer's solution for 60 days	274
10.6	Vickers hardness of commercially available antibiotic-loaded cements and liposomal Palacos R before and after storage in Ringer's solution for 60 days	282
10.7	T_g of commercially available antibiotic-loaded cements and liposomal Palacos R before and after storage in Ringer's solution for 60 days	283
11.1	Clinically approved liposomal-based therapeutics	302
11.2	Liposomal-based therapeutics in clinical trials	303

List of abbreviations

AFM	Atomic force microscopy
ANOVA	Analysis of variance
ASTM	American Society for Testing and Materials
ATR	Attenuated total reflectance
BaSO ₄	Barium sulphate
BMA	Butylmethacrylate
BMP	Bone morphogenic protein
BPO	Benzoyl peroxide
C	Cholesterol
Ca	Calcium
Ca ²⁺	Calcium ions
CaCl ₂	Calcium chloride
CaCO ₃	Calcium carbonate
CMC	Critical micelle concentration
CT	Computed tomography
DDAB	1,2-dimethyl-1-octadecylammoniumbromide
DISMA	3,5-diiodine salicylic methacrylate
DMPC	1--dimyristoylphosphatidylcholine
DMPG	1--dimyristoylphosphatidylglycerol
DMPT	N,N-dimethyl-p-toluidine
DMRIE	1,2-dimyristoxypropyl-3-dimethyl-hydroxyethyl ammonium
DMTAP	1,2-dimyristoyl-3- trimethylammoniumpropane
DOBAQ	N-(4-carboxybenzyl)-N,N-dimethyl-2,3-bis(oleoyloxy)propan-1-aminium
DODAc	Diocetyl dimethylammonium chloride
DODAP	1,2-Dioleoyl-3-dimethylammonium-propane
DOGS	Diocetylamidoglycylspermine
DOPC	1,2-Dioleoyl-sn-glycero-3-phosphocholine
DOPE	Dioleoylphosphatidylethanolamine
DOSPA	2,3-dioleoyloxy-N- (2(sperminecarboxamide)ethyl)-N,N-dimethyl-1-propanaminium
DOTAP	1,2 dioleoyl-3-trimethylammonium-propane
DOTMA	2-dioleoyl-3-N,N,N- trimethylaminopropanechloride
DPCC	Dipalmitoylphosphatidylcholine
DPPG	Dipalmitoylphosphatidylglycerol
DSPC	Distearoylphosphatidylcholine

LIST OF ABBREVIATIONS

DSPE	Distearoylphosphatidylethanolamine
DSPG	Distearoylphosphatidylglycerol
DSTAP	1,2-distearoyl-3- trimethylammoniumpropane
EDS/EDAX	Energy-dispersive X-ray spectroscopy
EO	Ethylene oxide
EPC	Egg phosphatidyl choline
EPG	Egg phosphatidyl glycerol
FBS	Fetal bovine serum
FDA	Food and Drug Administration
FGF	Fibroblast growth factor
FRV	Freeze/rehydrated vesicles
FTIR	Fourier transform infrared spectroscopy
HA	Hydroxylapatite
HLB	Hydrophilic-lipophilic balance
HPLC	High-performance liquid chromatography
HSPG	Hydrogenated soy phosphatidyl choline
IPMA	4-iodophenol methacrylate
ISO	International Organization for Standardization
KBr	Potassium bromide
KCl	Potassium chloride
LEFM	Linear elastic fracture mechanics
LUV	Large unilamellar vesicles
MA	Methylacrylate
MMA	Methyl methacrylate
MgO	Magnesium oxide
MIC	Minimum inhibitory concentration
MLV	Multilamellar vesicles
mPEG 2000-DSPE	Methoxy-polyethylene glycol-distearoyl phosphatidylethanolamine
MRSA	Methicillin-resistant <i>Staphylococcus aureus</i>
MRSE	Methicillin-resistant <i>Staphylococcus epidermidis</i>
MSPC	Monostearoylphosphatidylcholine
MTS	3-(4,5-dimethylthiazol-2-yl)-5-(3-carboxymethoxyphenyl)-2 -(4-sulfophenyl)-2H-tetrazolium
MVV	Multivesicular vesicles
NaCl	Sodium chloride
NaF	Sodium fluoride
NaHCO ₃	Sodium bicarbonate
NaOH	Sodium hydroxide
NBF	Neutral buffered formalin
NHS	National Health Service
NJR	National Joint Registry
PA	Phosphatidic acid
PBS	Phosphate buffered saline
PC	Phosphatidyl choline

LIST OF ABBREVIATIONS

PDGF	Platelet-derived growth factor
PE	Phosphatidyl ethanolamine
PEG 2000-DSPE	Polyethylene glycol 2000-distearoylphosphatidylethanolamine
PEO	Polyethylene oxide
PG	Phosphatidyl glycerol
PHT	o-phthaldialdehyde
PI	Phosphatidyl inositol
PMMA	Poly(methyl methacrylate)
PO	Propylene oxide
PO ₄	Phosphate
PPO	Polypropylene oxide
PS	Phosphatidyl serine
PTFE	Polytetrafluoroethylene
SA	Sterylamine
SBF	Simulated body fluid
SEM	Scanning electron microscopy
Si-OH	Silanol group
SPC	Soy phosphatidylcholine
SrO	Strontium oxide
SUV	Small unilamellar vesicles
TEM	Transmission electron microscopy
TGF- β	Transforming growth factor beta
TIBMA	2-[2',3',5'-triiodobenzoyl] ethyl methacrylate
TiO ₂	Titanium dioxide
TSA	Tryptone soya agar
TSB	Tryptic soy broth
UK	United Kingdom
XPS	X-ray photoelectron spectroscopy
XRD	X-ray diffraction
ZrO ₂	Zirconium dioxide
α -MEM	Minimum essential medium alpha

Nomenclature

A	y-intercept at $x=1$ ($\Delta K=1\text{MPam}^{1/2}$)
A_i	Area of indentation
a	Distance between the inner and outer loading points or the crack length
B	Bending strength
b	Sample thickness
d	Diagonal length of indentation
da/dn	Crack growth rate
E	Young's modulus
E_b	Bending modulus
E_{fract}	Modulus of elasticity related to fracture properties K_{IC} and G_{IC}
E_Q	Modulus of elasticity
E_{stiff}	Modulus of elasticity related to stiffness S
E'	Storage modulus
E''	Loss modulus
e	Material thickness
F	Load
F_5	Point of intersection with 5% offset
F_{fract}	Force at fracture
F_{max}	Maximum load
F_Q	Load at crack initiation
f	Difference between deflection at 15N and 50N
f	Geometry calibration factor
G	Rate at which strain energy is released
G_{IC}	Critical energy release rate
G_s	Amount of gentamicin in 0.4g of cement
H	Thickness of the specimen
h	Average thickness of the specimen
I	X-ray intensity passing through material
I_o	Original x-ray intensity transmitted
K	Stress intensity factor
K_{IC}	Critical stress intensity factor
k	Diffusion constant
l	Distance between the outer loading points

NOMENCLATURE

m	Slope of the linear regression
M_o	Weight at initial time point
M_t	Solvent absorbed per unit area, or weight at time t
M_w	Average molecular weight
n	Diffusion exponent
P_{max}	Maximum load
P_{min}	Minimum load
R_c	Cumulative gentamicin sulphate release
R_{diff}	Liquid diffusion rate
R_{relax}	Polymer relaxation rate
R_t	Percentage gentamicin release at time t
S	Stiffness of the specimen
T_{amb}	Recorded ambient temperature prior to mixing
T_c	Phase transition temperature of lipid
T_g	Glass transition temperature
T_{max}	Maximum temperature reached during curing
T_{set}	Setting temperature
t	Time
t_{set}	Setting time
w	Width of the specimen
Y	Stress intensity shape correction factor
α	Crack length divided by width of sample (a/W)
γ_s	Surface energy
ΔF	Load range in N
ΔK	Stress intensity factor range
δ	Phase lag
ϵ	Strain
θ	Contact angle
μ	Linear attenuation coefficient
μ/ρ	Mass attenuation coefficient
ρ	Material density
σ	Stress
σ_f	Stress to fracture
σ_c	Compressive strength
σ_L	Surface tension of liquid
σ_L^D	Disperse proportion of liquid
σ_L^P	Polar proportion of liquid
σ_S	Surface tension of solid
σ_S^D	Disperse proportion of solid
σ_S^P	Polar proportion of sample
ϕ	Energy calibration factor

Chapter 1

Introduction

1.1 Ageing population

Recent advances in health care have led to an increase in the average life expectancy of populations. The increase in life expectancy has resulted in an increase in the number of elderly people in the country and an ageing population which has considerable consequences for public services. It is estimated that around 10 million people in the UK are over 65 years old. This is expected to increase by 5.5 million in 20 years time and double to around 19 million by 2050. Currently one-in-six of the UK population is aged 65 and over and this is expected to become one-in-four by 2050¹. This dramatic increase in the elderly population poses significant problems, one of which is the ability of health care and health care technology to keep up with the number of ageing citizens requiring treatment. Furthermore recent data has shown that in 2007/08, the NHS expenditure was on average almost double for retired households (£5,200) when compared to non-retired households (£2,800) as elderly patients require more treatment due to health deterioration¹.

Joint related problems are one of the most common reported in elderly patients. As a person ages, bone mass is lost and the bones begin to lose calcium and other minerals. The range of motion becomes limited and the amount of fluid around the joints decreases, causing the the cartilage to gradually erode. Minerals may also begin to deposit in and around certain joints (calcification)². Almost all elderly people experience joint changes, ranging from minor stiffness to severe arthritis. In severe cases, the loss of joint function

or pain may require surgical intervention and artificial joints. In England and Wales in 2009 alone, there were approximately 150,000 hip and knee replacement surgeries carried out, with patients having an average age of around 70 years³.

1.2 Clinical conditions

The main clinical condition requiring surgical intervention and the use of artificial joints is osteoarthritis³. Osteoarthritis is a degenerative joint disease and is the most common joint disorder in the world⁵. Degradation of articular cartilage and changes to subchondral bone (as shown in Figure 1.1) results in joint pain and stiffness.

Currently, treatment for arthritis is limited to drug therapies, physical therapies and surgery. Drug and physical therapies may help overcome symptoms of osteoarthritis such as pain, swelling and stiffness; however as the disease progresses, patient quality of life is reduced and joint replacement surgery is required.

Inflammatory arthritis, such as rheumatoid arthritis involves the inflammation of articulating joints. In rheumatoid arthritis the synovium, a soft tissue found between articulating

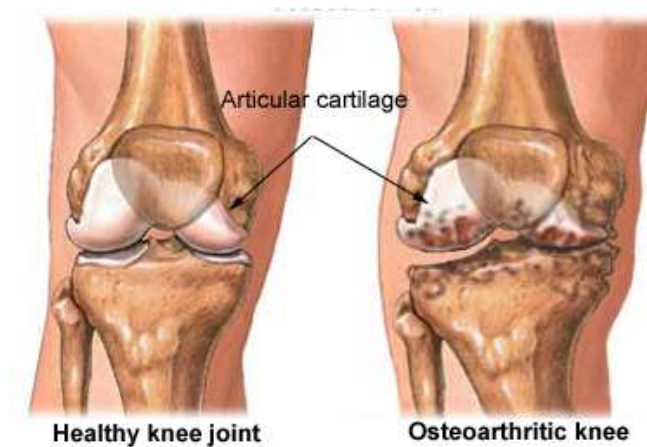


Figure 1.1: Osteoarthritis of the knee joint⁴

joints, becomes inflamed causing the patient to experience reduced joint function and pain⁶. Treatment options are similar to osteoarthritis, however drug therapies are more effective as anti-inflammatory medications can be used to suppress symptoms. Therefore a significantly smaller percentage of hip and knee replacements are carried out as a result of inflammatory arthritis³. Similarly, osteonecrosis (death of bone), trauma (physiological injury) and infection account for only a small percentage of joint replacements when compared to osteoarthritis.

1.3 Biomaterials

The treatment of many clinical conditions, such as those discussed would not be possible without the development of biomaterials. Biomaterials are materials intended to interact with biological systems to treat, augment, or replace any tissue, organ or function of the body⁷. The applications of biomaterials are vast and include joint and limb replacements, artificial arteries and skin, contact lenses and dentures. Biomaterials can be classified into three groups: inert materials, which elicit no or minimal tissue response; active materials, which encourage bonding to surrounding tissue and degradable and resorbable materials, which over time either dissolve or are broken down in the body. A requirement for all biomaterials is that they do not elicit an adverse reaction when implanted in the body.

A variety of biomaterials are currently used, these include: metallic biomaterials, which are used for load bearing applications; ceramic biomaterials, due to their hardness and wear resistance and polymeric biomaterials, which are used for their flexibility and low friction properties. Other biomaterials are used as they induce biological responses from the surrounding tissue, such as hydroxylapatite which promotes bone growth.

A biomaterial of particular interest is poly(methyl methacrylate) (PMMA). PMMA-based biomaterials have been developed for joint arthroplasty, cranioplasty, vertebroplasty and

dentistry⁸. PMMA can be formulated as a self-setting mixture, it can be combined with other materials to form a composite and it can be formulated to have a range of viscous properties. This makes PMMA a versatile biomaterial with a variety of applications. As a significant problem with the ageing population is joint degradation, this thesis will focus on the biomaterial PMMA, which is extensively employed in hip and knee replacements.

1.4 Cemented and cementless joint replacements

Total knee and hip replacements remain the most effective treatment for severe degenerative joint conditions such as osteoarthritis. There are currently two forms of total joint replacements: cemented, which use PMMA bone cement and cementless, which use coated implants.

In cemented total joint replacements the diseased or damaged joint is completely removed and a cavity is drilled into the bone. The cavity is then filled with PMMA bone cement and the implant, usually metallic, is inserted and positioned whilst the cement sets. Cementless total joint replacements follow a similar procedure however, the implant is placed directly in contact with the bone without the presence of a polymeric cement.

In the UK, bone cement has been used since the late 1950s when Sir John Charnley first used PMMA for a hip replacement^{3,9}. In the United States, the use of cement for securing joint replacements is less favoured as the American Food and Drug Administration (FDA) did not approve PMMA for use in surgery until much later^{10,11}. The Swedish Hip Registry annual report for 2010 demonstrated that approximately 70% of all hip replacements in Sweden used bone cement¹². Furthermore, in the UK, cementless replacements were found to have a higher failure rate for both hip and knee replacements as will be discussed later³. In terms of intra-operative incidents, cementless hip replacement surgeries had 510 incidents (out of a total of 27,492 surgeries) whilst cemented hip replacement surgeries

were reported to have only 252 intra-operative incidents reported (out of a total of 23,414 surgeries). Therefore for hip replacements, cementless implants reported approximately double the number of intra-operative incidents when compared to cemented hip implants. With this in mind, cemented techniques, which utilise PMMA, are still considered the best option.

The three main functions of PMMA in a total joint replacement are to secure the implant in place; transfer stresses and strains from the implant to the bone and prevent post-surgical infections if antibiotics are incorporated, as shown in Figure 1.2. The Young's modulus of cancellous bone is approximately 0.5 to 1GPa, rising to 10 to 15GPa for cortical bone compared to approximately 200GPa for metallic implants¹³. This difference in modulus may result in poor stress transfer between the implant and bone and may be damaging under high impact loads. Bone cement, with a Young's modulus of approximately 2GPa, assists in transferring some of the stresses between the implant and bone, reducing the likelihood of bone damage.

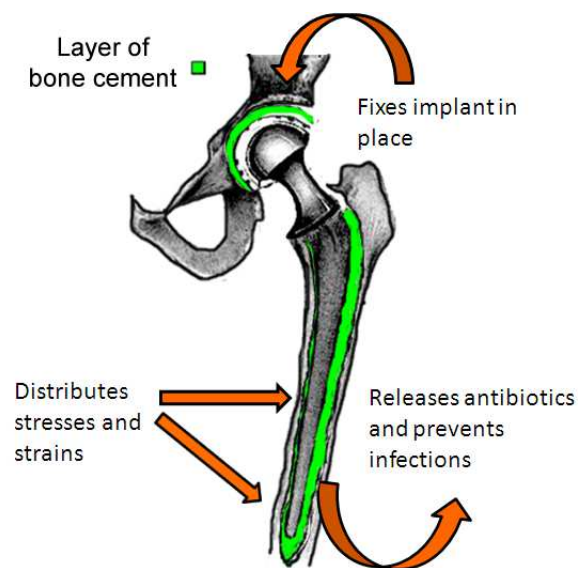


Figure 1.2: Cemented total hip replacements

Although bone cements have been used in joint replacements since the late 1950's, the failure mechanisms are still not fully understood. With cemented implant revision rates stated to be approximately 10% after 10 years¹⁴, understanding why bone cement fails is of clinical relevance and is the first step to reducing revision rates. Once the cause of failure is identified, improvements to the current bone cement systems can then be made to help reduce failure rates. With novel materials and drug delivery systems constantly being developed, there is an opportunity to improve some aspects of bone cements such as mechanical, fatigue, bone growth and anti-microbial properties. If successful these novel formulations may benefit future patients by reducing failure rates and therefore the number of revision surgeries.

1.5 Revision surgery

Revision surgeries are those which are performed as a result of implant failure. Revision surgeries take longer to perform, the prostheses are more expensive and the patient's hospital stay is prolonged, incurring higher costs for hospitals^{15,16}. Furthermore, revision surgery is more complex than primary surgery and there is a higher risk of failure and poorer prognosis associated with it^{15,17}. This is as a result of soft tissue and bone defects being present and the implant requiring removal, making the surgery technically challenging. Studies have shown that the cost of revision surgeries are substantially greater than for primary surgeries as highlighted in a recent review by Vanhegan et al.¹⁸. In the year 2000 in the UK, the total cost associated with revision surgery of the hip and knee carried out by the National Health Service (NHS) exceeded £60 million¹⁹. On average in 2007, Trusts were reimbursed between £6000 and £12000 per revision procedure depending on the expected costs associated with the procedure²⁰. The National Joint Registry (NJR) for England and Wales declared that in 2008, around 10,000 revision surgeries were carried out in the UK for both hip and knee replacements and this increased to around 12,000 in 2009^{3,21}. This is as a result of the number of joint replacement surgeries increasing

annually, highlighting the need for improvements in the materials and techniques used. It is also clear that revision procedures incur high costs, are less profitable for hospitals and subject patients to multiple high-risk surgeries and therefore there is a need to avoid them.

The aim of this study was to investigate the properties of current commercially available cements and potential methods to improve them. The ageing and moisture uptake of commercial cements were also investigated to obtain a better understanding of how the cement properties change *in vivo* over time. A review of previous studies and published literature was carried out to understand what has already been attempted and helped to form the basis of experimental work.

Although previous studies have already attempted to address several of the problems associated with PMMA bone cements, as will be discussed later, there is a need for a novel approach to this problem. Biomaterials that can interact with the surrounding tissue in a beneficial way whilst mechanically performing to a required standard are essential. In order to achieve this, the current problem requires a multidisciplinary approach, combining expertise from multiple scientific fields.

The first half of this thesis will look at the literature on bone cements, how it fails and ages and novel materials that can be used to prevent cement failure. The use of a silane-treated TiO₂ radiopacifier is particularly interesting due to its ability to encourage bone growth. The second half of this thesis will focus more on the pharmaceutical and drug delivery aspects of bone cements by investigating the behaviour of commercially available antibiotic bone cements and also by developing and testing a completely novel drug delivery system. This novel system employs liposomes, which improve the release and toughness of the cement. This system has the exciting potential to reduce failure in cemented joint replacements, by delivering synergistic antibiotic combinations and osteogenic material.

1.6 Background on PMMA bone cements

1.6.1 History of bone cements

Acrylic acid was first discovered in 1843, which led to the subsequent formulation of methacrylic acid in 1865²². When reacted with methanol, methacrylic acid forms methyl methacrylate, the basis for the polymer polymethyl methacrylate (PMMA). It was not until 1877 that the polymerisation from methyl methacrylate to PMMA was discovered by Fittig and Paul²³. The synthesis and further development of acrylates was carried out by Otto Röhm, which led to the patenting of PMMA as Plexiglas in 1928 and the formation of the company Röhm and Hass^{11,24}. In 1936 it was found that mixing fine ground PMMA particles with a liquid monomer resulted in a dough-like substance²⁴ and in the same year PMMA was used as a dental implant for the first time⁸. The first reported use of PMMA for a medical purpose was to fix cranial defects in monkeys in 1938²⁴, which was shortly followed by fixing cranial defects in humans in 1941²⁵. In 1943 the company Degussa and Kulzer developed a method of cold curing the polymer using a co-initiator (tertiary aromatic amines) as opposed to curing under heat^{24,26}.

The Judet brothers were the first to employ PMMA in arthroplastic surgery in the 1950s when they created PMMA femoral heads²⁷. This however, was unsuccessful due to biocompatibility and mechanical reasons²⁴. In 1953 PMMA was utilised as a grout to improve the fixation of implants to bone²⁸ and this was later followed by Sir John Charnley in 1958 who successfully anchored a femoral head prosthesis in the femur with the use of auto-polymerizing PMMA⁹. This resulted in the development of a completely novel surgical technique whereby acetabular and femoral implants could be secured to bone using PMMA during hip replacements²⁹. Antibiotic loading of the cement with gentamicin, penicillin, erythromycin soon followed, with gentamicin still incorporated in bone cements today³⁰.

It is estimated that in the year 2000, around 1 million orthopaedic implants were secured with bone cement worldwide and more recent datum has shown that the total number of cemented hip and knee replacements in England and Wales in 2009 was around 84,000 (not accounting for revision surgeries and hybrid implants)²¹. This highlights the large role that bone cement plays in orthopaedic surgery and how an improvement to the current system could have a significant impact on the quality of life of thousands of patients.

1.6.2 Poly(methyl methacrylate)

Commercial poly(methyl methacrylate) (PMMA) bone cement is made up of two parts, a liquid component and a powder component, which when mixed undergoes free radical polymerisation to form polymer chains. In commercially available PMMA bone cements, the liquid component comprises of methyl methacrylate (MMA, a monomer as shown in Figure 1.3), N,N-Dimethyl-p-Toluidine (DMPT, an activator) and a small amount of hydroquinone, which prevents the monomer from polymerising during storage. The powder component consists of polymethyl methacrylate polymer particles (Figure 1.4), barium sulphate (BaSO_4) or zirconium dioxide (ZrO_2) (a radiopaque agent for viewing under X-ray imaging) and benzoyl peroxide (BPO, an initiator for the polymerisation reaction)³¹. Depending on the manufacturer of the bone cement, the composition and quantities of these materials can vary as can the powder to liquid ratio as shown in Table 1.1³².

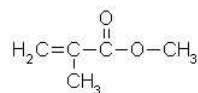


Figure 1.3: Methyl methacrylate monomer

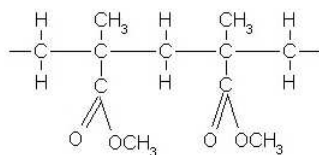


Figure 1.4: Poly(methyl methacrylate) polymer

Table 1.1: Composition of commercially available PMMA bone cements

	Cemex Isoplastic ^(a)	Cemex RX ^(b)	Cemex XL	Cemex Gun 1310/S	CMW1	CMW3	Palacos R ^(c)	Simplex P ^(d)	Zimmer Hi- fatigue ^(e)
Liquid component / g	13.30	13.30	18.33	22.00	18.37	17.90	18.78	20.00	20.00
Methyl Methacrylate / %w/w	99.10	99.10	98.20	98.20	99.18	97.49	97.98	97.50	99.35
N-N Dimethyl-p-Toluidine / %w/w	0.90	0.90	1.80	1.80	0.82	2.51	2.02	2.50	0.65
Hydroquinone / ppm	75.00	75.00	75.00	75.00	25.00	25.00	60.00	80.00	60.00
Powder Component / g	40.00	40.00	50.00	60.00	39.99	37.00	40.00	40.00	40.85
Polymethyl Methacrylate / %w/w	84.30	88.27	85.00	85.00	88.84	87.03	84.50	88.50	86.90
Barium Sulphate / %w/w	13.00	9.00	12.00	12.00	9.10	10.81	-	10.00	-
Benzoyl Peroxide / %w/w	2.70	2.73	3.00	3.00	2.05	2.16	0.50	1.50	0.86
Zirconia / %w/w	-	-	-	-	-	-	15.00	-	12.24
Powder : Liquid ratio	3.01	3.01	2.73	2.73	2.18	2.07	2.13	2.00	2.04

Note: (a) - High viscosity, (b) - Low viscosity, (c) - Poly(methyl methacrylate/methyl acrylate), (d) - 73.5%w/w poly(methyl methacrylate)/styrene co-polymer, 15.0%w/w pre-polymerised PMMA and (e) - MMA Styrene

The four main stages in the preparation of surgical bone cements are: mixing of the powder and liquid components, a short waiting period, handing/application of the cement and setting of the cement. Each stage has a different time duration which can vary according to cement manufacturer's specifications.

PMMA bone cements undergo free radical polymerisation. Free radical polymerisation is essentially an addition polymerisation reaction and occurs in three stages: initiation, propagation and termination. The ability of bone cement to undergo such a process allows it to be self curing.

Initiation

The initiation involves the formation of benzoyl peroxide free radicals which are created from the reaction between benzoyl peroxide and a tertiary amine, in this case DMPT (Figure 1.5). The benzoyloxy radical carries an unpaired electron in the outer shell, which results in high reactivity with the monomer molecules²⁵.

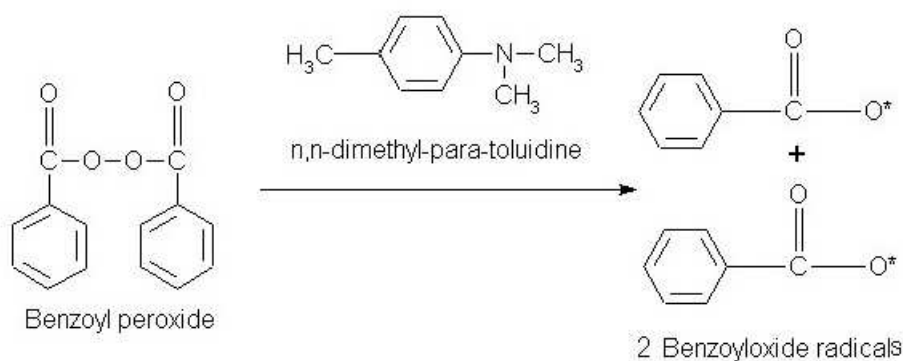


Figure 1.5: Benzoyloxy radical formation

When the benzoyloxy radical reacts with the monomer (MMA), a primary radical is formed (Figure 1.6). This primary radical acts as an active centre, allowing the reaction to propagate.

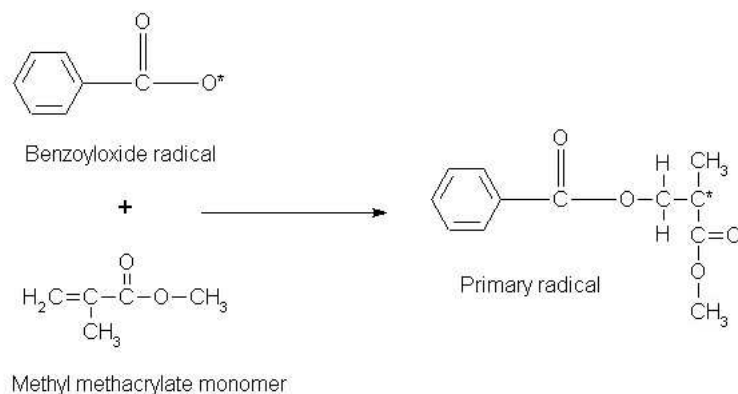


Figure 1.6: Primary free radical formation

Propagation

As described, the primary radical acts as an active centre and reacts with MMA molecules. After it attaches itself to an MMA molecule, it reacts with other MMA molecules, elongating the polymer chain as shown in Figure 1.7. With each addition of an MMA molecule, energy is released and this gives the reaction its exothermic properties.

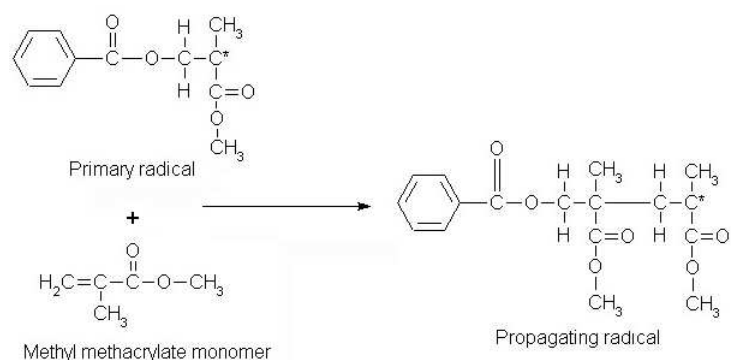


Figure 1.7: Free radical propagation

Termination

The polymerisation reaction is known to terminate by two mechanisms, either by combination or by disproportionation. The combination mechanism occurs when two active centres with unpaired electrons of growing chains react with one another to form a single bond, pairing up electrons and terminating chain propagation (Figure 1.8).

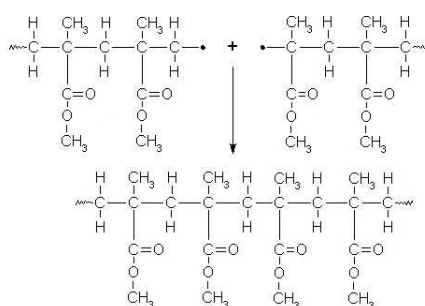


Figure 1.8: Free radical termination by combination

Disproportionation involves the unpaired electron of the radical removing not only an electron from another growing chain, but a hydrogen ion as well (Figure 1.9). This terminates the chain propagation as the first chain now has no unpaired electrons and the end carbon now shares a stable eight electrons.

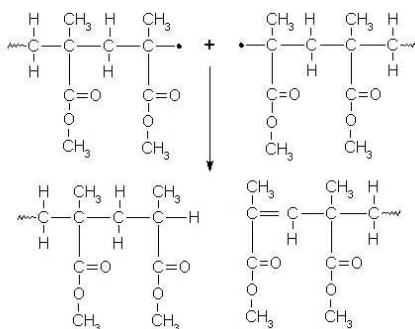


Figure 1.9: Free radical termination by disproportionation

1.6.3 Implant technique

The method of mixing and inserting bone cements into a patient varies according to the cement manufacturer and the surgeon's preference. Currently, methods of mixing include hand, vacuum and centrifuge mixing. Hand mixing simply involves placing both the powder and liquid component in a plastic bowl and mixing with a spatula for a specified amount of time. This is the simplest method, however studies have shown that pores develop due to entrapped air, potentially weakening the cement³³⁻³⁵. This will be discussed later in further detail. The majority of surgeons have adopted newer generation mixing techniques such as vacuum mixing as the standard mixing method. A reduced pressure during mixing (ranging from -39kPa to -86kPa) creates a vacuum which removes air, reducing airborne vapours during surgery and also alters the porosity of the final cement mixture. Mixing under a vacuum, as demonstrated in a study by Bettencourt et al.³⁶, significantly decreases the amount of residual monomer released from the cement when compared to manual mixing. This may also benefit the patient in terms of toxicity. Centrifuge mixing involves mixing the powder and liquid component at high rotary speeds (up to 3000rpm). Centrifuge and vacuum mixing are considered second generation mixing methods and studies tend to place both of them at the same level in terms of porosity and mechanical properties. The effect of mixing method on the performance of bone cements is the subject of much debate and will be discussed in more detail later in this chapter.

Once mixed, the cement is then inserted into the patient. Depending on the viscosity of the cement being used, this can be achieved by injection or manual handling. Bone cement can be injected either through a fine needle, usually with low viscosity cements for vertebroplasty, or using a cement gun system. For the cement gun system, the mixed cement is either poured into a cartridge or the cement is mixed within the cartridge, which



Figure 1.10: Typical cement gun system³⁷

is then attached to a pressure gun system as shown in Figure 1.10. This system applies pressure to the mixture and extrudes the cement out of an orifice into the bone cavity. The other method involves the surgeon manually applying the cement to the required area and applying pressure via digitation to compact it.

The setting of current commercially available cements tends to take place in four steps: mixing, waiting, handling and application/setting. Generally, mixing should take no longer than 1 minute, after which a dough-like mass will form. This mass will remain of dough-like consistency for up to a maximum of 4-5 minutes so the waiting period after mixing should not exceed 1 minute. This waiting period allows the PMMA beads to soak up the MMA monomer and polymerization to commence. The cement is then applied as previously discussed. For standard cements this period is between 5 to 8 minutes, allowing the surgeon time to carefully apply the cement, followed by the implant (ensuring the correct positioning) and also allows the surgeon to remove any excess cement while it is still soft. The cement then hardens and sets over 2-3 minutes, securing the implant in place. For the majority of cements, this entire process does not take more than 15 minutes, which is sufficient for the surgeon to successfully complete the procedure whilst minimising the risks associated with lengthy surgeries. Figure 1.11 shows the recommended setting times for several commercially available cements.

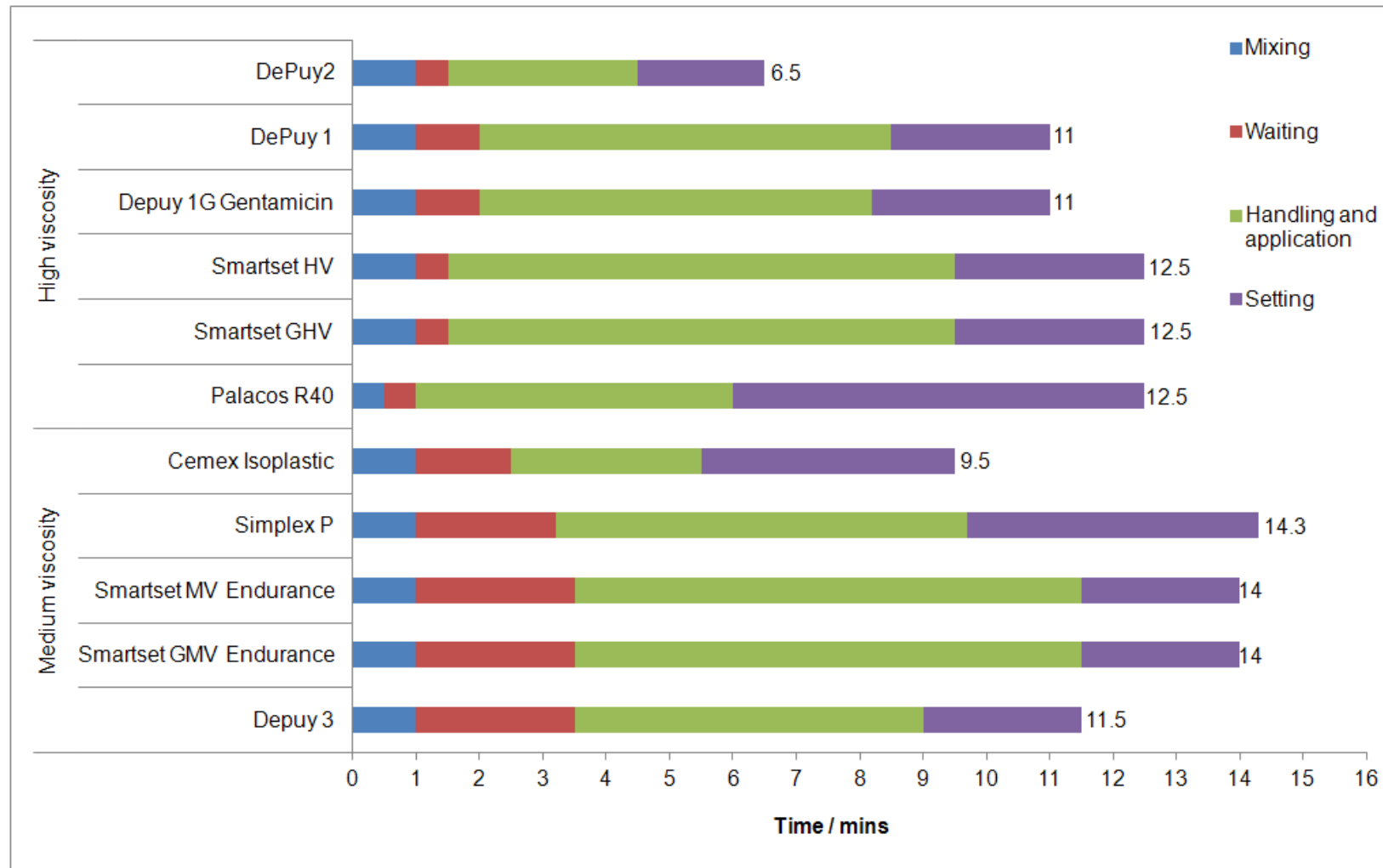


Figure 1.11: Recommended setting times at 23°C for commercially available cements

1.6.4 Surgical complications

Although surgical complications account for a small percentage of failure rates in total joint replacements, they are of great concern as they greatly impact morbidity and mortality rates. As previously discussed, bone cement cures slowly to allow surgeons to correctly align the implant, however if the surgeon does not achieve this in time, the cement must be removed and the procedure repeated. A malaligned total knee or hip replacement can greatly affect the functionality of the implant and may subject the cement to abnormal stresses and strains which may lead to premature cement failure. In order to repeat the procedure, more bone must be removed, which is not desirable, to accommodate for the new cement. Proper surgical training may help reduce the likelihood of such an event occurring. Other complications may also arise as a consequence of introducing a foreign material into the human body or as a result of the procedure itself. It has been observed that a drop in blood pressure immediately after implantation of PMMA bone cement occurs for up to five minutes³⁸. Initially bone cement was thought to be the cause of this with authors blaming the exothermic curing temperatures³⁹ or leaching monomer⁴⁰. Bright et al.⁴¹ found however that the hypotensive effects of MMA only occurred in animals at MMA concentrations around tenfold of those found to occur in humans during surgery. Furthermore Homsby et al.⁴² found no statistical correlation between MMA concentrations and pressure drop and death in animals was found to occur only with hundredfold concentrations of MMA. Although the initiator (DMPT) is known to be toxic, Shlag et al.⁴³ demonstrated that the initiator is totally depleted during the polymerisation of bone cement.

Cemented joint replacements have been shown to carry higher risks of embolisms over cementless joint replacements⁴⁴. Cardiac arrest during joint replacement surgery has also been well documented^{24,38}. This condition is known as “cardiac arrest syndrome” and in most cases is manageable with resuscitation but is not always reversible, leading to mortal-

ity, as a number of cases have reported²⁴. Autopsy of some of these cases showed extensive pulmonary fat embolisms had developed and in some cases cancellous bone fragments and even bone cement were present in the fat embolisms⁴⁵. These develop as manipulation of the bone cavity increases the intramedullary pressure and fat, bone marrow and air embolises into the venous system and to the lung. This can in turn lead to acute hypotension and, as reported in some cases, even cardiac arrest. Parvizi et al.⁴⁵ conducted a large retrospective study on hip surgeries (38,488 patients) and found the mortality rate to be around 0.06%. Patients with fractured femoral necks were found to be at a particularly higher risk (0.18%) as were patients with pertrochanteric fracture (1.6%). A separate study by Leidinger et al.⁴⁶ on a smaller cohort of patients (150 patients) also found mortality rates of patients with femoral neck fractures to be much higher at 8%. Elective total hip replacement surgery however, is generally rated as having a risk well below 0.1%²⁴. This is due to the novel techniques employed during surgery to reduce the likelihood of embolisms forming such as the use of pulsatile jet-lavage on the bone canal during surgery and continuous echocardiographic monitoring intraoperatively. Furthermore identifying high risk patients in which morbidity and mortality can be minimized by using uncemented replacements is possible and should be carried out prior to surgery⁴⁷.

According to the 2009 annual report from the National Joint Registry for England and Wales, less than 1% intra-operative incidents occurred for all hip and knee replacements²¹. As previously discussed, for hip replacements, cementless implants accounted for twice the number of intra-operative incidents when compared to cemented implants. For intra-operative cemented hip implant incidents, 20% were pelvic penetrations, 19% were trochanteric fractures (as shown in Figure 1.12), calcar cracks accounted for 14%, 3% were shaft fractures and 2% were shaft penetrations²¹. Penetration related cases in cement implants may be as a result of excess cement causing discomfort to the patient, whilst cracks and fractures are most likely caused by the removal or drilling of bone during surgery.

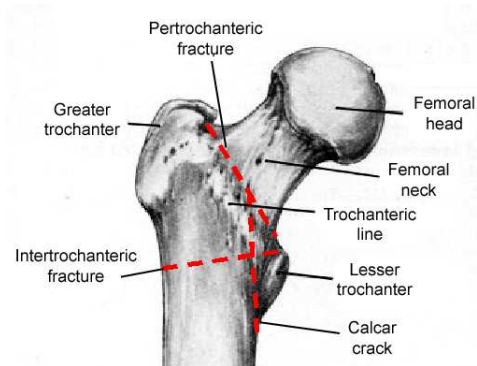


Figure 1.12: Common hip fractures in untoward intra-operative incidents⁴⁸

Untoward intra-operative events in knee replacements were found to be greater in cemented cases (440) than in uncemented cases (12), however this figure reflects the high number of cemented surgeries carried out on knee replacements (60,882) when compared to uncemented surgeries (4,445). Intra-operative incidents for cemented knee replacements in 2009 were found to be as a result of fracture (20%), ligament injury (9%) and patellar tendon avulsion (6%)²¹. Again, fracture of the bone may have resulted due to drilling and removal of the articulating joint, whilst ligament injury and patellar tendon rupture is most likely caused by surgical errors. It should be noted that complicated revision surgeries tend to employ cemented techniques due to the simplicity of the procedure and the lower likelihood of untoward intra-operative events.

1.6.5 Failure rates

In order to understand the current problems of PMMA bone cements and to highlight the need for improvements, it is essential to analyse recent data on the failure rates of cemented implants. In orthopaedics, the two most discussed and popular surgeries that use PMMA bone cement are total hip and knee replacements. By focusing primarily on these two procedures, a good representation of the overall performance of bone cements in orthopaedics can be obtained. The following information has been reproduced from the National Joint Registry's (NJR) annual report for 2010²¹. The NJR was set up by

the Department of Health and Welsh Assembly Government to collect information and monitor the performance of all hip, knee and ankle replacements in England and Wales.

In 2009 there were 72,432 hip replacement surgeries in England and Wales. Of these surgeries, 90% (65,229 surgeries) were primary procedures and 10% (7,203 surgeries) were revision procedures. This signifies an estimated 10% failure rate for all hip replacements. Within primary hip replacement surgeries, 36% (23,414 surgeries) were cemented, with the remainder being either cementless, hybrid (or not classified) or resurfacing procedures. Therefore, even with the introduction of novel technology such as cementless and hybrid implants, over one third of all hip replacements in England and Wales still use PMMA bone cement.

When comparing cemented and cementless hip implants between the 1st April 2003 and the 31st December 2009, cemented hip implants (99,359 cases) had a failure rate of 0.6% after one year, 1.4% after three years and 2.0% after five years. Cementless hip replacements (62,937 cases) were found to have higher failure rates, with 1.3% after one year, 2.5% after three years and 3.4% after five years. Therefore, even with the introduction of novel cementless hip implants, it is clear that cemented hip implants perform better clinically over time. Over a 10 year study, other sources have found cemented hip replacements to fail at a higher rate of approximately 10%¹⁴.

The main reasons for hip revision surgeries in England and Wales in 2009 were found to be aseptic loosening (49%, 3,524 surgeries), lysis (14%, 999 surgeries) and infection (14%, 1,020 surgeries). This agrees with a significant amount of published literature which states aseptic loosening to be the main cause of implant failure^{11, 14, 49, 50}.

For total knee replacements in 2009 (77,545 total surgeries), 94% were primary procedures (72,980 surgeries) and out of these procedures 79% were cemented (60,882 surgeries). This shows cemented techniques to be more popular in knee replacements, possibly related to their lower failure rate. 6% of the total surgeries were for revision purposes (4,565 surgeries), again caused mainly by aseptic loosening 35% (1,554), followed by infection 23% (1,026) and lysis 10% (448). When compared to hip replacements, the failure rate seems to be less, possibly due to the loading conditions of the cement. In total knee replacements it is thought that the majority of loading occurs in compression whereas in hip replacements the femoral stem is thought to apply more bending and tensile stresses on the cement.

Between 1st April 2003 and 31st December 2009 the failure rates for cemented knee replacements were 0.6% after one year, 2.1% after three years and 3.0% after five years. Cementless knee replacements on the other hand experienced a 0.7% failure rate after one year, 2.7% after three years and 3.7% after five years. Again, cemented knee replacements outperform uncemented implants after the first 5 years. Although the failure rate after 5 years for cemented knee replacements is higher than hip replacements, other studies have shown the overall failure rate after 10 years to be around 5%, half that of hip replacements⁵¹.

Although this data highlights important information on the clinical use and success of cemented implants in orthopaedics, further analysis of published studies and literature is required to better understand the failure mechanisms in PMMA bone cement. Bone cements have been used since the late 1950's and the literature on the subject is considerable and a complete review of the literature on the matter would be difficult to achieve. By necessity, therefore, this section will pay particular attention to the causes of failure and those methods that have already been employed in an attempt to reduce this failure. The test methods reported in the literature will also be summarised.

1.6.6 Failure of PMMA bone cement

Aseptic loosening is known to be the main cause of failure for cemented orthopaedic implants. The cement surrounding the prosthesis fractures and fails, which results in the loosening of the implant. The reason for the cement failure is widely disputed and substantial research has been carried out to better understand it.

Fatigue

As previously discussed, the rate of failure in cemented hip and knee replacements after 1 year is less than 1% and this increases to a much higher rate of 5% and 10% for cemented knee and hip replacements respectively after 10 years. These figures help in understanding the failure mechanism of cement. As failure rates increase dramatically after long-term usage, it is suspected that fatigue plays a role in the fracture and eventual failure of PMMA bone cements³². Cement fatigue is either thought to be a primary event, directly contributing to implant loosening (Topoleski et al.⁵² and Culleton et al.⁵³) or a secondary event preceded by other failure phenomena, such as debonding at the cement-implant interface (Jasty et al.⁵⁴). Cracks in the cement are thought to initiate at voids, pores, agglomerations, imperfections, damaged areas, areas of concentrated stress or due to cement shrinkage during polymerisation. Loading and unloading of the cement can cause these cracks to grow and coalesce over prolonged periods of time, gradually weakening the cement until failure of the implant occurs. This causes the cement to fail at stresses below its yield strength. This concept has been investigated using fatigue testing methods and a variety of different loading simulations with varying loads, frequencies and environments.

Overloads

The forces applied to bone cement *in vivo* vary significantly depending on the activity undertaken. For example, standing, walking, stair climbing, standing from a seated position and other activities will generate widely varying forces and stresses in the cement⁵⁵, and

these variations have a significant effect on crack propagation in PMMA^{56,57}. Therefore to model such activity, overloads can be applied.

An overload is a force of greater magnitude than that which is being applied. Evans et al.⁵⁸ studied the effects of loading regimes on crack formation and found that overloads in PMMA at low crack growth rates actually had a retarding effect on crack growth. The overloads were thought to slow crack growth by plastic deformation due to crazing or shear yielding ahead of the crack tip. This resulted in either blunting the crack tip, releasing stresses, plastically inducing crack closure or changing the path of the crack itself. With a more complex, commercially available cement however the results were not as clear, demonstrating that cement composition is vital to preventing fatigue failure. Overall it was found that overloads could decrease crack growth by a factor of 2 or increase it by a factor of 6⁵⁸. Further studies into overloads showed that overloads at a certain ratio above the baseline load accelerate cracks by overcoming microstructural obstacles. The retardation of crack growth by overloads can be explained by the main crack re-directing itself to smaller secondary cracks and defects ahead of it³³. The formation and accumulation of crazes at low stress intensities ahead of the crack tip however can be extremely damaging when an overload is applied. If the overload is large enough, it can cause the crazes to coalesce and induce a burst in crack growth which may lead to the eventual failure of PMMA below the expected threshold^{33,59}. As overloads and constant loading/unloading commonly occurs during long-term *in vivo* use of cemented implants, it is difficult to avoid this problem. Therefore to overcome this inevitable problem, some form of toughening is required which will absorb energy at the crack tip. This may be achieved by changes in the composition and microstructure of the cement.

Porosity

Porosity is widely discussed in the failure of bone cements and is caused by entrapped air during the mixing process, evaporating monomer and cement shrinkage^{34,60-62}. Figure 1.13 shows a pore in PMMA bone cement.

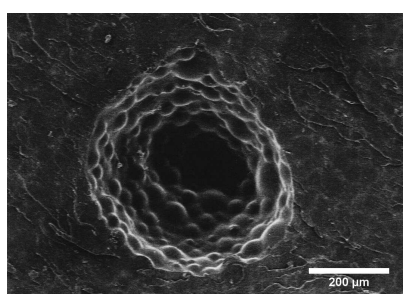


Figure 1.13: Scanning electron microscopy image of a pore in PMMA bone cement

As previously discussed, the method of mixing has been found to greatly affect the porosity of the cement, however the effect this has on the mechanical and fatigue properties are still debated. Some authors have claimed that pores decrease fatigue life by decreasing the load bearing area, which increases nominal stresses and creates stress concentrations³³⁻³⁵. Nevertheless, pores are also known to be beneficial for drug delivery, bone ingrowth and are thought to have a blunting effect on cracks by forming microcracks ahead of the crack tip^{63,64}. This can force large cracks to change direction or branch out into smaller cracks and can induce a greater amount of plastic deformation in the cement which requires a higher amount of energy for the crack to propagate. Other authors claim that the size of pores and the distance between them has a greater effect on fatigue life. It was found using both experimental and analytical methods that fatigue life is reduced with larger pores as the maximum principal stresses occur around the equator of the pore. This causes larger pores to initiate failure cracks as well as speed up the crack growth rate around them^{59,60,65}. The effect of this is further increased as the distance between the pores is reduced^{60,63,65}. It was found that a 2mm pore is equally as damaging as two 1mm pores

in close proximity as pores can link up to act as a larger void⁶³. This can be mathematically predicted using the theory of critical distances which implies that if pores are sufficiently far apart they act as single entities and do not interact. A recent finite element and micro-CT study by Coultrup et al.⁶⁶ also hypothesised that the damage accumulation process is most affected by larger pores, followed by smaller pores and radiopacifier agglomerations. Smaller pores however, have been found to be insufficient in initiating cracks by themselves⁶⁰. They are also thought to help reduce polymerisation shrinkage, reducing the likelihood of residual stress-induced cracks⁶¹.

It is clear that porosity affects the *in vivo* performance of bone cement and therefore the mixing technique employed plays a vital role in reducing failure rates. Newer generation mixing techniques such as vacuum mixing and centrifugation are reported to have improved the survival rate of bone cements by altering the porosity^{67,68}. As previously discussed, vacuum mixing employs a reduced pressure (-39kPa to -86kPa) which helps to remove some of the air during the mixing process. This system has been shown in a study by Hansen et al.⁶⁹, to increase the peak setting temperature of the cement. Reduced oxygen levels are thought to initially inhibit the chemical reaction, resulting in a greater number of free radicals reacting at the final polymerisation stage over a shorter period of time. Vacuum mixing also reduces porosity to a certain extent as well as the residual monomer as the vacuum removes any evaporated methyl methacrylate^{60,70}. Other authors have found however, that the vacuum mixing systems used do not give significantly different results to hand mixed samples^{34,71-76}. This is due to the weak vacuum not significantly reducing porosity. It was also found that altering the level of the vacuum pressure has an effect on the fatigue life of samples^{71,77}. Therefore with newer mixing systems, it is the type of porosity created that changes, rather than the amount of pores⁷⁶. It is thought that vacuum mixing creates fewer but larger pores whilst hand mixing creates smaller clusters of pores, which when grouped together are thought to initiate failure^{59,61,63}. A

study comparing laboratory fatigue tests and finite element models has shown that in laboratory tests, pores tend to act as sites for crack initiations whilst in simulations crack initiation is governed by local stress singularities. This would explain why modern mixing techniques have failed to demonstrate improvements clinically⁷⁸.

Pelletier et al.⁷⁹ has shown that mixing temperature also affects porosity as cooler temperatures (20°C) resulted in smaller pores around the outside of samples, warmer temperatures (50°C) resulted in larger pores nearer to the centre, which interestingly gave better mechanical properties. Walker et al.⁸⁰ has shown that reducing the temperature to 4°C decreases the overall porosity. Altering the mixing temperature however is known to affect the setting/handling time and temperature. Cooling the powder and liquid prior to mixing was found to increase the handling time and decrease the peak setting temperature, as demonstrated by Li et al.⁸¹. Preheating the femoral stem of the implant is a technique that has been investigated and it was found to reduce porosity at the cement-metal interface as the cement would set faster closer to the stem⁸¹.

Radiopacifiers

Radiopacifiers in PMMA bone cements can be used to observe the location and penetration of the cement in a non-invasive manner. When implant failure occurs *in vivo* it is essential to assess the cause of failure using non-invasive techniques such as X-ray imaging. This provides the surgeon with the necessary information to prepare and perform the appropriate procedure to correct the problem. This also reduces the number and length of risky surgeries the patient will have to undergo. To assess whether cement failure has occurred the cement itself must be visible under X-rays. As PMMA is considered radiolucent, it is essential to incorporate inorganic particles which will attenuate the X-rays sufficiently to view cracks and fractures in the cement. As previously outlined, commercial cements tend to use either BaSO₄ or ZrO₂ in the powder component at percentages of 8-15%w/w

(Table 1.1)^{25,32,82}. It has been speculated that these micron-sized particles contribute to cement failure. A recent study by Baleani et al.⁸³ has shown that the addition of 10% BaSO₄ to plain PMMA lowered the endurance limit and fracture toughness of the material by 13% but also decreased the crack growth rate by up to 66%. A similar study by Ginebra et al.⁸² found that BaSO₄ decreased the tensile strength, did not affect fracture toughness but improved crack propagation resistance whilst ZrO₂ was found to improve all three. A review by Lewis et al.⁸⁴ on the fatigue performance of acrylic bone cements has highlighted the positive effect radiopacifiers can have on the fatigue life of cements drawing on 5 different studies^{85–90}. Similar conclusions were drawn from these studies with regards to crack propagation. It is hypothesised that inorganic filler particles retard crack propagation by redirecting and deviating the crack tip. Other studies however have shown agglomerations of the radiopacifier (both BaSO₄ and ZrO₂) to be detrimental to the fatigue life of the cement. The agglomerations (as shown in Figure 1.14²⁴) act as sites for crack initiation and debonding of the radiopacifier from the PMMA matrix was also found to cause defects^{35,66,91–95}. An analytical study using stress analysis and fracture mechanics techniques by Evans et al.⁶⁰ also found that stress concentrations from small spherical voids such as pores are too small to account for crack initiation and therefore cracks must be initiated at additional stress raisers such as radiopacifier particles. A similar study by Janssen et al.⁷⁸ comparing laboratory tests and finite element models has drawn a similar conclusion. Furthermore in static tests, the radiopacifier may act as inclusions,

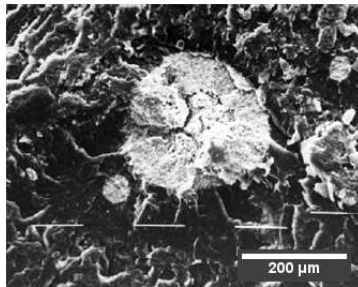


Figure 1.14: SEM of a BaSO₄ agglomeration in PMMA bone cement²⁴

weakening the matrix. Therefore, although radiopacifiers have been found to reduce crack propagation, they are also thought to be the cause of crack initiation. Similarities can be drawn between pores and radiopacifier particles. It seems under stress, agglomerations of radiopacifier particles act in the same way as large pores, initiating cracks. Similarly, well-dispersed radiopacifier particles may act in the same way as small pores, retarding crack propagation. Further problems have also been linked to radiopacifiers in terms of tribology and biology. It is thought that released radiopacifier particles can be abrasive, causing damage to articulating surfaces as well as enhancing macrophage-osteoclast differentiation, contributing to bone resorption and aseptic loosening^{96–99}. It is clear however that several characteristics of the radiopacifier play a vital role on the performance and success of the cement. These are the size, morphology, dispersion, adhesion to the polymer matrix and the material properties of the filler particle itself.

Polymerisation temperature

PMMA bone cement undergoes an exothermic free radical polymerisation reaction as previously discussed. The conversion from MMA to PMMA comes with a breakdown of covalent bonds which releases 52kJ per mole of MMA²⁴. This results in heat being produced at approximately 1.4 to $1.7 \times 10^8 \text{ J/m}^3$ ²⁵. The heat is produced rapidly and peaks over a short period of time. This heat has been previously thought to cause thermal necrosis of the bone due to temperatures exceeding 50°C , which may consequently cause aseptic loosening of the implant^{100,101}. *In vitro* studies have shown that the maximum temperatures achieved in models of cemented hip replacements were approximately 70°C ^{102–104}. These studies have also found that higher monomer to polymer ratios and thicker cement mantles increase the amount of heat produced¹⁰³. Finite element studies by Hansen et al.¹⁰⁵ on the cement-implant interface have found maximum temperatures achieved during the curing of cement to be around 53°C , however peak temperatures found *in vitro* do not necessarily correspond with temperatures reached *in vivo*. Clinical tests have shown

significantly lower intra operative peak temperatures ranging from 40 to 46°C, with the higher limit only reached when a thickness of 3mm or greater without cancellous interdigitation occurs²⁴. Similar *in vivo* setting temperatures have been found in several other studies. A recent review by Whitehouse et al.¹¹ has summarised these findings. Reckling et al.¹⁰⁶ found a mean maximum temperature of 48°C whilst temperatures in excess of 56°C have been recorded for periods of two to three minutes in a study by Harving et al.¹⁰⁷. The reasons for the lower *in vivo* maximum temperatures are due to thinner layers of cement (3-5mm), blood circulation and heat dissipation to the prosthesis and to the surrounding tissue^{24,108}. The temperature at which necrosis of cells occurs has also been well documented. Moritz and Henriques¹⁰⁹ suggested that a temperature of 55°C for 30 seconds was sufficient to cause necrosis of epithelial cells. At lower temperatures however, the time for necrosis was much greater (five hours at 45°C). Lundskog et al.¹¹⁰ found bone cells had a lower threshold, 30 seconds at 50°C, and the regenerative capacity of bone was only compromised at temperatures above 70°C. Using vital microscopy, Eriksson et al.¹¹¹ found evidence of widespread tissue damage in rabbit bone after one minute at 50°C, however a previous animal study by Lindner et al.¹¹² indicated that there is no change in bone regeneration following the use of bone cement. From these studies it is clear that although the high setting temperatures of bone cements are a concern in terms of necrosis of tissue, it appears it does not significantly contribute to the aseptic loosening of cemented implants due to lower *in vivo* setting temperatures and the regenerative nature of bone.

Shrinkage stresses

As well as high setting temperatures, PMMA bone cement shrinks during curing. During the polymerisation reaction of MMA, many short MMA monomer molecules combine to form a few long polymer molecules. This conversion from monomer to polymer comes with a reduction in volume. When polymerising pure MMA, a large volume shrinkage of 21% is observed²⁴, the process is very time consuming and the exothermic temperature is not

controlled. To overcome these problems, pre-polymerised beads of PMMA are employed in bone cement, which allows the amount of MMA employed to be halved. This reduces the volumetric shrinkage to 6-7% and possibly less depending on to the level of porosity in the cement. Volumetric shrinkage is also compensated via the uptake of water *in vivo*. Nevertheless, the volumetric shrinkage experienced combined with a high exothermic setting temperature can induce stresses, sufficient to initiate cracks in the cement.

Several studies have been conducted investigating the shrinkage of acrylic cement around hip replacement stems and it was found that cracks originated from the inner surface of the cement mantle, suggesting that they were caused by hoop stresses as a consequence of shrinkage of the cement during polymerisation^{54,113,114}. A theoretical model using thick-walled cylinder theory further confirms that stresses during curing are sufficient to initiate cracks prior to functional loading. The same study also demonstrated that pores are capable of expanding in order to reduce shrinkage stresses within the bulk of the cement therefore preventing crack initiation. Experimental studies quantified these residual stresses to be between 4 and 10MPa within the cement mantle^{115,116}. Using acoustic emission techniques, Roques et al.¹¹⁵ found partial relaxation of these stresses to occur due to cracking and sliding mechanisms at the cement-implant interface during curing. Two studies, one using an acoustic emission technique combined with micro-computed tomography (Mavrogado et al.⁶²) and the other using experimental and computer models (Lennon et al.¹¹⁶) found that thermal contraction due to the peak exothermic temperature played a larger role in cement damage than volumetric shrinkage alone. From this information it can be deduced that shrinkage as a result of high setting temperatures contributes to crack initiation and aseptic loosening to a greater extend than bone necrosis. Increased porosity may help reduce these stresses, however porosity can be detrimental to the mechanical performance of the cement. The exothermic nature of PMMA allows it to be self-curing, making its application simpler during surgery. Therefore, little can be done to completely

remove both the heat from curing and shrinkage stresses. Manipulating porosity to benefit both shrinkage stresses and mechanical properties would be difficult to achieve. Therefore, slight changes in the composition of PMMA bone cements may provide greater benefits to both shrinkage stresses and mechanical properties.

Sterilization

As with any implant used in the human body, bone cements must be sterilized before being introduced into the body. This process will remove microbial contamination in the cement and help prevent bacterial infection *in vivo*. Sterilization and packaging of the cement components is carried out by the manufacturer to ensure maintenance of the sterility of the product between the manufacturing location and the operating theatre. The monomer, MMA is typically sterilized using membrane filtration⁶⁸. For the powder component, two techniques are used, gamma irradiation or ethylene oxide sterilization. Both of these techniques have their respective advantages and disadvantages. Gamma irradiation has a high penetration depth which allows the material to be sterilized in its final packaging whilst ethylene oxide gas is an effective surface sterilant. Gamma irradiation however, has been known to affect molecular weight and cause free radical generation, which is harmful to the body. Furthermore these free radicals may interact with the benzoyloxide radical and affect the polymerisation process of PMMA. Ethylene oxide on the other hand does not have a high penetration depth and produces toxic by-products so the material must also be desorbed after sterilization²⁴.

Several studies have been conducted on the effects that the sterilization technique has on the properties of PMMA bone cements. Overall it was found that gamma sterilization lowered the molecular weight of PMMA powder when compared to ethylene oxide sterilization as a result of chain scission^{24,68,117-119}. This in turn had a detrimental effect on the fatigue performance and fracture resistance of the cement^{68,117,119}. The reduc-

tion in molecular weight on the static properties of PMMA are not as obvious. Certain authors have claimed to have observed a reduction in tensile strength, Young's modulus and strain-to-failure as well as changes in setting properties as a consequence of molecular weight reductions^{24,119}, whilst other authors found there to be no significant effect on quasi-static properties, such as bending and compression^{117,118}. It was also highlighted by Graham et al.⁶⁸ that the porosity of the final mixture due to the mixing technique employed had a larger effect on the mechanical properties than the sterilization method. Developments in novel sterilization techniques may benefit bone cements in the future, however at present it is a vital method for preventing bacterial-related surgical complications. The effectiveness of these techniques, although disadvantageous at times, is reflected upon in the low number of septic loosening cases for cemented implants. In 2009, it was reported that in England and Wales, only 14% of hip revision surgeries were due to infection, whilst 49% were due to aseptic loosening. Similarly 35% of knee revision surgeries were required due to aseptic loosening and to a lesser extent 23% due to septic loosening²¹. Although fewer cases of septic loosening are reported, there is still a need to implement added measures to prevent it such as the use of local antibiotic delivery systems in bone cements as will be discussed in detail later.

Composition

Table 1.1 summarizes the different compositions of several commercially available bone cements. These formulations have been optimised throughout the years to give the best performance *in vivo*. As previously described, changes in the radiopacifier used and the molecular weight of the polymer will have a significant effect on the setting and mechanical properties of bone cements. Different manufacturers have taken different approaches to their formulations. For example Cemex has a much higher powder to liquid ratio ($\simeq 3$), which the company (Tecres) claims to reduce the polymerization heat, the amount of residual monomer that the patient is subjected to and the shrinkage stresses³⁷. Cemex

has also a lower amount of toxic N,N-Dimethyl-p-Toluidine (DMPT) and a higher amount of benzoyl peroxide (BPO). Palacos R has a lower powder to liquid ratio ($\simeq 2$) and a higher DMPT content with lower amounts of BPO. Palacos also has a copolymer (methyl acrylate) and ZrO_2 as a radiopacifier in an effort to improve the mechanical properties of the cement as well as a small amount of chlorophyll to give the cement enhanced visibility during surgery. Heraeus claims that Palacos has “half the risk of revision after 10 years compared to other cements”, “very high visibility” and “excellent fatigue strength”¹²⁰.

Two compositional changes of interest are the initiator/activator ratio and the monomer/polymer ratio. As previously discussed the initiator (BPO) reacts with the activator (DMPT) to give a benzoyloxy radical which reacts with MMA to polymerise into PMMA. DMPT is toxic and therefore a lower level is favoured to prevent toxicity problems. In order for the MMA to self polymerise however, sufficient benzoyloxy radicals must be produced, therefore a high BPO to DMPT ratio is also favoured, as is a lower amount of MMA to reduce the amount of residual monomer. Studies have shown that more MMA results in higher setting temperatures^{103,121–124}. These studies also showed that the BPO and DMPT concentrations are proportional to the maximum curing temperatures and inversely proportional to setting times^{124–126}. A separate study by Noble et al.¹²⁷ however has revealed that different formulations of cement only affect the duration of the heat generation as opposed to the quantity of heat generated. Therefore increasing the amount of initiator and activator increases the rate at which the cement cures which in turn makes the curing parameters (temperature and time) less favourable. In terms of mechanical properties, it was found that decreasing the powder to liquid ratio by introducing more MMA results in a reduction in compressive strength^{128,129}. A recent study carried out at the Cardiff School of Engineering has led to similar conclusions¹³⁰. There was no correlation in terms of maximum temperature between the powder to liquid ratio, however more monomer was found to increase the setting time and decrease the compres-

sive strength of the cement. Altering the initiator to activator ratio also did not change the maximum setting temperature, however lowering the BPO to DMPT ratio resulted in a stiffer cement with higher compressive strength. Cement manufacturers have attempted to have a low powder to liquid ratio to prevent reductions in compressive strength but also enough monomer to allow the surgeon sufficient working time. The initiator/activator and the monomer/polymer ratios have been carefully optimised by manufacturers for specific purposes. Changing the initiation chemistry of PMMA bone cements improve some properties of the cement, however detrimental effects on other properties are likely to occur in the process.

Interfaces

In cemented implants there are two interfaces of interest where potential failure can cause implant loosening. These are the cement-metal interface and the cement-bone interface. The former bond arises as a result of direct contact between the cement and the metallic implant. This bond primarily develops from hydrogen bonds between the superficial metal oxide layer and PMMA. Macro and micro-retention can also be achieved as a result of surface roughness¹³¹. As water diffuses through cracks and is absorbed in the cement, this interface is subjected to hydrolysis which over time decreases its mechanical stability. This was further demonstrated by Ahmed et al.¹³² as samples immersed in saline over time showed significant reductions in bond strength. A study by Davies et al.¹³³ has developed a technique to monitor debonding *in vitro* using acoustic emissions in conjunction with ultrasound. From this study it was found that cracks in the cement and around the implant stem caused loosening of the implant, whilst cement without cracks maintained a good bond with the implant, however it was not deduced if the cracking originated from the cement itself or as a consequence of the debonding. To overcome hydrolytic debonding, implant coatings have been developed using polymers, silica and/or silane coatings which so far have proved to be successful^{131,132,134}, however it is postulated that improv-

ing this bond may increase the stresses transferred to the weaker cement-bone interface¹³⁵.

Although the cement-metal interface is important, the cement-bone interface has been more widely researched and discussed in publications. It is believed that the cement-bone interface is more prone to failure due to biological processes and micro-structural features. Acoustic emission techniques and computer tomography showed that damage was initiated at this interface and was found to be related to stress-raising micro-structural features in the cement. These features were as a result of irregularities in the geometry of the bone, creating recesses and notches filled with cement, as outlined by Leung et al.¹³⁶. Furthermore an ideal cement thickness of 1.0-1.5mm has been recommended by Terrier et al.¹³⁷ as too thin a cement layer will not support loads and too thick a cement layer will not elastically deform, subsequently increasing interfacial stresses and micromotion at the cement-bone interface. An animal study by Radin et al.¹³⁸ using sheep has demonstrated failure at the cement-bone interface to be more prevalent and most likely caused by a decreased torsional rigidity. A more biological approach to the cement-bone interface failure, taken by Goldring et al.¹³⁹, showed retrievals from aseptically failed hip replacements contained synovial-like tissue with the capacity to generate prostaglandin E2 and collagenase which can cause progressive bone lysis and resorption. Separate studies also found a similar membranous tissue or osteoid lining to occur in loosened implants^{140,141}. These studies also detected cement particles and debris such as radiopacifier particles in the bone surrounding the implant. Particles released by the cement and implant may therefore contribute to loosening after extended periods of time, as certain amounts of bone resorption and macrophagic reactions were found to occur even in successful implants¹⁴².

The technique used to apply bone cement was also found to affect cement penetration into bone and therefore affects the cement-bone interface as well. As outlined, bone cement can be introduced using a cement gun or manually using a “finger packing” method.

Studies have been conducted that have looked at the cement penetration of these two techniques. It was found that the use of a cement gun over finger packing resulted in higher pressures which in turn resulted in greater interdigitation of the cement into the cancellous bone^{143,144}. This allows the cement to interlock with the pores of the bone and anchor itself more effectively. Nevertheless the same studies found there were no advantages in terms of mechanical and fatigue properties by employing one system over the other. Another study by Leung et al.¹³⁶ found that interdigitation of cement with bone initiated damage by creating high levels of stress at the interface causing the cement to fracture. Furthermore concerns were also brought up as high levels of cement penetration may cause bone necrosis due to high curing temperatures. An *in vitro* study by Klein et al.¹⁴⁵ which pressurized test samples during curing found that increased pressure does in fact increase ultimate strength to a value similar to that of vacuum mixed cement but found there to be no difference in tensile properties and porosity. A separate study by Askew et al.¹⁴⁶ also highlights the fact that although cement penetration into bone may be beneficial, the strength of the fixation will always be limited by the intrinsic strength of the bone.

From these studies it seems that cement-metal interface failure tends to be mechanically and chemically induced whilst failure of the cement-bone interface tends to be induced by wear and debris particles as well as mechanically and biologically induced. Greater cement penetration into bone may not improve the cement-bone interface strength. Therefore changes to bone cement which can improve the biological and mechanical interactions between these interfaces and strengthen the bonds between them may prove more successful in reducing implant failure rates. For the cement-metal interface a mechanically stronger bond that resists hydrolytic degradation is required, whilst for the cement-bone interface, reduction of debris particles and bone growth and osseointegration into the cement as opposed to interdigitation would be beneficial.

Ageing

The final topic on cement failure involves the ageing of PMMA. As previously described, failure rates dramatically increase 5 years after surgery, demonstrating how bone cement tends to fail as a result of fatigue and ageing. Bone cement must function in the harsh environment of the human body and over time, water, higher temperatures and cells cause the cement to degrade, changing many of its properties. Although current commercially available cements must possess certain mechanical properties to pass standards, over time these properties can deteriorate *in vivo*. Recent studies have found that ageing *in vivo* and in simulated physiological conditions resulted in a reduction in mechanical properties. It was found that mechanical properties increased during the first week due to polymerization and formation of interpenetrating molecular networks, after which a decrease was observed due to the plasticising effect of water uptake¹⁴⁷. Testing in dry conditions, as dictated by standards, was found to always give higher values for mechanical properties which increased over time as the cement was found to polymerise over a period of 5 years⁵⁰. The plasticising effect of water also increased the creep rate of bone cements. Conditions which increase plasticisation (longer ageing, higher temperatures and stresses) were found to increase creep rates up to a maximum temperature of 40°C, above which the effects were diminished due to increased molecular mobility in the material¹⁴⁸. Ageing of bone cements not only affected mechanical properties, but it was also found to affect the structure and surface properties of the cement. Cement retrievals from hip replacements were found to have a decrease in molecular weight and scission-based degradation was found to occur over long periods of time, changing the actual structure of the PMMA molecule, as described in a study by Hughes et al.¹⁴⁹. Bettencourt et al.¹⁵⁰ showed that biological fluids cause hydrolysis of the PMMA ester groups, not only changing the composition of the cement but also the wettability of its surface. which may play a role in the loosening of the implant.

1.6.7 Novel Formulations

Having examined some of the causes of failure in PMMA bone cements, focus will now be placed on techniques that have been used in an attempt to overcome some of the problems previously highlighted.

Boneloc cement

To overcome the problem of high setting temperatures causing bone necrosis, Boneloc cement (Biomet Inc., Indiana, USA) was developed. Boneloc replaced half of the MMA content in the liquid component of the cement with n-decylmethacrylate isobornylmethacrylate, changed the activator to a mixture of adihydroxypropyl-p-toluidine and DMPT and added butyl-methacrylate-MMA co-polymers to the powder component of the cement¹⁵¹. This resulted in a 20°C to 33°C reduction in setting temperature when compared to other vacuum mixed cements but unfortunately, the changes had a detrimental effect on clinical results. Aseptic loosening rates were increased to 34% after three years¹⁵². This was due to a significantly lower glass transition temperature which meant the cement satisfied the standard tests at room temperature, but *in vivo* at 37°C, the cement had unacceptably high levels of stress relaxation and creep leading to clinical failure¹⁵¹.

Two-solution cements

Two-solution type cement mixtures are currently being developed in an attempt to overcome problems associated with porosity and inhomogeneities. These systems involve dispersing PMMA powder and an activator in MMA in one part and in the second part dispersing PMMA powder and an initiator in MMA. A study by Hasenwinkel et al.¹⁵³ looking at the effect of BPO and DMPT content on the properties of these two-solution cements found that setting times, setting temperature and maximum strains were within the range of commercial cements and an increase in flexural strength and modulus by 54% and 43% respectively was experienced. A later study by the same author showed the

fracture toughness and fatigue strength were comparable to a commercial cement, however these experiments did not employ radiopacifiers¹⁵⁴. A separate study by Rodrigues et al.¹⁵⁵ showed that the addition of zirconia to the two-solution cement increased its viscosity and also affected its mechanical properties, acting as a reinforcing phase when cross-linked PMMA spheres were added. Furthermore the amount of MMA used is much larger than in conventional cements, meaning more residual monomer will be present in the patient after surgery¹⁵⁴. The storage of MMA containing BPO over long periods of time is also a topic of concern as spontaneous polymerisation over time will limit the shelf life of two-solution cements. A study found that shelf life was very much temperature dependant and storage at 4°C yielded a shelf life of approximately 12 months whilst shelf life at 70°C resulted in setting of the cement in 5-7 minutes. Higher levels of initiator concentrations also shortened the shelf life, as demonstrated by Shim et al.¹⁵⁶. Changing the polymerisation chemistry of bone cement systems and altering the state of its components may successfully overcome problems such as porosity and high setting temperatures. In doing so however, unwanted problems that are less well understood than the current problems with traditional bone cement systems may develop. The unsatisfactory failure rates of Boneloc and potential future problems of two-solution cements make changes such as these very high risk. Therefore it may be better to modify only slightly current cement formulations by introducing novel materials as opposed to developing a completely different system. Slight modifications to the current cement system would be simpler to implement in an industrial scale and less likely to cause problems that have not been experienced before.

Copolymers

An example of this is the recent use of methylacrylate (MA), butylmethacrylate (BMA) and styrene copolymers in commercial bone cements in order to improve mechanical and fatigue properties. MA is a small molecule with a low glass transition temperature (6°C)

that makes the cement more hydrophilic and flexible resulting in a higher failure strain, a relatively low compressive strength and a relatively higher strength and failure strain in tension. Therefore MA makes the cement less brittle and less susceptible to stress risers like pores. BMA has a much higher molecular weight than MMA and the addition of a small amount of BMA gives the PMMA powder a more porous and open structure. This may improve the bond between polymer chains, which will entangle with the outer surface of the PMMA beads. BMA also has a low glass transition temperature (20°C) and adding a small percentage of BMA to the powder component ($\leq 5\%w/w$ but preferably $\leq 1\%w/w$) is claimed to result in enhanced fatigue strength¹⁵⁷. Styrene copolymers on the other hand are more hydrophobic with a higher glass transition temperature (120°C) and so the time and energy needed to make a homogeneous mixture will be longer than MMA-MA, MMA-BMA mixtures. It is thought that the addition of styrene to PMMA bone cements is beneficial to the fatigue strength, however little datum is published on this matter²⁴.

Cross-linking agents

A similar approach to copolymers involves the use of cross-linking agents. Cross-linking agents are thought to strengthen polymers by linking polymer chains together via covalent bonds. This process may strengthen the material however, chain mobility is reduced, making the polymer rigid and more prone to brittle failure. A study by Deb et al.¹⁵⁸ looking at different cross-linking agents in bone cement found that small amounts of cross-linking was beneficial to reducing creep and improving mechanical properties in bone cement, however too much cross-linking was detrimental to the cement. The same author also found that the use of these agents improves the bond between the polymer matrix and radiopacifier particles and improves tensile strength¹⁵⁹. Similarly a study by Nien et al.¹⁶⁰ implementing poly(methylmethacrylate-acrylic acid sodium salt) into bone cements found that too much cross-linking agent was detrimental to the mechanical properties and another study found cross-linking monomers to improve mechanical properties only

when used in conjunction with glass fibre^{161,162}. It seems as though small amounts of cross-linking agents improves mechanical properties by improving the bond between filler particles and the PMMA matrix. The biocompatibility of cross-linking agents is also questioned and further research is required in this field before such materials can be implemented in bone cements.

Plasticisers

Plasticisers function in the opposite way to cross-linkers. They work by sitting between polymer chains, spacing them apart, increasing the free volume and allowing for greater chain mobility. This decreases the glass transition temperature of polymers and makes them softer and more ductile. Citrate esters were tested in pure PMMA and found to lower the glass transition temperature, tensile strength and Young's modulus. The percentage elongation also increased dramatically after 20%w/w plasticiser was used¹⁶³. When added to bone cement at up to 12%w/w, castor oil plasticiser was found to decrease yield strength from 88 to 15 MPa, Young's modulus from 1500 to 446 MPa and maximum polymerization temperature from 41.3 to 25.6°C, without affecting the setting time. Castor oil also interfered with the polymerization reaction and had a negative effect on cell viability, as demonstrated by Lopez et al.¹⁶⁴. Similarly, Lam et al.¹⁶⁵ found reductions in modulus and compressive strength to occur when linoleic acid coated strontium was added to bone cements. Although plasticisers may be of use in vertebroplasties where a lower modulus cement is favourable to prevent brittle failure and damage to vertebral discs, in total joint replacements the reduction in mechanical properties may lead to early failure of the implant. Lowering of the glass transition temperature may also result in high levels of creep at *in vivo* temperatures, which can again may lead to premature failure of the cement. Furthermore as previously described, water uptake has a plasticising effect on PMMA over time and therefore synthetic plasticisers may not be required to achieve a more ductile material. The disadvantages outlined, coupled with lack of information on

the biocompatibility of plasticisers currently rules out the viability of this option.

Rubber Particles

Having eliminated the use of plasticisers in PMMA for total joint replacements, there is still a need to reduce brittle failure in bone cements. In an effort to achieve this, several authors have attempted to modify PMMA with rubber particles in order to achieve higher levels of toughness. Several studies have found that using rubber particles in PMMA improves the overall fracture toughness of the cement^{166–168}. Cho et al.¹⁶⁹ found that toughening in three-point bending occurred as a result of crazing and under impact shear yielding was induced by cavitation of the rubber particles. Further investigation into using poly-(*n*-butyl acrylate) for toughening either as a particle or in a core-shell configuration with PMMA showed that both methods work equally well. It was also found that at low strain rates the interfacial adhesion between the rubber particle and PMMA matrix is sufficient to induce matrix deformation whilst at high strain rates failure at the interface of the rubber particle and PMMA occurs¹⁶⁶. A similar study by Lalande et al.¹⁶⁸ using PMMA-*b*-polybutylacrylate triblock copolymers also showed high impact stresses to induce brittle failure associated with increased localization of the crack tip deformation. Rubber toughening appears to be an effective method of retarding fatigue failure in bone cements under low strain conditions, however at higher strain rates improved adhesion between the particle and the PMMA matrix is required to prevent brittle failure.

Iodine-based radiopacifiers

Another area of recent interest is the use of iodine-based radiopacifiers to replace conventional powdered radiopacifiers such as BaSO₄ and ZrO₂. As previously identified, conventional radiopacifiers have been associated with many problems, even failure of bone cements. The use of a liquid radiopacifier may overcome such problems. A study by Artola et al.¹⁷⁰ using 4-iodophenol methacrylate (IPMA) instead of BaSO₄ found that

15%v/v in the liquid component gave similar radiopacity as 10%w/w BaSO₄ as shown in Figure 1.15. Furthermore there was no change in glass transition temperature and there was enhanced compressive strength, tensile strength, and elastic modulus¹⁷⁰. The same author also investigated adding 5%v/v 2-[2',3',5'-triiodobenzoyl] ethyl methacrylate (TIBMA) and 3,5-diiodine salicylic methacrylate (DISMA) to the liquid component of bone cement and found that the mechanical properties were better than those of the BaSO₄ containing cement. The radiopacity was found to be comparable with BaSO₄ and all samples showed good biocompatibility¹⁷¹. Lewis et al.¹⁷² investigated using an iodine-containing copolymer in the powder component of bone cement and found similar results, stating iodine-based cements are a viable candidate cement for arthroplasties. Closer examination of this study however, found that the mean fatigue life of the iodine-containing cement is lower, there is no significant difference in work to fracture and fracture toughness and the iodine-based cement had higher variability (larger standard deviations). A study by Manero et al.¹⁷³ looking at fatigue crack propagation of three iodine-containing cements (IPMA, TIBMA and DISMA) in comparison with conventional BaSO₄ cement found that the BaSO₄ cement demonstrated the best performance in terms of fatigue crack propagation, then the iodine-based cements followed by radiolucent cement. Therefore although iodine-based cements may provide enhanced static mechanical properties

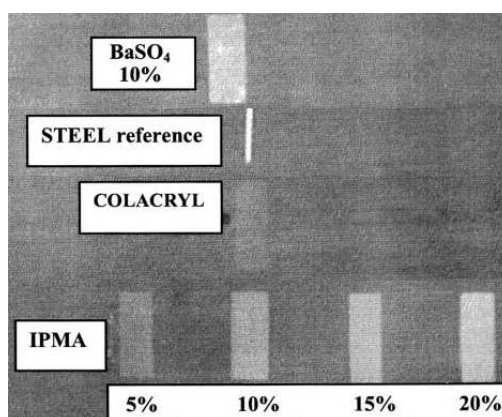


Figure 1.15: X-ray of iodine-based bone cements¹⁷⁰

over conventional cements, they do not perform better in terms of crack propagation. This may be due to the fact that iodine-based radiopacifiers cannot redirect crack tips like conventional radiopacifier particles. Also this technique has not been commercialised due to the risks associated with iodine allergies in patients²⁴.

Fibre reinforcement

Different studies have taken a similar approach to improving bone cements by adding novel materials to improve certain properties. A commercial example is the use of ZrO_2 to replace $BaSO_4$. ZrO_2 has been widely used for dental cements due to its mechanical properties and is also employed in Palacos bone cement for that same reason. Further research into ZrO_2 by Kotha et al.¹⁷⁴ found that the use ZrO_2 fibres instead of particles further improves the ultimate strength and fracture toughness of cements. Similarly, when PMMA fibres were added to pure PMMA in a study by Gilbert et al.¹⁷⁵, improvements in tensile, fracture toughness and fatigue properties were observed. The biocompatibility of fibres however and the effect they may have on the human body is still disputed.

Improving bone growth

Other novel materials such as strontium oxide (SrO) for improving bone growth into the cement have been investigated and suggested for total joint replacements by Lewis et al.¹⁷⁶. Replacing $BaSO_4$ with SrO however, results in higher hardness values, a greater elastic modulus and a lower mean fatigue life. When discussing bone growth, the use of hydroxylapatite (HA) is well documented as it is widely used as a material for bone repair. The addition of HA to PMMA by Tihan et al.¹⁷⁷ was found to increase the hydrophilicity and water absorption of PMMA and as a result, leads to good cell growth, proliferation and viability on the material. The addition of HA to PMMA however, has been documented to reduce mechanical properties and increase water absorption which may accelerate ageing or hydrolytic degradation mechanisms^{178,179}. Sodium fluoride, which is also thought to

promote bone growth, has also been tested by Minari et al.⁸⁸ in cements with BaSO₄ but did not show significantly different mechanical properties or increased radiopacity and its effect on bone growth in cements is yet to be tested. Although improving bone growth properties would be beneficial to the long-term performance of bone cements, it is vital for the novel materials to not reduce the mechanical and fatigue properties of the cement. Other cement types such as calcium phosphate and apatite based cements promote bone growth well, however do not have sufficient mechanical properties for load bearing applications such as joint arthroplasty. The use of titanium dioxide (TiO₂) as a radiopacifier may provide a solution to this problem. Titanium is the main material of hip and knee replacements due to its good biocompatibility, mechanical properties and its ability to bond with bone. A recent study by Fukuda et al.¹⁸⁰ using rutile TiO₂ in bone cement found it to have high levels of osteoconductivity and good mechanical properties. A separate study by Chou et al.¹⁷⁸ however showed TiO₂ to decrease the strain at break and the flexural strength, which was due to agglomerations of TiO₂ and brittle failure.

Chemical coatings

Gillani et al.¹⁸¹ investigated the functionalisation of ZrO₂ and BaSO₄ using a silane coupling agent and found that cements with unfunctionalised radiopacifiers exhibited brittle failure whilst functionalised radiopacifiers exhibited plastic failure modes. This was due to a stronger bond forming between the radiopacifier and the polymer which under stress induced plastic deformation of the polymer matrix as opposed to separation of the radiopacifier from the matrix, which can initiate cracks and brittle failure. Cement adhesion to the metallic implant is usually not desirable in joint replacements as hip replacements with polished, tapered stems have been shown to have a lower failure rate when compared to hip replacements with roughened stems. It is thought that the polished stem, under load, can loosen and wedge itself deeper in the cement, whilst roughened stems create wear debris which may contribute to the loosening of the implant. Nevertheless, several

studies have been carried out investigating the use of chemical coatings to enhance the bond strength between bone cement and the metallic implant in an effort to prevent excess movement of the implant. Coating of cobalt-chrome alloy implants with a silane was found to significantly improve their bond strength with PMMA bone cement, as demonstrated by Yerby et al.¹³⁴. The same silane was added to the monomer of PMMA in a separate study by Gbureck et al.¹⁸² and the bond strength between the titanium implant and the bone cement was assessed. It was found that the mechanical properties of the cement itself were not altered by the addition of the silane, the cement-metal interface was more hydrolysis resistant and the bond strength between the metal and PMMA was significantly improved. Furthermore Miyazaki et al.¹⁸³ observed accelerated apatite formation on the surface of bone cements using the same silane in conjunction with calcium chloride. It was found that the silanol group (Si-OH), provided by the silane after hydrolysis, induced apatite formation as well as a dissolution of calcium ions (Ca^{2+}) from the material. A similar chemical known as Span 60, which forms a bond with the hydroxyl group of TiO_2 in the same way a silane does, was found to improve the dispersion of TiO_2 particles, increasing its hydrophobicity and reducing agglomerations, as demonstrated by Li et al.¹⁸⁴. As the surface of radiopacifier particles tend to have high surface energies and are highly hydrophilic, the coating of the surface using a hydrophobic and low surface energy silane coupling agent may also offer improved dispersion characteristics which will reduce agglomerations¹⁸⁵. Although the biocompatibility of silanes is questioned, the use of small amounts as coatings for radiopacifier particles may not have a detrimental effect on cells. The use of silanes, coupled with a novel bioactive material such as TiO_2 may improve bone growth, bonding to the metallic implant, dispersion of the radiopacifier particles and as a result of this, improve mechanical and fatigue properties and the long-term success of cemented implants.

Nanoparticles

With the recent development of nanotechnology, there has been a great deal of interest in using such technology to improve bone cements. Current radiopacifiers used are in the range of 1-3 μm , which when poorly dispersed can lead to 50-200 μm agglomerates. Several studies using nano-particle radiopacifiers found that agglomerations were reduced, mechanical and fatigue properties were improved, osteoblast adhesion was improved, decreases in curing temperatures were experienced and increases in radiopacity occurred¹⁸⁶⁻¹⁸⁸. Due to the size of the radiopacifier nanoparticles, cell and tissue interactions must be investigated to ensure nano-sized particles released from the cement do not have a detrimental effect on the surrounding tissue and patient's well being. A study by Hill et al.⁴⁹ using nano-calcium carbonate (CaCO_3), which is known to be biocompatible, in bone cements found that energy to maximum load, elastic modulus, bending strength and bending modulus were improved by the addition of less than 1%w/w. Coating the nano- CaCO_3 with sodium citrate to improve dispersion also increased the energy to maximum load and elastic modulus but had a detrimental effect on bending properties. The cement used to achieve these results however, did not contain any radiopacifier particles and the study focused only on mechanical properties as opposed to fatigue and cytocompatibility tests.

Nanotubes

The development of super strong carbon nanotubes, which exhibit extremely high tensile strength and modulus has been of great interest to material scientists for many years. The ability of nanotubes to undergo plastic deformation under excessive tensile strain makes it applicable to countless materials including PMMA bone cement. Carbon nanotubes, although strong in tension are not as strong in compression, bending and torsion as they tend to buckle. Nevertheless, it was found that nano-tubes enhanced the mechanical and fatigue properties of bone cement both in tension and compression^{189,190}. Furthermore, the

addition of multi-walled carbon nanotubes was found to reduce the setting temperature due to the good thermal conductivity of the nanotubes. Carbon nanotubes were also found to improve the mechanical properties by retarding crack growth by a bridging effect in the crack, normal to the direction of crack growth. Agglomerations of the multi-walled nanotubes were also found to occur, but this was dependant upon the method used to incorporate the nanotubes into the cement, as outlined by Ormsby et al.^{191,192}. A biological study by Usui et al.¹⁹³ on the effects of multi-walled carbon nanotubes found that they “induce little local inflammatory reaction, show high bone-tissue compatibility, permit bone repair, become integrated into new bone, and accelerate bone formation”. Nanotubes therefore offer an exciting new approach to improving bone cements, however there is speculation regarding its biocompatibility and as this technology is still under development, the costs of manufacturing nanotubes are relatively high, making its use in bone cements not economically viable. Nevertheless, as more efficient production methods are being developed, the use of nanotubes in orthopaedics is very likely as they become more economically viable.

1.6.8 Drug delivery systems and antibiotics

Powdered gentamicin

Powdered antibiotics, such gentamicin sulphate, have been employed in PMMA bone cements in an effort to prevent septic loosening of the implant. This technique is currently under much debate due to the fear of resistant bacteria becoming established and the effect of gentamicin on the mechanical and fatigue properties of the cement. Gentamicin is generally added to the powder component of the cement in doses of 0.5-1g of gentamicin sulphate powder per 40g of cement. Dunne et al.^{194,195} showed that the addition of 1-4g of gentamicin resulted in a significant decrease in compressive and bending strength. Likewise an earlier study by Lautenschlager et al.¹⁹⁶ investigating the addition of gentamicin to Simplex P bone cement found the antibiotic to cause gradual, proportional decreases

in compressive and tensile strengths. The amount of antibiotic released was also found to increase with increased dosage, however the majority of the gentamicin release occurred within the first 6 hours in a “burst” type mode^{194,195,197}. When testing on *Staphylococcus spp.* clinical isolates the increased release initially reduced the amount of bacterial colonisation but at 72 hours there was no beneficial effect as biofilms formed regardless of gentamicin release^{194,195}. Separate studies obtained similar results and conclusions demonstrate that the use of gentamicin sulphate powder in bone cements does not completely inhibit the formation of infectious biofilms^{198,199}. Furthermore there have been studies that showed the antibiotic to have a detrimental effect on the fatigue life of cements^{194,200}. In contrast other studies have found that there was no significant difference in terms of fatigue performance^{201,202}. It has been shown that the porosity and therefore the mixing method also plays a role on the elution of antibiotics as vacuum and hand mixing have been found to affect gentamicin release^{203,204}. In general the manual addition of gentamicin in-situ prior to surgery is not recommended due to a lack of homogeneity achieved in the mixing²⁰⁰, but this is also disputed²⁰⁵.

Gentamicin solution

To overcome the problem of dispersion and homogeneity of antibiotic-loaded cements as well as to reduce costs, gentamicin solution has been tested and was found to have good release characteristics, but was also found to reduce the mechanical properties significantly^{206,207}. This may be due to the phase separation of the two liquids occurring as MMA is hydrophobic, not mixing well with water-based gentamicin solutions, creating large voids in the cement upon polymerisation. To overcome this, Miller et al.²⁰⁸ tested employing emulsifiers with liquid gentamicin in bone cement but found little success in terms of mechanical performance. The use of gentamicin solution with vancomycin also yielded positive results in terms of antibiotic release but poor mechanical properties, as demonstrated by Hsieh et al.²⁰⁹.

Alternative therapeutic agents

Different antibiotics in a powdered form such as vancomycin have also been tested in bone cements, either alone or in conjunction with other antibiotics. Laine et al.²¹⁰ demonstrated the use of powdered vancomycin in PMMA had a similar effect as gentamicin, as a reduction in mechanical strength was observed regardless of mixing method. When employed in conjunction with gentamicin loaded cements, vancomycin was found to reduce the compressive strength and porosity of the cement but maintained a compressive strength above the minimum values required by ISO standards (70MPa). Furthermore the combination of gentamicin and vancomycin was found to inhibit the growth of more strains whilst gentamicin alone selected for methicillin-resistant *Staphylococcus aureus*^{211,212}. Another therapeutic agent tested in bone cements is chitosan, however this has met with little success. It was found that chitosan did not have any antimicrobial benefit or benefit to the gentamicin release. Setting properties were also altered and a detrimental effect on the mechanical properties of the cement over time was observed²¹³⁻²¹⁵. Fusidic acid and clindamycin was also tested in combination with gentamicin in bone cements in a study by Neut et al.²¹⁶. It was found that fusidic acid in combination with gentamicin was effective against a higher number of clinical isolates when compared to gentamicin and gentamicin with clindamycin, however mechanical properties are yet to be assessed²¹⁶. The addition of lactose to gentamicin was found to increase the amount of antibiotic released but also increased porosity which reduced mechanical properties^{217,218}. It appears that the addition of other therapeutic agents to bone cement either in conjunction with gentamicin or by itself, can improve the antimicrobial efficacy of the cement, however the changes in mechanical properties experienced are not beneficial to the long-term success of the implant. Therefore a different approach such as redesigning the delivery system may prove more effective in preventing implant infections whilst preserving mechanical and fatigue performance.

Silver nanoparticles

An example of a different antimicrobial system in PMMA is the recent use of silver nanoparticles. Silver has a wide spectrum antimicrobial activity, however due to the cytotoxicity of silver salts it is unsuitable for continuous clinical use. Silver nanoparticles however may overcome this issue. When introduced in PMMA, silver nanoparticles were found to have high antibacterial efficacy even against methicillin-resistant *Staphylococcus epidermidis* (MRSE) and methicillin-resistant *Staphylococcus aureus* (MRSA)^{219,220}. Also the *in vitro* cytotoxicity of silver nanoparticle containing bone cement was not significantly different from plain bone cement²²⁰. A recent animal study by Moojen et al.²²¹ however showed that silver bone cement was not effective in preventing methicillin-sensitive staphylococcal infections *in vivo* as the antimicrobial effect is only exhibited at the cement surface rather than the surrounding tissue. This may be due to the fact the silver nanoparticles are not released from the cement into the surrounding fluid and tissue like antibiotics. Also results on mechanical and fatigue properties of silver bone cements are yet to be published.

1.7 Test methods

1.7.1 Test parameters

From the reviewed literature it is clear that a wide range of different test methods have been applied to assess different properties of PMMA bone cements. The properties tested have been categorized into static, dynamic, crack growth, fracture toughness, viscoelastic and rheological tests in a review by Saha et al.²²². These properties can be altered by many factors, including: the preparation method, the composition/additives used in the cement, the sterilization techniques employed, the porosity of the cement and the storage/ageing conditions. Furthermore parameters such as test temperature, environment, specimen preparation method and strain/loading rates also affect the results obtained.

1.7.2 Standard tests

To prevent test parameters from affecting results, the majority of reported tests are performed according to guidelines published by the International Organization for Standardization (ISO) and the American Society for Testing and Materials (ASTM). The standards used for PMMA bone cements are either the “ISO5833:2002 Implants for surgery - Acrylic resin cements” standard²²³ or the “ASTM F451-08 Standard Specification for Acrylic Bone Cement” standard²²⁴. The ISO5833 guidelines have established minimum requirements that all novel cements must achieve, as shown in Table 1.2.

Table 1.2: ISO5833 Requirements for acrylic resin cements

Parameter		Requirement
Maximum setting temperature	Average / °C	90
	Maximum deviation / °C	± 5
Doughing time	Average / min	≤ 5
	Maximum deviation / min	± 1.5
Setting time / min		3 to 15
Compressive strength / MPa		≥ 70
Bending modulus / MPa		≥ 1800
Bending strength / MPa		≥ 50

ISO5833 also specifies procedures for establishing setting, compression and flexural properties. ASTM F451 is similar to the ISO standard, however uses tensile tests as opposed to flexural tests. These standards also specify the required conditioning of samples prior to testing and the strain rates that must be applied during testing as static properties of bone cement have been found to be affected by these parameters²²². The availability of such standards has made the comparison of bone cement properties across different studies possible. From three separate studies that have used the standards, the average values for static properties of polymerised commercial bone cements were found to be: 35.3MPa tensile strength, 64.2MPa bending strength, 93.0MPa compressive strength and 2552MPa bending modulus^{24, 25, 74, 222}.

1.7.3 Alternative tests

PMMA bone cement is subjected to complex loading *in vivo*, however the standards do not fully establish how the cement will perform *in vivo*. Several different methods are used in the literature that have been developed to better understand bone cement properties. These include: hardness^{92, 225}, fatigue^{32, 74}, crack propagation^{33, 58, 173, 226, 227}, fracture toughness^{74, 228, 229}, creep^{230–234} and stress relaxation tests^{235–238}. The use of rheometric testing to understand the rheological and setting properties of bone cement have also been outlined^{74, 239–244}. Similarly methods to investigate the molecular structure of bone cements have also been developed^{24, 50, 148–150, 245}. The radiopacity, porosity and cracking of cements has been investigated using X-ray imaging^{62, 79, 136, 170, 246}; and the bone growth properties of novel cement formulations have been investigated using simulated body fluids^{247–253}, cell culture methods^{254–256} and animal trials^{138, 180, 257, 258}. The antibiotic release from bone cements is of great interest and has been studied using HPLC and chemical assay methods^{195, 213, 217, 259} as well as mathematical methods.¹⁹⁷ Similarly the effectiveness of the antibiotic release on different strains of bacteria has also been investigated^{203, 216, 220}.

Some of the methods listed have been used throughout this thesis and will be discussed in more detail in subsequent chapters. The effectiveness of the methods used and the results obtained will also be discussed and compared to previous studies.

Chapter 2

General Methods

This chapter will refer to some of the common methods that have been used to test the different properties of bone cements throughout this thesis. Later chapters will refer back to these methods to reduce repetition. Test methods that are specific to certain chapters will be described in detail in the appropriate chapter.

2.1 Mixing bone cements

As previously stated, PMMA bone cement is composed of a liquid and powder component which when mixed undergoes free radical polymerisation to form a rigid polymer. When preparing commercially available bone cement, mixing was carried out according to the manufacturer's instructions. When preparing the authors own formulation of bone cement, the ISO 5833:2002 (Implants for surgery - Acrylic resin cements) standard²²³ was used as a guideline. All the contents of the cement were stored at room temperature in the dark and conditioned at 23°C for 2 hours prior to mixing. Each material of the powder component was put through a 35 mesh sieve (0.5mm opening) before being carefully weighed out to an accuracy of $\pm 0.01\text{g}$ and mixed together thoroughly. Separately each chemical of the liquid component was weighed out and mixed together. Both components were then introduced into a clean polypropylene bowl and hand mixed at approximately 1Hz with a polypropylene spatula for 1 minute. The cement was then applied into a mould or appropriate container.

Moulds were prepared out of polytetrafluoroethylene (PTFE) in order to make uniform samples with specific dimensions. PTFE was chosen as it does not adhere to or react with bone cement, it can withstand the setting temperatures, allows for the easy removal of samples and has no leachables. The cement was mixed as previously specified and poured into the mould. The mould was then clamped with two steel endplates covered with PTFE film at either end. After 10 minutes, the samples were pushed out of the mould using a steel removal rod and allowed to cure at 23°C for 24±2 hours. After 24 hours the samples were sanded down to the correct dimensions using 320 grit silicon carbide paper.

2.2 Setting properties

Measurements and calculations for the setting properties were carried out according to the ISO5833:2002 standard using a high density polyethylene mould and a K-type wire thermocouple connected to a Picotech ADC11 Data Logger. The ambient temperature was recorded prior to mixing and 25g of cement was prepared. Recording of the temperature and time commenced as soon as the liquid came into contact with the powder. Temperatures were recorded to an accuracy of ±0.5°C. The setting temperature was calculated as shown in Equation 2.1 and the setting time (t_{set}) was defined as the time when the setting temperature was reached (T_{set}).

$$T_{set} = \frac{T_{max} + T_{amb}}{2} \quad (2.1)$$

Where:

- T_{set} is the setting temperature
- T_{max} is the maximum temperature reached during curing
- T_{amb} is the recorded ambient temperature prior to mixing

2.3 Mechanical properties

2.3.1 Compressive strength

Compressive strength was determined as specified in the ISO 5833:2002 standard²²³. Cylindrical bone cement samples were prepared with $12\pm 0.1\text{mm}$ length and $6\pm 0.1\text{mm}$ diameter (Figure 2.1(a)). Prior to loading, the dimensions of the samples were recorded to an accuracy of $\pm 0.01\text{mm}$. Each individual sample was then loaded incrementally in compression using a Zwick Roell ProLine table-top Z050/Z100 materials testing machine (Zwick Testing Machines Ltd., Herefordshire, UK) at a constant cross-head speed of $20\text{mm}/\text{min}$. Load and displacement was recorded and loading was stopped when failure occurred or the upper yield point had been passed.

To calculate the compressive strength (σ_c) in MPa, F_{max} , the load to cause fracture, the 2% offset load or the upper yield point load (whichever occurred first, in N) was divided by the original cross-sectional area (in mm^2) of the sample as shown in Equation 2.2. An average of five samples were used.

$$\sigma_c = \frac{F_{max}}{\text{cross sectional area}} \quad (2.2)$$

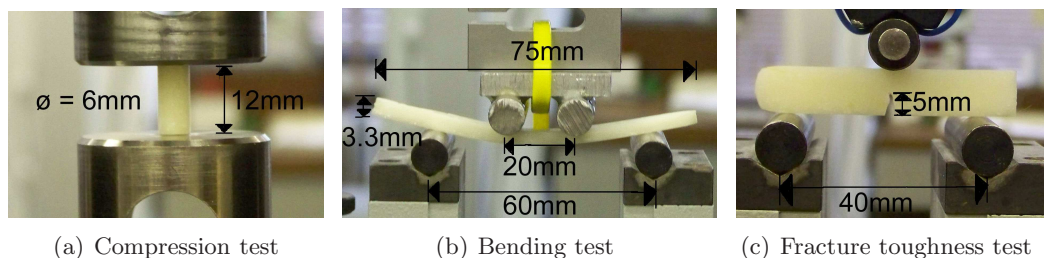


Figure 2.1: ISO5833 and ISO13586 tests

2.3.2 Bending modulus and strength

Bending modulus and strength was determined as specified in the ISO 5833:2002 standard²²³. Rectangular bone cement samples were prepared with a length of 75 ± 0.1 mm, width of 10 ± 0.1 mm and thickness of 3.3 ± 0.1 mm (Figure 2.1(b)). Prior to loading, the width and thickness of the samples were noted to an accuracy of ± 0.01 mm. A four-point bending test rig was used with a distance between the outer loading points of 60 ± 1 mm and a distance between the inner loading points of 20 ± 1 mm (Figure 2.1(b)). Each individual sample was carefully placed in the centre of the four-point bending rig and loaded incrementally using a Zwick Roell ProLine table-top Z050/Z100 materials testing machine at a constant cross-head speed of 5mm/min. Displacement as a function of applied force was recorded. Loading was stopped when failure of the specimen occurred.

Equation 2.3 was used to calculate the bending modulus and Equation 2.4 was used to calculate the bending strength of each sample. Five samples were used to obtain an average bending modulus and bending strength for each group.

$$E_b = \frac{\Delta F a}{4 f b h^3} (3l^2 - 4a^2) \quad (2.3)$$

$$B = \frac{3F_{fract} a}{bh^2} \quad (2.4)$$

Where:

- f is the difference between the deflections at 15N and 50N in mm
- b is the average width of the specimen in mm
- h is the average thickness of the specimen in mm
- l is the distance between the outer loading points (60mm)
- ΔF is the load range (50N - 15N)
- a is the distance between the inner and outer loading points (20mm)
- F_{fract} Force at fracture in N
- a is the distance between the inner and outer loading points (20mm)

2.4 Fracture toughness tests

The ISO13586:2000 Plastics - Determination of fracture toughness (G_{IC} and K_{IC}) - Linear elastic fracture mechanics (LEFM) approach standard was used to determine the fracture toughness of samples²²⁸. This was similar to the bending tests, but with a sharp chevron notch (roughly 4.5-5.5mm) through the centre of the sample, created using a sharp razor blade. Prior to loading in three-point bending (Figure 2.1(c)) using a Zwick Roell ProLine table-top Z050/Z100 materials testing machine, a Pye Scientific travelling microscope (Pye Scientific, Cambridge, UK) was used to measure the length of the crack and the width and length of each sample was measured using a Vernier caliper. The results from five samples for each group were recorded to obtain an average.

Determination of the load at crack growth initiation (F_Q)

A tangent to the load displacement curve of a specimen was drawn to determine the initial stiffness (S). This stiffness was then reduced by 5% and a line from the zero-point was drawn. If the maximum of the load displacement curve fell between the two lines drawn, then F_Q was equal to F_{max} . If the second line (stiffness reduced by 5%) intersects with the load curve before the maximum then the point of intersection (F_5) was considered to be F_Q . The conditions of linear elastic fracture mechanics (LEFM) were met when:

$$\frac{F_{max}}{F_5} \leq 1.1$$

Calculating the critical stress intensity factor (K_{IC})

The critical stress intensity factor (K_{IC}) was calculated using Equation 2.5 which used the load (F_Q) at crack growth initiation and the original crack length (a).

$$K_{IC} = f \frac{F_Q}{H\sqrt{w}} \quad (2.5)$$

Where:

F_Q	is the load at crack growth initiation in N
H	is the thickness of the specimen in m
w	is the width of the specimen in m
a	is the crack length in m
f	is the geometry calibration factor (retrieved from Annex A of the BS ISO 13586:2000)

Validity of results

Equations 2.6 and 2.7 were used to check the accuracy of the results obtained. If the value for E_{stiff} was 15% larger than E_{fract} then K_{IC} and G_{IC} was checked for errors or the test was carried out again.

$$E_{stiff} = \frac{2f^2\phi S}{H} \quad (2.6)$$

$$E_{fract} = \frac{K_{IC}^2}{G_{IC}} \quad (2.7)$$

Where:

E	is the modulus of elasticity in Pa
H	is the thickness of the specimen in m
S	is the stiffness of the specimen in Pa
ϕ	is the energy calibration factor (retrieved from Annex A of the BS ISO 13586:2000)
$f(a/w)$	is the geometry calibration factor (retrieved from Annex A of the BS ISO 13586:2000)
K_{IC}	is the critical stress intensity factor MPam ^{1/2}
G_{IC}	is the critical energy release rate Nm ⁻¹

2.5 Fatigue testing

For fatigue testing, the ISO15850:2002²⁶⁰ (Plastics - Determination of tension-tension fatigue crack propagation) and ASTM E399²⁶¹ standards were used as guidelines. Fatigue

tests were conducted at 37°C using an Instron environmental chamber (Instron SFL, Bristol, UK) and a 5kN Dartec servohydraulic testing machine with an MTS FlexTest GT controller (MTS, Minnesota, USA). Circular disc compact tension samples were prepared according to Section 2.1 with a diameter of 27mm and thickness of 9mm with two drilled 5mm holes (as shown in Figure 2.2(a)). A chevron notch (roughly 5mm in length) was cut into the sample to ensure symmetric crack growth using a modified microtome. Sample dimensions were measured using a travelling microscope (Pye Scientific, Cambridge, UK) as shown in Figure 2.2(b). Symmetric loading was applied using the drilled oversized holes allowing the loading pins to rotate without friction. Krak gages (KG-A10, Hartrun Corporation, Minnesota, USA) were attached to the samples (Figure 2.2(b)) and connected to a constant current supply and amplifier built and designed by Evans et al.⁵⁸ to measure crack lengths with an accuracy of $\pm 0.001\text{mm}$ even at low crack growth rates. Prior to testing, samples were conditioned for 2 months to ensure their material properties had stabilised.

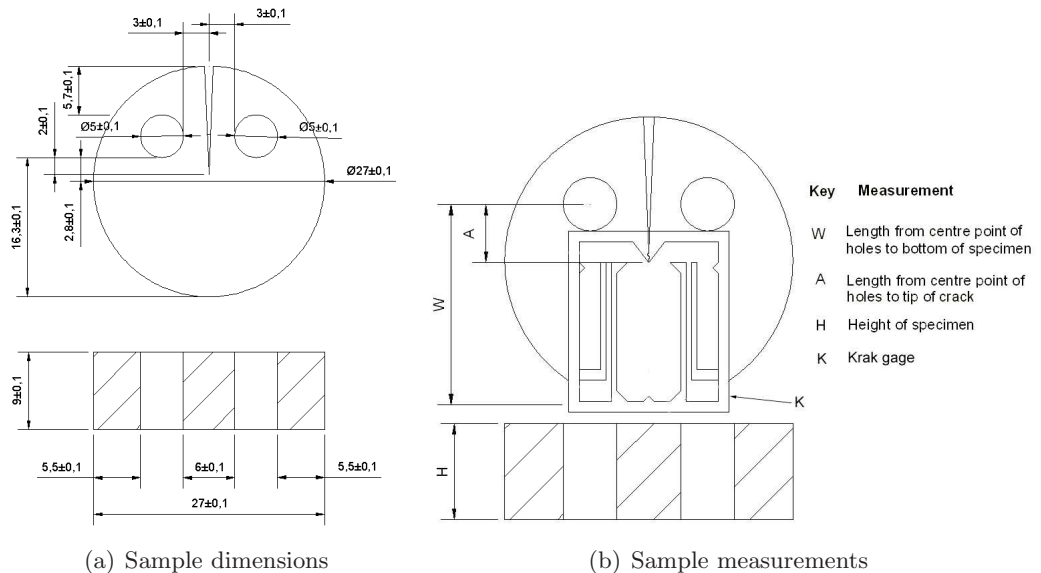


Figure 2.2: CT fatigue testing samples

Samples were cyclically tested in load control with a sine wave at 5Hz between 70N and 7N (or 100N and 10N for Palacos cements) (R-ratio of 0.1) allowing for measurements of crack growth rates through stress intensities of 0.3 to 0.8MPam^{1/2} as the crack grows through the length of the sample. Prior to loading, samples were subjected to a precracking procedure to ensure a steady crack growth rate of 10⁻⁹m/cycle to begin with. For precracking, a high cyclic load of 235N at 5Hz was applied and reduced by no more than 20% after 0.2mm of crack growth until the test loads were reached (70N for Cemex and 100N for Palacos cements). 5Hz was selected as it represents a loading cycle between walking (1Hz) and running (20Hz) and also allows for a faster testing time when compared to the standard walking load cycle (1Hz).

The crack length and number of cycles was measured during loading. The crack growth rate (da/dN) was then calculated from this data every 0.2mm. Similarly the corresponding stress intensity factor range (ΔK) for each sample and crack length (ranging from 6-12mm, in steps of 0.2mm) was calculated using Equation 2.8.

$$\Delta K = \frac{(P_{max} - P_{min})}{b\sqrt{W}} \times \frac{(2 + \alpha)}{(1 - \alpha)^{3/2}} (0.76 + 4.8\alpha - 11.58\alpha^2 + 11.43\alpha^3 - 4.08\alpha^4) \quad (2.8)$$

Where:

ΔK	is the stress intensity factor range in MPam ^{1/2}
P_{max}	is the maximum load in N
P_{min}	is the minimum load in N
Y	is the stress intensity factor function
b	is the sample thickness in m
α	is a/W and is greater than 0.2
a	is the crack length from centre point of the holes to the tip of the crack gage in m
W	is the width of the specimen from centre point of the holes to the bottom of the specimen in m

Two samples were tested to obtain an average plot of crack growth rate (da/dN) as a function of the stress intensity factor range (ΔK) on a logarithmic scale. A linear regression was used to fit the data and the Paris Law was then applied to give the constants 'A' and 'm' (as shown in Equation 2.9)²⁶². 'A' represents the intercept at the da/dN axis when $\Delta K=1$ and therefore is the crack growth rate at $1\text{MPam}^{1/2}$; and 'm' is the slope, which is a measure of the crack acceleration as it increases in length. Therefore a more fatigue resistant cement would have a reduction in both 'A' and 'm' material constants.

$$\frac{da}{dN} = A\Delta K^m \quad (2.9)$$

Where:

da/dn	is the crack growth rate (y-axis) in m/cycle
ΔK	is stress intensity factor range in $\text{MPam}^{1/2}$
A	is the y-intercept at $x=1$ ($\Delta K=1\text{MPam}^{1/2}$)
m	is slope of the linear regression

2.6 Vickers hardness tests

Disc shaped samples with a 10mm diameter, a 2mm height were prepared and the surfaces polished with a 4000 grit silicon carbide paper. Samples were then tested for hardness under the ISO6507-2 standard²⁶³ for Vickers hardness testing. Five small indentations, 1mm apart and from the edges of the sample, were put on both sides of each sample using a Zwick 3212 indenter (Zwick Testing Machines Ltd., Herefordshire, UK) fitted with a 136° square-based pyramid diamond indenter to obtain a mean hardness value. Indentations that occurred near to or on pores were disregarded and repeated. The load was set at 200g and was held for 10 seconds after initial contact with the sample. For each indentation a travelling microscope was used to measure the two diagonal lengths from which a mean value was obtained. Using Equation 2.10 the hardness values for each sample in Kg/mm^2 were calculated, where 'F' is the load in Kg (0.2), ' A_i ' is the area of the indentation and 'd' is the mean diagonal length of the indentation in mm.

$$\text{Hardness}(HV) = \frac{F}{A_i} = F / \frac{d^2}{2\sin(136^\circ/2)} \simeq 1.854 \frac{F}{d^2} \quad (2.10)$$

2.7 Glass transition temperature

A Rheometric Scientific V500 (TA Instruments Ltd., Elstree, UK) testing machine was used to determine the glass transition temperature of samples by dynamic mechanical analysis. Small matchstick like samples were used with a length of roughly 30mm, width of 2-3mm and a height of 1-2mm. Samples were loaded sinusoidally at a frequency of 1Hz in a dual cantilever configuration as the sample was heated from 35°C to 200°C at a rate of 10°C/min. The applied stress and strain was measured as shown in Figure 2.3.

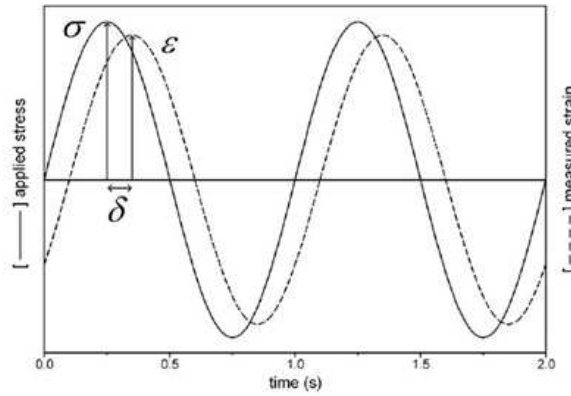


Figure 2.3: Stress (σ) and strain (ϵ) during a dynamic mechanical analysis

The phase lag (δ) between the stress and strain was measured and the storage modulus (E') and loss modulus (E'') was calculated using Equations 2.11 and 2.12 respectively.

$$E' = \frac{\sigma}{\epsilon} \cos\delta \quad (2.11)$$

$$E'' = \frac{\sigma}{\epsilon} \sin\delta \quad (2.12)$$

From this the complex viscosity in the form of $\tan\delta$ was calculated as shown in Equation 2.13. For perfectly elastic materials, $\tan\delta=0$ and for perfectly viscous materials $\tan\delta=\infty$. $\tan\delta$ was therefore plotted against temperature and the temperature at which $\tan\delta$ was at its maximum was considered to be the glass transition temperature. Five samples were tested to obtain a mean value for glass transition temperatures.

$$\tan\delta = \frac{E'}{E''} \quad (2.13)$$

2.8 Scanning electron microscopy

Throughout the course of this study, scanning electron microscopy (SEM) was employed to study surfaces of samples to assess fractures and porosity. Prior to imaging with an EBT1 Scanning Electron Microscope (SEM Tech Ltd, Southampton, UK) at 15KeV, the samples were gold coated using an E65x sputter coater (Emitech, Kent, UK).

2.9 Statistical analysis

An analysis of variance (ANOVA) was carried out to establish significant differences between groups of samples using the data analysis package in Excel (Microsoft, Reading, UK). Significance between groups was defined as those with a calculated p-value of less than 0.05.

Chapter 3

Mechanical properties of commercial cements and the development of a standardised model of cement

3.1 Introduction

In order to improve current bone cement performance, novel materials must be tested in a standardised formulation. Commercial cements come premixed as separate powder and liquid components (as discussed in Chapter 1), modifying the composition of a commercial cement is thus very difficult. Commercial cements also vary in formulation and as a result, propriety products have many different properties, making unpredictable the effect of compositional change.

The approach undertaken was to develop a simple model cement with a similar composition and similar properties to commercial cements. By doing so, it was possible to change individual components of the model cement to investigate the effect of those changes.

Static mechanical tests, as outlined by the ISO5833 standard for acrylic-based cements, falls short in predicting clinical success. Therefore, research studies have introduced alternative tests in an attempt to create more accurate predictability for clinical application. This chapter establishes a series of tests, mechanical and physical, by which formulation

performance can be analysed. By studying the formulations of several commercial cements (Table 1.1) and using average quantities for each ingredient, a basic model cement was developed and tested. Two different commercially available cements were also tested and the results defined a target performance range that the model cement would have to achieve. The failure mechanisms of the commercial cements tested were also investigated to provide an insight into potential areas that could be improved. The properties of the commercial cements obtained in this chapter were used in subsequent chapters for comparison with novel formulations.

3.1.1 Failure modes and toughening in polymers

When a polymer is subjected to high stresses, crack growth may be initiated by the fracture of covalent bonds or the breaking of weaker van der Waal forces. It has been suggested that the polymer fracture process can be simplified into 3 steps²⁶⁴:

1. The excitation of bonds under the action of an applied stress
2. The scission of the excited, over-stressed bonds by thermal fluctuations
3. The formation of small microcracks in crazes which coalesce to form larger cracks

Furthermore propagation of cracks can be classified into three different modes as shown in Figure 3.1. Mode I represents crack growth due to tensile stresses perpendicular to the plane of the crack; mode II represents a sliding mode due to in-plane shear and mode III represents a tearing mode caused by out-of-plane shear. Crack propagation may occur as a result of a combination of these three modes.

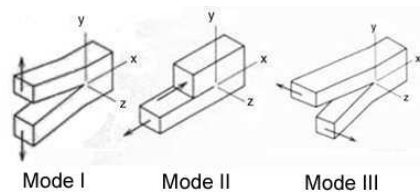


Figure 3.1: Crack propagation modes²⁶⁵

During these fracture processes, there is a degree of shear yielding which consists of a change in shape without a significant change in volume. This viscoelastic and plastic energy dissipating process is localised and usually occurs in the vicinity of the crack tip. In order to prevent crack propagation it is essential to incorporate energy absorbing mechanisms from many sites rather than a few, which increases the overall volume of the polymer and blunts the crack. Crazeing, shear deformation and crack pinning are forms of energy absorbing mechanisms which naturally occur in polymers under load. When such mechanisms are not present, brittle fracture tends to occur. To promote these mechanisms throughout the bulk of the material and to improve the mechanical properties of the polymer, additional particles can be incorporated. This second phase can be rubber particles, which is known as rubber toughening or rigid-particle fillers with a higher stiffness than the polymer.

Crazeing

Crazes are a network of small, fine cracks which are initiated when an applied tensile stress causes microvoids to nucleate at points of high stress concentrations created by scratches, flaws or molecular heterogeneities. This usually occurs ahead of the crack tip and creates fibrils of plastically deformed, oriented polymeric material spanning the craze (Figure 3.2(a)). Crazeing is a cavitation process and unlike shear yielding, it occurs with an increase in volume.

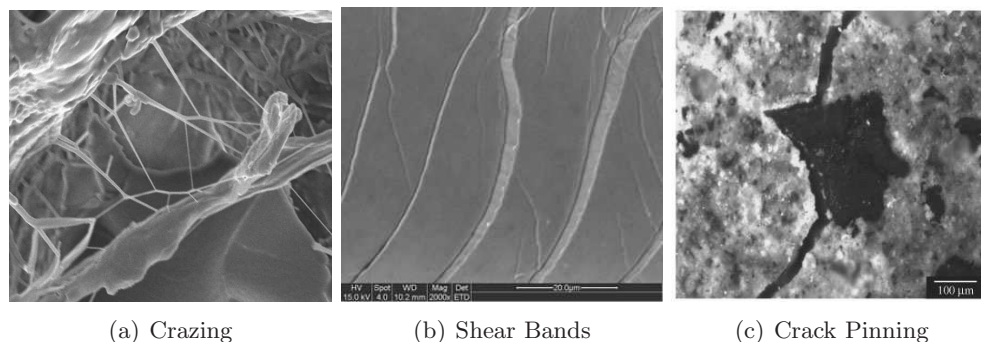


Figure 3.2: Crack blunting mechanisms in polymers^{266–268}

Although considerable plastic deformation and local energy adsorption are involved in craze initiation, growth and breakdown, this is highly localised to a small volume. If stable crazes can be initiated in a larger volume, it may lead to a tough and ductile material response.

Using transmission electron microscopy (TEM) on high-impact polystyrene, it has been proven that craze growth occurs by meniscus instability^{269,270}. In this mechanism, yielded polymer particles at the concave air/polymer interface break off and produce new craze matter (Figure 3.3). As crazes grow and coalesce, they gradually break down into a crack. If the applied stress is parallel to the orientation of the craze however, then crack initiation can be inhibited and will only occur at much higher stress levels²⁶⁴.

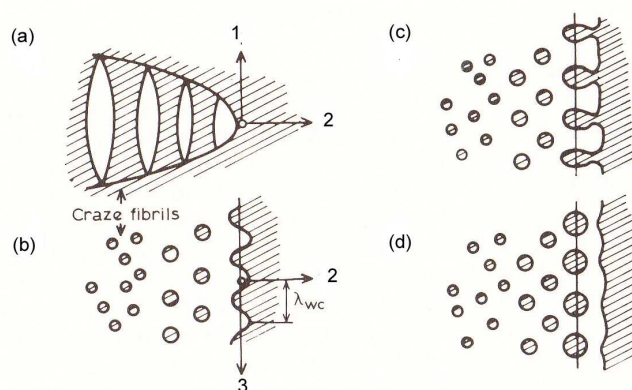


Figure 3.3: Craze formation. (a) Side view of the craze tip; (b)-(d) sections through the midline of the craze showing the craze advance by meniscus instability²⁷⁰

Shear deformation

Shear deformation consists of a change in shape without a significant change in volume. It is important because it is the factor that limits the strength of the polymer if brittle fracture is suppressed. Shear yielding in the form of micro-shear bands also plays a key role in crack initiation and even brittle crack propagation in polymers usually involves localised viscoelastic and plastic energy dissipation in the crack tip vicinity.

Large plastic shear deformations result in the formation of shear bands (Figure 3.2(b)), a lens-like region, roughly 45° to the applied force. When both crazes and shear bands are present in a polymer, one of the following may take place:

1. The shear band may terminate the craze when grown into the craze tip.
2. When a growing craze meets a pre-existing shear band, no termination takes place, rather crack nucleation begins.

If upon crack extension only highly localised shear deformations occur around the crack tip, then the material will generally exhibit a brittle fracture at a low stress intensity since plastic deformation is confined to a small volume of polymer²⁶⁴.

Crack pinning

The inclusion of particles into a polymer matrix allows for crack pinning to occur. This is when a crack grows from particle to particle, bowing between each one as shown in Figure 3.2(c). This bowing shape results in a new fracture being formed and a longer distance for the crack to grow. This in turn results in more energy dissipated at the crack tip and thus retardation of the crack. For this mechanism to work effectively, the particles must be spaced an optimum distance apart²⁶⁴.

Crack branching and deviation

The formation of microcracks ahead of the crack tip also plays a role in the toughening of materials. Microcracks located in the vicinity of the crack tip may cause the main crack to change direction or branch out into smaller cracks in order to coalesce with the microcrack. This deviation or branching of the main crack requires a greater amount of energy to propagate the crack and reduces the stress intensity at the main crack tip. Microcrack formation also requires the utilisation of energy and the creation of multiple microcracks requires a substantial increase in the amount of work required for the crack to advance.

3.1.2 Fracture mechanics theory

It has long been understood that the theoretical strength of a material is much greater than the apparent strength due to the presence of flaws in the microstructure of the material. Fracture mechanics is a method that can account for such flaws and can be used to investigate how cracks will propagate through a material. Analysis of stresses at the crack tip can be used to predict the potential for crack growth and therefore failure⁶⁰. Using conservation of energy arguments and the crack tip stress analysis developed by Inglis²⁷¹, Griffith²⁷² developed an equation in the 1920's to derive the tensile strength of a brittle material with crack-like flaws (Equation 3.1), where the stress to fracture is dependant upon the length of the crack and the surface energy as the crack propagates through the material. σ_f is the stress to fracture, a is the length of the crack, γ_s is the surface energy and E is the Young's modulus. The underlying assumptions in this equation are that all the energy required to generate a new crack surface is accounted for by the surface energy and that fracture occurs when the rate of energy supplied to the body exceeds that dissipated through crack advance.

$$\sigma_f = \frac{2}{\pi} \left(\sqrt{\frac{E}{\gamma_s a}} \right) \quad (3.1)$$

Griffith discovered that a high stress concentration is necessary for crack propagation to occur, however energy is also required to break intermolecular bonds within the material to generate cracks²⁷². Such energy was found to come from stored strain energy in the material around the crack^{60,262}. This equation was further developed to take into account the irreversible effects of plastic flow at the crack tip and resulted in a single property called work of fracture (energy required per unit area of a new crack) which takes into account all the forces involved in crack growth. This value is then compared to the rate at which strain energy is released (G) and if the work of fracture is less than G , then the crack will propagate.

Another approach carried out by Irwin et al.²⁷⁴ studied the stress intensity just beyond the crack tip as theoretically the stress at the tip itself is infinite. These stresses were investigated using polar coordinates, which led to a simple relationship whereby all stresses beyond the crack tip were found to be proportional to the term $\sigma\sqrt{\pi a}$. This led to the stress intensity (K) being defined as Equation 3.2, whereby if the critical value of K (fracture toughness) is reached, the crack will propagate. A shape correction factor (Y) can be added to this equation to account for different loading methods, geometries and proximity to external boundaries^{60,262}. This equation is the basis for those described in Sections 2.4 and 2.5.

$$K = Y\sigma\sqrt{\pi a} \quad (3.2)$$

When this theory is applied to crack growth tests as described in Section 2.5, it is possible to obtain an accurate measure of the fatigue endurance of a material. The characteristic shape of the results obtained is shown in Figure 3.4 where: region I represents crack initia-

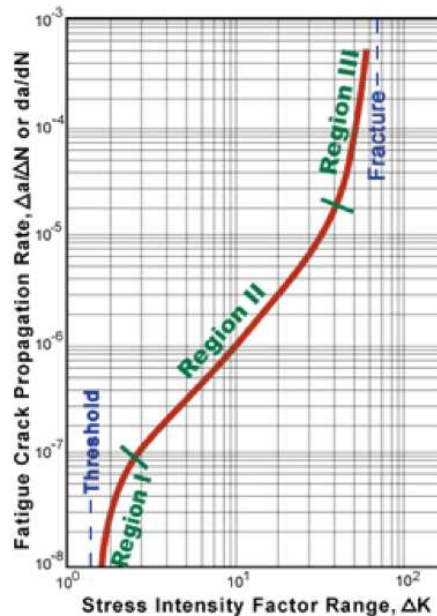


Figure 3.4: Characteristic crack propagation results, reproduced from Motarjemi et al.²⁷³

tion after the critical stress intensity factor threshold is reached; region II represents stable crack propagation and region III represents unstable crack growth followed by fracture²⁷³. As previously described, the Paris Law can be applied to region II in order to describe a material's crack propagation properties.

3.2 Methods

3.2.1 Materials

Cemex Isoplastic was obtained from Tecres (Sommacampagna, Italy) and Palacos R was provided by Heraeus (Newbury, UK). Methyl methacrylate with 75ppm hydroquinone, N-N dimethyl-p-toluidine and benzoyl peroxide were purchased from Sigma Aldrich (Gillingham, UK); polymethyl methacrylate powder with a methylacrylate copolymer (Colacryl TS1713) was provided by Lucite International UK (Southampton, UK); and barium sulphate was obtained from Fisher Scientific UK (Leicestershire, UK). The composition of the commercial cements are shown in Table 3.1 along with the formulation for the model cement. This formulation was developed by averaging compositional values from a wide range of different cement brands as shown in Table 1.1.

Table 3.1: Composition of the model cement and the commercial cements used

	Cemex Isoplastic	Palacos R	Model Cement
Liquid component / g	13.30	18.78	16.93
Methyl Methacrylate / %w/w	99.10	97.98	98.50
N-N Dimethyl-p-Toluidine / %w/w	0.90	2.02	1.50
Hydroquinone / ppm	75.00	60.00	75.00
Powder Component / g	40.00	40.00	40.00
Polymethyl Methacrylate / %w/w	84.30	84.50	88.30
Barium Sulphate / %w/w	13.00	-	10.00
Benzoyl Peroxide / %w/w	2.70	0.50	1.70
Zirconia / %w/w	-	15.00	-
Powder : Liquid ratio	3.01	2.13	2.36

3.2.2 Mechanical testing

Compression and bending samples were prepared and tested according to Sections 2.1, 2.3.1 and 2.3.2.

3.2.3 Setting properties

The setting temperature and time was measured as detailed in Section 2.2. This ensured the model bone cement tested was not significantly different from commercially available cements.

3.2.4 Fracture toughness

The fracture toughness of each cement was tested as specified in Section 2.4.

3.2.5 Fatigue testing

Fatigue tests were carried out as described in Section 2.5 under load control to determine any differences in fatigue properties between commercial cements and the model cement.

3.2.6 SEM images

SEM images of the fracture surfaces of fatigue samples were assessed as described in Section 2.8 and the morphology of Palacos R and Cemex powders were also observed.

3.3 Results

3.3.1 Setting properties

Figure 3.5 and Table 3.2 show the setting profiles and setting properties respectively for Palacos R, Cemex and the model cement. Cemex Isoplastic took the longest time to set and had the lowest maximum setting temperature whilst Palacos R set the quickest and had the highest maximum setting temperature. The model cement was found to set in a time between that of Palacos R and Cemex and also with an intermediate maximum setting temperature.

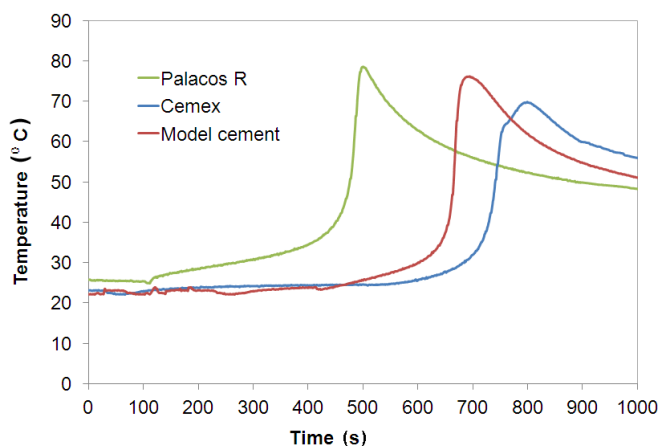


Figure 3.5: Setting profiles of commercial bone cements and the model cement

Table 3.2: Setting properties of commercial bone cements and the model cement

	Setting time (t_{set}) / s	Setting temperature (T_{set}) / ° C	Maximum temperature (T_{max}) / ° C
Cemex	738	46.5	69.8
Palacos R	479	52.1	78.5
Model cement	665	49.2	76.2

3.3.2 Mechanical properties

Table 3.3 shows the compressive strength, bending modulus and bending strength of Palacos R, Cemex and the model cement. Palacos R had significantly higher compressive strength (ANOVA - $p < 0.05$, $p = 4.99 \times 10^{-05}$), bending modulus ($p = 0.02$) and bending strength ($p = 1.48 \times 10^{-03}$) when compared to Cemex.

In terms of compressive strength there were significant differences between all three cements ($p = 8.59 \times 10^{-06}$), however the model cement had a compressive strength halfway between that of Palacos R and Cemex.

The bending modulus of the model cement was higher than both the commercial cements. There was no significant difference between the model cement and Palacos R ($p = 0.11$), however the difference with Cemex was found to be significant ($p = 0.01$).

In terms of bending strength, the model cement was found to be halfway between Palacos R and Cemex. There was no significant difference in bending strength between the model cement and Cemex ($p = 0.14$) but Palacos R had a significantly higher bending strength than the model cement ($p = 0.01$). Overall with the exception of bending modulus, the model cement formulation has demonstrated ideal mechanical properties, between what is considered a “good” cement and a “poor” cement in terms of mechanical properties.

Table 3.3: Mechanical properties and fracture toughness of commercial and model cements

	Compressive strength (σ_c) / MPa	Bending modulus (E_b) / MPa	Bending strength (B) / MPa	Fracture toughness (K_{IC}) / MPam ^{1/2}
Palacos R	104.6±2.6	3410±123	69.7±7.7	2.5±0.2
Cemex	85.2±4.2	3080±205	46.0±6.5	1.16±0.1
Model cement	95.5±2.67	3730±319	53.7±6.9	1.5±0.2

3.3.3 Fracture toughness

Table 3.3 shows the results of the fracture toughness tests. Similar to the results of the mechanical properties, Palacos R had significantly enhanced fracture toughness with a higher critical stress intensity factor value than Cemex ($p=5.81 \times 10^{-07}$). All three cements were found to be significantly different ($p=2.54 \times 10^{-07}$) but the model cement had a critical stress intensity factor value between that of Palacos R and Cemex.

3.3.4 Fatigue

Using the Paris Law on the crack propagation data, two constants were obtained, constant 'A' (crack growth at $\Delta K=1\text{MPam}^{1/2}$) and constant 'm' (crack growth rate as stress intensity increases), as shown in Table 3.4. Palacos R demonstrated the best crack growth resistance at $\Delta K=1\text{MPam}^{1/2}$. The model cement was found to have a value for constant 'A' between that of Palacos R and Cemex. For constant 'm' the model cement had a lower value than the commercial cements, signifying less change in crack growth rate with increased stress intensity. An 'm' value of 1 would mean crack growth rates for all stress intensities are the same. From this data it is clear that Cemex also performs poorly in fatigue.

Table 3.4: Fatigue constants of commercial and model cements

	A	m
Palacos R	3.73×10^{-07}	4.65
Cemex	5.39×10^{-07}	5.92
Model cement	4.83×10^{-07}	3.73

Figure 3.6 shows the crack growth rates obtained for varying stress intensities for the commercial and model cements. All three cements obtained similar crack growth rates through the stress intensities tested. At lower crack growth rates the model cement performed poorly in comparison to Cemex and Palacos R, however the slope of the model

cement data is less steep, demonstrating less change in crack growth rate throughout the range of stress intensities tested.

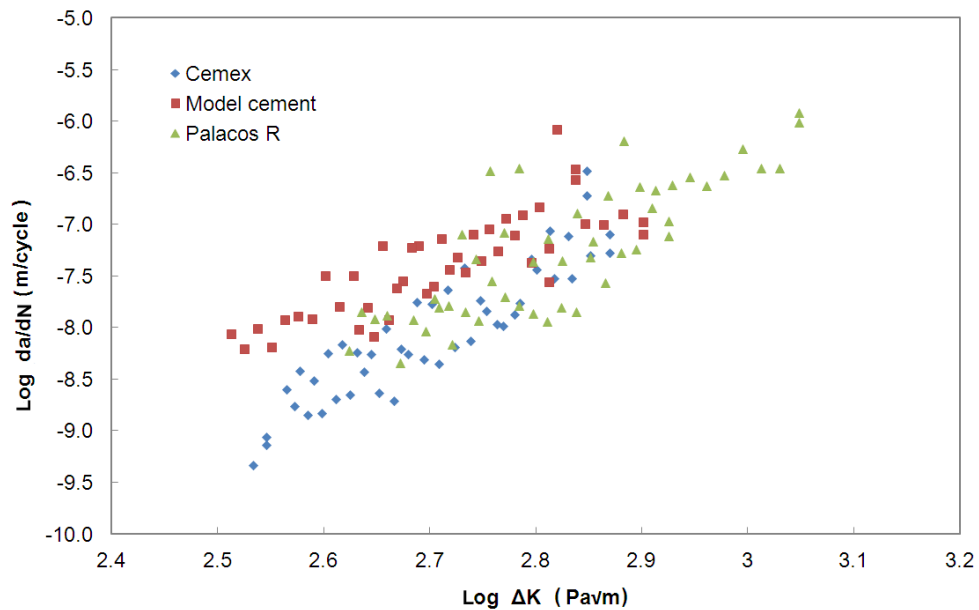


Figure 3.6: Crack propagation of commercial bone cements and the model cement

3.3.5 SEM images

Figure 3.7 shows scanning electron microscopy images of the fatigue fracture surfaces of Palacos R, Cemex and the model cement. Palacos R and Cemex bone cement fracture surfaces were found to have significantly more pores (which appear as dark circles) than the model cement. PMMA beads were not visible in the fracture surfaces of Palacos R, whilst in the Cemex and the model bone cement, PMMA beads were observed as light grey circles in the SEM images. Closer inspection of the fracture surfaces revealed that Palacos R and the model cement had a greater amount of small cracks whilst Cemex appeared to have fewer but larger cracks. The fracture surface of Palacos R also shows shear deformation as a large shear band is visible on the fracture surface. As previously described this shear band appears to have terminated several crazes, acting as a toughening mechanism.

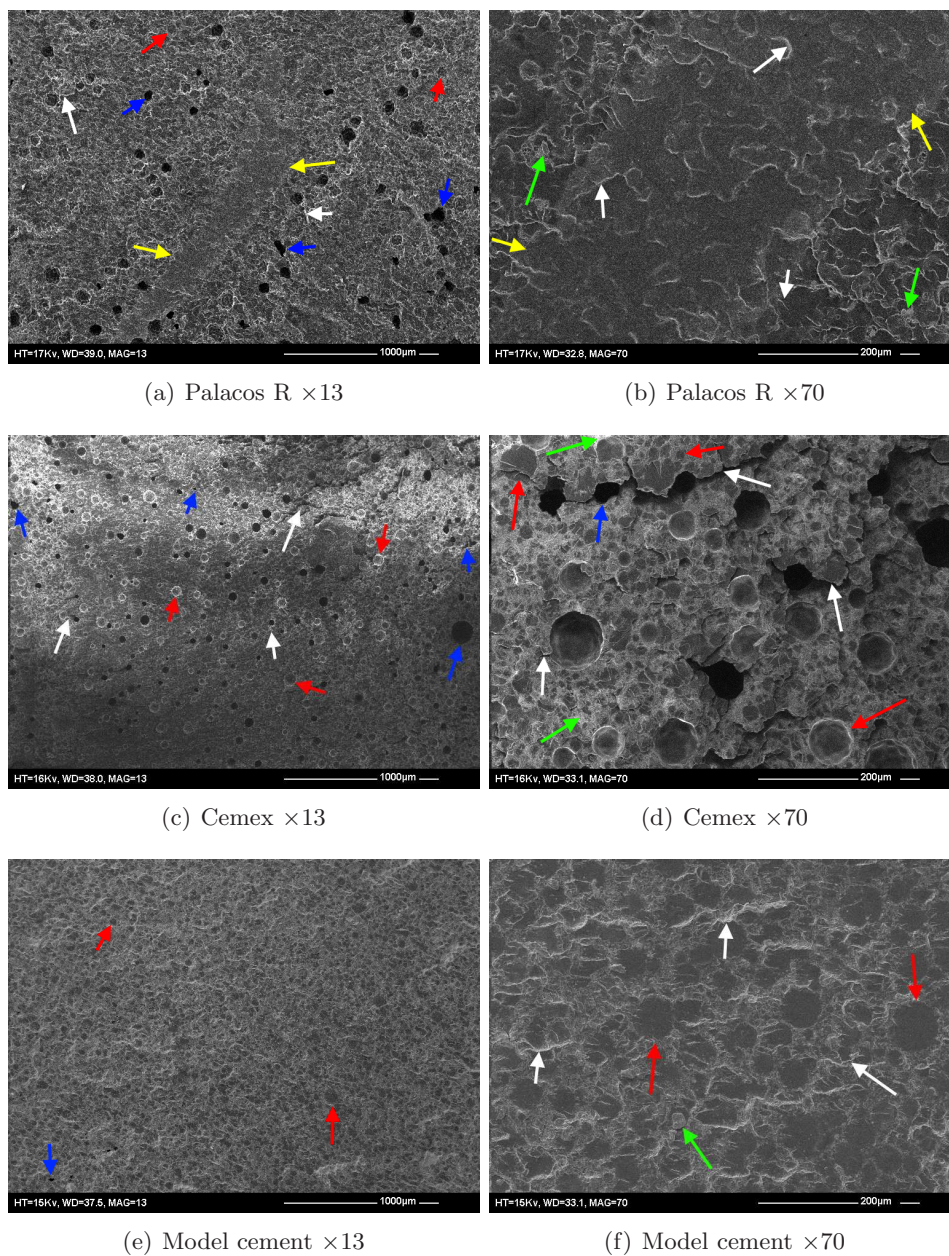


Figure 3.7: SEM images of the fracture surfaces of fatigue samples for (a-b) Palacos R, (c-d) Cemex and (e-f) the model cement - Red arrows indicate the location of PMMA beads, green arrows indicate radiopacifier particles, blue arrows indicate pores and voids, yellow arrows indicate the edges of shear bands and white arrows indicate microcracks

The morphology of the powders differed, as shown in Figure 3.8, whereby Palacos beads were clearly separated whilst Cemex beads are fused together. Both cements however had similar PMMA bead sizes ($\approx 50\mu\text{m}$) and were found to have accumulated radiopacifier particles on the surface of the PMMA beads.

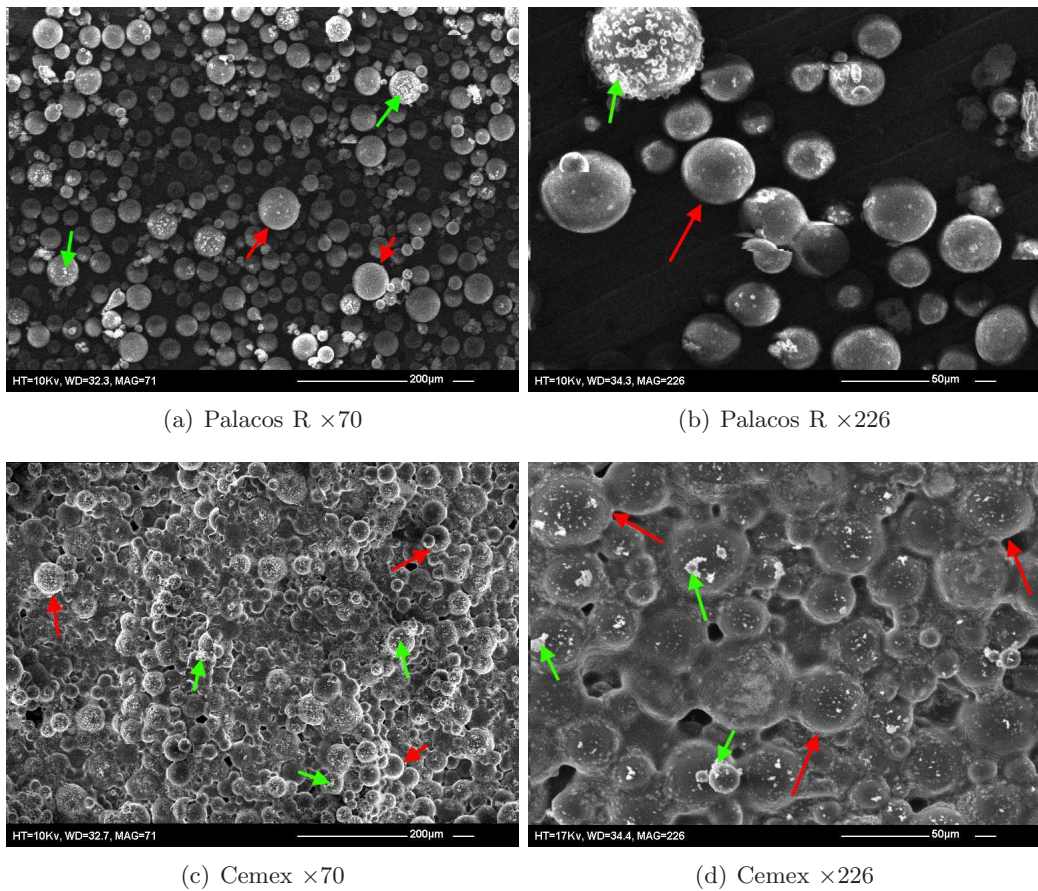


Figure 3.8: SEM images of the powder morphologies of (a-b) Palacos R and (c-d) Cemex - Red arrows indicate PMMA beads and green arrows indicate radiopacifier particles

3.4 Discussion

Studying the effects that a change in formulation or the addition of a novel material will have on the properties of PMMA bone cement is of great interest and essential for developing better cement formulations. Numerous studies have attempted to test novel materials

in bone cements but few obtain results that can be compared with commercial cements or truly test the effects of the novel material. For example Lewis et al.¹⁷² tested the use of iodine-containing copolymers and compared it with conventional BaSO₄ cement. The BaSO₄ containing cement was very similar in composition to the cement used in this study and to other commercial cements, however it used butylmethacrylate (BMA) in the liquid component, which is not generally employed in commercial cements. Furthermore the iodine based cement had lower levels of PMMA, BPO and higher levels of MMA, butylmethacrylate (BMA) and DMPT when compared to the BaSO₄ cement employed. Therefore improvements or changes to the properties of the iodine-based cement in comparison to the BaSO₄ cement may be as a result of the different levels of polymer, initiator or activator used and not as a direct result of the iodine radiopacifier. Gillani et al.¹⁸¹ used a liquid MMA to powder PMMA ratio of 5:1 (10g of MMA to 2g of PMMA) with 1g of radiopacifier particles and the catalyst 1,1-Azobis(cyclo-hexanecarbonitrile) (0.05% by mass of MMA) which was mixed in a 70°C water bath. This composition bears no resemblance to commercial PMMA bone cements and the catalyst and the method of mixing is not relevant to orthopaedic cements. Many other studies employ diverse compositions or do not specify the cement compositions used^{82,188,275}. Another study using strontia (SrO) in Simplex P, prepared cements with an identical composition to Simplex P and only altered the amount of SrO and BaSO₄¹⁷⁶. This study proved to be more effective in identifying key changes as a result of replacing BaSO₄ with SrO, however the study was limited to the Simplex P formulations only and although carefully and thoughtfully prepared, the homogeneity of the mixtures obtained cannot be compared to industrial preparations due to the mixing/sterilization techniques employed. The work presented in this chapter attempted to create a model cement with similar properties to two PMMA bone cements currently used in orthopaedics. The model cement is intended to allow for novel materials to be tested in an unbiased way, whilst still providing results which may be compared to commercial cements.

The formulation of the model cement was selected as it incorporated characteristics of many different commercial cements. For example, a poly(methyl methacrylate/methyl acrylate) copolymer was used for the model cement as is employed in Palacos R. Similarly a powder to liquid ratio between that of Palacos R and Cemex was used. BaSO₄ was used as the radiopacifier instead of ZrO₂ as the majority of commercial cements use BaSO₄. Combining these specific attributes has resulted in a model cement with average properties between what can be considered a mechanically “good” cement and a “poor” cement.

Palacos R was found to have a shorter setting time than Cemex in this study. This does not correspond with the datum from the manufacturers which shows Palacos R to have a longer setting time. This may be attributed to the methods employed by the manufacturers to determine setting times. As claimed by Tecres, the setting temperature of Cemex was much lower than Palacos R, due to the lower quantity of MMA employed.

The results for the mechanical properties obtained for Cemex and Palacos R correlate well with results from previous literature^{74,222}. There was a positive correlation between $\log \Delta K$ and $\log da/dN$ for all fatigue results and the shape of the curves agrees with other studies^{58,82}. As demonstrated in the results, the copolymer used in Palacos R enhanced bending and fatigue properties when compared to Cemex bone cement. As discussed in Chapter 1 copolymers prevent brittle fracture and make the cement less susceptible to stress raisers. This is clear in the model cement and Palacos R where many small cracks or crazes were observed as opposed to Cemex where a few large cracks were seen, particularly around pores. The positive effect of copolymers is further highlighted by the fact that both the model cement and Palacos R had better fatigue properties than Cemex. This is as a result of crazing mechanisms in the bulk of the cement, encouraged by the copolymer, which caused crack propagation to occur only at the higher levels of stress. Shear bands were also visible on the fracture surface of Palacos R, demonstrat-

ing a further toughening mechanism. The lack of copolymer in Cemex may have created stress concentrations around the pores, resulting in crack initiation and weakening of the cement. The pores however, may have also caused crack pinning, blunting the crack tip and retarding crack growth. Although the effect of these pores is not well understood and there is a clear difference in porosity between the commercial and model cements, studies have shown that small sub-millimeter spherical pores as seen in the images, do not affect the fatigue behaviour of sharp notched specimens³⁴ and are of limited significance compared to other stress concentrations such as agglomerations of radiopacifier particles⁶⁰.

Although the use of a copolymer appears to enhance the mechanical and fatigue performance of the model cement and Palacos R, the use of BaSO₄ as a radiopacifier in the model cement seems to be a limiting factor on its performance. The use of BaSO₄ coupled with the same copolymer and a similar powder to liquid ratio as Palacos R did not yield results comparable to Palacos R. Furthermore the use of copolymers can be detrimental to the compressive strength of the cement, however Palacos R still achieved the highest compressive strength. Therefore it can be speculated that the radiopacifier has a critical effect on the properties of the cement and may be key to improving the cement. Several other authors have reached similar conclusions^{82,83,91,92,95}.

Another key parameter is the amount of MMA used. Palacos R had the greatest MMA content and as a result had the highest setting temperature and shortest curing time. Furthermore PMMA beads were not visible on the fracture surfaces of Palacos R whilst they were clearly present in the model cement and Cemex fracture surfaces. It can be speculated that the slightly higher amount of MMA used in Palacos R may lead to higher levels of dissolution of PMMA beads in MMA during mixing and curing. As Cemex and the model cement had less MMA, the PMMA beads were more visible. The presence of BaSO₄ around the PMMA may have also contributed to the enhanced visibility of the

PMMA beads on the SEM images of the fracture surfaces. Although the size of the PMMA beads were similar for both commercial cements, the morphology differed. This however, did not affect the propagation of the crack as the fracture was found to grow through the PMMA beads for both cements.

Overall the properties and characteristics of commercial cements have been investigated and can be used for reference in future chapters and studies. Similarly a model cement has been developed, which will allow for the effect of novel additives to be investigated.

3.5 Conclusions

A model cement with similar properties to both Palacos R and Cemex bone cement has been successfully developed. Although not all properties were found to fall between the values of the two commercial cements (bending modulus and 'm' constant for fatigue), the majority of properties achieved the required criteria. Furthermore, fatigue fracture surfaces demonstrated the model cement to have attributes from both Palacos R and Cemex. Therefore, the model cement is thought to represent effectively a wide range of properties found in most commercial cements.

Several examples of toughening mechanisms were also observed on the fracture surfaces of the commercial cements, proving such mechanisms are beneficial to the performance of the cement. Having established that the radiopacifiers used can limit the performance of a cement composition, it is now possible to use alternative radiopacifiers in the model cement in an attempt to improve bone cement performance.

Chapter 4

Development of novel radiopacifiers

4.1 Introduction

Radiopacifiers such as barium sulphate (BaSO_4) and zirconium dioxide (ZrO_2) are incorporated into bone cements to permit the inspection of cement integrity non-invasively. It is disputed whether such materials could have a detrimental effect on the performance of the cement^{60,66,82,83,88,91,92,95}. Titanium dioxide (TiO_2) has the potential for use as a radiopacifier because of its biocompatibility, capacity to attenuate X-rays as a solid metal, and its ability to encourage bone growth²⁷⁶. The anatase form of TiO_2 is of particular interest as several studies have shown it to be highly beneficial to bone growth and osseointegration^{277–279}. Yttria-stabilised ZrO_2 , which has a transformation toughening mechanism, and is used in ceramics, may also be a suitable radiopacifier. Following on from the development of a model cement in Chapter 3, both can now be tested as alternative radiopacifiers and this is considered in this chapter.

4.1.1 Radiopacifiers as functional fillers

The primary function of a radiopacifier in bone cement is to attenuate X-rays and allow for the non-invasive inspection of the cement. The presence of these materials may also enhance the stiffness and strength of the cement and therefore are thought to have a secondary function. Authors have reported a moderate increase in toughness when using rigid-particles in polymers^{83,173}. Since rigid particles do not deform under stress it is initially difficult to understand how rigid particles can contribute to an increase in tough-

ness. It is hypothesised however, that the presence of rigid particles induces a toughening mechanism in the polymer matrix. As described in Chapter 3, crack branching and crack deviation also toughens materials and a dispersion of rigid particles can potentially induce this behaviour. Bartzak et al.²⁸⁰ demonstrated that when the distance between rigid particles is lower than a critical value, polymer crystallites orient preferentially on the surface of those rigid particles, leading to higher levels of toughness. As the rigid particles do not cavitate, debonding from the polymer matrix occurs. Debonding and stretching of the polymer matrix requires high levels of energy which also makes the material tougher. The degree of toughness is governed mainly by the adhesion between the rigid particle and the polymer matrix and also the dispersion of the particles as agglomerations have been known to act as points of high stress concentration.

4.1.2 Barium sulphate

Barium sulphate (BaSO_4) is a radiopacifier commonly used in bone cements due to its ability to effectively attenuate X-rays. BaSO_4 is an insoluble salt used clinically as an orally administered radiocontrast agent. Although barium itself is a toxic heavy metal, the insolubility of BaSO_4 prevents harmful amounts of the metal being absorbed and allows for easy removal from the body. This makes BaSO_4 non-toxic and biocompatible for use in bone cement. Nevertheless, BaSO_4 has been known to weaken bone cement, particularly when agglomerated, as it may act in a similar way to a pore due to its low mechanical strength and therefore present as a site for potential crack initiation⁹⁴.

4.1.3 Zirconium dioxide

Zirconium dioxide (ZrO_2 , otherwise known as zirconia or zirconium oxide) is a material commonly used in ceramics and polymers as a rigid-particle filler to help strengthen and improve material properties. This arises from its high strength and toughness, chemical and wear resistance, and the structural transformations ZrO_2 undergoes during heating.

When heated from room temperature to 950°C , ZrO_2 adopts a monoclinic crystal structure (Figure 4.1(a)). Above 950°C it converts to tetragonal (Figure 4.1(b)) and later cubic (Figure 4.1(c)), which is accompanied by a 1-4% volume reduction. Usually when cooled, it returns to a monoclinic structure, however the addition of oxides (magnesium oxide (MgO), yttrium oxide (Y_2O_3), calcium oxide (CaO) or cerium oxide (Ce_2O_3)) results in a stable tetragonal state at room temperature. Each tetragonal ZrO_2 precipitate is under stress and full of strain energy. When a crack tip approaches the ZrO_2 particle, it expands and transforms back into the monoclinic phase, releasing energy and applying compression to the crack tip. This mechanism is known as transformation toughening and triggers a uniform distribution of low level internal strain within the bulk of the material. ZrO_2 is currently used in certain commercial bone cements, however the use of yttria-stabilised ZrO_2 as a radiopacifier has yet to be evaluated.

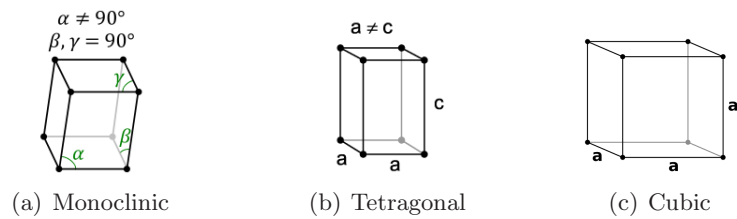


Figure 4.1: Crystal structures of ZrO_2

4.1.4 Titanium dioxide

Titanium dioxide (TiO_2 , otherwise known as titania or titanium(IV) oxide) is a naturally occurring oxide of titanium also used as a rigid-particle filler for its high refractive index, electrical properties and mechanical properties. It is used in medical implants due to its biocompatibility and ability to interact with bone. TiO_2 is an inexpensive, non-toxic, thermally-stable and photostable material. The surface of TiO_2 itself is hydrophilic due to the presence of a charged oxide layer which makes it suitable for surface treatments. When used in polymers, changes to the material properties are dependent upon the composition, size and concentration of the TiO_2 particles.

4.1.5 X-ray imaging

Incorporating radiopacifiers into bone cements allows X-ray imaging techniques to be carried out to assess potential problems *in vivo* in a minimally invasive manner. Radiopacifiers attenuate and absorb X-rays which produces an image according to the level of absorption and attenuation that takes place. The ability of a radiopacifier to attenuate and absorb X-rays is governed by its atomic number and density, which in turn affects what are known as its mass attenuation coefficient and mass energy absorption coefficient²⁸¹. The mass attenuation coefficient is a measure of the total loss of X-ray intensity due to both scattering and absorption, whereas the mass energy absorption coefficient is a measure of loss of X-ray intensity caused by absorption only. Therefore using the mass attenuation coefficient is more useful when studying the radiopacity of a material. Both coefficients however are dependent upon the energy levels employed by the imaging equipment. This is shown in Figures 4.2 and 4.3 for PMMA, barium, titanium and zirconium. Beyond energy levels of around 15keV PMMA is no longer capable of attenuating or absorbing X-rays, highlighting the need for a radiopacifier.

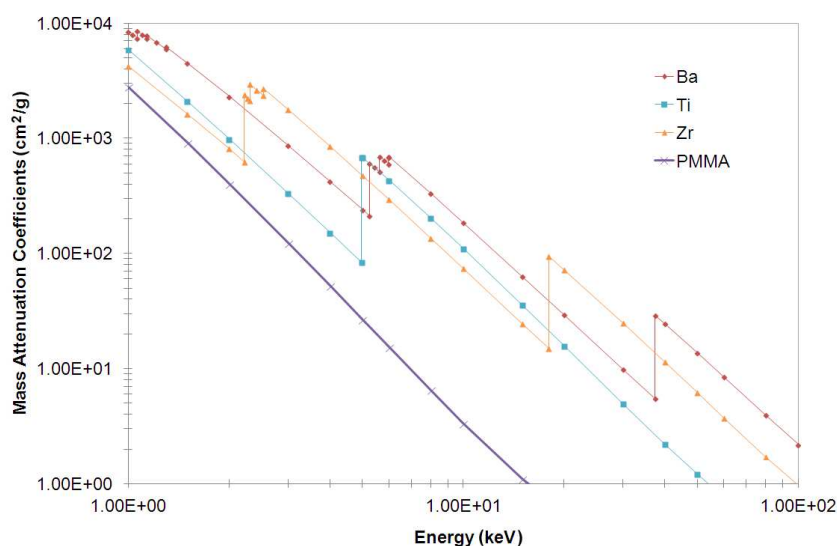


Figure 4.2: Attenuation spectra for Barium, Titanium, Zirconium and PMMA

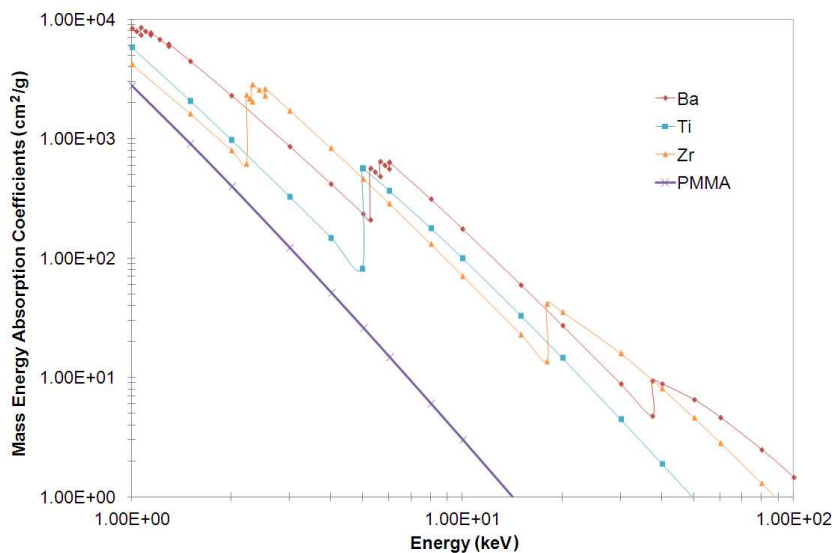


Figure 4.3: Absorption spectra for Barium, Titanium, Zirconium and PMMA

X-rays performed clinically employ an energy level of 70keV, 63mAs to minimise the radiation dose given to a patient. Figure 4.2 can be used to deduce the mass attenuation coefficient (μ_m) of a material at 70keV. For example, barium at 70keV has a mass attenuation coefficient (μ_m) of approximately $10\text{cm}^2/\text{g}$. This value multiplied by the density of the material (ρ) provides the linear attenuation coefficient (μ_l). The negative exponential function of the product of the linear attenuation coefficient (μ_l) and the thickness of the sample (e) will provide a ratio of the X-ray intensity that will pass through the material (I) from the original X-ray intensity transmitted (I_o) as demonstrated in Equation 4.1. It is therefore possible to theoretically deduce the intensity of X-rays that are transmitted through certain materials. This provides a measure of how effectively a material attenuates and absorbs X-rays²⁸².

$$\frac{I}{I_o} = \exp(-\mu_l e), \quad \mu_l = (\mu_m)\rho \quad (4.1)$$

Table 4.1 shows the calculated I values for barium, titanium, zirconium and PMMA at two different X-ray intensity settings. At a clinical setting (70keV) barium ($I=1.3 \times 10^{-6}$) will provide the best contrast and radiopacity followed by zirconium ($I=36.4 \times 10^{-6}$), titanium ($I=7.9$) and PMMA ($I=60.7$), which only attenuates around 20% of the transmitted X-ray. At 35keV however, a setting which is employed for research and analytical purposes, zirconium ($I=2.0 \times 10^{-50}$) would perform best followed by barium ($I=9.2 \times 10^{-10}$), titanium ($I=3.3 \times 10^{-6}$) and PMMA ($I=25.5$). This is a theoretical approximation which assumes unit thickness for the material and only considers elemental materials as opposed to compounds.

Table 4.1: Transmitted intensity values at varying energy levels

Material	Original Intensity (I_0) /keV	Density (ρ) /gcm ⁻¹	Mass attenuation coefficient (μ/ρ) /cm ² /g	Linear attenuation coefficient (μ) /cm ⁻¹	Material thickness (e) /cm	Transmitted Intensity (I) /keV
Barium	70	3.5	5.1	17.9	1	1.3×10^{-6}
	35		6.9	24.4		9.2×10^{-10}
Titanium	70	4.5	0.5	2.3	1	7.9
	35		3.6	16.2		3.3×10^{-6}
Zirconium	70	6.5	2.2	14.5	1	3.6×10^{-5}
	35		18.1	118.0		2.0×10^{-50}
PMMA	70	1.18	0.2	0.2	1	60.7
	35		0.3	0.3		25.5

4.1.6 Thermal conductivity and heat transfer

Metal oxides are known to enhance the thermal conductivity of polymers²⁸³⁻²⁸⁶. The use of radiopaque agents with a high thermal conductivity (e.g. TiO₂, Table 4.2) in PMMA will result in an increase in the thermal conductivity of the polymer. If well-dispersed, the radiopacifier may prevent areas of local heat concentration by spreading and dissipating heat. This may result in lower setting temperatures and less heat induced stresses on the cement.

Table 4.2: Thermal conductivity and expansion of radiopacifier materials

Material	Thermal conductivity / W/mK	Coefficient of thermal expansion / K ⁻¹
^a PMMA	0.17 - 0.19	70-77×10 ⁻⁶
^b BaSO ₄	1.72	10×10 ⁻⁶
^a ZrO ₂	2.50	10×10 ⁻⁶
^a TiO ₂	2.50-5.00	8-9×10 ⁻⁶

Note: Data obtained from (a) www.goodfellow.com and (b) Weidenfeller et al.²⁸⁶

After the peak setting temperature is reached, the bone cement cools and decreases in volume. This is caused by the volumetric contraction of the polymer chains during polymerisation. When polymer molecules relax, shrinkage stresses can occur. The addition of fillers helps to reduce shrinkage as they prevent the molecules from relaxing during cooling^{287,288}. Filler particles also reduce shrinkage due to the significantly lower coefficient of thermal expansion, which results in smaller volume changes with changing temperatures.

4.2 Methods

4.2.1 Materials

Anatase TiO₂, yttria-stabilised ZrO₂, methyl methacrylate with 75ppm hydroquinone, N-N dimethyl-p-toluidine and benzoyl peroxide were obtained from Sigma Aldrich (Gillingham, UK) and BaSO₄ was obtained from Fisher Scientific UK (Leicestershire, UK). Polymethyl methacrylate powder with a methylacrylate copolymer (Colacryl TS1713) was provided by Lucite International UK (Southampton, UK).

4.2.2 Particle Sizing

The particle size distributions of BaSO₄, anatase TiO₂ and yttria-stabilised ZrO₂ were examined using a Malvern Mastersizer X (Malvern Instruments Ltd, Worcestershire, UK)

attached to an ultrasonic bath mixer. A small sample of the radiopacifier was added to deionised distilled water in the ultrasonic bath mixer. This disperses the particles, preventing agglomeration in order to obtain accurate size readings. The solution was then pumped into the Mastersizer X and the particle size distributions were obtained by laser diffraction.

4.2.3 Mechanical testing

Compression, bending and fracture toughness samples were prepared and tested as stated in Chapter 2. Data on the properties of commercial Cemex Isoplastic, Palacos R and the model cement were used from Chapter 3. Model cement samples without any radiopacifier (radiolucent) and model cement samples containing 5 to 25%w/w of the different radiopacifiers (TiO_2 and ZrO_2 , Table 4.3) were prepared and tested.

Table 4.3: Composition of tested bone cements

	Radio-lucent	Model cement	5% TiO_2 or ZrO_2	10% TiO_2 or ZrO_2	15% TiO_2 or ZrO_2	20% TiO_2 or ZrO_2	25% TiO_2 or ZrO_2
Liquid component / g	16.93						
Methyl Methacrylate / %w/w	98.50						
N-N Dimethyl-p-Toluidine / %w/w	1.50						
Hydroquinone / ppm	75.00						
Powder Component / g	40.00						
Polymethyl Methacrylate / %w/w	98.30	88.30	93.30	88.30	83.30	78.30	73.30
Barium sulphate / %w/w	-	10.00	-	-	-	-	-
Benzoyl Peroxide / %w/w	1.70						
ZrO_2 or TiO_2 / %w/w	-	-	5.00	10.00	15.00	20.00	25.00
Powder : Liquid ratio	2.36						

4.2.4 Setting properties

Data from Chapter 3 on the setting time, setting temperature and maximum temperature of commercial cements and the model cement were taken from Chapter 3. The radiolucent model cement and model cement with 10%w/w TiO₂ and 10%w/w ZrO₂ were tested according to Section 2.2.

4.2.5 Fracture toughness

Fracture toughness results for the commercial cements and the model cement were taken from Chapter 3 and fracture toughness measurements were taken according to Section 2.4 for the model cement samples containing 0 to 25%w/w of the different radiopacifiers (TiO₂ and ZrO₂).

4.2.6 Fatigue testing

The fatigue properties of Cemex Isoplastic, Palacos R and the model cement have already been determined in Chapter 3. The radiolucent model cement and model cement with 10%w/w TiO₂ and 10%w/w ZrO₂ were tested as described in Section 2.5. Two fatigue samples for each cement type were tested.

4.2.7 SEM images

SEM images of the fracture surfaces of fatigue samples were taken to study surface roughness and the presence of agglomerations, voids, pores and microstructure as described in Section 2.8.

4.2.8 X-ray imaging

2±1mm thick by 10±1mm square samples of Cemex Isoplastic, Palacos R, the model cement and model cement samples containing 0 to 25%w/w of the different radiopacifiers (TiO₂ and ZrO₂) were prepared for the X-ray study. The dimensions were selected to

represent the minimum cement mantle thickness usually found *in vivo*²⁸⁹. Two samples for each test group were used and an energy level of 35keV, 150 μ A was employed in air. Image analysis was carried out using ImageJ (National Institutes of Health, Maryland, USA) to assess the optical density of samples in terms of average brightness of the image picture elements (pixels). The results were obtained as mean grey values, ranging from 0 to 255, where 0 is black and 255 is white. A mean grey value of 255 would indicate complete absorption of X-rays, whilst a value of 0 would indicate complete transmission.

4.3 Results

4.3.1 Particle size

Figure 4.4 shows the particle size distributions for the radiopacifiers tested. The median diameters (D50) for BaSO₄, TiO₂ and ZrO₂ were 2.72 μ m, 0.53 μ m and 0.74 μ m respectively. Both TiO₂ and ZrO₂ had unimodal distributions whilst BaSO₄ had a partially bimodal distribution.

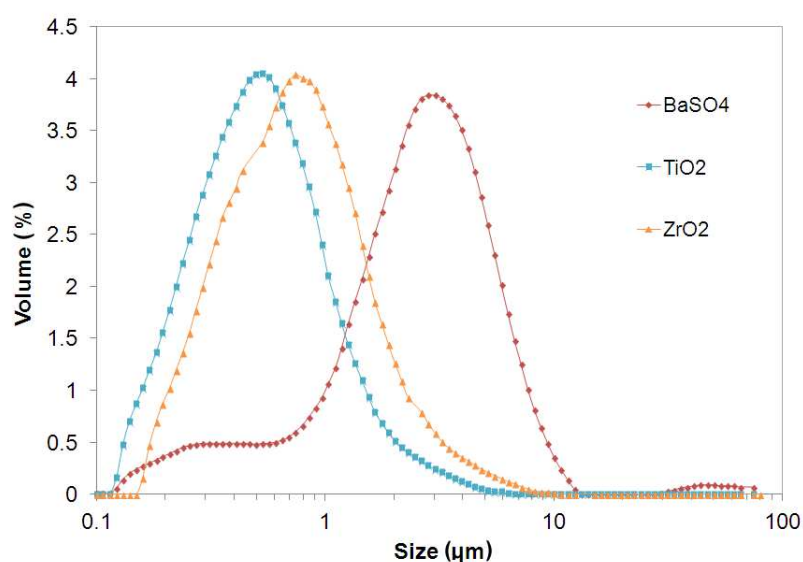


Figure 4.4: Particle size of BaSO₄, TiO₂ and ZrO₂ in water

4.3.2 Setting properties

Table 4.4 shows the setting properties of the commercial and novel bone cement formulations. 10%w/w ZrO₂ had the shortest setting time and highest setting and maximum temperatures (similar to Palacos R), whilst Cemex had the longest setting time and lowest setting and maximum temperatures. 10%w/w TiO₂ and radiolucent cements had similar setting properties and were found to have shorter setting times and higher temperatures than the model cement.

Table 4.4: Setting properties of commercial bone cements, the model cement, radiolucent cement and the cement with novel radiopacifiers

	Setting time (t_{set}) / s	Setting temperature (T_{set}) / °C	Maximum temperature (T_{max}) / °C
Cemex	738	46.5	69.8
Palacos R	479	52.1	78.5
Model cement	665	49.2	76.2
Radiolucent	615	51.4	81.6
10%w/w TiO₂	631	52.9	82.1
10%w/w ZrO₂	441	53.3	82.2

4.3.3 Mechanical properties

Compressive strength

Figure 4.5 shows the compressive strength for samples with varying amounts of TiO₂ and ZrO₂. The model bone cement (with 10%w/w BaSO₄) had a significantly higher compressive strength over other formulations (ANOVA, $p < 0.05$), whilst there were no significant differences between Cemex bone cement and the different formulations ($p = 0.06$). ZrO₂ gave significantly higher values when compared with TiO₂ at 5%w/w ($p = 7.52 \times 10^{-05}$) and 15%w/w ($p = 0.03$), however TiO₂ was significantly stronger at 20%w/w ($p = 0.04$). When compared to radiolucent cement (0%w/w radiopacifier), 10%w/w ($p = 0.01$) and 20%w/w ZrO₂ ($p = 0.01$) and 20%w/w TiO₂ ($p = 1.48 \times 10^{-03}$) had significantly higher compressive

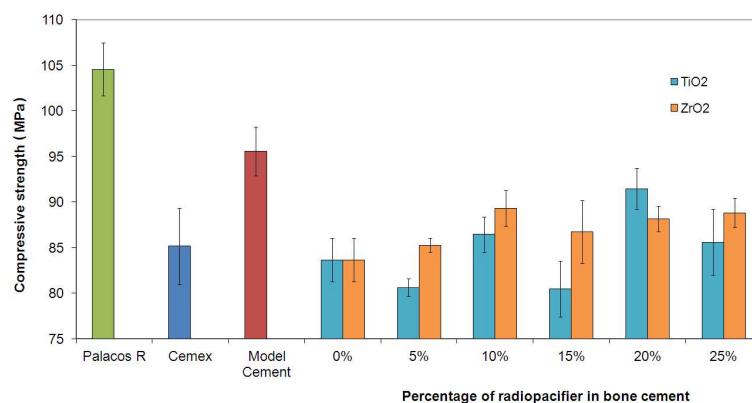
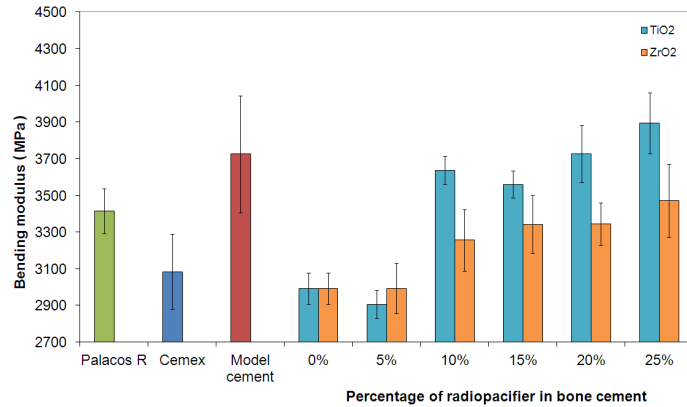


Figure 4.5: Average compressive strength

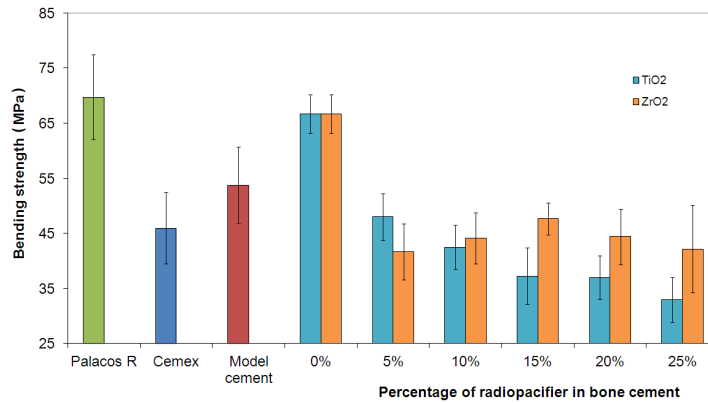
strength, whilst the other formulations were found to have no significant difference. It was expected that the compressive strength of bone cement would increase linearly with increased radiopacifier content as the rigid particles would resist compression more effectively. The results however, demonstrate that there is no linear relationship between the percentage of TiO₂ and ZrO₂ in bone cement and compressive strength. Overall it can be said that there were no improvements in compressive strength with the use of TiO₂ and ZrO₂ as radiopacifiers when compared with BaSO₄. Nevertheless, all cement formulations were found to be above the ISO5833 minimum standard for compressive strength, demonstrating that additives from 5%w/w to 25%w/w TiO₂ and ZrO₂ are suitable in terms of compressive strength for bone cements.

Bending modulus and strength

Figures 4.6(a) and 4.6(b) show the bending modulus and bending strength respectively for bone cements with varying amounts of TiO₂ and ZrO₂. There is a clear trend for both TiO₂ and ZrO₂ where an increase in the percentage of radiopacifier used results in an increase in bending modulus and a decrease in bending strength. TiO₂ containing samples had a significantly higher modulus after 10%w/w additive when compared to Cemex bone cement ($p < 0.05$). Bone cement with ZrO₂ had a significantly higher modulus than Cemex



(a) Bending modulus



(b) Bending strength

Figure 4.6: Average flexural properties

at 25%w/w ($p=0.03$). The addition of 5%w/w TiO₂ or ZrO₂ did not significantly affect the bending modulus when compared to the radiolucent cement (0%w/w radiopacifier, $p=0.27$ and $p=1.00$ respectively). The addition of 10%w/w or more TiO₂ or ZrO₂ significantly increased the bending modulus ($p<0.05$). After 10%w/w or more radiopacifier, TiO₂ was found to have a significantly higher modulus than ZrO₂ ($p=3.31 \times 10^{-03}$, $p=0.04$, $p=4.35 \times 10^{-03}$ and $p=0.01$ for 10, 15, 20 and 25%w/w respectively).

Samples with no radiopacifier were found to have significantly higher bending strength over Cemex ($p=4.78 \times 10^{-04}$), the model cement ($p=2.54 \times 10^{-04}$), cements with TiO₂ and

ZrO₂ ($p < 0.05$) and comparable bending strength to Palacos R. By adding only 5%w/w TiO₂ or ZrO₂, a significant decrease in bending strength was observed ($p = 4.68 \times 10^{-04}$ and $p = 1.10 \times 10^{-03}$ respectively). Cemex was found to be significantly stronger when compared to 25%w/w TiO₂ samples ($p = 0.01$) and the model cement was significantly stronger than samples with 25%w/w TiO₂ ($p = 0.03$). Overall ZrO₂ samples demonstrated enhanced bending strength when compared with TiO₂ as 15%w/w and 20%w/w ZrO₂ was significantly stronger than the same composition of TiO₂ ($p = 7.73 \times 10^{-03}$ and $p = 0.04$ respectively). All samples were found to have bending moduli above the ISO5833 minimum requirement, however TiO₂ and ZrO₂ containing samples failed to meet the minimum requirement of 50MPa for bending strength.

Fracture toughness

There was a gradual reduction in fracture toughness with increased TiO₂ content in the bone cement (Figure 4.7). This however does not occur with ZrO₂ possibly as a result of the toughening mechanism of yttria-stabilised ZrO₂. When compared to Cemex in terms of critical stress intensity factor, all TiO₂ and ZrO₂ samples showed significant (ANOVA, $p < 0.05$) improvements with the exception of 25%w/w formulations ($p = 0.33$). There were no significant differences between the model cement and samples containing TiO₂ and

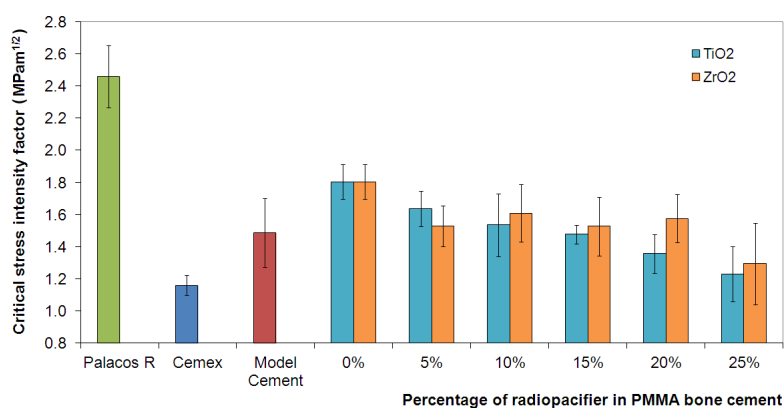


Figure 4.7: Average fracture toughness

ZrO₂ ($p > 0.05$). When compared to radiolucent cement (0%w/w radiopacifier), all the samples experienced a reduction in critical stress intensity factor, however the reduction was only significant for 25%w/w ZrO₂ ($p = 0.01$) and 15%w/w or more TiO₂ samples ($p = 7.25 \times 10^{-04}$, $p = 5.61 \times 10^{-04}$ and $p = 4.67 \times 10^{-04}$ for 15, 20 and 25%w/w respectively).

4.3.4 Fatigue

Figure 4.8 and Table 4.5 show the fatigue testing results and the analysis when the Paris Law²⁶² was applied to the data respectively. 10%w/w ZrO₂ performed most poorly in fatigue even though the yttria stabilisation should have enhanced its crack resistance. The use of 10%w/w TiO₂ also reduced the fatigue properties when compared to the model cement and the commercial cements, however a moderate improvement was observed in the ‘A’ coefficient when compared to radiolucent (0%w/w radiopacifier) cement. A great deal of variance in crack growth per cycle for the 10%w/w TiO₂ cement was observed when compared to the model and commercial cements. This is shown in Table 4.5 by the lower correlation coefficient when the Paris Law was applied.

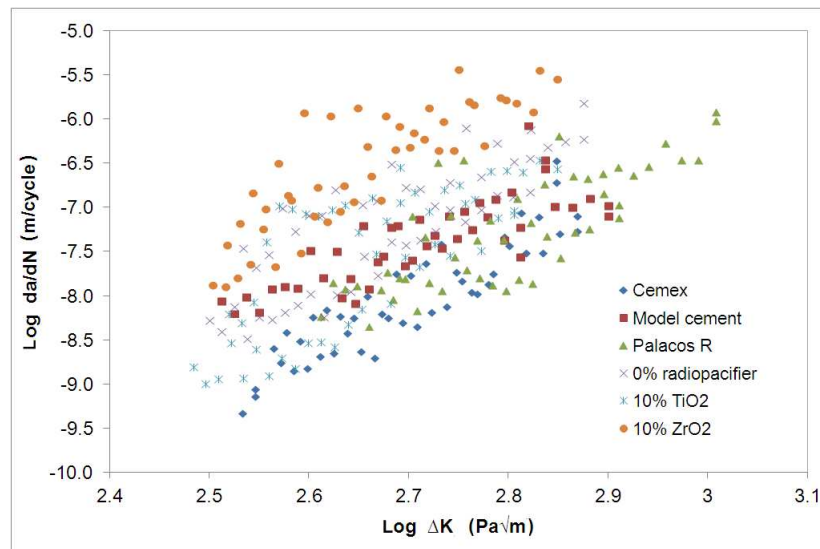


Figure 4.8: Fatigue results for commercial, model and novel cements

Table 4.5: Fatigue constants of commercial, model and novel cements, where ‘A’ is the crack growth at $\Delta K=1\text{MPam}^{1/2}$ and ‘m’ is the slope of the data

	A	m	Correlation coefficient
Palacos R	3.73×10^{-07}	4.65	0.61
Cemex	5.39×10^{-07}	5.92	0.82
Model cement	4.83×10^{-07}	3.73	0.67
0%w/w radiopacifier	3.53×10^{-06}	5.49	0.69
10%w/w TiO_2	3.00×10^{-06}	6.03	0.57
10%w/w ZrO_2	6.92×10^{-05}	6.88	0.73

4.3.5 SEM

Figure 4.9 shows large agglomerations of radiopacifiers. The agglomerations ranged from 20 to 200 μm in length, up to a hundred times the size of the individual radiopacifier particles. Agglomerations of this size were not expected, given the particle sizing results. Surrounding the agglomerations were large voids, possibly caused by the absorption of MMA monomer or caused by the deformation of the polymer matrix around the rigid particle during fracture. Such void formation is expected to reduce the bending strength and fracture toughness of the cement.

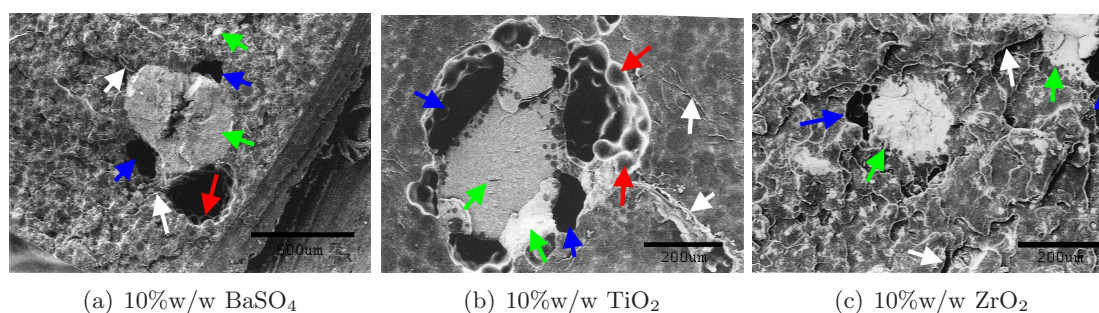


Figure 4.9: Void formation around agglomerations of radiopacifiers - Red arrows indicate PMMA beads, green arrows indicate radiopacifier particle agglomerations, blue arrows indicate pores and voids and white arrows indicate microcracks

When comparing the different radiopacifiers, BaSO₄ samples were found to have rougher fracture surfaces than TiO₂ and ZrO₂ samples (Figure 4.10). This demonstrates enhanced crack resistance in BaSO₄ samples, whilst TiO₂ and ZrO₂ samples were found to fracture in a more brittle manner.

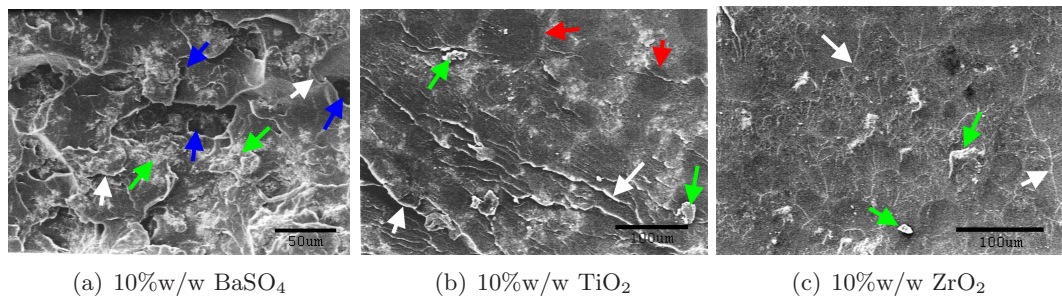


Figure 4.10: Surface roughness of fractures - Red arrows indicate PMMA beads, green arrows indicate radiopacifier particle agglomerations, blue arrows indicate pores and voids and white arrows indicate microcracks

4.3.6 Radiopacity

Figure 4.11 shows the calculated mean grey values for X-ray imaging at 35keV, 150μA. An ANOVA ($p < 0.05$) found that there were no significant differences between formulations with 10%w/w or more radiopacifier and the commercially available and model cements ($p = 0.15$). There was however, a significant difference between the samples without any

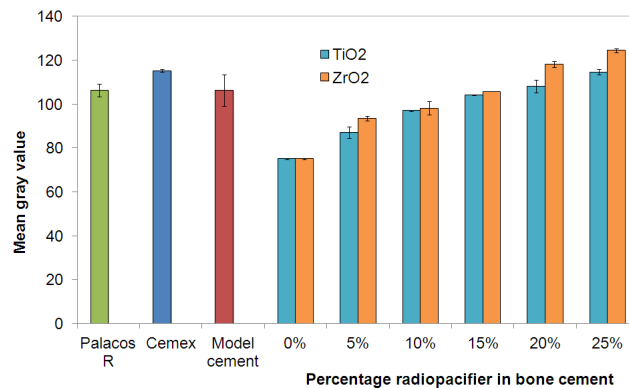


Figure 4.11: Mean grey values of X-ray images

radiopacifier (radiolucent) and all other cement samples ($p < 0.05$). It was expected that the radiolucent cement would produce lower grey values, demonstrating PMMA has a natural opacity under X-ray imaging at 35keV. This may not be the case at higher clinical settings (70keV).

4.4 Discussion

The use of radiopacifiers in PMMA bone cement is essential for the examination of cement integrity *in vivo*, however the radiopacifier may have a possible effect on the mechanical and fatigue performance of bone cement. BaSO_4 , which is widely utilised by bone cement manufacturers, is known to agglomerate²⁴, in turn negatively affecting the performance of the cement⁸²⁻⁸⁴. Anatase TiO_2 and yttria-stabilised ZrO_2 have been incorporated into the model cement, developed in Chapter 3, in an effort to overcome the problems associated with conventional bone cements. The use of TiO_2 in orthopaedic implants is well documented, however few studies have attempted to use powdered anatase TiO_2 as a radiopacifier in PMMA bone cement. On the contrary the use of ZrO_2 in PMMA to improve material properties is widely recognised in both bone and dental cements; the ZrO_2 used in this study was yttria-stabilised, which is claimed to benefit fracture toughness properties.

The particle size distributions of the anatase TiO_2 and yttria-stabilised ZrO_2 used were found to be very similar whilst the results for the BaSO_4 used in the model cement indicate a larger particle size. It is possible that the larger particle size and bimodal distribution experienced by the BaSO_4 could be a result of agglomerating BaSO_4 particles in distilled water. The plateau experienced at lower particle sizes either indicate that the BaSO_4 used has a wide particle size distribution or simply that few non-agglomerated particles were detected.

The higher thermal conductivity of anatase TiO_2 did not improve the setting properties and heat dissipation of bone cement. This may be attributed to poor dispersion of the radiopacifier or that the differences in thermal conductivity are not sufficient to induce improvements in the setting properties. Furthermore, the changes in thermal conductivity observed in the literature correspond to higher levels of metal oxide fillers ($\simeq 40\%w/w$)^{283–286}. Chou et al.¹⁷⁸ found the peak setting temperature of bone cement to reduce with increased filler loading. It is possible that higher quantities of radiopacifier may be required before a change is observed. Nevertheless the setting properties were changed when using $10\%w/w$ yttria-stabilised ZrO_2 . The properties were found to be similar to that of Palacos R, which also uses ZrO_2 as a radiopacifier. It is hypothesised that ZrO_2 interacts with, and affects, the polymerisation reaction of bone cement, however the mechanisms affecting the reaction are not understood. It is speculated that the polymer orientates itself on the surface of the ZrO_2 particle when polymerising. If this is the case, the change in setting properties observed may be linked to the specific surface properties, which are governed by the surface oxides and crystal structure of ZrO_2 .

The increase in modulus that was experienced as a result of higher levels of radiopacifier can be linked to the fact that stiffer particles have replaced a portion of the PMMA powder in the compositions used. The results show that the amount of rigid particles used is directly proportional to the final bending modulus obtained and in the case of TiO_2 , inversely proportional to the bending strength. Therefore high percentages of TiO_2 or ZrO_2 make bone cement more brittle. Similar studies by Fukuda et al.^{178,180,290} found the same trend. Values from these studies were much higher than the values obtained in this study as the cement was different in composition to commercial cements as it had significantly lower quantities of PMMA and the PMMA beads were a different size.

It is speculated that poor adherence between the $\text{TiO}_2/\text{ZrO}_2$ particles and the polymer matrix has caused the decrease in bending strength. The rigid particle filler can easily be detached under strain, creating microvoids between the particle and the polymer matrix, weakening the cement. As discussed, the thermal coefficient of expansion of the radiopacifiers used are significantly higher than that of PMMA. This may have induced cracking and void formations as the PMMA expanded and contracted at a higher rate than the radiopacifier, weakening the cement. Particle size has also been known to affect flexural properties as larger particles are unable to deform and therefore create greater stress concentrations. The reduction in strength of the novel formulations with increased radiopacifier content may also be caused by agglomerations.

The anticipated transformation-toughening mechanism of yttria-stabilised ZrO_2 did not improve the fracture toughness of the cement. Again, this may be as a consequence of poor dispersion and particle adhesion to the polymer matrix. Similarly, yttria-stabilised ZrO_2 was expected to improve fatigue properties, however closer examination of the fracture surfaces revealed highly agglomerated radiopacifier particles for both TiO_2 and yttria-stabilised ZrO_2 . In previous studies agglomerations of radiopacifiers have been found to be detrimental to the fatigue life of bone cements^{35,66,91–95}. Further, the addition of stiff radiopacifiers appears to have made the cement fail in a more brittle manner.

In terms of radiopacity, in theory ZrO_2 containing cements were expected to be the most radiopaque at 35keV, but the differences observed were not significant. The theoretical calculations only accounted for elemental metals and not compounds such as the metal oxides used. The low percentages of radiopacifiers tested in PMMA would also make subtle differences in the radiopacity of the various materials difficult to distinguish. It is clear that in order to obtain similar radiopacity as the commercially available cements, a minimum of 10%w/w anatase TiO_2 or yttria-stabilised ZrO_2 is required.

4.5 Conclusions

Overall the the novel radiopacifiers tested did not improve the mechanical, fatigue and setting properties of the model cement. Furthermore, certain properties were found to be poorer when using high percentages of anatase TiO_2 and yttria-stabilised ZrO_2 . 10%w/w radiopacifier was found to provide sufficient radiopacity without significantly compromising many of the material properties.

Yttria-stabilised ZrO_2 did not improve the fracture toughness or fatigue properties of the cement and affected the setting properties. Anatase TiO_2 had suitable setting properties, however it did not demonstrate any significant improvement in terms of mechanical and fatigue properties. It should be recognised however, that anatase TiO_2 still may have potential as a radiopacifier due to its ability to enhance bone growth and osseointegration.

Further, it is clear that agglomerations and poor bonding of radiopacifier particles to the polymer matrix are problems that must be overcome in order to improve the properties of bone cement. A potential method to overcome these limiting features was investigated in the following chapter.

Chapter 5

Improving radiopacifier dispersion and adhesion

5.1 Introduction

Radiopacifier agglomerations and poor adhesion between the radiopacifier particles and the polymer matrix is suspected to weaken bone cement. To ensure that the radiopacifier particles toughen the cement effectively, they must be well-dispersed throughout the cement and must be sufficiently well bonded to the polymer matrix to induce toughening mechanisms. The use of silane coupling agents may help achieve this.

Silane coupling agents (herein referred to as silanes) are solutions that have the ability to form durable bonds between organic and inorganic materials. These bonds modify the wetting and adhesion characteristics of the substrate used (e.g. the radiopacifiers). In general, silanes are composed of an organofunctional group, a linker, a silicon atom and a hydrolyzable group as shown in Figure 5.1¹⁸⁵.

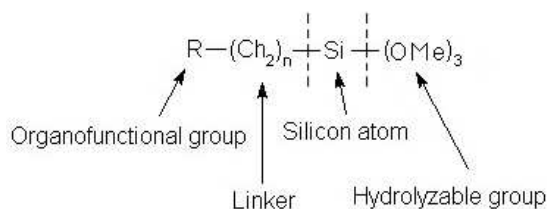


Figure 5.1: Silane structure

A silane couples to the substrate in four steps (Figure 5.2):

1. Hydrolysis of the 3 labile groups occurs.
2. Condensation to the oligomers follows.
3. Oligomers then hydrogen bond with hydroxyl groups on the substrate surface.
4. Finally during drying and/or curing, a covalent linkage is formed with the substrate with concomitant loss of water.

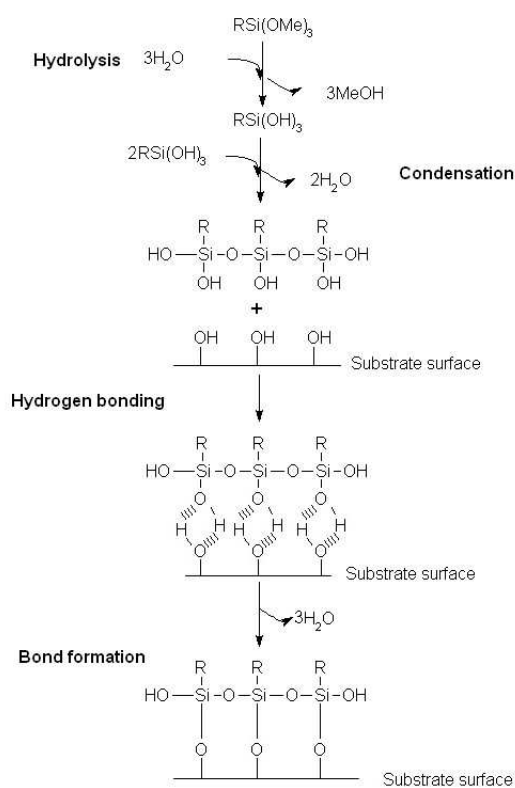


Figure 5.2: Hydrolytic deposition of silanes

The latter 3 steps can occur simultaneously after the initial hydrolysis event. At the interface there is usually only one bond from each silicon atom to the substrate surface. The R group remains available for covalent reaction or physical interaction with other phases. It should be noted that these steps represent hydrolytic deposition of silanes and therefore water is required for the process to take place. Water may be added or may come from the substrate surface or the surrounding atmosphere. The degree of polymerisation is de-

terminated by the amount of water available, the organic substituent and the concentration of silicon atoms. Factors which may influence the effectiveness of silane coupling agents include the concentration of surface hydroxyl groups; the type of surface hydroxyl groups; the hydrolytic stability of the bond formed and the physical dimensions of the substrate or substrate features.

The linker length of the silane also imposes a number of physical properties. If the linker length is long, the functional group has greater mobility and extends farther from the inorganic substrate. Furthermore a longer linker length will increase the distance between adjacent particles improving dispersion characteristics.

TiO₂ and ZrO₂ have hydrolytically stable surface oxides, however the oxidised surface has sufficient hydroxyl functionality to allow coupling by the hydrolytic deposition process outlined.

A methacrylate based functional silane was selected for this study, methacryloxypropyltrimethoxysilane (also known as 3-(trimethoxysilyl)propyl methacrylate); this has been employed as a coating for implants in studies investigating the surface adhesion between bone cement and metallic implants^{134,291}. The structure of methacryloxypropyltrimethoxysilane is shown in Figure 5.3. As this particular silane has three carbon atoms between the functional group and the silicon atom, it is a gamma substituted silane, which is thermally stable up to 350°C in the short term and 160°C in the long term and there-

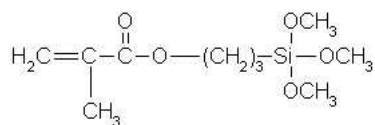


Figure 5.3: Methacryloxypropyl trimethoxysilane

fore, the silane will not be affected by the exothermic polymerisation reaction of bone cement and the temperatures experienced *in-vivo*. This particular silane has a toxicity similar to that of MMA (LD50>3000mg/Kg) and will only be present in small quantities¹⁸⁵. Therefore it should not significantly alter the toxicity of PMMA bone cements; this will be investigated in Chapter 6.

5.2 Methods

5.2.1 Materials

Methacryloxypropyltrimethoxysilane, HPLC grade ethanol ($\geq 99.8\%$), anatase TiO_2 , yttria-stabilised ZrO_2 , methyl methacrylate with 75ppm hydroquinone, N-N dimethyl-p-toluidine and benzoyl peroxide were obtained from Sigma Aldrich (Gillingham, UK). Whatman grade 6 filters (185mm diameter) were purchased from Fisher Scientific UK (Leicestershire, UK). Polymethyl methacrylate powder with a methylacrylate copolymer (Colacryl TS1713) was provided by Lucite International UK (Southampton, UK).

The model cement formulation was used when making cement samples, however the 10%w/w BaSO_4 was replaced with either 10%w/w silane-treated TiO_2 or 10%w/w silane-treated ZrO_2 . The silane-treated oxides were added to the liquid component of the cement (MMA) to improve dispersion. 10%w/w silane-treated radiopacifier was selected as the results from the previous chapter show 10%w/w radiopacifier to provide sufficient radiopacity without significantly compromising mechanical properties.

5.2.2 Silane treatment

The procedure used to treat the radiopacifier particles is based on industrial processes used to coat metallic surfaces and glassware^{185,292}. The radiopacifiers treated with the silane were anatase TiO_2 and yttria-stabilised ZrO_2 .

A 100mL solution of 95% ethanol, 5% distilled water was produced for 5g of radiopacifier powder. Acetic acid was used to adjust the pH to 4.5-5.5. The silane (methacryloxypropyltrimethoxysilane) was added at a 2%v/v concentration and allowed to hydrolyse at room temperature for 5 minutes. The radiopacifier powder was added and the solution was stirred using a magnetic stirrer for 24 hours. The solution was allowed to settle and the upper clear layer decanted. The remaining solution was filtered through a funnel with a Whatman grade 6 filter. The slurry was rinsed twice briefly with ethanol to remove any excess unreacted silane before drying in an oven at 80°C for 24 hours. Once dried the powder was crushed using a pestle and mortar and put through a 30-mesh sieve followed by a 300 mesh sieve to ensure a powder size of less than 50µm. The powder was then dispersed in the liquid component of the cement (MMA).

5.2.3 FTIR of treated radiopacifiers

To characterise and assess the success of the treatment process, fourier transform infrared spectroscopy (FTIR) was used. Potassium bromide (KBr) discs containing the radiopacifier powders were prepared as described in Chapter 7 and the spectra obtained using a Perkin Elmer Spectrum One FT-IR Spectrometer with FT-IR Spectrum software (Perkin Elmer, Massachusetts, USA) at the Cardiff School of History, Archaeology and Religion. TiO₂, ZrO₂, silane-treated TiO₂, silane-treated ZrO₂ and the silane alone were scanned from 4000cm⁻¹ to 450cm⁻¹ at a resolution of 4cm⁻¹.

5.2.4 Setting properties

The setting properties for commercial cements and model cements containing 10%w/w TiO₂ and 10%w/w ZrO₂ were previously determined in Chapters 3 and 4. Setting properties for 10%w/w silane-treated TiO₂ and 10%w/w silane-treated ZrO₂ were measured according to Section 2.2.

5.2.5 Mechanical testing

Compression and bending test samples with 10%w/w silane-treated TiO₂ and 10%w/w silane-treated ZrO₂ were prepared as described in Sections 2.3.1 and 2.3.2. Results were taken from Chapters 3 and 4 for comparison.

5.2.6 Fracture toughness

Fracture toughness values for commercial cements, the model cement and cements containing 10%w/w TiO₂ and 10%w/w ZrO₂ were previously determined in Chapters 3 and 4. Fracture toughness values for 10%w/w silane-treated TiO₂ and 10%w/w silane-treated ZrO₂ were obtained as described in Section 2.4.

5.2.7 Fatigue

Fatigue tests were carried out as outlined in Section 2.5 for both silane-treated oxides. Data for commercial cements, the model cement and cements containing 10%w/w TiO₂ and 10%w/w ZrO₂ were obtained from Chapters 3 and 4.

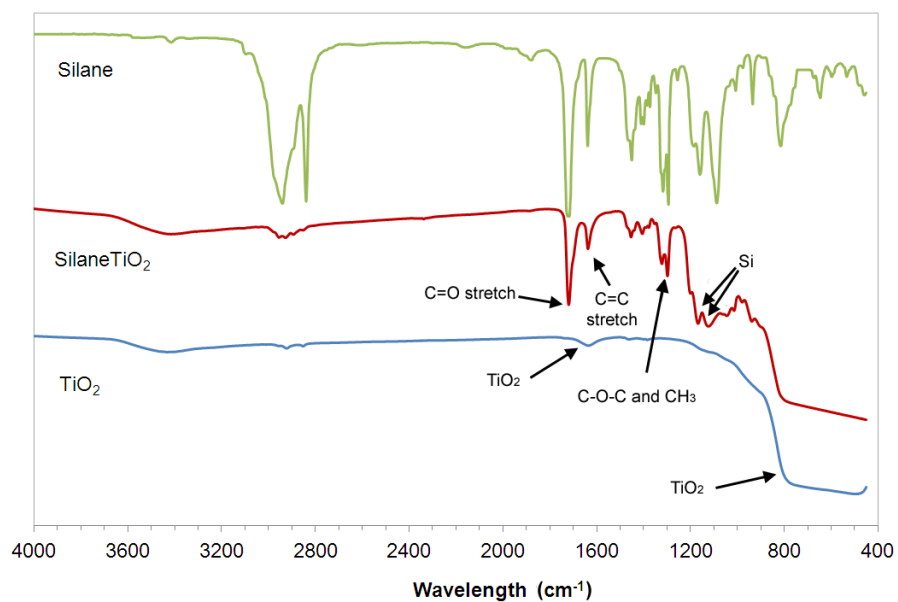
5.2.8 SEM images

SEM images for the fatigue samples were obtained as described in Section 2.8 in order to study radiopacifier dispersion, voids, porosity and fracture characteristics. SEM images of samples containing 10%w/w TiO₂ and 10%w/w ZrO₂ were taken from Chapter 4.

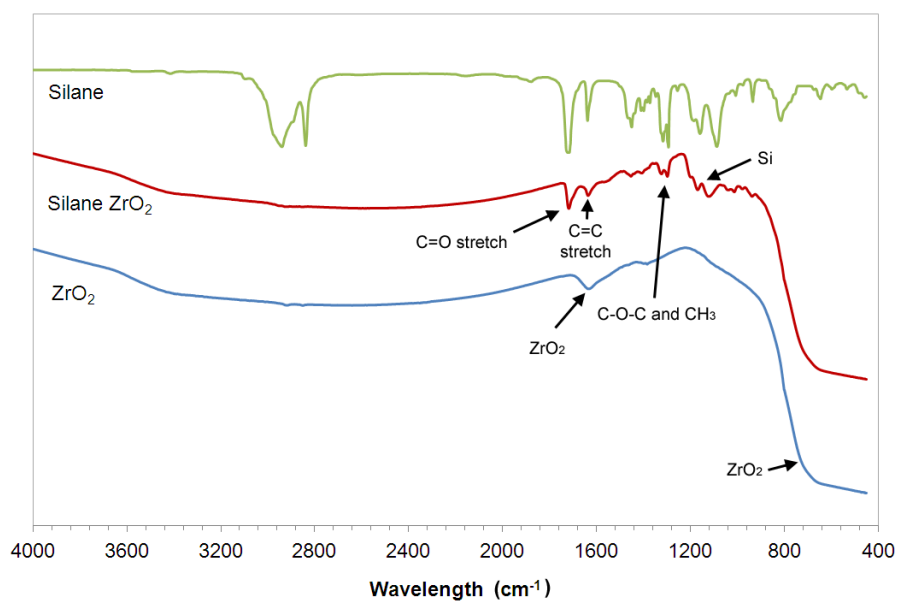
5.3 Results

5.3.1 FTIR analysis of treated radiopacifiers

Figure 5.4 shows the FTIR spectra for silane-treated TiO₂ and ZrO₂. Both radiopacifiers appear to have been successfully treated as both oxide particle spectra were found to contain similar peaks to the silane. The most prominent peaks were the C=O bond



(a) Silane-TiO₂



(b) Silane-ZrO₂

Figure 5.4: FTIR of silane-treated radiopacifiers using KBr discs

stretch at 1730cm^{-1} , the C=C stretch at 1600cm^{-1} , the C-O-C and CH_3 peaks around 1300cm^{-1} and the two peaks at 1100cm^{-1} and 1200cm^{-1} associated with silicon. The intensity of the silane-treated TiO_2 was found to be greater than that obtained from the silane-treated ZrO_2 . Both samples also show characteristics of their original untreated material in the form of a small broad peak at around 1600cm^{-1} and a drop in intensity for wavelength values below 900cm^{-1} .

5.3.2 Setting properties

Table 5.1 shows the setting properties for the commercial bone cements, the model cement, radiolucent cement and the cement with treated and untreated novel radiopacifiers. The cements containing silane-treated radiopacifiers gave similar results to the cements with untreated radiopacifiers. A slight reduction in the setting temperature and maximum temperature was observed with the silane-treated 10%w/w TiO_2 when compared to 10%w/w TiO_2 ; whilst a significant reduction was observed when comparing silane-treated 10%w/w ZrO_2 and 10%w/w ZrO_2 . A slight reduction in the setting time was observed when silane-treated 10%w/w TiO_2 was used and there was no significant change in setting time for silane-treated 10%w/w ZrO_2 .

Table 5.1: Setting properties of commercial bone cements, the model cement, radiolucent cement and the cement with untreated and silane-treated novel radiopacifiers

	Setting time (t_{set}) / s	Setting temperature (T_{set}) / °C	Maximum temperature (T_{max}) / °C
Cemex	738	46.5	69.8
Palacos R	479	52.1	78.5
Model cement	665	49.2	76.2
Radiolucent	615	51.4	81.6
10%w/w TiO_2	631	52.9	82.1
Silane-10%w/w TiO_2	579	51.0	79.6
10%w/w ZrO_2	441	53.28	82.2
Silane-10%w/w ZrO_2	442	46.1	69.1

5.3.3 Mechanical testing

Figure 5.5 shows the average compressive strength values for commercial cements, 10%w/w TiO₂ and ZrO₂, and silane-treated 10%w/w TiO₂ and ZrO₂. An ANOVA ($p < 0.05$) found that the silane-treated 10%w/w TiO₂ and ZrO₂ had significantly higher compressive strength than their untreated counterparts ($p = 3.94 \times 10^{-06}$ and $p = 4.57 \times 10^{-04}$ respectively). Silane-treated 10%w/w TiO₂ had significantly higher compressive strength than all the cements ($p < 0.05$) except Palacos R ($p = 0.50$) which was found to be comparable. Silane-treated ZrO₂ had significantly higher compressive strength than Cemex ($p = 9.64 \times 10^{-04}$), 10%w/w TiO₂ ($p = 4.04 \times 10^{-05}$) and 10%w/w ZrO₂ ($p = 4.57 \times 10^{-04}$) but significantly worse when compared to Palacos R ($p = 7.45 \times 10^{-04}$).

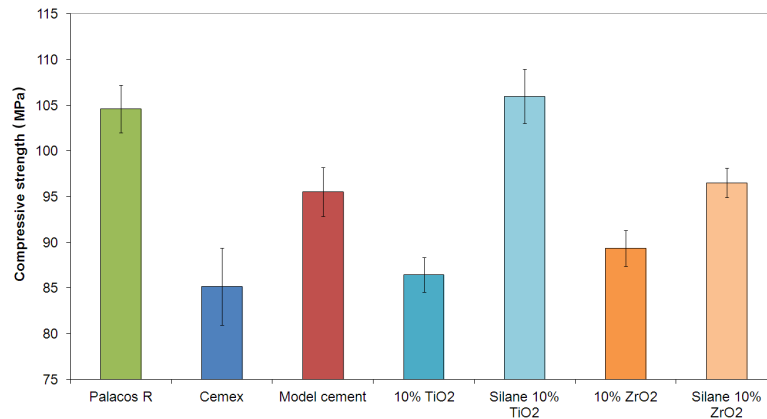
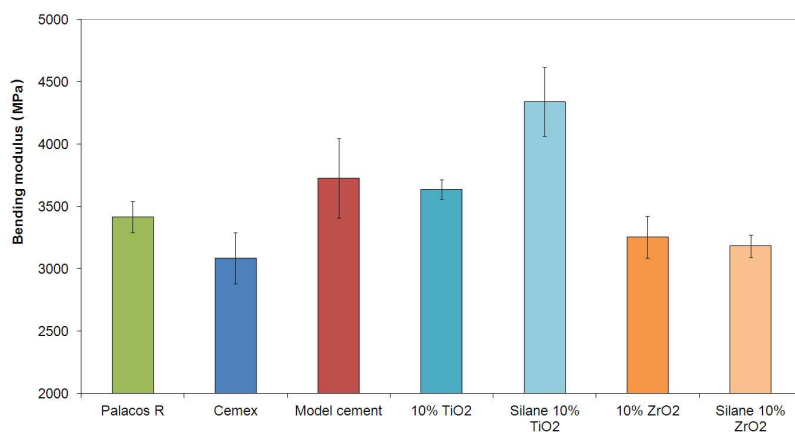
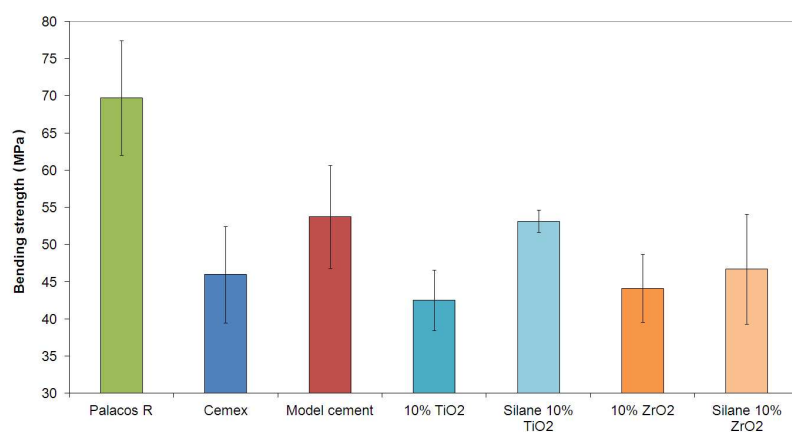


Figure 5.5: Average compressive strength

The bending modulus of silane-treated 10%w/w TiO₂ was significantly higher than all the other cement formulations ($p < 0.05$), as shown in Figure 5.6(a). There was no significant difference in modulus when using silane-treated ZrO₂ over untreated ZrO₂ ($p = 0.46$), however silane-ZrO₂ was found to have a significantly lower bending modulus than Palacos R ($p = 0.02$) and 10%w/w TiO₂ ($p = 6.32 \times 10^{-05}$).



(a) Bending modulus



(b) Bending strength

Figure 5.6: Average bending properties

Figure 5.6(b) shows the bending strength for the tested bone cement formulations. Silane-treated 10%w/w TiO₂ had a significantly higher bending strength than untreated 10%w/w TiO₂ ($p=2.52\times 10^{-03}$) and 10%w/w ZrO₂ ($p=0.01$) and was above the minimum requirements of the ISO5833 standard, which was not the case with 10%w/w TiO₂ cement. Silane-treated 10%w/w ZrO₂ on the other hand did not perform significantly better than untreated ZrO₂ ($p=0.57$) or the other cements. All formulations however were found to be significantly lower in bending strength when compared to Palacos R ($p<0.05$).

5.3.4 Fracture toughness

Figure 5.7 shows the fracture toughness of commercial cements, untreated 10%w/w TiO₂ and ZrO₂ and silane-treated 10%w/w TiO₂ and ZrO₂. The fracture toughness of 10%w/w TiO₂ was improved by the silane coating, but this was not significant ($p=0.24$). The silane-treated 10%w/w TiO₂ was found to be significantly better than Cemex ($p=1.22\times 10^{-04}$) and silane-treated 10%w/w ZrO₂ ($p=0.02$) bone cements. Similarly, the silane-treated 10%w/w ZrO₂ cement was found to be significantly better than Cemex ($p=0.02$). Cemex was found to have the poorest fracture toughness properties, whilst Palacos R was found to have significantly higher fracture toughness properties when compared to all the cements ($p<0.05$).

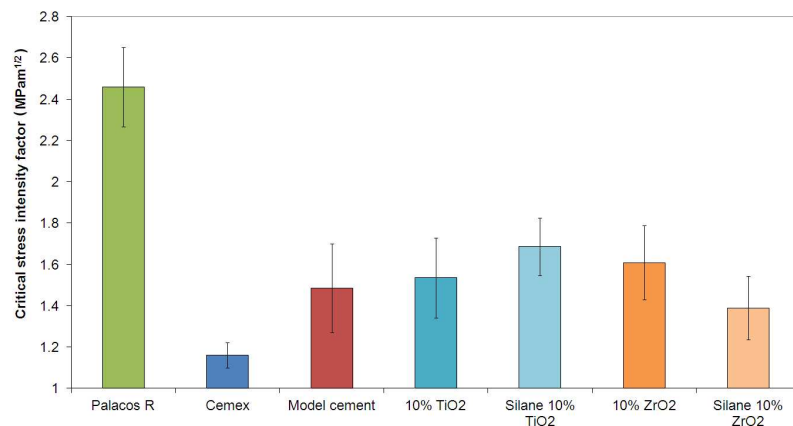
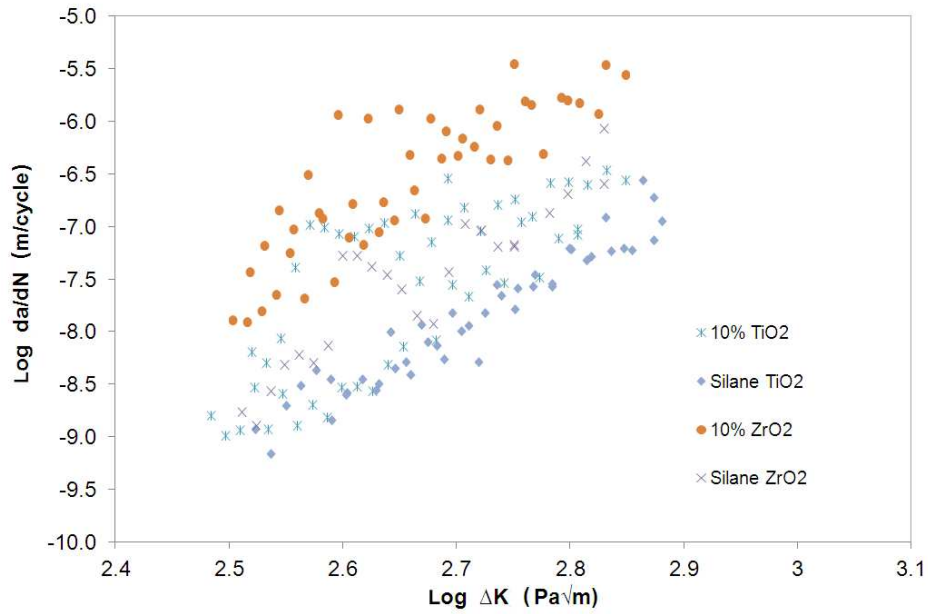


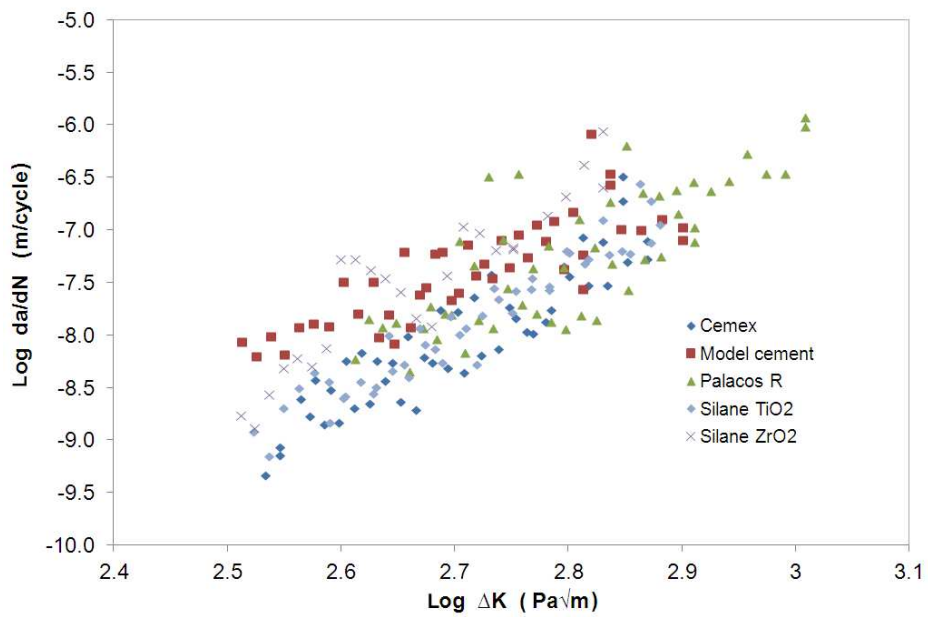
Figure 5.7: Average fracture toughness

5.3.5 Fatigue

Figure 5.8 and Table 5.2 show the fatigue results and fatigue constants respectively for commercial, model and novel untreated and silane-treated cements. The silane coating on TiO₂ and ZrO₂ has improved the crack growth rates at $\Delta K=1\text{MPam}^{1/2}$ (A coefficient), however the change in crack growth rates over the range of ΔK tested (m coefficient) was not improved. This is identifiable in Figure 5.8 where the fatigue plots have shifted



(a)



(b)

Figure 5.8: Fatigue test results

Table 5.2: Fatigue constants of commercial, model and novel silane-treated cements

	A	m	Correlation coefficient
Palacos R	3.73×10^{-07}	4.65	0.62
Cemex	5.39×10^{-07}	5.92	0.82
Model cement	4.83×10^{-07}	3.73	0.67
0%w/w radiopacifier	3.53×10^{-06}	5.49	0.69
10%w/w TiO₂	3.00×10^{-06}	6.03	0.57
Silane-10%w/w TiO₂	6.80×10^{-07}	5.94	0.92
10%w/w ZrO₂	6.92×10^{-05}	6.88	0.73
Silane-10%w/w ZrO₂	5.51×10^{-06}	6.76	0.84

down to lower crack growth rates for silane-treated cements. The silane-treated cements achieved low crack growth rates at low stress intensities and comparable crack growth rates at higher stress intensities when compared to the model and commercial cements as shown in Figure 5.8. Furthermore the silane treatment of the novel radiopacifiers has achieved less variability in the crack growth rates as demonstrated by an increase in the correlation coefficient with the Paris Law (Table 5.2). The decrease in variance of the results is attributed to the reduction in agglomerations resulting in a more homogeneous cement. This in turn produces more consistent results between samples.

5.3.6 Scanning electron microscopy

Figure 5.9 shows SEM images taken from the fracture surfaces of fatigue samples with 10%w/w TiO₂ and ZrO₂ and silane-treated 10%w/w TiO₂ and ZrO₂. Silane treatment has improved the dispersion of TiO₂ particles, however for silane-treated 10%w/w ZrO₂ large agglomerations were still present, suggesting poor silanisation. Both silane fracture surfaces however, were found to be rougher than the untreated TiO₂ and ZrO₂ fracture surfaces demonstrating less brittle failure. Furthermore semi-circular microcracks were found to have developed on the fracture surface of the silane-treated 10%w/w TiO₂, indicative of microcracks forming ahead of the crack tip. The microcracks would induce plastic deformation ahead of the crack tip and cause the main crack to deviate or branch out, slowing crack propagation and reducing the stress intensity at the tip of the crack.

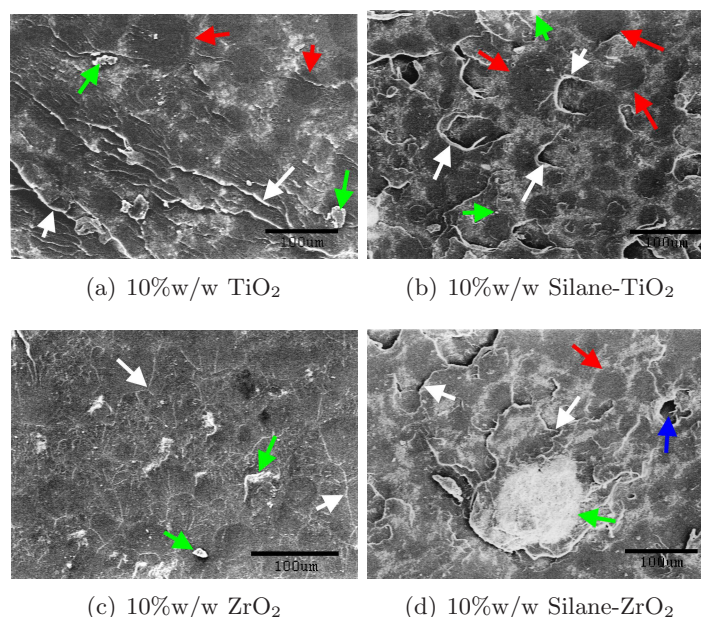


Figure 5.9: SEM images of fracture surfaces - Red arrows indicate PMMA beads, green arrows indicate radiopacifier particle agglomerations, blue arrows indicate pores and voids and white arrows indicate microcracks (bar=100µm)

5.4 Discussion

Silane coupling agents have been shown to enhance the bond strength and interfacial properties of implants made of titanium^{291,293}, zirconium^{294,295} and cobalt-chrome alloys¹³⁴. Silanes have also been used with PMMA containing glass fibres²⁹⁶, calcium chloride¹⁸³, hydroxylapatite²⁹⁷, silver and aluminium²⁹⁸. In all cases, the performance of PMMA with the additional materials was enhanced by the use of silanes. Although the initial results from Chapter 4 show that anatase TiO₂ and yttria-stabilised ZrO₂ do not improve the properties of bone cement, the use of silanes in conjunction with the novel radiopacifier may enhance the properties of the cement. A recent study has shown when methacryloxypropyltrimethoxysilane is added directly to MMA, the interfacial strength and the hydrolysis resistance of the metal-PMMA interface is improved, however the compressive and bending strength of the cement remain unaltered¹⁸². Similarly, the addition of silanes to dental cements did not result in significantly enhanced properties²⁹⁹. In order for the

silane to improve the mechanical properties of bone cement, it must first be applied to the surface of the radiopacifier.

The technique used to treat the radiopacifiers was judged successful for anatase TiO_2 using FTIR analysis, whilst for ZrO_2 the results are equivocal due to the intensity of the FTIR peaks and the presence of agglomerations. In both samples however, characteristic peaks of both the radiopacifier materials and the silane were detected. Several studies have used similar treatment and analytical procedures to characterise silane-treated surfaces^{293–295,300}. Other studies have used alternative methods to analyse coatings, including X-ray photoelectron spectroscopy (XPS)²⁹⁵, scanning electron microscopy (SEM) and contact-angle measurements³⁰⁰.

Silane treatment of the novel radiopacifiers alters the surface characteristics and allowed the powders to be dispersed in the liquid component of the cement (MMA). When successfully treated, the substrate surface will be covalently linked to the silane with the organofunctional group of the silane on the outermost layer of the substrate. This group in methacryloxypropyltrimethoxysilane is a methacrylate which renders the surface of the substrate hydrophobic. Furthermore the interactions between the methacrylate molecules on the outer surface of the substrate and the methacrylate molecules in MMA allowed for a well-dispersed stable suspension to be formed. Visual inspection of the suspensions found that the treated TiO_2 dispersed more readily than the treated ZrO_2 . Sedimentation of the treated substrate particles were found to occur over time due to gravity and differences in density, however the particles could be resuspended by agitation. The ability of the silane-treated TiO_2 and ZrO_2 to be suspended in MMA enhanced the dispersion of the radiopacifier. Furthermore, interactions between the methacrylate molecules in MMA and on the surface of the treated radiopacifiers would ensure some degree of bonding between the treated radiopacifier particles and the polymer matrix during polymerisation.

Overall the silane treatment did not significantly affect the setting properties of the cement. The amount of silane used and the extent of the coating on the surface of the radiopacifier may not have been sufficient to affect the polymerisation of PMMA. The setting time for the silane-treated 10%w/w ZrO₂ cement was similar to Palacos R and the 10%w/w ZrO₂ cement, further highlighting the impact of ZrO₂ on the polymerisation of bone cement.

In theory, the silane coating of the radiopacifier particles should improve the dispersion of the particles throughout the cement and improve the adhesion between the particles and the PMMA matrix. This was clearly the case with silane-treated TiO₂ where improvements in compressive strength, bending strength, bending modulus, fracture toughness and fatigue characteristics were observed. Similar results were observed in other studies whereby improvements in compressive and flexural properties occurred as a result of silane use^{298,301,302}. A moderate increase in toughness was observed with the silane-treated TiO₂ and this agrees with results from other publications^{83,173}. The SEM images of the fracture surface of the silane-treated TiO₂ sample showed few agglomerations and rougher fracture surfaces with semi-circular cracks. The well-dispersed TiO₂ may have increased the modulus of the cement, however, good dispersion of the radiopacifier would result in less stress concentrations and stress risers, which initiate cracks. The dispersion of rigid particles in the polymer matrix would also have distributed stresses away from the crack tip, acting as a toughening mechanism. Moreover, good adhesion between the TiO₂ particle and the PMMA matrix would require higher stresses to break the covalent bonds, and cause debonding of the particle from the polymer matrix. Good adhesion would also induce higher levels of deformation in the surrounding polymer as rigid particles do not deform. Both mechanisms would result in a tougher, stronger material as observed in the results.

Although these improvements were found to occur with silane-treated TiO₂ samples, this was not the case with silane-treated ZrO₂ samples. Few significant improvements were observed as a result of silane coating ZrO₂ and large agglomerations were still visible on the fracture surfaces of the fatigue samples. By assessing the surface coatings in the FTIR results, it is probable that the silane-treatment of ZrO₂ was incomplete. Recent studies experienced similar difficulties in achieving complete silane treatment of yttria-stabilised and non-stabilised ZrO₂³⁰³⁻³⁰⁵. Sandblasting with silica-coated alumina prior to silane treatment has been shown to improve the outcome of silane treatment and may offer a solution to this problem^{294,295}.

5.5 Conclusions

In conclusion, the silane treatment of TiO₂ is thought to have been successful, whilst difficulties in achieving complete treatment of ZrO₂ was experience. Silane treating TiO₂ greatly improved the mechanical and fatigue properties of the cement and did not significant alter the setting properties. Moreover, silane-treated TiO₂ cement met all the ISO5833 minimum requirements for acrylic cements. The use of a silane on the surface of TiO₂ enhanced the the surface characteristics of the radiopacifier, allowing it to be dispersed effectively in MMA. This in turn would have improved the dispersion and adhesion between PMMA and the radiopacifier, allowing several of the toughening mechanisms discussed to be induced. Introducing silane-treated TiO₂ into a commercial cement as a substitute for BaSO₄ or ZrO₂, using industrial mixing and preparation techniques, may result in further improvements to mechanical and fatigue properties.

The biocompatibility of the silane used has previously been questioned and although only a small quantity is employed on the surface of each radiopacifier particle, it is essential to study the effect this has on surrounding cells and tissues. Furthermore the use of anatase TiO₂ may yield positive results in terms of bone growth and osseointegration. The fol-

lowing chapter focuses primarily on bone growth and the interactions between the novel silane-treated radiopacifiers and MC3T3-E1 cells, an osteoblast precursor cell line derived from mouse calvaria.

Chapter 6

Biocompatibility and osseointegration of PMMA bone cements

6.1 Introduction

Anatase TiO_2 and yttria-stabilised ZrO_2 have the potential to be used as radiopacifiers for bone cements. Improvements in the setting, mechanical, fracture toughness and fatigue properties of the cement containing anatase TiO_2 and yttria-stabilised ZrO_2 were not observed due to agglomerations of the radiopacifiers and poor bonding to the polymer matrix. Consequently, a silane coating on the surface of the radiopacifier particles was tested and significant improvements to the mechanical and fatigue properties were observed. PMMA is generally considered to have little to no influence on bone growth and the use of novel materials such as silane treated TiO_2 and ZrO_2 may have the potential to enhance bone growth at the cement-bone interface. The work in this chapter assessed the bioactivity of the novel cement formulations in terms of hydroxylapatite (HA) growth on the surface of the cement and interactions with MC3T3-E1 cells. If demonstrated to be functionally bioactive, bone growth at the cement-bone interface may be improved, perhaps preventing micromotion and potentially encouraging new bone to grow into fatigue cracks in the cement over time.

6.1.1 Bone growth

When an implant is introduced into the body, there is an initial inflammatory response with the arrival of phagocytes and other repair cells. The subsequent tissue response will then determine the outcome of the implant. A toxic tissue response would cause death to the surrounding tissue and cells. An inert response may result in the formation of a thin protective layer around 1-3 μm in thickness and if micromotion occurs, a fibrous tissue can form, preventing any bond from forming. Bioactive materials have the ability to evoke a positive response with the surrounding tissue, rapidly creating chemical bonds and encouraging natural healing mechanisms. In the case of bone cements, a bioactive material would deposit layers of bone minerals rapidly³⁰⁶.

Bone consists primarily of collagen fibres and crystalline salts. The two main components of the crystalline salts deposited in bone matrix are calcium (Ca) and phosphate (PO_4), which combine to form HA crystals ($\text{Ca}_{10}[\text{PO}_4]_6[\text{OH}]_2$). These crystals have good compressive strength whilst the collagen fibres have good tensile strength. When combined with a degree of bonding between the collagen fibres and the crystals, a bony structure is formed with good properties in both compression and tension.

Within bone there are also blood vessels, nerves and cells, which play a vital role in bone remodelling, growth and healing (Figure 6.1). The main cells within bone are fibroblasts, fibrocytes, osteoblasts, osteocytes, osteoclasts and osteoprogenitors. Fibroblasts and fibrocytes are responsible for collagen formation, which enhances tensile properties. Osteoprogenitor cells are found deeper in the periosteum and in bone marrow and differentiate into osteoblasts under the influence of growth factors such as bone morphogenic proteins (BMPs), fibroblast growth factor (FGF), platelet-derived growth factor (PDGF) and transforming growth factor beta ($\text{TGF-}\beta$). Osteoblasts are responsible for forming new bone. They form the organic component of bone, osteoid, which is predominantly

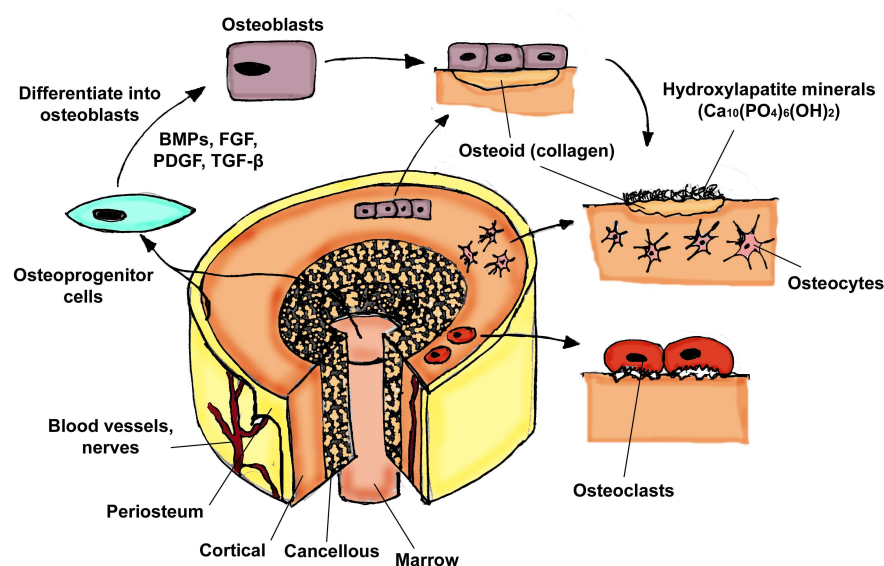


Figure 6.1: Structure of bone and its remodelling process

made of collagen. Minerals then begin to form around this collagen to form HA. Osteocytes are mature osteoblasts that have become trapped in the bone matrix. Osteocytes are sensitive to pressure, enabling bone to remodel itself in response to loads, and move nutrients and waste through the bone matrix. Osteoclasts counterbalance the role of osteoblasts and are responsible for bone resorption.

Beneficial interactions between cells involved in bone remodelling and hydroxylapatite (HA) has resulted in a variety of orthopaedic applications for HA, as detailed in a review by Oonishi et al.³⁰⁷. Numerous studies have investigated the use of HA in bone cement^{178, 179, 297, 308, 309}, bone spacers and scaffolds^{255, 256} and as a surface coating for implants^{250, 310–313}. Osteoblast cells proliferate on bone-like apatite layers and form a biological matrix of natural HA and collagen, whilst consuming the apatite in the bone-like material and later remodelling it³¹⁴. This process, which occurs between artificial materials and natural bone, is identical to the process that occurs naturally in bone remodelling. HA not only induces mechanisms of natural bone growth but is also non-toxic, reducing unwanted inflammatory responses. Although successfully used in bone scaffolds and

non-load bearing applications, recent studies have shown that incorporating HA into bone cement may have a detrimental effect on mechanical and fatigue properties³⁰⁸.

The interaction between cells and the surface of an implanted material depends on a range of material properties such as chemical composition, particle size, surface roughness and surface energy^{310,315}. These properties dictate how effectively biological molecules and cells behave on, and adsorb to, surfaces. Proteins such as vitronectin (contained in serum which mediates osteoblast adhesion)³¹⁶, fibronectin and albumin have been shown to adsorb more rapidly onto hydrophilic surfaces with high surface energies, therefore enhancing the rate of adhesion of specific anchorage-dependent cells (e.g. osteoblasts, fibroblasts and endothelial cells)³¹⁷. Recent studies have shown how surface energy plays a vital role in the efficiency of cell-material interactions, affecting both protein adsorption³¹⁸ and cell attachment³¹⁹. Materials with improved physical and chemical properties could therefore enhance cell behaviour at the surface of the implant and extend its lifetime.

The surface energy of a material defines how a liquid behaves at that surface. A low surface energy, demonstrated by a high water contact angle between the solid surface and water, represents a hydrophobic surface. Surfaces with a high surface energy and a low contact angle tend to be more hydrophilic. This concept is highlighted in Figure 6.2

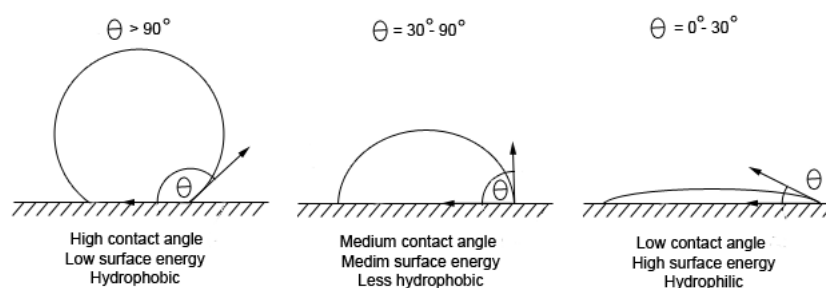


Figure 6.2: Contact angle technique to measure surface energy or the hydrophobic/hydrophilic properties of a material

which demonstrates the degree of wetting of different surface types. As previously discussed, hydrophilic surfaces tend to enhance cell interaction, adsorption and adhesion and is also favourable for HA formation³²⁰. Negatively charged surfaces were also reported to enhance hydroxylapatite formation³²¹. By replacing the radiopacifier of PMMA bone cement with a more hydrophilic and negatively charged material, there is the potential to enhance bone growth properties.

Titanium is widely employed in orthopaedics due to its low toxicity and ability to bond to bone. The low toxicity is due to the thin oxide layer (2-7nm)³²²⁻³²⁴ that naturally forms when titanium is exposed to oxygen, creating TiO₂, a stable and inert compound. In addition to being stable in the physiological environment, TiO₂ has been found to increase calcium ion interactions, which is important for protein and osteoblast adhesion as well as HA formation³²⁵. In particular, the anatase crystal structure of TiO₂ is speculated to have a higher bioactivity than rutile or amorphous TiO₂. This is due to the closer lattice match with HA, higher acidity and lower surface zeta potential caused by a larger number of hydroxyl groups on the surface. Deposition of HA on anatase at a pH of 7.4 is faster than on the rutile form at the same pH³²⁶.

The surface energies of PMMA, BaSO₄, TiO₂, ZrO₂ and the silane (methacryloxypropyltrimethoxysilane) used in the previous chapter were obtained from published literature and are shown in Table 6.1. From this datum it is expected that commercial bone cements

Table 6.1: Surface energies of different materials

Material	Surface energy / mN/m
PMMA	39 ³²⁷
BaSO ₄	33 ³²⁸
Anatase TiO ₂	91 ¹⁸⁵
Yttria-stabilised ZrO ₂	42 ³²⁹
Methacryloxypropyltrimethoxysilane	34 ³⁰⁰
HA	72-95 ³³⁰

containing roughly 10%w/w BaSO₄ will have the lowest surface energy and thus be more hydrophobic in nature, whereas bone cements containing anatase TiO₂ will have a higher surface energy with a lower contact angle and be more hydrophilic. It is also expected that silane treating TiO₂ and ZrO₂ will reduce the surface energy of the cement when compared to cements with untreated TiO₂ and ZrO₂. This is due to the hydrophobic nature of the silane. As previously discussed in Chapter 5 the hydrolyzable group of the silane creates a covalent bond with the oxide surface of the metal, leaving the organofunctional group of the silane free to attach to the surrounding polymer. When TiO₂ and ZrO₂ particles are coated with the silane, the hydrophobic organofunctional group will be left on the surface, rendering the particle more hydrophobic. It is therefore expected that particles that have been treated to increase hydrophobicity for dispersion and adhesion purposes will have a lower surface energy and possibly poorer bone growth properties. Recent studies however have shown that the silane functional groups and silanol groups (Si-OH) can enhance apatite formation^{183,311}. Furthermore osteoblast-like cell behaviour has been shown to be more dependent on surface chemistry rather than general surface properties such as surface energy and wettability³³¹.

6.2 Methods

6.2.1 Surface energy determinations

Surface energy measurements were taken according to the British Standards EN828³³². Small cylindrical bone cement samples (10mm diameter, 2mm thickness) containing 10%w/w BaSO₄, TiO₂, ZrO₂, silane-treated TiO₂ and silane-treated ZrO₂ were prepared as described in Section 2.1. The flat surfaces of the samples were sanded with a 500 grit silicon carbide paper. Three test liquids were used in this experiment: water, methanol and glycerol.

2 μ L of the test liquid was pipetted onto the surface of the bone cement sample at a 90° angle and an image was taken of the profile of the droplet (perpendicular to the surface) using a high definition digital camera. The images were then imported into ImageJ (National Institutes of Health, Maryland, USA) and the right and left contact angles were measured to give an average contact angle per sample (θ) as shown in Figure 6.3. The experiment was repeated five times for each sample.

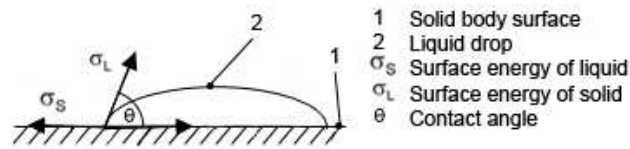


Figure 6.3: Contact angle measurements

A linear variation ($y = mx + c$) of Young's equation is shown in Equation 6.1 and was used to calculate the total surface free energy of each sample. The interfacial tension values for the test liquids (Table 6.2) and the average contact angles for each liquid on a sample were used in Equation 6.2 to produce y and x points. Plots for each sample were produced and the slope and y-intercept determined using linear regression. The square of the slope corresponds to the polar proportion of the solid body surface energy (σ_S^P) and the square of the y-intercept corresponds to the disperse proportion of the solid body surface energy (σ_S^D). The sum of these two proportions gives the total surface free energy of the sample (σ_S), as shown in Equation 6.3.

$$\frac{(1 + \cos\theta) \times \sigma_L}{2\sqrt{\sigma_L^P}} = \sqrt{\sigma_S^P} \times \frac{\sqrt{\sigma_L^P}}{\sqrt{\sigma_L^D}} + \sqrt{\sigma_S^D} \quad (6.1)$$

$$y = \frac{(1 + \cos)\theta \times \sigma_L}{2\sqrt{\sigma_L^D}}, \quad x = \frac{\sqrt{\sigma_L^P}}{\sqrt{\sigma_L^D}} \quad (6.2)$$

$$\sigma_S = \sigma_S^P + \sigma_S^D \quad (6.3)$$

Where:

- θ is the measured contact angle;
- σ_L is the surface tension of the liquid used;
- σ_L^D is the disperse proportion of the liquid used;
- σ_L^P is the polar proportion of the liquid used;
- σ_S is the surface tension of the sample;
- σ_S^D is the disperse proportion of the sample;
- σ_S^P is the polar proportion of the sample;

Table 6.2: Interfacial tensions of test liquids

Test liquid	Surface tension σ_L / mN/m	Disperse proportion σ_L^D / mN/m	Polar proportion σ_L^P / mN/m
Water	72.8	21.8	51.0
Methanol	22.5	18.2	4.3
Toluene	28.5	28.5	0.0

6.2.2 Hydroxylapatite growth

HA growth was determined using the ISO23317:2007 standard³³³. 10x10x2mm square bone cement samples were prepared for the model cement with 10%w/w BaSO₄, 10%w/w TiO₂, 10%w/w ZrO₂, 10%w/w Silane treated TiO₂ and 10%w/w Silane treated ZrO₂ as described in Section 2.1. Two samples for each group and time point were used (n=2, 36 samples in total). Each sample was stored in 30mL of simulated body fluid (SBF) based on a solution developed by Kokubo et al.³³⁴ with a composition and preparation method as specified in ISO 23317:2007. The samples and SBF were stored in a V-bottom container at 37°C for 1 hour, 1 week and 4 weeks. After each time point, the samples were removed and washed twice with distilled deionised water to remove any unattached HA precipitates. The samples were then desiccated without heat to prevent crystallisation. The sample surface was examined by X-ray diffraction (XRD) using a Philips PW3830 X-ray generator with a PW1710 Diffractometer control (Philips Research, Eindhoven, The Netherlands) and X'pert Industry v1.1c software (PANalytical B.V., Almelo, The

Netherlands). The scan was run between 3° and 50° (2θ) at a scan speed of $0.020^\circ/\text{s}$. After XRD, one sample from each group was imaged using scanning electron microscopy (SEM) for visual inspection of apatite crystals as described in Section 2.8. The second sample was incubated in SBF for a total of 6 weeks and imaged using SEM.

6.2.3 MC3T3-E1 cell culture

Gibco[®] Minimum Essential Medium alpha (α -MEM) with nucleosides (L-Glutamine, sodium pyruvate, lipoic acid, B₁₂, biotin, and ascorbic acid) was purchased from Life Technologies Ltd (Paisley, UK) and prepared according to the manufacturer's instructions. MC3T3-E1 osteoblasts of passage 14-16 were cultured in α -MEM supplemented with 10% fetal bovine serum (FBS) and 1% penicillin/streptomycin at 37°C , 5% CO₂. Once confluent, the cells were trypsinized, resuspended in α -MEM and counted using a haemocytometer.

6.2.4 Osteoblast adhesion

The ability of a cell to adhere and anchor itself to a specific surface will dictate how quickly it will interact with the surface and carry out its intended function. The rate of osteoblast cell adhesion is important as it will define how rapidly the cells can deposit minerals on the surface of the material and begin forming new bone.

10mm diameter by 2mm height cylindrical bone cement samples were prepared in a similar manner to the samples used for surface energy measurements. The samples consisted of bone cement containing 0%w/w radiopacifier (radiolucent), 10%w/w BaSO₄, 10%w/w TiO₂, 10%w/w ZrO₂, 10%w/w silane-treated TiO₂ and 10%w/w silane-treated ZrO₂. Four samples for each test group and time point were prepared (n=4, 72 samples in total). The cylindrical samples were sterilized by soaking in 100% ethanol for 5 minutes and allowed to air dry under aseptic conditions. MC3T3-E1 cells were cultured as previously described.

The cement samples were placed in a 24 well-plate and 6000 cells in 150 μ L of culture medium (α -MEM) was carefully seeded directly onto the top of each sample and incubated. After 4 hours each well was flooded with 750 μ L of medium and incubated for 1, 4 and 24 hours.

After each time point, the medium was removed from each well and the samples were washed with phosphate buffer saline (PBS) to remove any non-adherent cells. The PBS was then removed and the adherent cells fixed with 10%v/v neutral buffered formalin (NBF) for 10 minutes. The NBF was removed and the samples were washed with PBS and stained with 1%w/v toluidine blue for 10 minutes after which the stain was removed and the samples were washed twice with distilled water. The samples were left to dry and four different areas on the surface of each sample were imaged using an Olympus IX50 light microscope (Olympus, Southend-on-Sea, UK). The number of adherent cells were counted using ImageJ software (National Institutes of Health, Maryland, USA).

6.2.5 Osteoblast proliferation

Cell proliferation refers to the growth of a cell population. The ability of a material to increase the rate of cell proliferation would be beneficial to healing processes such as the one experienced during total joint replacements. The faster the cells reproduce and develop, the more cells that are available to carry out specific tasks, such as developing new bone material. Therefore, the rate of cell proliferation is a parameter that must be evaluated. Furthermore, cell proliferation tests evaluate the number of live cells and therefore also provide a measure of how detrimental a material or chemical is to cell activity.

10mm diameter by 2mm height cylindrical bone cement samples were also used for the proliferation test and three samples and one control for each test group and time point was used (n=3, 48 samples in total). The cylindrical samples were sterilized in 100%

ethanol for 5 minutes and allowed to air dry under sterile conditions. MC3T3-E1 cells were cultured as previously described. The cement samples were placed in a 24 well-plate and each well was flooded with 3000 cells in 500 μ L of α -MEM or α -MEM medium alone for the controls. The well plate was gently agitated to ensure an even distribution of cells on the sample surfaces then incubated at 37°C in 5% CO₂ for 3 and 7 days, with the medium replaced every 2 days.

After 3 and 7 days the well plates were removed from the incubator and the medium removed from each well. The samples were then washed with PBS and moved into a new well plate. 500 μ L of α -MEM and 100 μ L of CellTiter 96[®] AQueous One Solution Proliferation Assay (Promega Corporation, WI, USA) was added to each well containing samples and the plate was incubated in the dark at 37°C in 5% CO₂ for 2 hours. The assay is composed of a tetrazolium compound (MTS, 3-(4,5-dimethylthiazol-2-yl)-5-(3-carboxymethoxyphenyl)-2-(4-sulfophenyl)-2H-tetrazolium). MTS reacts with living cells to produce a formazan precipitate, which can be determined at 490nm. The absorbance values are therefore a direct measure of the number of living cells in the medium. After 2 hours, 100 μ L of the assay medium was moved to a 96-well plate and the absorbance was read at 490nm using a Packard Spectracount plate reader. The absorbance of the control samples were subtracted from the absorbance of samples with cells to account for background colouration arising from interaction with the bone cement

6.3 Results

6.3.1 Surface Energy

Table 6.3 shows the results of the surface energy measurements. Bone cement with no radiopacifier and the model cement which contains 10%w/w BaSO₄ had significantly lower surface energies than the other cements (ANOVA, p<0.05) demonstrating a more hy-

Table 6.3: Experimental surface energies

	Surface energy / mN/m
0%w/w Radiopacifier (Radiolucent)	30.6±3.8
Model cement	28.8±3.0
10%w/w TiO₂	44.5±3.5
Silane 10%w/w TiO₂	42.5±3.3
10%w/w ZrO₂	36.7±3.8
Silane 10%w/w ZrO₂	41.6±6.2

drophobic surface. The cement formulations with treated and untreated TiO₂ and ZrO₂ had the highest surface energies making them more hydrophilic. There was no significant difference in surface energy as a result of silane treatment ($p=0.43$ for TiO₂ and $p=0.21$ for ZrO₂). Samples with 10%w/w TiO₂ had a significantly higher surface energy than samples with 10%w/w ZrO₂ ($p=0.02$), however the difference between silane-treated TiO₂ and silane-treated ZrO₂ was not significant ($p=0.80$).

6.3.2 Hydroxylapatite growth

Figures 6.4 to 6.8 show the XRD spectra for the model, TiO₂, silane TiO₂, ZrO₂ and silane ZrO₂ cements respectively after storage in SBF for 1 hour, 1 week and 4 weeks. The top spectrum for each figure corresponds to peaks obtained from XRD scans of HA, whilst the bottom spectra were obtained from XRD scans of the radiopacifier material used in the cement samples. It is expected that if a material successfully promotes bone growth, then full surface coverage will occur and only peaks from HA will be observed. For materials that gradually nucleate bone minerals, it is expected that peaks from both HA and the radiopacifier material will be present. When peaks from both HA and the radiopacifier occur at the same position (2θ), then an overall increase in peak intensity should be observed.

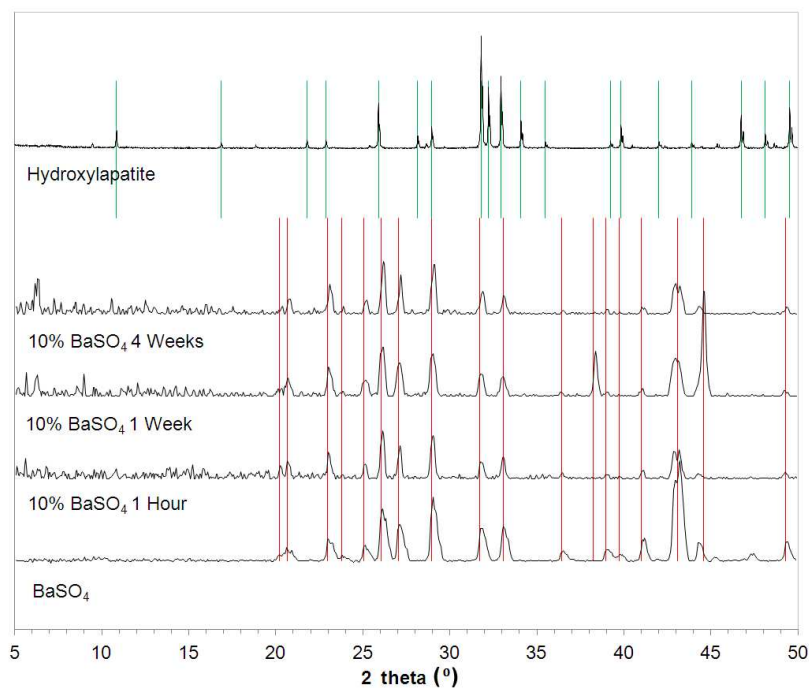


Figure 6.4: XRD spectra of the model cement samples stored in SBF over time

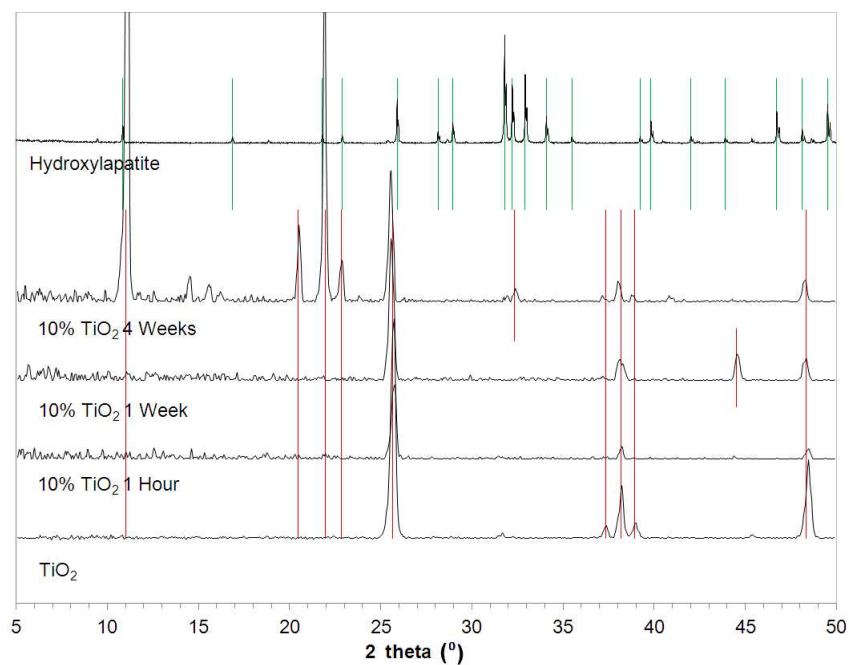


Figure 6.5: XRD spectra of TiO₂ samples stored in SBF over time

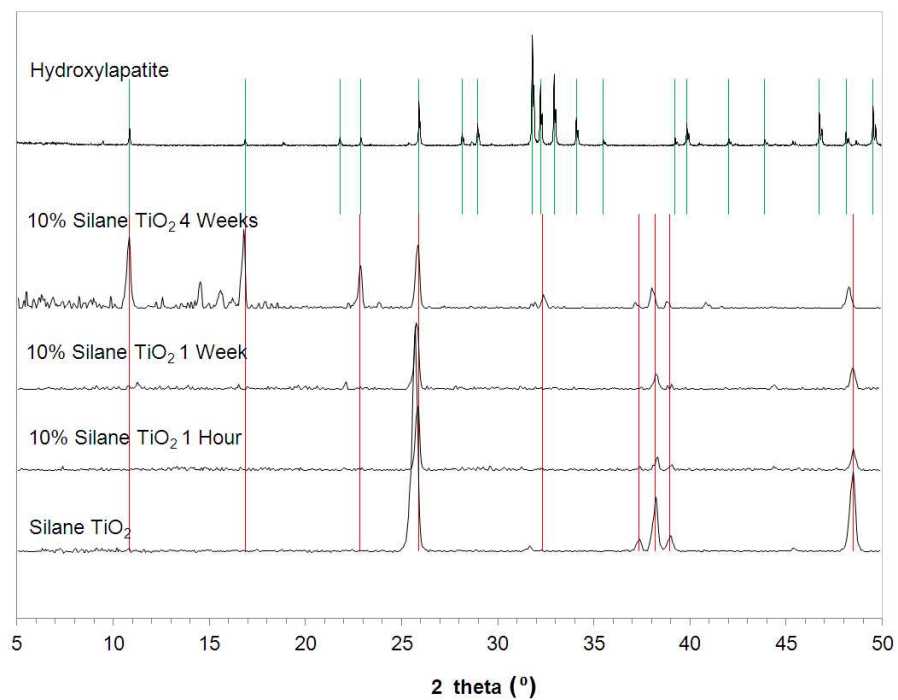


Figure 6.6: XRD spectra of silane TiO₂ samples stored in SBF over time

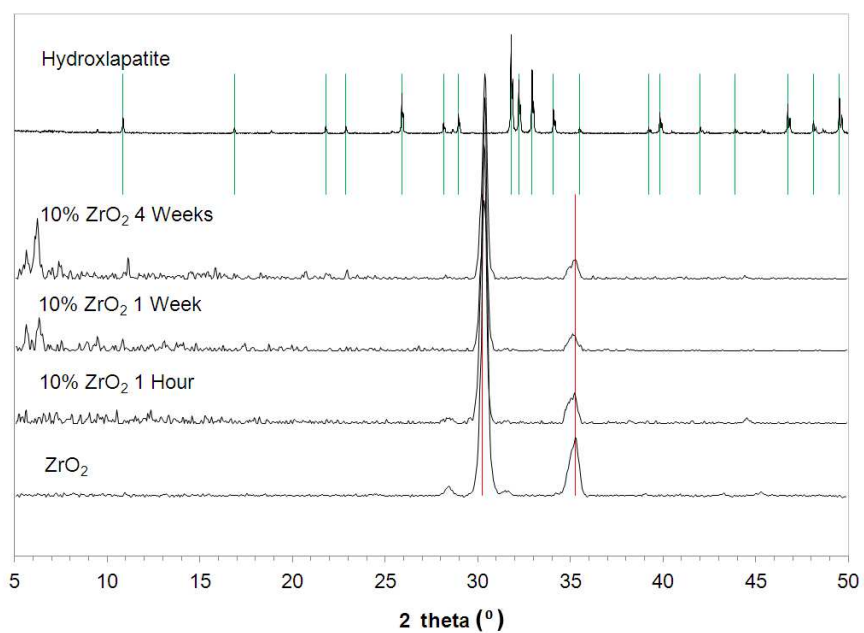


Figure 6.7: XRD spectra of ZrO₂ samples stored in SBF over time

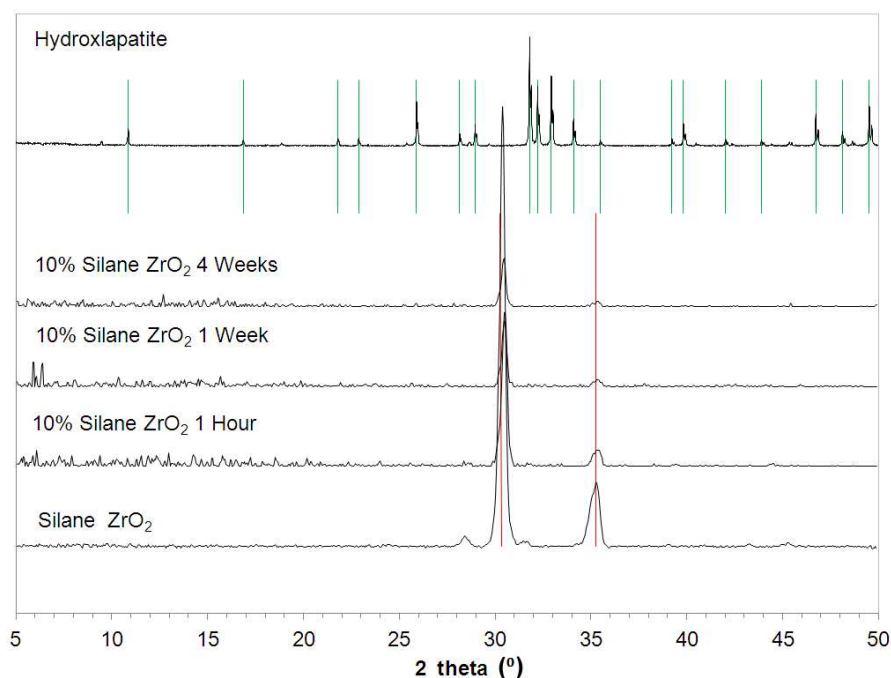


Figure 6.8: XRD spectra of silane ZrO₂ samples stored in SBF over time

All XRD spectra had peaks at the same positions as the radiopacifier materials, demonstrating the presence of the radiopacifier material on the surface of all the samples. Similarly, the XRD spectra demonstrate that the anatase phase of TiO₂ and the cubic phase ZrO₂ were present.

From the model cement XRD scans, it is clear that no HA growth took place on the surface of the cement. All the peaks coincided with the BaSO₄ spectrum, with the exception of one peak at 38.25° after 1 week in SBF. This peak did not match with those of HA and was not present at 4 weeks, therefore the deposition of HA can be ruled out.

Bone cement containing TiO₂ on the other hand demonstrated strong peaks after 4 weeks in SBF at 11.03°, 21.95°, 22.83° and 32.33° which coincided with HA peaks. Peaks at 44.53° after 1 week and 20.48° after 4 weeks were shown on the XRD scans, however they

do not match the HA peaks. The source or cause of these peaks is not understood. Bone minerals were not detected at 1 hour and 1 week and the strongest peak for HA (31.80°) was not present in any of the scans, demonstrating the crystal structure of HA may not have fully formed after 4 weeks.

Similar to TiO_2 , silane-treated TiO_2 samples were found to have peaks at the same positions as HA after 4 weeks in SBF. These peaks occurred at 10.85° , 16.86° , 22.83° and 32.33° . The peaks obtained by the silane TiO_2 samples were not exactly the same as those obtained with the TiO_2 samples as a peak at 16.86° was present but not at 21.95° . Similarly, there was no peak at 31.8° .

ZrO_2 and silane-treated ZrO_2 had identical spectra with strong ZrO_2 peaks at 30.24° and 35.28° . No other peaks were detected at 1 hour, 1 week or 4 weeks. Although XRD may not detect very thin surface layers of HA, it can be assumed no minerals were present on the surface of samples containing ZrO_2 and silane-treated ZrO_2 .

Figure 6.9 shows the SEM images of the samples stored in SBF for 1 week. At 1 week there are no discernible features on the surfaces of the model cement, ZrO_2 and silane-treated ZrO_2 samples that would indicate the growth of HA crystals, however on the surface of TiO_2 and silane TiO_2 at 1 week, small straight edged structures were observed.

Figure 6.10 shows samples stored in SBF for 4 weeks. After 4 weeks the surfaces of the model, ZrO_2 and silane-treated ZrO_2 samples appear altered, however there were no visible crystal formations on the surfaces. TiO_2 and silane TiO_2 samples after 4 weeks had many irregular shaped structures forming on the surface. This time point coincides with the results from the XRD scans, which show selected peaks associated with HA forming.

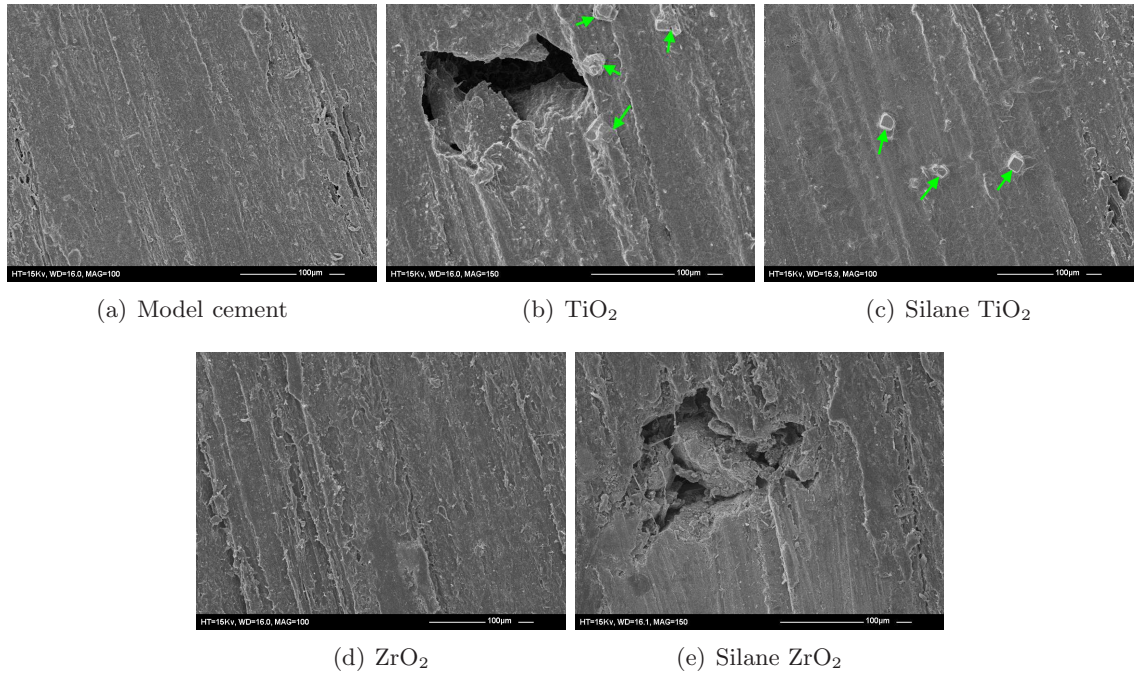


Figure 6.9: SEM images of the surface of samples stored in SBF for 1 week - Green arrows indicate potential HA crystal structures on surface of samples

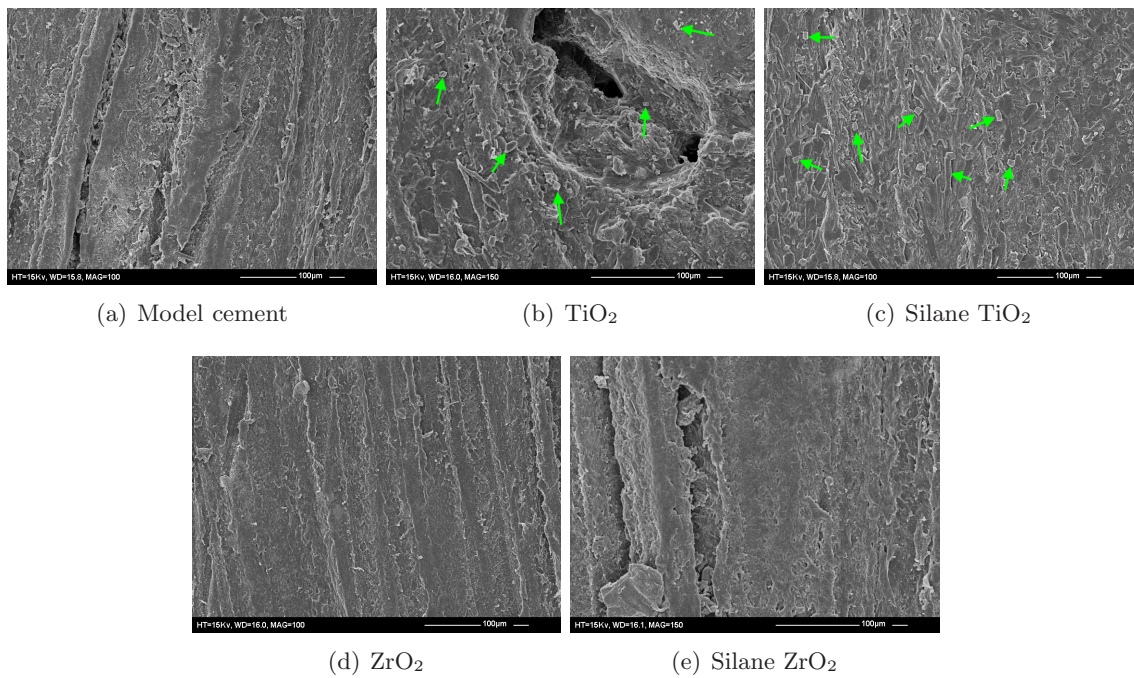
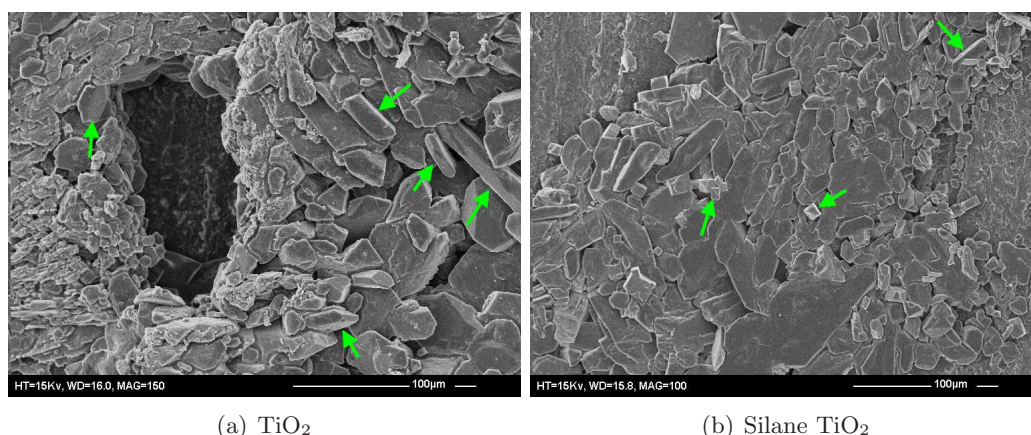


Figure 6.10: SEM images of the surface of samples stored in SBF for 4 weeks - Green arrows indicate potential HA crystal structures on surface of samples



(a) TiO_2 (b) Silane TiO_2
 Figure 6.11: SEM images of the TiO_2 and Silane TiO_2 samples after storage in SBF for 6 weeks - Green arrows indicate potential HA crystal structures on surface of samples

After 6 weeks in the SBF solution, clear straight edged geometrical shapes were observed on the surfaces of TiO_2 and silane TiO_2 samples, indicative of crystal structures (Figure 6.11).

6.3.3 Osteoblast adhesion

Figure 6.12 shows the osteoblast adhesion at 1, 4 and 24 hours for the tested cements. At all time points silane- TiO_2 had the highest level of MC3T3-E1 cell adhesion. Cell adhesion was significantly higher at 1 hour incubation compared to the other cements ($p < 0.05$).

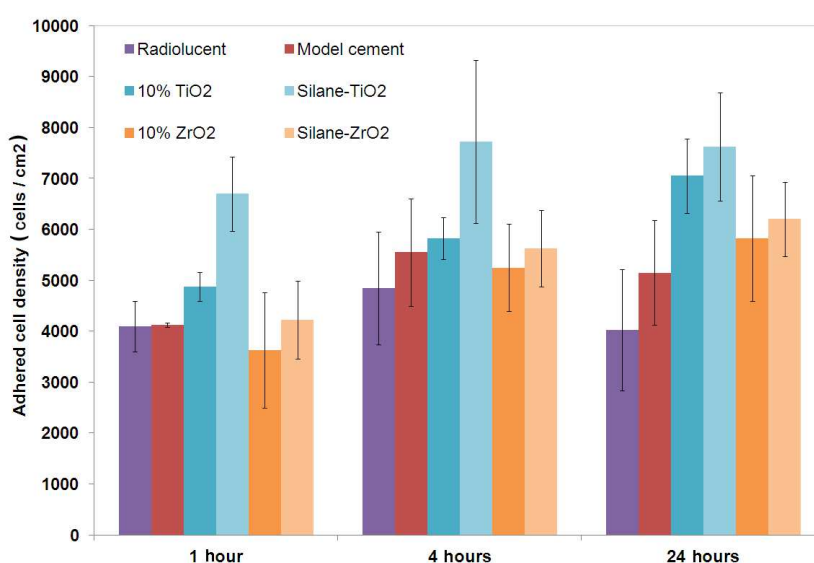


Figure 6.12: Osteoblast adhesion

10%w/w TiO₂ cement had significantly higher levels of cell adhesion than the model cement at 1 hour ($p=4.15 \times 10^{-03}$), whilst there were no significant differences between the rest of the cements ($p>0.05$). At 4 hours however, all the cements had performed similarly with the exception of silane-TiO₂ which was found to be significantly better than the control radiolucent (0%w/w radiopacifier) cements ($p=0.04$). Finally at 24 hours, TiO₂ and silane-TiO₂ were significantly more adherogenic than radiolucent cement ($p=0.01$) and the model cement ($p=0.04$), whilst silane-ZrO₂ performed significantly better than radiolucent cements ($p=0.04$). Overall it was observed that the silane-TiO₂ cements performed the best in terms of MC3T3-E1 cell adhesion, closely followed by the 10%w/w TiO₂ cement and then the ZrO₂ cements. From these initial results, the interaction between TiO₂ and MC3T3-E1 cells was found to be beneficial for cell adhesion as was the silane treatment.

Figures 6.13 to 6.18 show images of the stained cells at 1, 4 and 24 hours on the surface of the different cement samples. For all cements, the cells were found to change morphology as the incubation times increased. Initially, at 1 hour, cells were rounded and by 24 hours the MC3T3-E1 cells began to spread and appear similar in morphology to osteoblast cells. From the images it is clear that TiO₂ containing cements had a significantly higher number of cells adhered to the surface. Furthermore, the cells on the TiO₂ containing cements were found to be more widely spread at 1 and 4 hours.

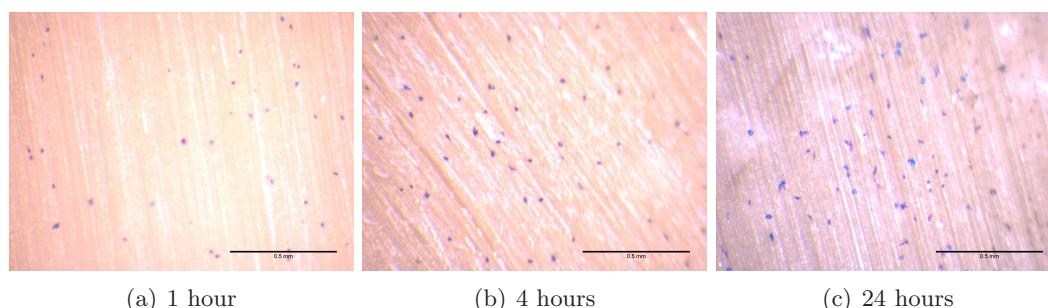
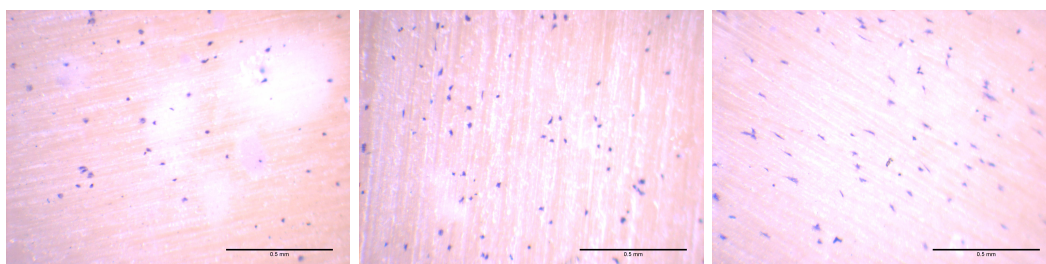
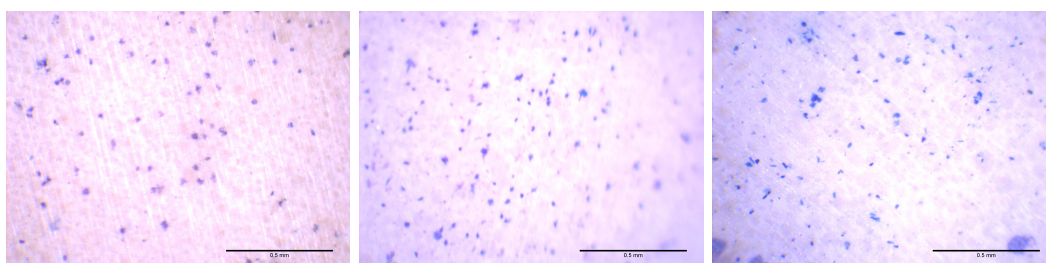


Figure 6.13: Stained MC3T3-E1 cells on the surface of the radiolucent cement



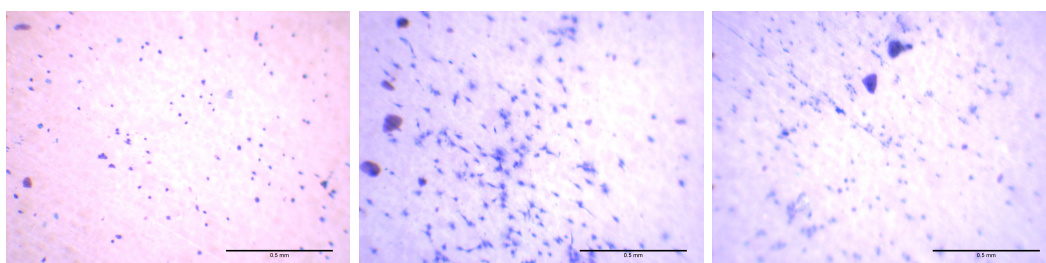
(a) 1 hour (b) 4 hours (c) 24 hours

Figure 6.14: Stained MC3T3-E1 cells on the surface of the model cement



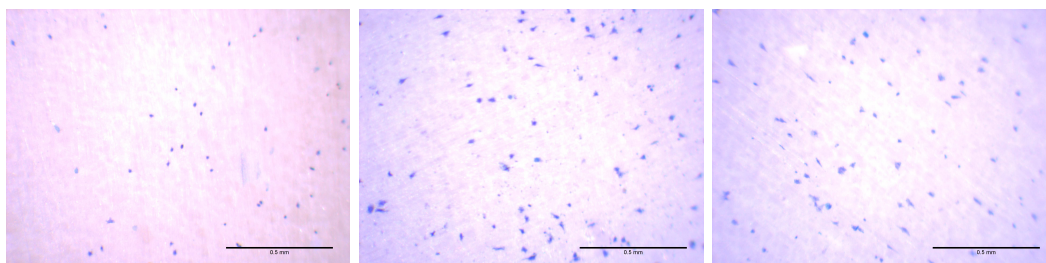
(a) 1 hour (b) 4 hours (c) 24 hours

Figure 6.15: Stained MC3T3-E1 cells on the surface of the TiO₂ cement



(a) 1 hour (b) 4 hours (c) 24 hours

Figure 6.16: Stained MC3T3-E1 cells on the surface of the silane TiO₂ cement



(a) 1 hour (b) 4 hours (c) 24 hours

Figure 6.17: Stained MC3T3-E1 cells on the surface of the ZrO₂ cement

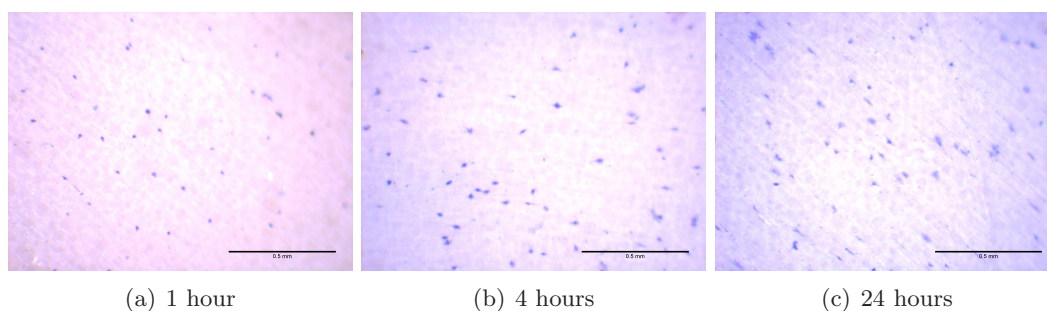


Figure 6.18: Stained MC3T3-E1 cells on the surface of the silane ZrO₂ cement

6.3.4 Osteoblast proliferation

The results of the proliferation test are shown in Figure 6.19. Although osteoblasts were found to attach more readily on the surface of silane-TiO₂ samples, the results for cell proliferation demonstrates that silane treatment has a detrimental effect on MC3T3-E1 cell proliferation. Absorbance values at 490nm on silane-treated samples were found to be lower than those obtained from 10%w/w TiO₂ and ZrO₂ samples. Although a reduction in cell proliferation was experienced, this was not significant for silane-TiO₂ at both 3

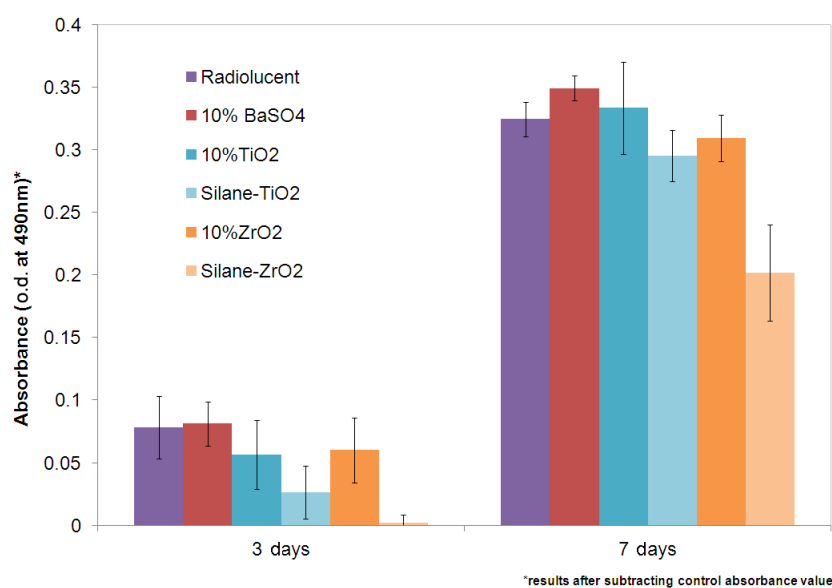


Figure 6.19: Osteoblast proliferation

days ($p=0.29$) and 7 days ($p=0.27$). Silane-TiO₂ however was significantly worse than the model cement on day 7 ($p=0.03$) and Silane-ZrO₂ was significantly worse than the model cement on days 3 ($p=3.83\times 10^{-03}$) and 7 ($p=6.34\times 10^{-03}$). On day 7, silane-treated ZrO₂ was significantly worse than all of the cements ($p<0.05$). Nevertheless, the percentage change between day 3 and 7 for proliferation was found to be 75.9% for radiolucent, 76.7% for BaSO₄, 83.0% for TiO₂, 80.6% for ZrO₂, 91.1% for silane-treated TiO₂ and 98.8% for silane-treated ZrO₂. Therefore, although lower yields were obtained for live cells at days 3 and 7, the percentage increase in the number of live cells were highest for cements containing silane-treated TiO₂ and ZrO₂, followed by 10%w/w TiO₂ and ZrO₂ cements and finally BaSO₄ and radiolucent cements. This demonstrates that the radiopacifier used can affect the rate of MC3T3-E1 cell proliferation.

6.4 Discussion

PMMA is not considered bioactive as it does not readily interact and bond with bone.^{74,302,335} This is believed to have contributed to the loosening of the implant at the cement-bone interface and is a significant problem in total joint replacements. As discussed in the introduction, cases of loosened implants were found to be accompanied by bone lysis, resorption and macrophagic reactions^{139,142}. In order to prevent such biological mechanisms, there is a need to encourage osseointegration and enhance the bone growth properties of PMMA bone cements. Several studies have attempted to improve this aspect of bone cement using calcium salts (CaCl₂, Ca(CH₃COO)₂ or Ca(OH)₂) with and without a silane³³⁵, magnesium oxide (MgO)¹⁸⁸, apatite-wollastonite glass ceramic particles³⁰², strontium oxide (SrO)¹⁷⁶, HA¹⁷⁷⁻¹⁷⁹, sodium fluoride (NaF)⁸⁸, and rutile TiO₂¹⁸⁰. The majority of these studies claim to have observed improvements in bone growth properties.

As Table 6.1 demonstrated, anatase TiO₂ had a surface energy similar to HA and significantly higher than PMMA and BaSO₄, whilst yttria-stabilised ZrO₂ had a moderately

higher surface energy than PMMA and BaSO₄. By incorporating materials with higher surface energies into PMMA bone cement, the overall surface energy of the cement was increased. Higher surface energies result in a more hydrophilic surface, which is favourable for cell adhesion and cell interactions³¹⁷. It was expected that the silane coating would significantly decrease the surface energy of the cement, however this did not occur. The wettability of the radiopacifiers were found to influence the overall surface properties of the cement to a greater extent than the silane treatment.

Overall it was found that bone cement containing BaSO₄ or ZrO₂ did not precipitate any mineralisation on the surface of the cement when submerged in SBF over time. Bone cement containing TiO₂ and silane-TiO₂ however, demonstrated some mineralisation after 4 weeks in SBF as crystals were detected by XRD and SEM imaging. This may be linked to the increased surface energy of the cement as a result of using TiO₂. The crystal structure and surface oxides of TiO₂ may also enhance the interaction with calcium ions. Full surface coverage with minerals however, was only achieved after incubation in SBF for more than 4 weeks, demonstrating the process of HA deposition on PMMA *in vitro* requires extended incubation periods.

The morphology of the HA obtained differed from the morphology obtained in other studies. Ciobanu et al.³¹² found that titanium alloy, surface treated with sodium hydroxide (NaOH) solution and heat treated, established petal rose-like HA crystals roughly 2-5 μ m in size, when submerged in a supersaturated calcification solution. Wen et al.³¹³ utilised the same simulated body fluid (SBF) as this study and obtained similar HA morphologies on the surface of titanium-zirconium alloys after just one day. Furthermore, at 8 and 15 days in SBF, a much denser coating of fine HA precipitates were obtained. In a different study which precipitated HA on the surface of porous silicon, the floccules of HA obtained were similar in morphology to the HA obtained in this study and similar peaks were

found using XRD ($\simeq 10^\circ$ and 32°), however the HA precipitates were significantly smaller ($\simeq 100\text{nm}$)³³⁶. Larger ($\simeq 200\text{-}300\text{nm}$) lath-like HA particles were obtained by Mitsionis et al.³³⁷ when precipitating HA in the presence of spherical TiO_2 particles. Lath-like particles were also obtained in this study after 4 weeks in SBF, however the particles were much larger ($10\text{-}100\mu\text{m}$) than the HA precipitates described in the literature. The larger sized HA crystals obtained may be due to the longer soaking periods used (up to 4 weeks) and the surface properties of the cement inducing specific crystal sizes and morphologies to nucleate. Although differences in the HA morphologies were found between the results obtained and the results in the literature, the combination of scanning electron microscopy (SEM) and X-ray diffraction (XRD) have shown the precipitates to be calcium/HA based minerals.

All the studies discussed used scanning electron microscopy (SEM) and X-ray diffraction (XRD) techniques to characterise the HA precipitates. Other techniques that were used in the literature include, energy-dispersive X-ray spectroscopy (EDS / EDAX)^{312,313}, atomic force microscopy (AFM)³³⁶ and fourier transform infrared spectroscopy (FTIR)³³⁷. The use of XRD and SEM techniques to characterise apatite on the surface of materials is specified in the guidelines for the ISO 23317:2007 Standard (Implants for surgery - *In vitro* evaluation for apatite-forming ability of implant materials). This standard is based on a method developed by Kokubo et al.³³⁴ and has been used in numerous other studies²⁴⁷⁻²⁵³. This technique was deemed suitable for establishing the apatite-forming ability of the novel materials tested, however the use of EDAX/EDS would have proved useful in quantifying the amount of calcium deposited on the surface of the novel cement samples.

The results from the osteoblast adhesion experiments correlate well with the results obtained from the HA growth experiment. Cement samples containing either treated or untreated TiO_2 were found to have higher numbers of adhered osteoblast-like cells at each

time point when compared with other cements. The MC3T3-E1 cells on the surface of the cement samples containing TiO₂ were also found to be more spread out and less circular in shape. Cell spreading is important in osteoblast-like cells as it is the process that follows adhesion and precedes proliferation³¹⁵.

Bone cement with silane-treated TiO₂ was found to have high levels of cellular adhesion after 1 hour. This may be due to the functional groups of the silane interacting with the MC3T3-E1 cells. Recent studies have found that MC3T3-E1 osteoblast behaviour and HA formation is enhanced by the functional groups of silanes^{311,331}. Similarly, the silanol group (Si-OH) of silanes was also found to induce apatite formation¹⁸³. As the silane-treated ZrO₂ did not achieve high levels of adhesion after 1 hour, it can be assumed that either the combination of TiO₂ and the silane contributed to the high adhesion rates, or the silane treatment did not work for ZrO₂ as postulated in the previous chapter.

MC3T3 cells are a strain of tissue culture cells derived from *Mus musculus* (house mice) and are widely used as models for osteoblast studies as they are stated to be one of the most convenient and physiologically-relevant systems for the study of osteoblasts³³⁸. Extracting human osteoblast cells is a complex and time consuming process, therefore the MC3T3-E1 cell line was used. The use of MC3T3-E1 cells for assessing attachment, proliferation and mineralisation on the surface of materials is well documented²⁵⁴⁻²⁵⁶.

The adhesion of the MC3T3-E1 cells was tested after 1, 4 and 24 hours incubation as at these time points cell adhesion is most likely to occur. The proliferation tests were carried out after 3 and 7 days incubation as proliferation occurs after cell adhesion and spreading. After 3 days incubation, the majority of MC3T3-E1 cells are likely to have adhered to the cement surface and begun to proliferate. As cells adhered most quickly to the silane-treated TiO₂ surface it was expected that at 3 days the cell proliferation for

silane-treated TiO_2 would be highest. Cell proliferation however was found to be reduced by the presence of the silane when compared to other cement samples. The reduction in cell proliferation was significant for silane-treated ZrO_2 , but not for silane-treated TiO_2 . As the assay method measures the number of living cells, it is possible that the cells on the surface of the silane-treated TiO_2 cement samples attached rapidly, spread and proliferated but died before the 3 day time point, however between 3 and 7 days incubation, a significant increase in the number of living cells were detected for all cements, demonstrating cell proliferation still took place. Furthermore the percentage increase in the number of live cells between 3 and 7 days was found to be highest for cements containing silane-treated TiO_2 and ZrO_2 . Nevertheless, the results for cell proliferation draws questions with regards to the biocompatibility of the silane used. Although methacryloxypropyltrimethoxysilane has been tested in dental and orthopaedic materials, further biocompatibility testing is required if it is to be used in bone cements.

Overall the results from this study accord with previous publications which state that anatase TiO_2 is beneficial for bone growth *in vitro* and in animal studies^{180,278,279,325}. Further *in vitro* tests however are required to investigate the cytotoxicity of the silane-coated TiO_2 cements. For example, rat bone chips can be cultured on the surface of the novel cements to investigate cell behaviour, as a study on coated titanium surfaces has done³³⁹. Once *in vitro* studies prove successful, *in vivo* animal trials can then be undertaken. Trials using similar materials have performed tests on rats¹⁸⁰, rabbits²⁵⁷ and sheep^{138,258}.

6.5 Conclusions

Bone cement containing anatase TiO_2 demonstrated good bone growth properties as a result of TiO_2 increasing the overall hydrophilicity of the cement. Furthermore silane coating the anatase TiO_2 was found to achieve similar HA growth and improved cell adhesion due

to the functional groups of the silane interacting with the osteoblast-like cells. The silane coating however was found to have a detrimental effect on cell proliferation which raises questions with regards to the biocompatibility of methacryloxypropyltrimethoxysilane. Although silane coated anatase TiO_2 has proven to be an effective radiopacifier with potential to enhance the bone growth properties of PMMA bone cement, further cytotoxicity testing is required before any form of *in vivo* testing can be considered.

Chapter 7

Mechanical and structural changes in commercial bone cements due to ageing and moisture uptake

7.1 Introduction

Although there is an extensive literature on bone cement performance, few studies have been conducted on the ageing and moisture uptake of commercial bone cements and the effect this has on mechanical and fatigue properties over time. Bone cement fails predominantly after long-term use and the temperatures and conditions found *in vivo* may contribute to this. A study investigating the degradation of bone cement is of clinical relevance and may provide insight into how conditions experienced *in vivo* contribute to cement failure.

The current published standards for acrylic-based resin cements (ISO5833:2002²²³, ASTM F451-08²²⁴) are ill-defined and do not completely address the ageing effects of physiological conditions. In this Chapter the effects of moisture and temperature, at levels similar to those encountered *in vivo*, on water uptake, mechanical, fatigue, and structural properties were studied over time for two commercial cements.

7.1.1 Diffusion in polymers

Polymers have been known to undergo changes in mechanical and rheological properties when submersed in fluid over time. The extent of these changes can be attributed to the degree of fluid uptake, the nature of the immersion fluid, the temperature, the composition of the polymer and the duration of immersion. Typical changes include an increase in mass and a lowering of the glass transition temperature (T_g , when a polymer changes from a glassy to a rubbery state)³⁴⁰. The effects of physiological salts, body temperature (37°C) and fluid on the compressive strength, flexural properties, fracture toughness and fatigue properties of bone cements however are still unclear.

Diffusion in polymers is a complex process and difficult to predict. It is known that the diffusion of a liquid into a polymer is affected by the physical properties of the polymer network and the interactions between the polymer and the liquid itself. A classification method was proposed by Alfrey et al.³⁴¹, whereby diffusion is classified according to the polymer relaxation rate and liquid diffusion rate. The classifications fall into two categories, Fickian (Case I) and non-Fickian (Case II and anomalous) and can be related by Equation 7.1 where M_t is the amount of solvent absorbed per unit area at time t , k is a constant and n is a parameter related to the diffusion mechanism which lies between 1/2 and 1³⁴².

$$M_t = kt^n \tag{7.1}$$

The majority of polymers are known to follow a Fickian uptake curve (Fick's second law³⁴³), particularly when the temperature is above the glass transition point (T_g) and the polymer chains have high mobility, allowing for easy penetration of the liquid³⁴⁴. This behaviour is characterised by a high polymer relaxation rate, R_{relax} , and a low liquid diffusion rate, R_{diff} ($R_{relax} \gg R_{diff}$). The diffusion distance of this mechanism is proportional to the square root of time and therefore the n parameter is 1/2. Fickian diffusion has been

observed in polymers with plasticisers below the glass transition temperature and the literature shows a maximum value for total percentage weight change of roughly 2%^{50,344}. Interestingly, the diffusion into PMMA of methanol with water was found to follow Fickian diffusion below the glass transition temperature as water acted as a plasticiser, which increased chain mobility allowing for further water penetration³⁴⁴.

Non-Fickian diffusion is usually observed in glassy polymers below the glass transition temperature, where the polymer chains are not mobile enough to permit diffusion of liquids. Two non-Fickian diffusion processes can occur, case II and anomalous. These processes differ by the rates with which the liquid diffuses into the polymer. For case II diffusion, the rate is much higher than the polymer relaxation rate ($R_{diff} \gg R_{relax}$), whilst for anomalous diffusion, the rates are roughly the same ($R_{diff} \simeq R_{relax}$). For case II diffusion, the diffusion distance is directly proportional to time so n is equal to 1 and for anomalous diffusion, the rate is between that of Fickian diffusion and case II diffusion so n is between 1/2 and 1³⁴².

Water uptake in bone cements can arise through any of these diffusion processes, however Fickian diffusion is most likely as water may act as a plasticiser for bone cements. The actual mechanism of water uptake in polymers varies but can arise due to fluid occupying vacancies in the material, such as pores or voids, or by water diffusing between intermolecular spaces.³⁴⁵ With PMMA bone cements, vacancies are created by entrapped air during mixing and by leaching monomer. Water molecules are also small enough to diffuse into spaces within radiopacifier agglomerations and between the polymer molecules. The latter is more pronounced as a result of plasticisation and higher temperatures, which causes the polymer chains to relax and increase the intermolecular spaces. Fluid can therefore diffuse into bone cements either without any relationship to the polar molecules in the material (free volume theory) or it can be governed by specific molecular interactions^{346,347}.

7.2 Methods

7.2.1 Materials

Cemex Isoplastic was obtained from Tecres (Sommacampagna, Italy) and Palacos R was provided by Heraeus (Newbury, UK). Sodium chloride ($\geq 99.9\%$), potassium chloride ($\geq 99\%$), calcium chloride ($\geq 99\%$) and sodium bicarbonate ($\geq 99.7\%$) were purchased from Fisher Scientific (Fisher Scientific UK Ltd, Loughborough, UK).

7.2.2 Ageing conditions

Cemex Isoplastic and Palacos R compression and bending samples were prepared as described in Chapter 2. The compression test samples were weighed to an accuracy of $\pm 0.1\text{mg}$ prior to ageing. Both bending and compression samples were then aged in air at 23°C for 1, 2, 3, 7, 15 and 60 days or submerged in Ringer's solution at 37°C for the same periods. The Ringer's solution was replaced every 2 weeks. Ringer's solution (8.6mg/mL NaCl, 0.3mg/mL KCl and 0.33mg/mL CaCl_2 , buffered to a pH of 7.4 with NaHCO_3 ²⁷⁶) was selected as it is an isotonic solution and large quantities can be easily prepared. The solution was buffered to ensure a consistent pH throughout the experiment, as occurs *in vivo*. Control samples were aged according to the ISO5833 standard²²³ in air for 24 hours.

7.2.3 Moisture uptake and mechanical testing

After each time point the compression test samples were removed from their medium and the surface blotted dry with filter paper. The samples were then weighed and Equation 7.2 was used to establish the percentage change in mass. The samples were then tested in compression and bending samples were tested at each time point as outlined in Sections 2.3.1 and 2.3.2 respectively.

$$\% \text{ weight gain} = \frac{M_t - M_o}{M_o} \times 100 \quad (7.2)$$

Where:

M_t	Weight of the sample at time t
M_o	Weight of the sample at start (t=0)

7.2.4 Mathematical modelling

Three different types of diffusion can occur with PMMA bone cements (page 156). To better understand the type of diffusion taking place, Equation 7.1 ($M_t=kt^n$) was applied to moisture uptake at different time points (0-3 days and 3-60 days). As the amount of solvent absorbed per unit area (M_t) can be indirectly measured by the change in weight of the material, the total percentage weight change was used. Fickian and case II diffusion equations were applied to the data and the goodness of fit was investigated using the curve fitting toolbox in Matlab (MathWorks, Cambridge, UK), which calculated the coefficients by minimizing the sum of squared residuals. A modification to Equation 7.1, in the form of an additional coefficient to model leaching components from the cement was made to better model the data obtained.

7.2.5 Fracture toughness

Fracture toughness was tested for samples aged in air for 24 hours at 23°C and Ringer's solution for 60 days at 37°C as described in Section 2.4 to establish differences between aged samples and samples tested according to the ageing conditions outlined by the ISO5833 standard.

7.2.6 Fatigue testing

Four fatigue samples of each cement brand were prepared as described in Section 2.5. Two samples were aged in air at 23°C and the other two samples were aged in Ringer's solution at 37°C for a minimum of 60 days prior to testing.

7.2.7 Scanning electron microscopy

Scanning electron microscopy was used to analyse the fracture surfaces of fatigue samples aged in air and Ringer's solution.

7.2.8 Vickers hardness

Disc shaped samples were prepared and tested as described in Section 2.6 after 24 hours ageing in air at 23°C and 60 days ageing in Ringer's solution at 37°C.

7.2.9 Glass transition temperature

The glass transition temperature of samples aged in air for 24 hours and Ringer's solution for 60 days at 37°C was measured as described in Section 2.7.

7.2.10 Structural changes

Structural changes were monitored by Fourier Transform Infrared Spectroscopy (FTIR) using a Perkin Elmer Spectrum One FT-IR Spectrometer with FT-IR Spectrum software (Perkin Elmer, Massachusetts, USA) at the Cardiff School of History, Archaeology and Religion. Measurements were taken between 4000cm^{-1} and 450cm^{-1} with a resolution of 4cm^{-1} . Samples were scanned after being aged 24 hours in air at 23°C and 60 days in Ringer's solution at 37°C. The surface of aged bending samples was scanned using attenuated total reflectance (ATR) at 6 different sections on the sample, taking 30 scans at each section to obtain an average spectrum representative of the entire sample. To ensure components from the Ringer's solution did not interfere with FTIR measurements, samples were washed with deionised water and dried prior to scanning. To obtain a spectrum representing both the outer and inner parts of the sample a clean and sterile file was used to remove a small cross section of the sample and 1mg of the sample was combined and compressed with 100mg of potassium bromide (KBr) in a pestle and mortar until a fine uniform powder was obtained. The powder was then placed in a disc shaped

press between two stainless steel disks and subjected to a force of 10kN for 30 seconds, followed by 100kN for 30 seconds to create discs. Two discs were prepared per sample and 30 scans per sample were carried out to obtain an accurate spectrum.

7.3 Results

7.3.1 Moisture uptake

Figure 7.1 shows the weight changes of Palacos R and Cemex aged in Ringer's solution at 37°C or in air over the square root of time. This type of plot was employed to demonstrate Fickian diffusion, indicated by a linear relationship between moisture uptake and the square root of time. Both commercial cements aged in Ringer's solution experienced a total weight gain of around 1.5-2% whilst samples aged in air experienced a loss in weight of around 0.3%. The linear portions of the curves for samples aged in Ringer's solution occur within the first 7 days (168 hours/12.96 square root of hours), after which water absorption continued at a slower rate. Equilibrium for both cements was reached after

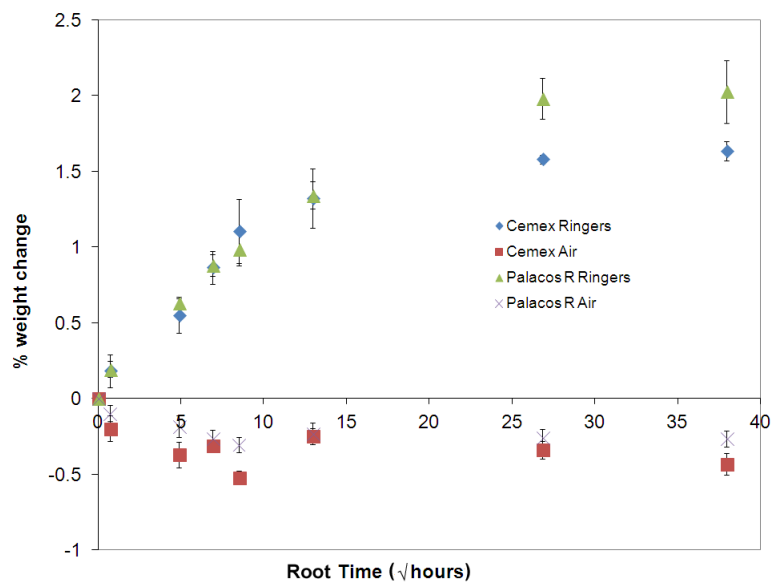


Figure 7.1: Moisture uptake over time for Cemex and Palacos R in Ringer's solution and in air

30 days and overall Palacos R had greatest moisture uptake at the end of the study (60 days).

7.3.2 Mathematical modelling

Figures 7.2(a) and 7.2(b) show the goodness of fit between the real datum and the datum obtained from the models. Similarly, Tables 7.1 and 7.2 show the results of modelling moisture uptake for Cemex and Palacos R respectively. For both cement brands the modified Equation 7.1 ($M_t = b + kt^n$) fit the data most accurately. This equation used an additional constant (b) to represent the leaching of monomer thereby creating vacancies for the water to diffuse into. For the first 3 days, both cements fitted a Fickian diffusion model well ($R\text{-value} \geq 0.95$) and when using Equation 7.1 ($M_t = kt^n$) Cemex and Palacos R had n values of 0.526 and 0.354 respectively, signifying a close relationship to Fickian diffusion. After 3 days however, the diffusion slowed and was no longer Fickian. The additional coefficient did not improve the goodness of fit for both cements between 3 and 60 days in Ringer's solution. This demonstrates the leaching monomer does not affect the moisture uptake after 3 days in Ringer's solution. The case II diffusion equation produced the poorest fit for all the data modelled and therefore water absorption was considered to be non-linear with time.

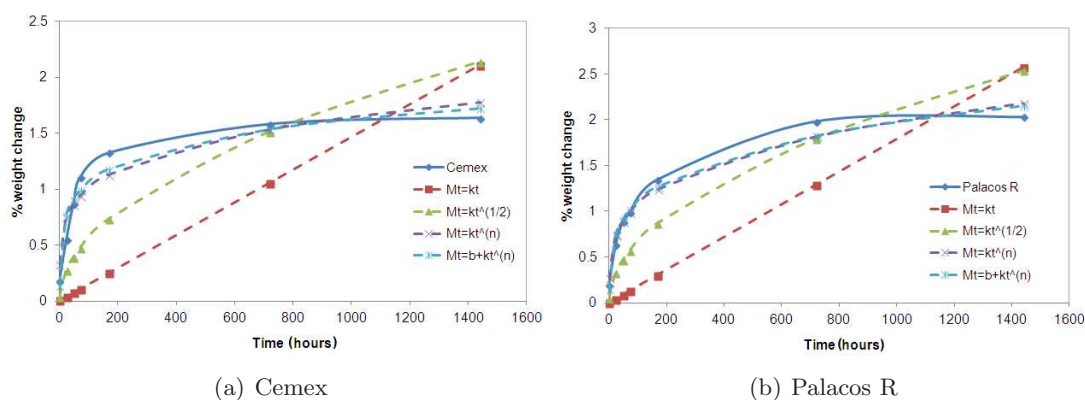


Figure 7.2: Moisture uptake data and model data for (a) Cemex and (b) Palacos R over time in Ringer's solution

Table 7.1: Mathematical modelling of diffusion types to moisture uptake results for Cemex

		Fickian	Case II	Equation 7.1	Modified equation 7.1
		$M_t = kt^{1/2}$	$M_t = kt$	$M_t = kt^n$	$M_t = b + kt^n$
Entire curve	k	0.056	0.001	0.380	1.581
	n	0.500	1.000	2.11	0.091
	b	-	-	-	-1.346
	R-value	0.2340	-1.0631	0.9144	0.9445
0-3 days	k	0.126	0.017	0.114	0.031
	n	0.500	1.000	0.526	0.801
	b	-	-	-	0.162
	R-value	0.9688	0.8662	0.9693	0.9992
3-60 days	k	0.052	0.001	0.798	0.463
	n	0.500	1.000	0.100	0.137
	b	-	-	-	0.400
	R-value	-0.6748	-28.7763	0.9674	0.9636

Table 7.2: Mathematical modelling of diffusion types to moisture uptake results for Palacos R

		Fickian	Case II	Equation 7.1	Modified equation 7.1
		$M_t = kt^{1/2}$	$M_t = kt$	$M_t = kt^n$	$M_t = b + kt^n$
Entire curve	k	0.067	0.001	0.319	0.568
	n	0.500	1.000	0.264	0.204
	b	-	-	-	-0.345
	R-value	0.6462	-0.3002	0.9719	0.9784
0-3 days	k	0.123	0.016	0.217	0.132
	n	0.500	1.000	0.354	0.451
	b	-	-	-	0.095
	R-value	0.9572	0.6390	0.9929	0.9961
3-60 days	k	0.063	0.002	0.526	0.443
	n	0.500	1.000	0.191	0.208
	b	-	-	-	0.103
	R-value	-0.6748	-5.3414	0.9078	0.9052

7.3.3 Mechanical properties

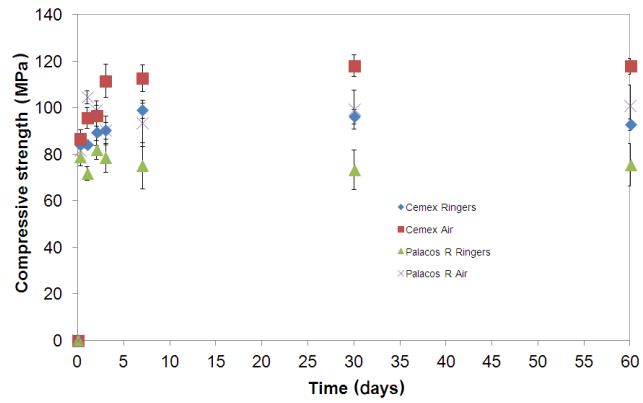
Figures 7.3(a), 7.3(b) and 7.3(c) show the compression, bending modulus and bending strength respectively for Palacos R and Cemex aged in Ringer's solution at 37°C and in air. For all mechanical properties, samples aged in air had significantly higher values compared to samples aged in Ringer's solution after 60 days (ANOVA, $p=1.98 \times 10^{-03}$ for Palacos R and $p=9.07 \times 10^{-07}$ for Cemex). At 24 hours, Palacos R had higher compressive strength but as the cement cured, Cemex became stiffer and stronger in compression. All compressive strength values were found to reach a maximum after 30 days and all cements were found to experience a peak in mechanical properties at around 24-48 hours. For bending strength and bending modulus it was difficult to establish subtle changes over time due to high variance experienced between samples, caused by the presence of pores. Nevertheless, after 60 days, Cemex samples aged in air had a significantly higher bending modulus than samples aged in Ringer's solution ($p=0.02$). There was no significant difference in bending strength after ageing in air or Ringer's solution after 60 days for Cemex ($p=0.13$) and Palacos R ($p=0.18$). Similarly Palacos R samples aged in air did not have a significantly different bending modulus than samples aged in Ringer's solution ($p=0.16$).

7.3.4 Fracture toughness

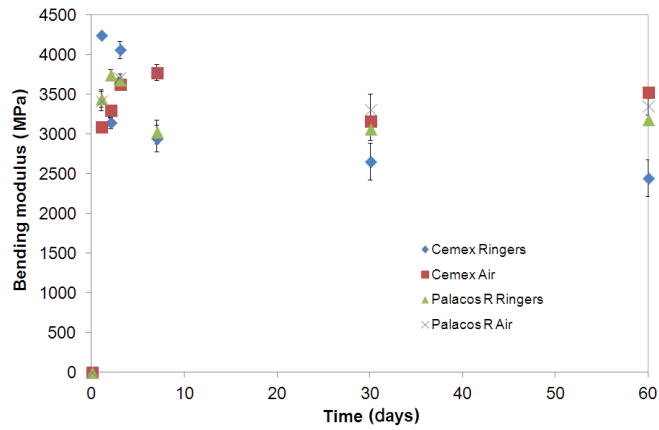
From fracture toughness tests, both commercial cements experienced a significant loss in critical stress intensity factor after ageing in Ringer's for 60 days ($p=2.63 \times 10^{-03}$ for Cemex and $p=3.87 \times 10^{-04}$ for Palacos R), as shown in Table 7.3.

Table 7.3: Fracture toughness of Cemex and Palacos R cements before and after ageing in Ringer's for 60 days

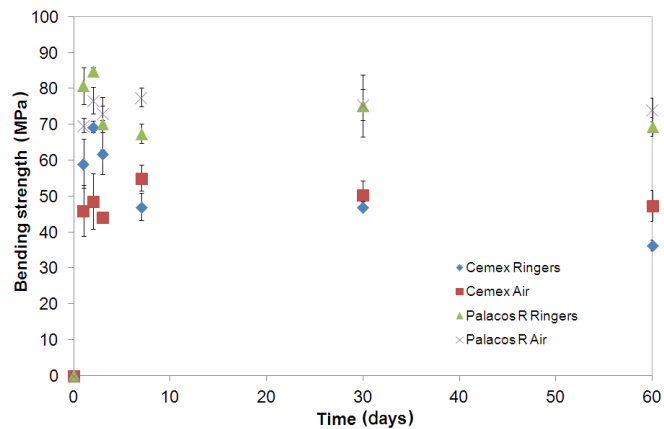
Critical stress intensity factor (K_{IC}) / MPam ^{1/2}		
Cemex	Air 1 day	1.7±0.1
	Ringer's 60 days	1.4±0.1
Palacos R	Air 1 day	2.5±0.2
	Ringer's 60 days	1.5±0.3



(a) Compression



(b) Bending modulus



(c) Bending strength

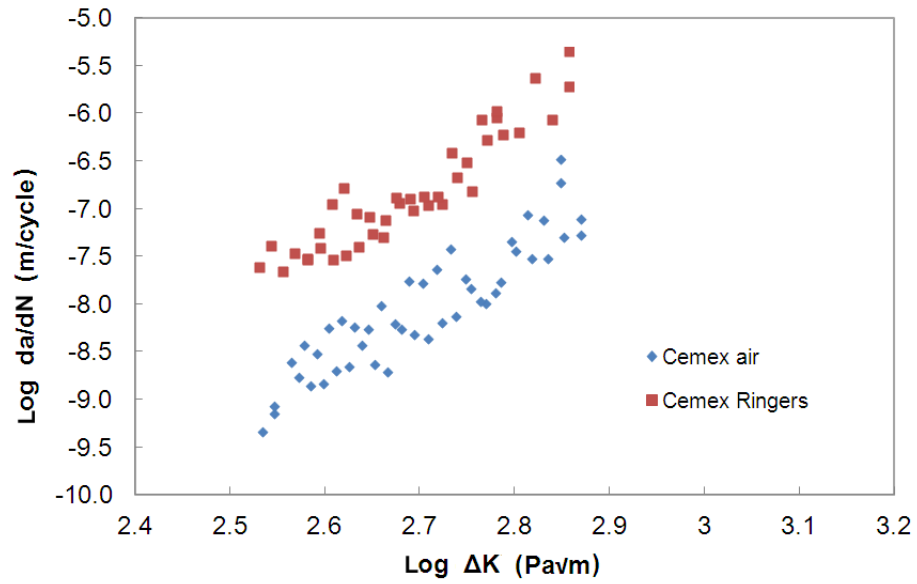
Figure 7.3: Changes in mechanical properties of Cemex and Palacos R over time in Ringer's solution and in air

7.3.5 Fatigue testing

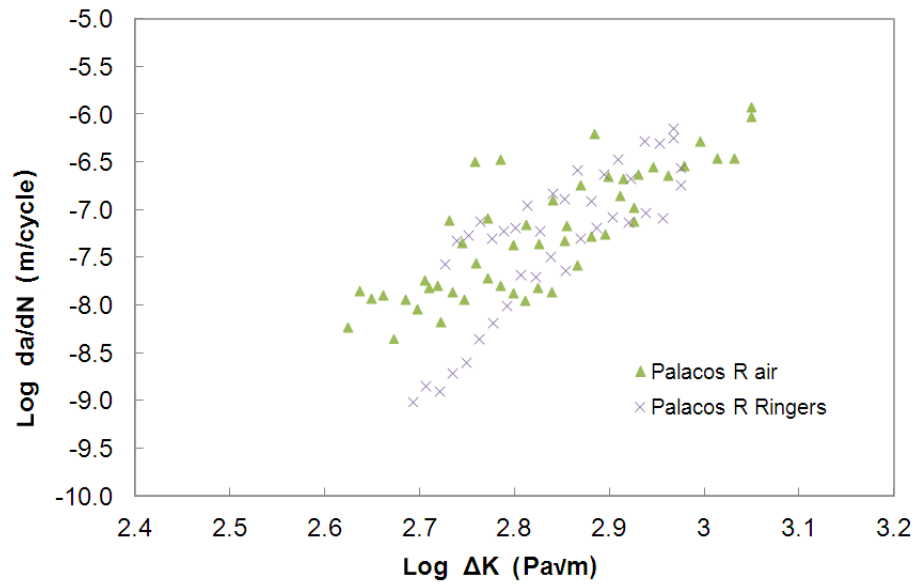
Figures 7.4(a) and 7.4(b) show the fatigue test results for Cemex and Palacos R respectively when aged in air and in Ringer's solution at 37°C for 60 days. Both cements experienced a reduction in fatigue properties as a result of ageing in Ringer's solution. Cemex aged in Ringer's solution experienced increased crack growth rates for all stress intensities, whilst Palacos R aged in Ringer's solution experienced a lesser detrimental effect on crack growth rates at high stress intensities. The change in crack growth rate for Palacos R was much more severe as the stress intensity increased as shown by a steeper slope. These results are highlighted when the Paris Law is applied to the data as shown in Table 7.4. Cemex samples aged in Ringer's solution experienced an increase in fatigue constants 'A' and 'm', whilst Palacos R increased slightly in fatigue constant 'A' and significantly in fatigue constant 'm'. All fatigue samples were found to have correlation coefficients above 0.60 when the Paris Law was applied, demonstrating a moderate to strong positive correlation between the data and the Paris Law. Palacos R had lower correlation coefficients when compared to Cemex, due to variations in the crack growth rates of the samples tested.

Table 7.4: Fatigue test constants of Cemex and Palacos R cements before and after ageing in Ringer's for 60 days. 'A' is the crack growth at $\Delta K=1\text{MPam}^{1/2}$ and 'm' is the slope of the data

	A		m		Correlation coefficient	
	1 day air	60 days Ringer's	1 day air	60 days Ringer's	1 day air	60 days Ringer's
Cemex	5.39×10^{-07}	1.29×10^{-05}	5.92	6.20	0.82	0.86
Palacos R	3.73×10^{-07}	7.34×10^{-07}	4.65	7.33	0.67	0.66



(a)



(b)

Figure 7.4: Fatigue results for (a) Cemex and (b) Palacos R over time in Ringer's solution and air

7.3.6 SEM images

The fracture surfaces for samples aged in Ringer's solution for 60 days were found to be rougher, containing a greater amount of small cracks (Figure 7.5) Fracture surfaces for both cements were found to have high levels of porosity before and after ageing in Ringer's solution.

7.3.7 Vickers hardness

Similar to fracture toughness, both commercial cements experienced a significant reduction in hardness after ageing in Ringer's solution at 37°C for 60 days ($p=5.53 \times 10^{-06}$ for Cemex and $p=0.03$ for Palacos R, Table 7.5).

Table 7.5: Vickers hardness of Cemex and Palacos R cements before and after ageing in Ringer's for 60 days

		Hardness (HV30/10) / MPa
Cemex	Air 1 day	24.8±2.0
	Ringer's 60 days	19.1±2.0
Palacos R	Air 1 day	19.8±1.8
	Ringer's 60 days	17.5±2.6

7.3.8 Glass transition temperature

Table 7.6 shows the glass transition temperatures obtained by dynamic mechanical thermal analysis for Cemex and Palacos R before and after ageing in Ringer's solution for 60 days at 37°C. A significant reduction in glass transition temperature was experienced for both Cemex ($p=3.60 \times 10^{-04}$) and Palacos R ($p=7.12 \times 10^{-04}$).

Table 7.6: T_g of Cemex and Palacos R cements before and after ageing in Ringer's for 60 days

		Glass transition temperature (T_g) / °C
Cemex	Air 1 day	127.3±1.6
	Ringer's 60 days	121.6±1.4
Palacos R	Air 1 day	126.2±3.3
	Ringer's 60 days	117.9±1.2

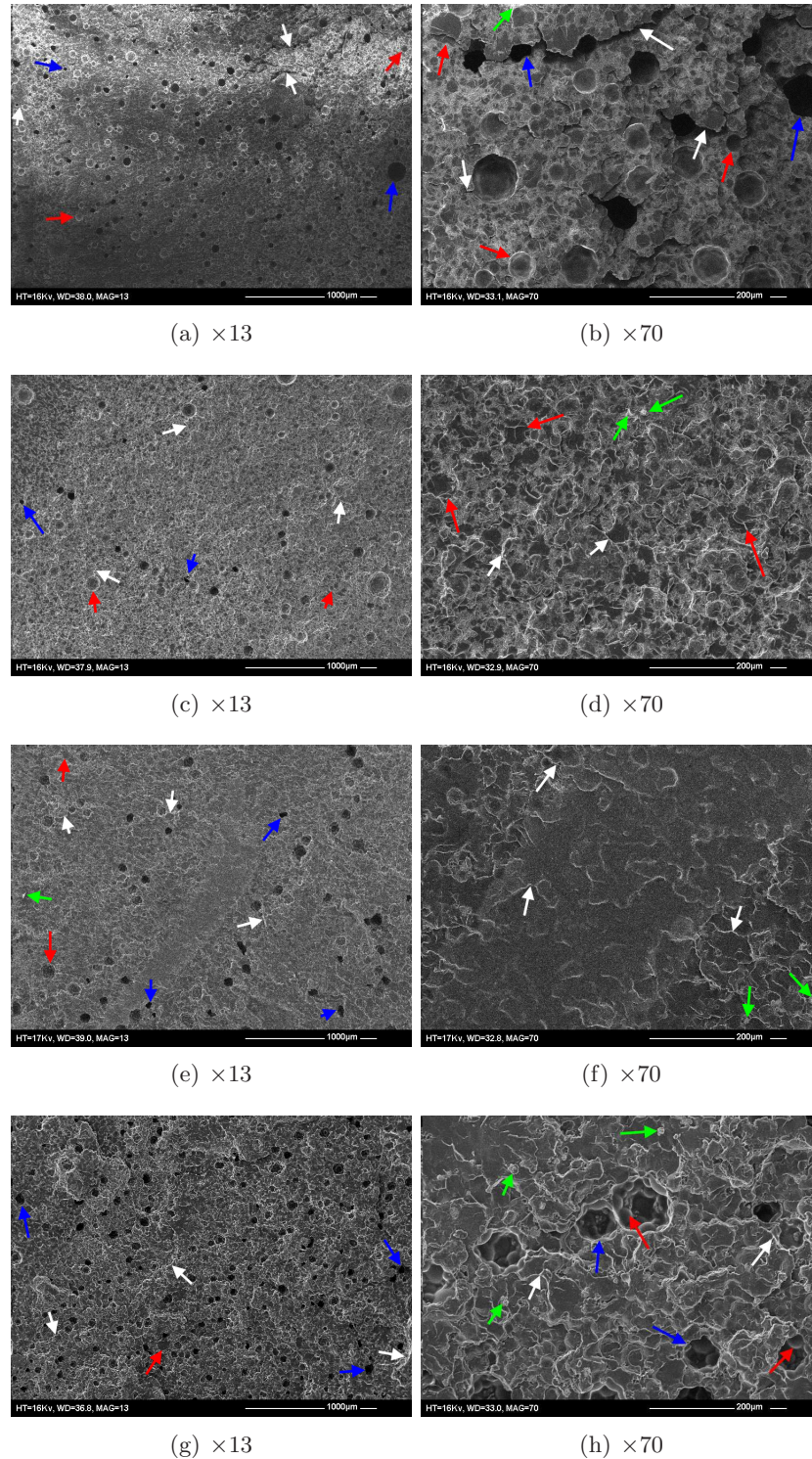


Figure 7.5: SEM images of the fracture surfaces of (a-b) Cemex aged in air, (c-d) Cemex aged in Ringer's solution, (e-f) Palacos R aged in air and (g-h) Palacos R aged in Ringer's solution - Red arrows indicate the location of PMMA beads, green arrows indicate radiopacifier particles, blue arrows indicate pores and white arrows indicate microcracks

7.3.9 Structural changes

Figure 7.6 shows the FTIR spectra obtained using ATR on the surface of samples and Figure 7.7 shows the FTIR spectra obtained using KBr discs of the cross section of samples for Cemex and Palacos R before and after ageing in Ringer's solution. Comparing the molecular structure of PMMA and the FTIR peaks obtained, characteristic bonds that form PMMA were found to be present in the FTIR spectra. The two peaks between 2850cm^{-1} and 2950cm^{-1} represent methylene (CH_2) and methyl (CH_3) stretches. Sharp peaks found at 1400cm^{-1} and 1450cm^{-1} also represent the methyl group (CH_3) of PMMA. Peaks found between 1300cm^{-1} and 1500cm^{-1} are attributed to the bending of CH molecules. The single peak at 1730cm^{-1} represents a C=O stretch, the peak at 1250cm^{-1} represents the C-C-O stretch, the peak at 1150cm^{-1} represents an O-C-C stretch and peaks between 1300cm^{-1} and 900cm^{-1} represent C-O stretches. ZrO_2 , the radiopacifier for Palacos R also has peaks between 2800cm^{-1} and 2950cm^{-1} , around 1450cm^{-1} , 1370cm^{-1} , 750cm^{-1} and a broad peak at 500cm^{-1} . BaSO_4 , used in Cemex has two large peaks located around 1000cm^{-1} and 550cm^{-1} . These peaks coincide with PMMA peaks and are assumed to be present.

Several changes occurred to the FTIR spectra as a result of ageing. Increases in peak intensity signify an increase in the number bonds formed and a shift in the position of peaks demonstrates a change in one chemical bond in favour of another. It was found that changes occurred to both cement brands after ageing for 60 days in Ringer's solution. The changes were only observed on ATR scans and not when using KBr discs. A decrease in intensity of peaks located between 2850cm^{-1} and 2950cm^{-1} were observed and is characteristic of a transition from unsaturated alkenes ($\text{C}=\text{C}$) to saturated alkanes ($\text{C}-\text{C}$), as occurs in the polymerization of MMA in PMMA and also indicates the absence of unreacted monomer, which leaches out of the cement over time. Similarly increases in peaks at 1730cm^{-1} , between 900cm^{-1} and 1300cm^{-1} were found, demonstrating an increase in

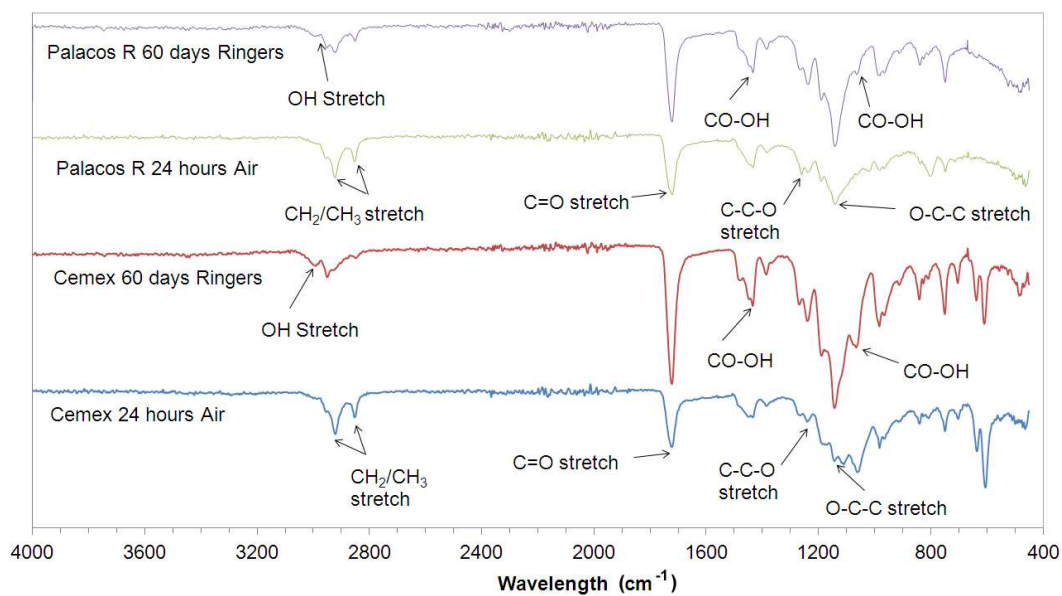


Figure 7.6: FTIR spectra using ATR of Cemex and Palacos R after ageing in air for 24 hours and Ringer's solution for 60 days

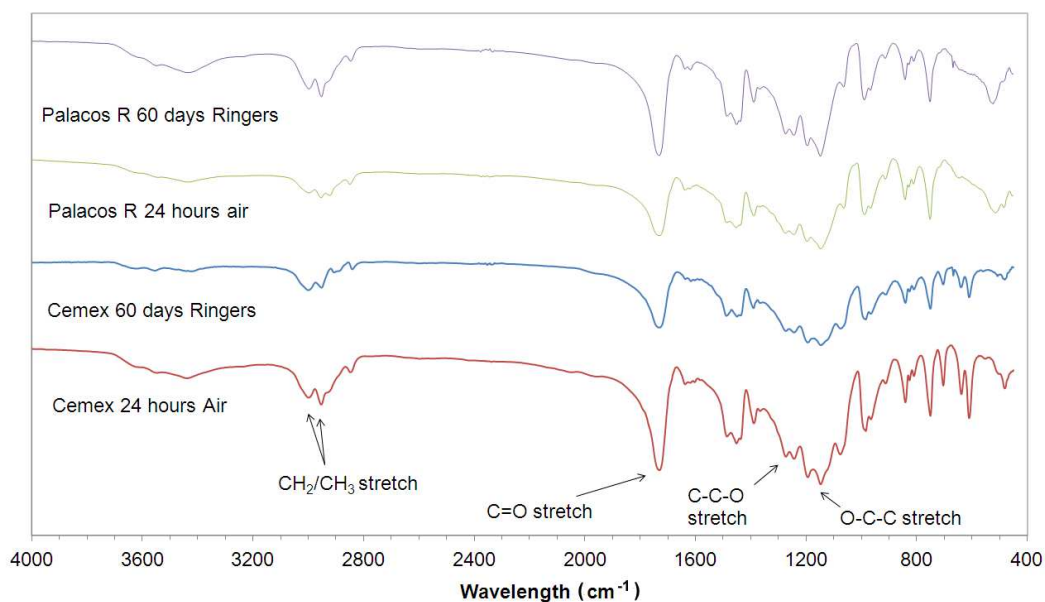


Figure 7.7: FTIR spectra using KBr discs of Cemex and Palacos R after ageing in air for 24 hours and Ringer's solution for 60 days

the number of C=O and C-O bonds as the cement polymerises and forms new bonds. The increase in peak intensity of ATR scans demonstrates the slow polymerisation of the outer layers of the cement over 60 days after mixing.

A peak located at 3000cm^{-1} began to develop whilst peaks at 2800cm^{-1} were found to decrease in intensity for ATR scans. This demonstrates a shift from CH stretches to OH stretches, which signifies CH bonds are slowly being converted to OH bonds. Similarly the peak located at 1430cm^{-1} and the peak located at 1060cm^{-1} were found to increase in intensity for ATR scans. This supports the theory that carboxyl groups (-COOH) are forming. These changes were only present on surface ATR scans and not KBr scans that use a cross-section of the cement. Therefore water is thought to only penetrate a short distance and not diffuse deep into the bulk of the cement over 60 days at 37°C .

7.4 Discussion

The mechanism of moisture uptake and ageing in PMMA bone cements is of clinical relevance as changes to the material properties over time may affect the performance of the cement and influence the likelihood of failure.

Three processes are thought to occur simultaneously during the ageing of bone cement: the cement polymerises further over a prolonged period of time, increasing the strength and modulus of the cement, unreacted monomer and other components will diffuse out of the cement and water will penetrate into the cement. Although several studies have been conducted with regards to structural and molecular changes^{149,150,348}, few have investigated moisture uptake and mechanical properties as a result of ageing. Therefore, this chapter considers moisture uptake and changes in mechanical, fatigue and structural properties using *in vitro* techniques in an attempt to better understand how *in vivo* conditions may contribute to cement failure.

To fully investigate how cement ages clinically, the cement must be subjected to *in vivo* conditions, which would require the removal of working implants. This can only be justified when implant failure occurs. Should the implant fail, the amount of cement available for testing would be limited and the cement would have been exposed to high stresses in the removal process, which in turn would affect the results obtained. The mixing and implant techniques adopted by the surgeon may also vary, influencing the properties of the cement, measuring moisture uptake over time would be difficult and all cement samples would have experienced different loading conditions. Therefore, for this particular study, *in vivo* tests were not carried out and cement retrievals were not used. *In vitro* conditioning of pre-moulded samples was adopted with a similar temperature, moisture, pH and salt concentration as found *in vivo*. Ringer's solution contains approximately the same concentration of Cl^- ions found in body and interstitial fluids²⁷⁶. It allowed for individual samples to be fully immersed and the solution to be changed regularly. Lipid solutions have been shown to be a preferable ageing medium as they replicate the fatty conditions found in bone marrow⁵⁰, however the shelf life of lipid solutions⁵⁰ would not suit the time scale of this study and may have interfered with FTIR measurements.

The increase in weight over time for samples aged in Ringer's solution was caused by the diffusion of water into the cement³⁰⁹. Similar levels of moisture uptake (1.8-2%) have been reported with other polymers^{50,349}. Although PMMA is a hydrophobic polymer, studies have shown it to absorb up to 2% of its weight in water³⁵⁰⁻³⁵². A recent study by N'Diaye et al.³⁵³ demonstrated that PMMA swells when submerged in water. This increase in mass may be beneficial in reducing shrinkage stresses associated with bone cements. The commercial bone cements achieved a total moisture uptake of between 1.5% and 2.3%. Palacos R had a greater moisture uptake when compared to Cemex due to the presence of methyl acrylate in Palacos R, which is more hydrophilic than methyl methacrylate. Therefore, the composition of the cement plays a role in the extent of mois-

ture uptake. For both cements, there was a linear relationship between weight change and the square root of time for the first 7 days. Mathematical modelling demonstrated that the initial diffusion of water into the cement follows Fickian diffusion, but only up to 3 days in Ringer's solution. This result is similar to a study by Grinstead et al.³⁴⁴ where Fickian diffusion was observed below the glass transition point of polymers as result of the plasticising effect of water. The standard deviations of the results for the initial moisture uptake period were large, demonstrating variance in the amount of water absorption. The variability in the levels of moisture uptake after initial immersion has implications on the efficiency and control of antibiotic release from bone cement. The decrease in weight experienced by samples aged in air occurred as a result of residual monomer from the polymerisation reaction evaporating over time. Although a decrease in weight was demonstrated for samples aged in air, the amount of MMA evaporating fluctuated, with no linear correlation between change in weight and time. It can be assumed that samples aged in Ringer's solution also experience leaching of the residual monomer. This is further highlighted by the improved goodness of fit for the mathematical models using the additional coefficient for leaching monomer (b). The goodness of fit was only improved for samples aged in Ringer's solution up to 3 days. Between 3 and 60 days the models were not improved when using the additional coefficient. Therefore it is thought that the leaching monomer does not influence moisture uptake beyond 3 days immersion. The initial diffusion of water into bone cement is thought to be governed by vacancies in the cement, whereby leaching monomer molecules are replaced by water molecules. This mechanism results in a dramatic increase in moisture uptake over the first 3 days, which slows as the amount of leached monomer reduces. After the initial uptake of water, diffusion between the polymer molecules is thought to take place at a lower rate, as water molecules slowly diffuse between the polymer chains. This period of moisture uptake may also be influenced by molecular changes in the cement and the relaxation of the polymer chains. The plasticising effect of water may increase chain mobility, allowing for water

to penetrate deeper into the cement. Similarly, porosity in the cement may prolong the moisture uptake process by creating pathways for further diffusion.

When examining changes in mechanical and structural properties, it was observed that the cement polymerised slowly over months, creating interpenetrating molecular networks, which in turn increased the strength and modulus of the cement. The major changes in mechanical properties occurred within the first few hours after mixing. It was also found that samples aged in Ringer's solution for 60 days always had poorer properties than samples aged in air for the same amount of time. This is due to water acting as a plasticiser and inducing structural changes and degradation in the polymer matrix as described by other authors^{147,348}. Samples aged in Ringer's solution were found to reach an equilibrium value for moisture uptake after 30 days, which coincided with the time when equilibrium values for compression and bending properties were achieved. This would indicate changes in mechanical properties lessen as water content reaches a maximum. Samples aged in Ringer's solution were also found to fail in a less brittle manner. Fatigue samples aged in Ringer's solution demonstrated this with rougher fracture surfaces. Schmitt et al.³⁴⁹ found that long-term soaking in Ringer's solution improves fatigue crack propagation resistance. It was theorised that water absorption increases polymer chain mobility and enhances crack tip blunting. This however, was not observed in this study as fracture toughness and fatigue properties were reduced after ageing in Ringer's solution. Degradation of the cement as a result of ageing may have caused the observed decrease in fracture toughness and fatigue properties.

The outermost surface of bone cement experiences the most water penetration and therefore is more prone to degradation and structural changes as a result of ageing in isotonic fluid. Hardness tests on the surface of samples demonstrated that the material softened over time when aged in Ringer's solution. Furthermore, FTIR scans highlighted structural

changes on the surface of samples (using ATR), but not through the bulk (cross-section) of the cement (using KBr). The increase in intensity of peaks for ATR scans may be attributed to molecular bonds continuously forming on the outermost layers of the cement. This is consistent with previous studies that state when bone cement is mixed, polymerisation occurs most rapidly in the centre of the cement mass, where the most heat is generated, whilst the outermost layers polymerise more slowly and less completely^{354,355}.

Polymers have been known to undergo hydrolysis when immersed in acidic conditions at high temperatures. The acid acts as a catalyst for the reaction and under weak acidic conditions, hydrolysis of the polymer may occur slowly over time. As OH groups were found to form when bone cement was immersed in Ringer's solution at 37°C, it is possible that hydrolysis of the ester groups of PMMA caused the change in polymeric structure. Any localised acidic pH in the area of the implant may further accelerate this reaction *in vivo*. This process results in the formation of methanol (CH₃OH) and carboxylic acid (-COOH) (as shown in Figures 7.8(a) and 7.8(b) for MMA and PMMA respectively). This theory has been postulated by other authors and demonstrated using a variety of techniques^{149,150}. Bettencourt et al.¹⁵⁰ found changes in the wetting properties and the

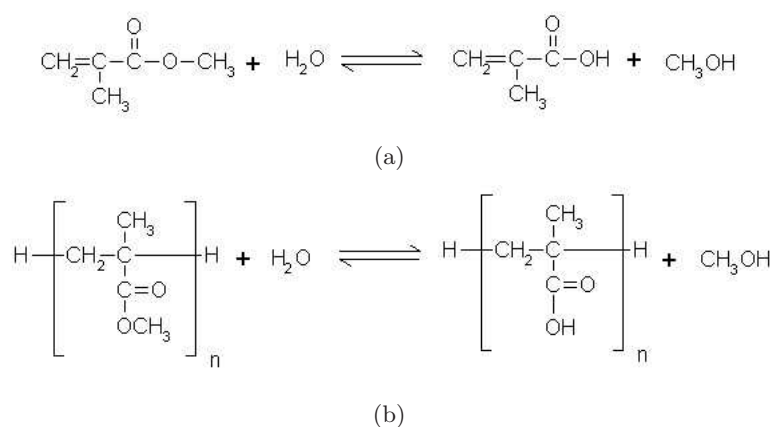


Figure 7.8: Hydrolysis of ester groups in (a) MMA and (b) PMMA

molecular structure of PMMA bone cement arising from artificial ageing using contact angle measurements and X-ray photoelectron spectroscopy (XPS). Hughes et al.¹⁴⁹ used gel permeation chromatography (GPC) to demonstrate changes in molecular weight and FTIR to demonstrate chemical changes in artificially and physiologically-aged cement. The changes observed by Hughes and Bettencourt were similar to the results of this study. Oonishi et al.³⁴⁸ also used FTIR to study structural changes of retrieved CMW1 cement samples. CMW1 cement, however did not undergo structural changes, as experienced with Cemex and Palacos R in this study. Structural changes in Cemex and Palacos R were further highlighted by a reduction in the glass transition temperature. Since the glass transition temperature is dependent upon molecular weight it can be assumed that a reduction in the molecular weight would also have occurred as a result of ageing. These findings correlate well with the majority of ageing studies on PMMA^{148–150,340}. A reduction in both these properties would result in polymer chains having greater mobility at body temperature. This greater mobility can be attributed to scission of polymer chains, via the hydrolysis mechanism outlined above, and would result in the cement behaving in a more elastic and less brittle manner, as observed in the results.

Overall, moisture uptake in two commercial bone cements were found to reach a maximum value of roughly 2% after 30 days. The amount of moisture uptake is dependent upon the composition of the cement. Initial water absorption is thought to occur via a Fickian process, governed by vacancies created by the leaching monomer and entrapped air, after which anomalous diffusion is thought to follow at a slower rate as the polymer chains relax and increase their intermolecular spacings. Maximum saturation of water was accompanied by a decrease in the mechanical, fatigue and fracture toughness properties. The reduction in these properties is attributed to the structural changes that PMMA undergoes as a result of hydrolysis over time. To prevent hydrolysis, novel hydrophobic materials may be incorporated in bone cement to alter surface properties. Gbureck

et al.¹⁸² incorporated a bifunctional coupling agent into the monomer of bone cement to successfully enhance hydrolysis resistance at the metal-polymer interface. This study has also highlighted the limitations of the ISO5833 guidelines for testing bone cements, which obtained significantly different results from aged cements. Physiological conditions are known to differ greatly from those specified by the standard. Boneloc cement, which performed to the requirements of the standard at room temperature failed clinically due to the temperatures experienced *in vivo*¹⁵¹. Therefore there is a need to improve current testing standards to address the effects of physiological conditions. Immersion in an isotonic fluid at high temperatures (e.g. 60°C) for a short period of time may be sufficient to accelerate the diffusion process and thus, the ageing of the cement.

Although a variety of properties of bone cement after ageing have been investigated, there are several limitations to this study. The samples were unloaded when aged in a basic isotonic fluid. *In vivo* it is expected that the cement will be subjected to loading and unloading regimes. It is also expected that the environment experienced *in vivo* is more hostile with the cement interacting with cells, enzymes, lipid material and wear particles. This may have a greater impact on the changes experienced in terms of molecular, mechanical and crack propagation properties. A great deal of variance was noted in the bending properties of aged cement as a result of variance between sample batches. Furthermore, the results from the tests conducted can be influenced by factors such as porosity and the presence of stress raisers, such as voids and agglomerations. Static tests do not replicate the loading conditions that occur *in vivo*. Nevertheless, the range of *in vitro* tests employed, which cover properties and loading conditions relevant to *in vivo* circumstances, can be used to establish baseline performance for comparative purposes.

7.5 Conclusions

Polymers have been known to undergo time-dependant changes in mechanical and rheological properties when submerged in aqueous fluid. The extent of these changes can be attributed to the amount of fluid uptake, the type of fluid, the surrounding temperature, the composition of the polymer and the immersion time³⁴⁰. Initial diffusion of water into PMMA bone cement was found to be Fickian and governed by the leaching of unreacted monomer from the cement, which created vacancies for water molecules. The *in vitro* ageing conditions resulted in a maximum of 2% change in weight after 30 days, which significantly affected the properties of the commercial bone cements tested. Not only were mechanical and fatigue properties of bone cements affected, but structural changes were also found to occur over time. Structural changes occurred on the outermost layer of the cement, where high levels of diffusion are thought to take place and where the cement polymerises most slowly.

The mechanisms of moisture uptake and degradation due to ageing have been investigated. The changes in mechanical and structural properties of cement as a result of ageing may contribute to the long-term failure of PMMA bone cements.

Chapter 8

Commercially available antibiotic-loaded cements

8.1 Introduction

The remaining chapters of this thesis will focus on the delivery of therapeutic agents via PMMA bone cements. The drug release, mechanical, fatigue and structural properties of commercially available antibiotic-containing cements are explored in this chapter and the results will be used for comparison in subsequent chapters.

8.1.1 Antibiotics

Fear of antibiotic resistance has led to a decrease in the local application of antibiotics. Joint replacement surgery is one of the few conditions where local application remains justified. Mineralised bone tissue cannot expand and inflammation of adjacent tissue results in reduced blood flow to the immediate area, which prevents the delivery of therapeutic agents transported via circulatory blood, necessitating localised delivery of antibiotics.

When implanting artificial joints there is a risk of infection as the presence of a small amount of bacteria on the surface of the implant may result in a poor surgical outcome. Bacteria at the implant surface may become sessile by forming a biofilm. If the bacteria in the biofilm subsequently revert to a planktonic form, infection can be induced in adjacent tissue. Although antibiotics administered systemically (e.g. intravenously or orally) are

able to affect planktonic bacteria in the surrounding soft tissue or bone, they are unable to affect sessile forms of bacteria in biofilms. Therefore, a revision surgery would be required as the sessile bacteria would act as a reservoir for recurrent infections. To prevent infections and the need for revision surgeries, it is essential to ensure the eradication of bacteria immediately after surgery.

The concept for using bone cement as a reservoir for local antibiotic delivery was developed in 1969 when it was observed that the acrylic monomer of bone cement was eluted from the cement over a long period of time after setting³⁰. The antibiotics were first introduced into the cement in the form of a powder. This method proved to be successful and has since been the method adopted in joint surgery.

The powdered antibiotic is incorporated between a meshwork of PMMA chains throughout the cement and therefore, the release of the antibiotic is dependent upon the penetration of water into the cement. As previously discussed in Chapter 7, diffusion of water into bone cement follows a Fickian relationship and maximum uptake was achieved after roughly 2 months. Although the diffusion of water into the cement is a slow process, it has been established that powdered antibiotics in PMMA bone cements are released within the first few minutes up to the first 6 hours³⁵⁶. Furthermore, the release was found to occur from the surface layers of the cement, with the majority of the antibiotic left inaccessible in the bulk of the cement^{194, 218, 357}.

Although a high burst of antibiotic in the moments directly following surgery is advantageous in eliminating the majority of the bacteria present, any remaining spores or biofilms of bacteria may lay dormant and reproduce after the initial burst of antibiotics. This in turn may develop into an infection over time resulting in the patient requiring a revision surgery. To overcome this problem, a delivery system is required which provides the initial

burst of treatment, followed by a prolonged release of the remaining antibiotic, above inhibitory concentrations. This must also be achieved without compromising the mechanical and fatigue performance of the cement.

When selecting an antibiotic for use in the bone cement, the following properties are required²⁴:

- High solubility
- Heat stability during polymerisation
- No chemical interaction with PMMA or mediators of polymerisation
- Low effect on the mechanical strength of the cement
- Good release from cured/polymerised bone cement

An antibiotic commonly employed in PMMA bone cements is gentamicin sulphate. Gentamicin is an highly hydrophilic, bactericidal, broad-spectrum antibiotic used for the treatment of various Gram-positive and Gram-negative infections including pathogenic species of *Escherichia*, *Enterobacter*, *Klebsiella*, *Salmonella*, *Serratia*, *Shigella*, *Staphylococcus aureus*, some *Proteus* and *Pseudomonas aeruginosa*. Gentamicin is also heat stable and has low allergenicity²², however the antimicrobial efficacy of gentamicin is concentration dependent and bacterial barriers and adverse effects such as nephrotoxicity and neurotoxicity limit its daily dosage when taken systemically³⁵⁸. Gentamicin sulphate is incorporated in large amounts in PMMA bone cements, roughly 1g per 40g of cement; however, only a small percentage is released when incorporated as a powder into PMMA bone cement.

Between 2003 and 2009 in England and Wales, the number of hip replacements using antibiotic-loaded bone cements was found to have increased from 85% to 92%. Similarly for cemented knee replacements, the use of antibiotic-loaded bone cements increased from

92% to 96%²¹. This trend demonstrates the recent popularity of antibiotic-loaded cements and the need to prevent septic failure. The antibiotic release mechanisms are still not well understood and the effect of adding powdered antibiotics on the mechanical and fatigue properties of bone cements is still of concern (see Chapter 1).

In this chapter the antibiotic release and the antimicrobial efficacy of commercially available cements was investigated. Furthermore, the impact of using powdered gentamicin sulphate on the mechanical, fatigue and structural properties of commercially available cements, both before and after elution of the antibiotic, was assessed.

8.2 Methods

8.2.1 Materials

Cemex and Cemex Genta were obtained from Tecres (Sommacampagna, Italy), Palacos R and Palacos R+G were provided by Heraeus (Newbury, UK) and CMW Smartset GHV was provided by Depuy (Blackpool, UK). O-phthaldialdehyde ($\geq 97\%$, HPLC), ethanol ($\geq 99.8\%$, HPLC), 2-mercaptoethanol ($\geq 99.0\%$) and sodium borate ($\geq 99.0\%$) were obtained from Sigma Aldrich (Gillingham, UK).

8.2.2 Antibiotic release

Commercially available antibiotic-loaded cements (Cemex Genta, Palacos R+G and CMW Smartset GHV) were prepared as described in Section 2.1. Standard Cemex and Palacos R bone cement samples were prepared and tested to ensure leaching components of the cement did not affect measurements of antibiotic release. Table 8.1 shows the compositions of the cements tested. A high-density PTFE mould was manufactured to produce 10mm diameter by 2mm thick cylindrical samples. All samples were finished with a 250 grit silicon carbide sandpaper to the stated dimensions with a tolerance of $\pm 0.2\text{mm}$. Each

Table 8.1: Composition of gentamicin containing bone cements

	Cemex	Cemex Genta	Palacos R	Palacos R+G	CMW Smartset GHV
Liquid component / g	13.30	13.30	18.78	18.80	18.88
Methyl Methacrylate / %w/w	99.10	98.20	97.98	97.87	97.50
N-N Dimethyl-p-Toluidine / %w/w	0.90	1.80	2.02	2.13	2.50
Hydroquinone / ppm	75.00	75.00	60.00	60.00	75.00
Powder Component / g	40.00	40.00	40.00	40.80	40.00
Polymethyl Methacrylate / %w/w	84.30	82.78	84.50	83.27	80.45
Barium Sulphate / %w/w	13.00	10.00	-	-	-
Benzoyl Peroxide / %w/w	2.70	3.00	0.50	0.50	2.00
Zirconia / %w/w	-	-	15.00	15.00	14.37
Gentamicin sulphate / %w/w	-	4.22	-	1.23	4.22
Powder : Liquid ratio	3.01	3.01	2.13	2.17	2.11

sample weighed 0.40 ± 0.01 g and five samples for each test group was examined. Each sample was stored in 5mL of Ringer's solution (8.6mg/mL NaCl, 0.3mg/mL KCl and 0.33mg/mL CaCl_2 , buffered to a pH of 7.4 with NaHCO_3 ²⁷⁶) at 37°C. After 6 hours, 1, 2, 3, 7, 15, 30 and 60 days the Ringer's solution was removed and stored in the dark at -20°C before assaying; 5mL of fresh Ringer's was added as replacement until the next time point. Ringer's solution was replaced at the selected time points in order to approach sink conditions, a condition where the drug concentration in the eluent can be assumed negligible in comparison to the maximum solubility of the drug.

The solutions were thawed overnight at room temperature in the dark and the concentration of gentamicin was determined using an o-phthaldialdehyde (PHT) method developed by Sampath et al.³⁵⁹ and Zhang et al.³⁶⁰, whereby a PHT reagent reacts with the amino groups of gentamicin sulphate to yield measurable fluorogenic products. The reagent was prepared by adding 2.5g of o-phthaldialdehyde, 62.5mL of ethanol and 3mL of 2-mercaptoethanol to 560mL of 0.04M sodium borate solution in distilled water. The PHT reagent was stored in an amber glass bottle in the dark for 24 hours prior to use.

Twelve calibration solutions with gentamicin concentrations from $0\mu\text{g}/\text{mL}$ to $100\mu\text{g}/\text{mL}$ in Ringer's solution were prepared for the calibration curve. 1mL of the calibration solution was added to 1mL PHT reagent and 1mL isopropanol and left for 40 minutes to react. The absorbance was then measured at 340nm using a Hitachi U-1900 spectrophotometer (Hitachi High-Technologies Europe GmbH, Mannheim, Germany) and a linear relationship between concentration and absorbance was produced. 1mL of the sample eluate was mixed with 1mL PHT reagent and 1mL isopropanol and left for 40 minutes to react and its absorbance compared against the calibration graph, in order to determine the concentration of gentamicin sulphate released by the samples at each time point. Average gentamicin concentrations for each time point were calculated from the 5 samples and the cumulative gentamicin release was calculated over 60 days.

Gentamicin release was also calculated as the cumulative release of gentamicin sulphate as a percentage of the theoretical maximum amount of gentamicin sulphate in each sample (Equation 8.1).

$$\text{Percentage release} = \frac{R_c \times 5}{G_s} \times 100 \quad (8.1)$$

Where:

R_c is the experimental cumulative gentamicin sulphate release in $\mu\text{g}/\text{mL}$
 G_s is the amount of gentamicin sulphate in 0.4g of cement in μg

8.2.3 Mathematical modelling

Mathematical models were applied to the antibiotic release data for the commercial bone cements to better understand release kinetics. In the equations described, R_t is the total percentage gentamicin sulphate released, t is the time period, n is an exponential function and k is a diffusion related constant. Equation 8.2 was developed by Korsmeyer et al.³⁶¹ who stated drug release was exponentially related to time.

$$R_t = kt^n \quad (8.2)$$

Higuchi et al.³⁶² proposed Equation 8.3, whereby the release of drugs is dependent upon Fickian diffusion of water into the material.

$$R_t = kt^{1/2} \quad (8.3)$$

Equation 8.4 is associated with a Noyes-Whitney dissolution process³⁶³. The Noyes-Whitney dissolution process states that the dissolution rate of a solid is dependent on its diffusion coefficient, the surface area of the solid, the concentration at the boundary layer and the length of the boundary layer.

$$R_t = k[1 - \exp(-nt)] \quad (8.4)$$

Equation 8.5 is an expanded version of Korsmeyer's work developed by Lindner and Lipold which takes into account an additional coefficient (b) to represent the initial burst of antibiotics from the surface of the cement³⁶⁴. The additional coefficient was added to the Higuchi and Noyes-Whitney equations (Equations 8.3 and 8.4) and applied to the release data.

$$R_t = b + kt^n \quad (8.5)$$

All models were applied to the data using the curve fitting toolbox in Matlab (MathWorks, Cambridge, UK), which calculates the coefficients by minimizing the sum of squared residuals.

8.2.4 Agar diffusion assay

10mm diameter by 2mm thick cylindrical bone cement samples were prepared as previously described. Tryptone soya agar (TSA) was prepared by dissolving 40g of tryptone soy agar medium in one litre of distilled water. The solution was boiled for one minute then sterilized in an autoclave at 121°C for 15 minutes. The solution was allowed to cool to 45-50°C before being dispensed into Petri dishes (9cm diameter). The Petri dishes were cooled to room temperature then stored at 8-15°C until use.

Staphylococcus aureus (*S. aureus*) was cultured in tryptic soy broth (TSB) for 18-24 hours at 37°C. A sterile cotton swab was used to spread the inoculum across the TSA Petri dish. The Petri dish was turned by 60° and the process was repeated to ensure complete surface coverage. A 10µg gentamicin disc was placed on the Petri dish as a control and pressure was applied to the top of the disc to ensure full surface contact. The dish was divided into segments and the bone cement samples were placed well separated on the agar, in the same manner. The Petri dish was then incubated at 37°C for 18-24 hours, after which, the zones of inhibition around the samples and gentamicin disc were measured. Images of the zones of inhibition were taken and measured using ImageJ software (National Institutes of Health, Maryland, USA). The zones of inhibition were measured as the radius of the zone minus the radius of the sample. Two measurements for each zone of inhibition were taken, perpendicular to one another. The experiment was repeated in triplicate (n=3). Observations on the appearance of the bacterial cultures and the zones of inhibition were also made.

8.2.5 Mechanical properties

Compression and bending samples of Cemex Genta, CMW Smartset GHV and Palacos R+G were prepared and tested as described in Sections 2.3.1 and 2.3.2. Samples were tested after 24 hours in air and after ageing in Ringer's solution at 37°C for 60 days, with

the Ringer's solution changed every 2 weeks. Results for Cemex and Palacos R cement were previously reported in Chapter 7.

8.2.6 Fracture toughness

Fracture toughness values for Cemex Genta, Palacos R+G and CMW Smartset GHV were obtained according to Section 2.4 for samples aged in both air for 24 hours and in Ringer's solution at 37°C for 60 days. Results for Cemex and Palacos R cement were previously obtained in Chapter 7.

8.2.7 Fatigue testing

Fatigue test samples were prepared and tested as described in Section 2.5. Results were obtained for samples aged in air for 24 hours and after ageing in Ringer's solution at 37°C for 60 days, with the Ringer's solution changed every 2 weeks. Results for Cemex and Palacos R cement were previously obtained in Chapter 7.

8.2.8 SEM images

SEM images of the fracture surfaces of the fatigue test samples were taken as described in Section 2.8. Higher magnification SEM images of the cement powders were prepared to study differences in particle morphology, and SEM images of the surfaces following release of the antibiotic into Ringer's solution for 60 days were compared with fresh samples. Cemex and Palacos R fatigue and powder images were taken from Chapter 7.

8.2.9 Vickers hardness

Hardness values for Cemex Genta, Palacos R+G and CMW Smartset GHV were obtained as described in Section 2.6 for samples aged in air for 24 hours and Ringer's solution at 37°C for 60 days, with the Ringer's solution changed every 2 weeks. Values for hardness for Cemex and Palacos R were taken from Chapter 7.

8.2.10 Glass transition temperature

The glass transition temperature (T_g) of Cemex Genta, Palacos R+G and CMW Smartset GHV were obtained for samples aged in air for 24 hours and Ringer's solution at 37°C for 60 days, with the Ringer's solution changed every 2 weeks, as described in Section 2.7. Cemex and Palacos R T_g values were taken from Chapter 7.

8.3 Results

8.3.1 Antibiotic release

Figure 8.1 shows the calibration graph obtained using the PHT assay method for varying concentrations of gentamicin sulphate in Ringer's solution. A good correlation was obtained (R-value of 0.9987) and the standard deviations were acceptable. It was noted that at concentrations approaching 100µg/mL, the standard deviations of the absorbance values increased resulting in reduced linearity between absorbance and gentamicin sulphate concentration. This technique was deemed accurate for absorbance values below 1.6 (gentamicin sulphate concentrations of up to 90µg/mL).

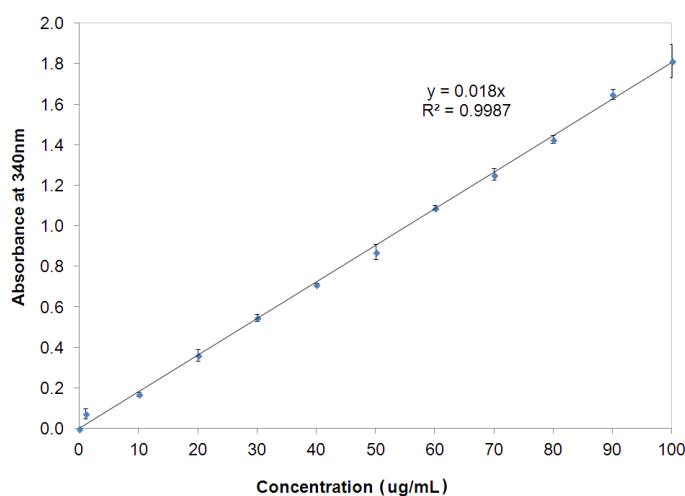
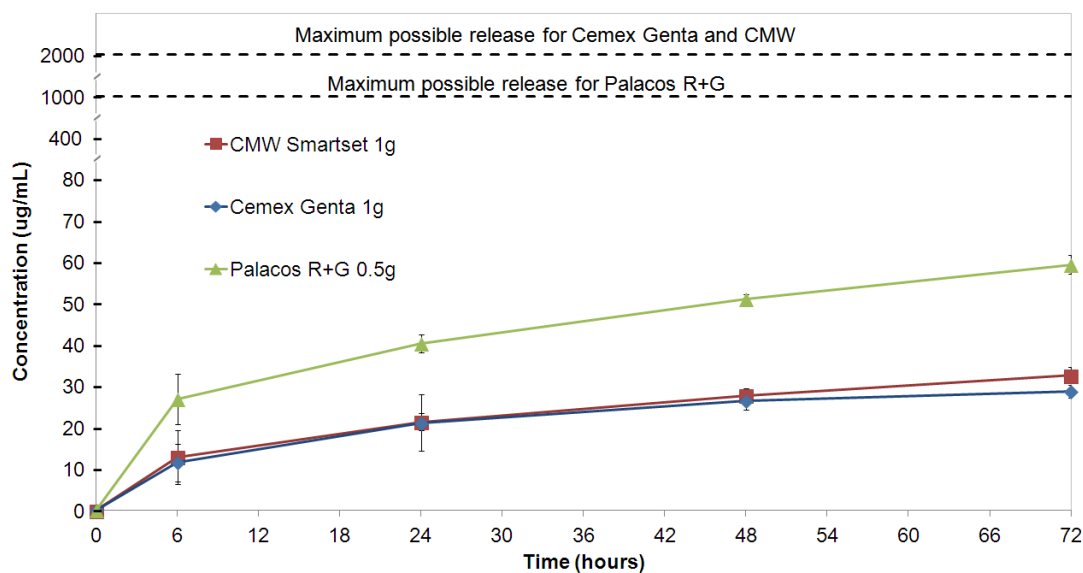


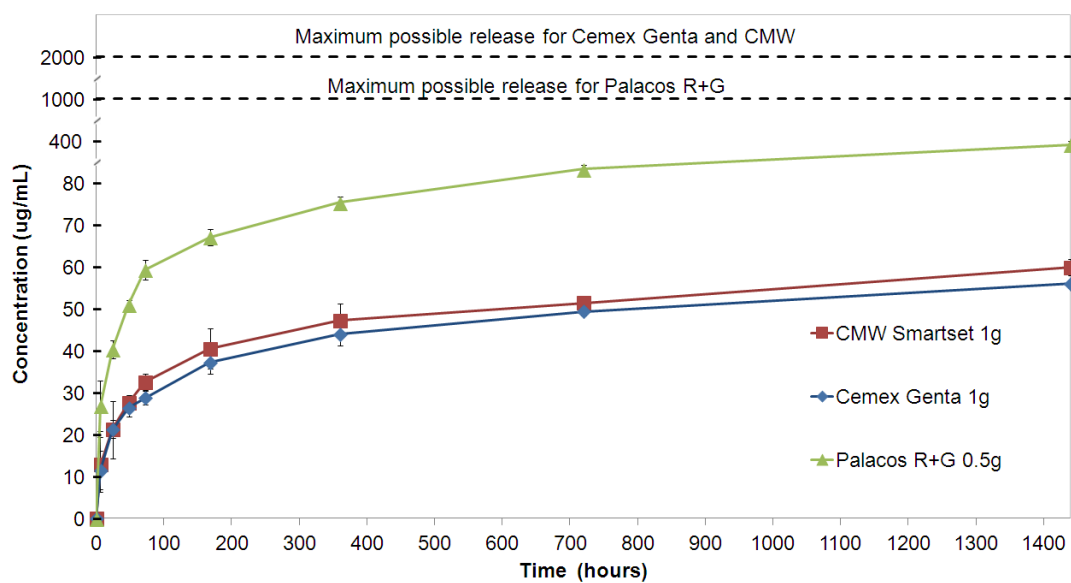
Figure 8.1: Calibration curve for the PHT assay of gentamicin sulphate

For Cemex and Palacos R bone cements the PHT assay resulted in absorbance values of 0 ± 0.005 for all time points, demonstrating that leached materials from the cement samples did not react with the PHT reagent and thereby compromise the assay. Figure 8.2 (a) and (b) shows the cumulative antibiotic release over 72 and 1440 hours (60 days) respectively for commercially available antibiotic cements. The dashed lines represent the maximum concentration which might be obtained if all the gentamicin sulphate in the cement sample had been released. The standard deviations of the assay were found to be below $\pm 7 \mu\text{g/mL}$, demonstrating low variance in release between samples and acceptable accuracy within the assay technique. It was noted that standard deviations were largest for the initial time points. All cements experienced a burst of gentamicin sulphate release within the first 72 hours. The majority of the release was found to occur within the first 6 hours, after which the rate of release decreased. After 720 hours, the release of gentamicin sulphate was found to have reached a maximum with limited further release over the next 720 hours. Overall Palacos R+G achieved significantly higher antibiotic release than Cemex Genta (ANOVA, $p=2.24 \times 10^{-04}$) and CMW Smartset ($p=4.63 \times 10^{-05}$), which released roughly half the amount of gentamicin sulphate.

Figure 8.3 shows the total percentage of gentamicin sulphate released from the commercial cements. Cemex Genta and CMW smartset released only approximately 1.5% of its total gentamicin sulphate content after 72 hours and 3% after 1440 hours incubation. As both cements have 1g of gentamicin sulphate per 40g of cement powder, this would result in roughly 15mg of antibiotic being released after 72 hours and 30mg over the course of 1440 hours from a single dose of cement. Palacos R+G obtained a much higher percentage release of approximately 6% after 72 hours and 9% after 1440 hours. As Palacos R+G has 0.5g of gentamicin sulphate per 40g of cement powder, this would result in roughly 30mg of antibiotic being released over 72 hours and 45mg over 1440 hours.

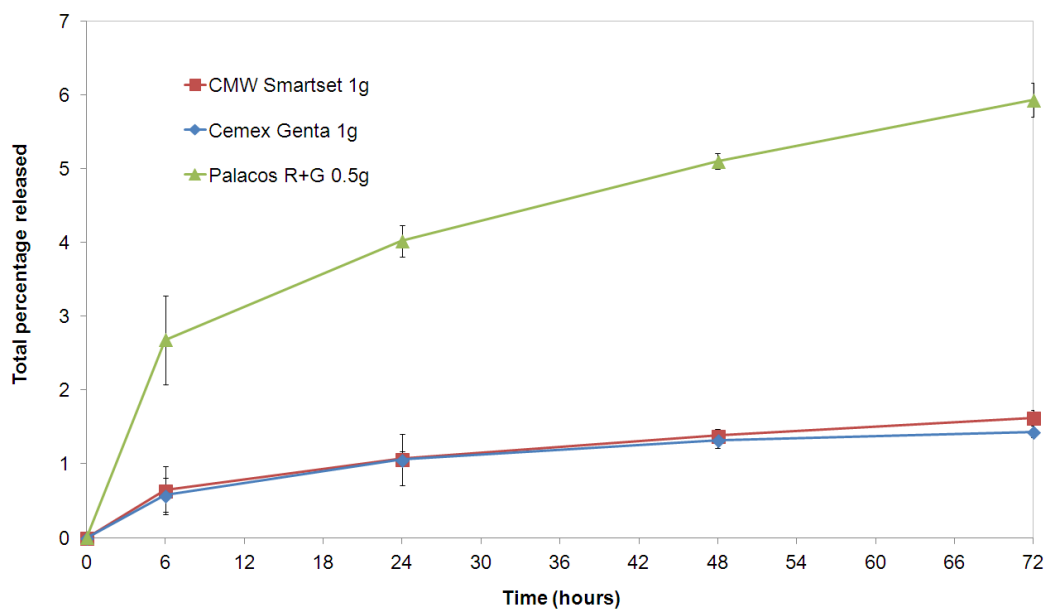


(a) Gentamicin release over 72 hours

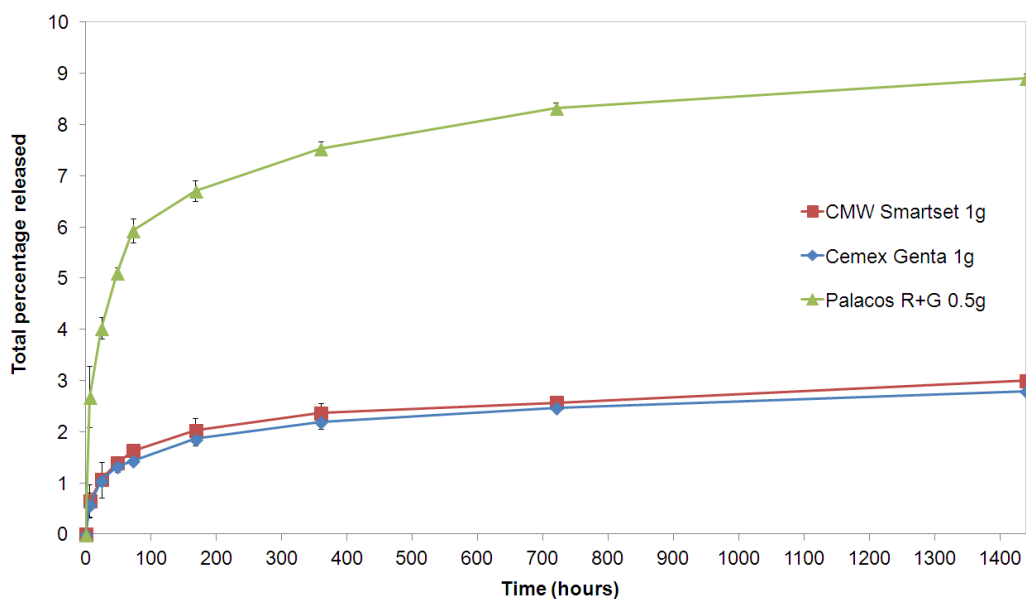


(b) Gentamicin release over 1440 hours

Figure 8.2: Cumulative antibiotic release from Cemex Genta, CMW Smartset GHV and Palacos R+G bone cement



(a) Percentage gentamicin release over 72 hours



(b) Percentage gentamicin release over 1440 hours

Figure 8.3: Cumulative percentage release from Cemex Genta, CMW Smartset GHV and Palacos R+G bone cement

8.3.2 Mathematical modelling

Table 8.2 shows the coefficient values that most accurately model the experimental antibiotic release data using the Korsmeyer-Peppas model, the Higuchi model and the Noyes-Whitney model for each cement. The table also shows the goodness of fit (R-value) between the experimental data and the models for each cement brand. The Korsmeyer-Peppas model was found to best model the antibiotic release for all three commercially available bone cements. The Higuchi model was found to have the poorest fit with the experimental data as the antibiotic release was not controlled by a single process alone. The n coefficient obtained using the Korsmeyer-Peppas model was found to be less than 0.5 for all three cements, demonstrating the antibiotic release was not governed by Fickian diffusion alone, however this may be as a consequence of the method employed. This is further highlighted by the poor correlation between the Higuchi model and the experimental data. The Noyes-Whitney model was found to have a moderate fit, demonstrating the possibility of dissolution based processes taking place during gentamicin sulphate release from PMMA bone cements.

Table 8.2: Mathematical modelling of antibiotic release for Cemex Genta, CMW Smartset and Palacos R+G

		Korsmeyer	Higuchi	Noyes-Whitney
		$R_t = kt^n$	$R_t = kt^{1/2}$	$R_t = k[1 - \exp(-nt)]$
Cemex Genta	k	0.507	0.094	2.397
	n	0.240	0.500	0.015
	R-value	0.9783	0.3655	0.8505
CMW smartset	k	0.552	0.100	2.343
	n	0.237	0.500	0.020
	R-value	0.9726	0.3320	0.9151
Palacos R+G	k	2.421	0.696	7.827
	n	0.284	0.500	0.011
	R-value	0.9559	-0.4704	0.8204

Table 8.3 shows the coefficient and correlation values obtained when an additional coefficient (b) was added to the Korsmeyer-Peppas model (as developed by Lindner and Lippold³⁶⁴), the Higuchi model and Noyes-Whitney model for each cement to represent the burst-type release of gentamicin sulphate from the surface of the cements. The goodness of fit between the experimental data and the expanded models were all improved by the additional coefficient. The expanded Korsmeyer-Peppas model produced the most accurate model, followed by the expanded Noyes-Whitney model and then the expanded Higuchi model. The improved fit of the expanded Higuchi model demonstrates a burst type release of gentamicin from the surface of the cement, followed by a much slower release, controlled by diffusion into the cement. For both the expanded Noyes-Whitney and the expanded Higuchi models, the burst coefficient was positive. For the expanded Korsmeyer-Peppas model however, the coefficient was negative and the reason for this is not understood.

Table 8.3: Mathematical modelling of antibiotic release for Cemex Genta, CMW Smartset and Palacos R+G using the additional coefficient

		Expanded Korsmeyer	Expanded Higuchi	Expanded Noyes-Whitney
		$R_t = b + kt^n$	$R_t = b + kt^{1/2}$	$R_t =$ $b + k[1 - \exp(-nt)]$
Cemex Genta	k	4.687	0.058	1.874
	n	0.065	0.500	0.006
	b	-4.700	0.844	0.734
	R-value	0.9988	0.9012	0.9602
CMW Smartset	k	6.333	0.061	1.998
	n	0.054	0.500	0.007
	b	-6.367	0.917	0.733
	R-value	0.9955	0.8919	0.9582
Palacos R+G	k	24.487	0.160	5.541
	n	0.039	0.500	0.010
	b	-23.426	3.764	2.744
	R-value	0.9885	0.8337	0.9570

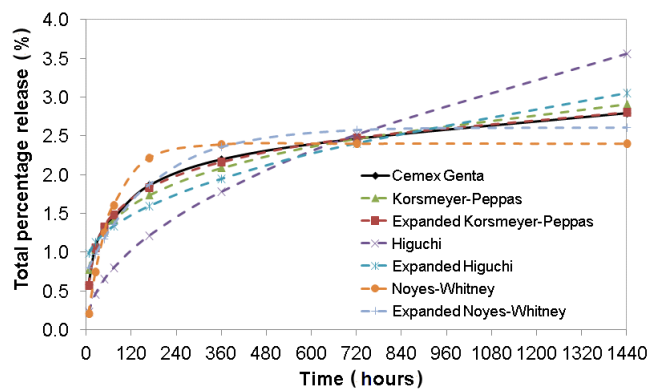
Figure 8.4 shows the goodness of fit between the experimental data and the values obtained using the mathematical models. As previously discussed, for all three commercial cements the Higuchi model demonstrated the poorest fit. The expanded Korsmeyer-Peppas model demonstrated the best fit for all three models. All models were found to be improved by the additional coefficient representing a burst of gentamicin sulphate release from the surface of the cement.

8.3.3 Agar diffusion assay

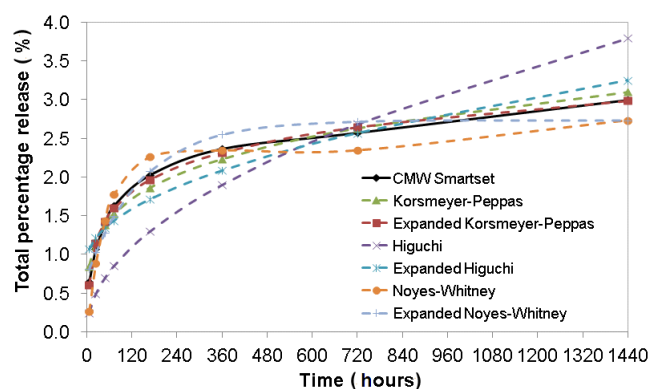
Good surface coverage of *S. aureus* was achieved on the agar plates using the technique described. Figure 8.5 shows the average zones of inhibition obtained for commercially available bone cements using a method based on the Kirby-Bauer agar diffusion assay. Susceptibility of strains may be defined as those with a zone of inhibition greater than 2mm³⁶⁵.

Consistent zones were obtained for the 10µg gentamicin discs, demonstrating the strain of *S. aureus* used was susceptible to gentamicin sulphate. The standard deviations for each 10µg gentamicin disc was small, reflecting the symmetrically circular zones obtained. Furthermore, the samples produced zones of similar diameter, demonstrating a consistent amount of gentamicin sulphate was released.

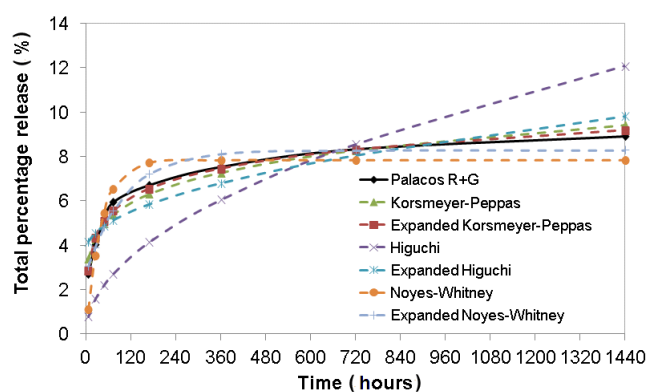
The commercial bone cements without gentamicin sulphate (Cemex and Palacos R) did not produce zones of inhibition and therefore showed no antimicrobial properties. Cemex Genta gave large zones of inhibition, however the results were not consistent as one of the samples was found to have a significantly smaller zone of inhibition. The standard deviations for each sample was small, demonstrating even diffusion of gentamicin sulphate from the surface of the sample. Palacos R+G had one of the largest zones of inhibition, however there were significant differences between samples. The standard deviation obtained from



(a) Cemex Genta



(b) CMW Smartset



(c) Palacos R+G

Figure 8.4: Antibiotic release models for (a) Cemex Genta, (b) CMW Smartset and (c) Palacos R+G

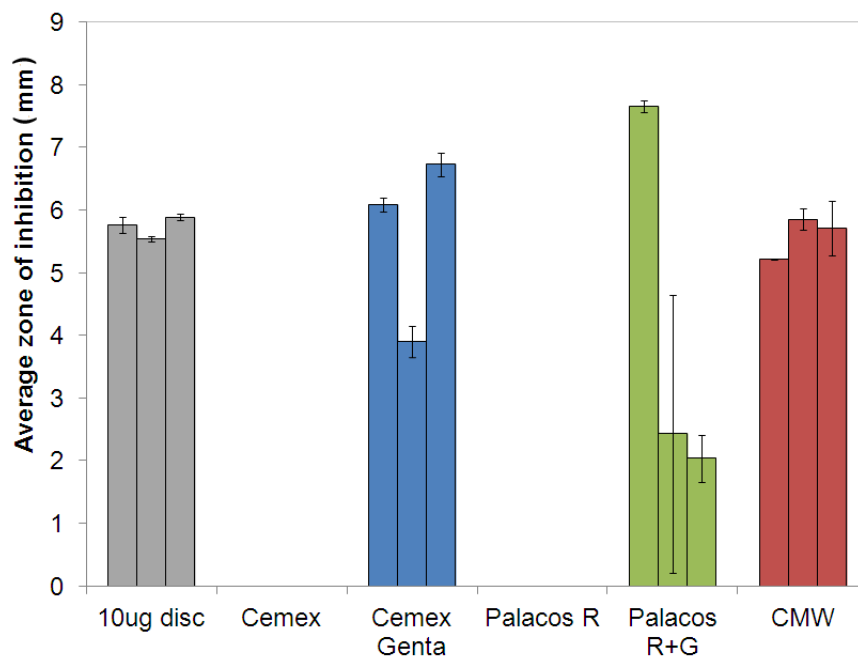


Figure 8.5: Average zones of inhibition for commercially available cements

one of the sample was particularly large due to an irregular-shaped zone. Overall, Palacos R+G produced substantially variable zones of inhibition. CMW was found to be the most consistent cement, obtaining similar zones to the 10 μ g gentamicin discs with acceptable standard deviations and minimum variation between samples.

Figure 8.6 shows images of the zones of inhibition obtained for the commercially available cements and the 10 μ g gentamicin control disc. As discussed, even release of gentamicin sulphate was obtained for the 10 μ g gentamicin discs and CMW bone cement. There were no zones of inhibition for commercial cements without antibiotic. Cemex Genta produced a slightly oval shaped zone and Palacos R+G demonstrated poor antimicrobial efficacy for two of the samples tested.

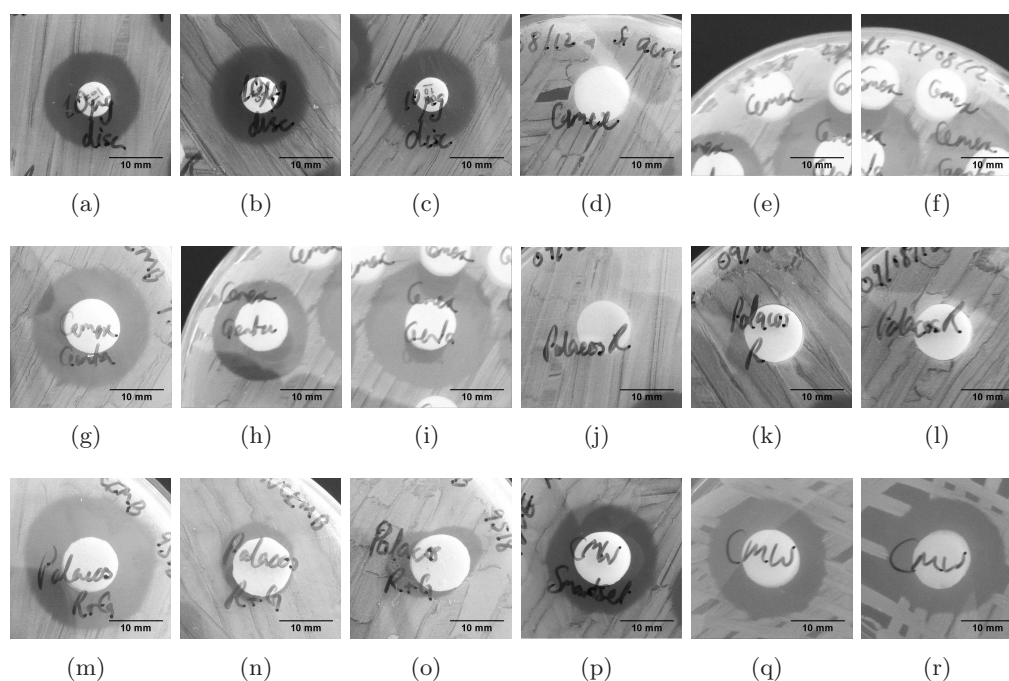


Figure 8.6: Zones of inhibition for (a-c) 10 μ g discs, (d-f) Cemex, (g-i) Cemex Genta, (j-l) Palacos R, (m-o) Palacos R+G and (p-r) CMW

8.3.4 Mechanical properties

The mechanical properties of the commercially available cements before and after ageing in Ringer's solution for 60 days are shown in Table 8.4. All of the cements tested experienced a significant reduction in compressive strength ($p < 0.05$), with the exception of Cemex bone cement, which demonstrated a significant increase ($p = 0.01$). There was no significant difference between Cemex and Cemex Genta at 24 hours air exposure ($p = 0.09$), however after 60 days in Ringer's solution, Cemex was found to be significantly stronger in compression when compared to Cemex Genta ($p = 6.07 \times 10^{-5}$). After 24 hours air exposure, the addition of gentamicin sulphate to Palacos R significantly reduced the compressive strength of the cement ($p = 2.74 \times 10^{-03}$). After 60 days in Ringer's solution however, there was no significant difference between Palacos R and Palacos R+G ($p = 0.15$).

Table 8.4: Mechanical properties of commercially available cements before and after ageing in Ringer's for 60 days

		Compressive strength (σ_c) / MPa	Bending modulus (E_b) / MPa	Bending strength (B) / MPa
Cemex	Air 1 day	85.2±4.2	3080±204	46.0±6.5
	Ringer's 60 days	92.7±2.5	2540±92	37.6±0.2
Cemex Genta	Air 1 day	89.7±2.1	3160±128	49.1±3.6
	Ringer's 60 days	81.9±1.9	2840±80	50.4±3.8
Palacos R	Air 1 day	104.6±2.6	3460±97	73.4±2.9
	Ringer's 60 days	75.5±5.7	3180±80	69.4±0.6
Palacos R+G	Air 1 day	95.7±3.3	3110±110	66.6±2.4
	Ringer's 60 days	80.3±3.3	2790±155	50.4±7.0
CMW Smartset	Air 1 day	85.8±2.6	3290±264	68.7±4.3
	Ringer's 60 days	80.7±4.0	2080±225	48.3±4.5

In terms of bending modulus, all cements experienced a significant reduction as a result of ageing in Ringer's solution for 60 days ($p < 0.05$). There was no significant difference after 24 hours between the bending moduli of Cemex and Cemex Genta ($p = 0.53$). After ageing in Ringer's solution, Cemex Genta was found to have significantly higher bending modulus ($p = 7.92 \times 10^{-03}$). With Palacos cement, the addition of gentamicin sulphate significantly reduced the bending modulus at both 24 hours in air ($p = 2.41 \times 10^{-03}$) and 60 days in Ringer's solution ($p = 0.02$).

Palacos R+G, CMW and Cemex cement were found to have significantly reduced bending strength after ageing in Ringer's solution for 60 days ($p = 1.27 \times 10^{-03}$, $p = 1.18 \times 10^{-04}$ and $p = 0.02$ respectively), whilst there was no significant difference for the other cements as a result of ageing in Ringer's solution ($p = 0.14$ for Palacos R and $p = 0.62$ for Cemex Genta). There was no significant difference in bending strength between Cemex and Cemex Genta at 24 hours ($p = 0.42$). After 60 days in Ringer's solution however, Cemex Genta was found to be significantly stronger than Cemex cement ($p = 6.34 \times 10^{-03}$). For Palacos cement, the

addition of gentamicin sulphate was found to significantly reduce the bending strength at both 24 hours in air ($p=8.06\times 10^{-03}$) and 60 days in Ringer's solution ($p=0.01$).

8.3.5 Fracture toughness

The fracture toughness of Cemex, Palacos R and CMW were found to be significantly reduced ($p=2.62\times 10^{-03}$, $p=3.87\times 10^{-03}$ and $p=2.23\times 10^{-03}$ respectively) as a result of ageing in Ringer's solution for 60 days, as shown in Table 8.5. After 24 hours in air, the addition of gentamicin sulphate did not significantly affect the fracture toughness ($p=0.30$ for Cemex and $p=0.81$ for Palacos). After 60 days in Ringer's solution, the fracture toughness of the cements with gentamicin sulphate were found to be significantly higher over their antibiotic-free counterparts ($p=3.78\times 10^{-04}$ for Cemex and $p=8.31\times 10^{-04}$ for Palacos).

Table 8.5: Fracture toughness of commercially available cements before and after ageing in Ringer's for 60 days

		Critical stress intensity factor (K_{IC}) / MPam ^{1/2}
Cemex	Air 1 day	1.7±0.1
	Ringer's 60 days	1.4±0.1
Cemex Genta	Air 1 day	1.6±0.1
	Ringer's 60 days	1.8±0.1
Palacos R	Air 1 day	2.5±0.2
	Ringer's 60 days	1.5±0.3
Palacos R+G	Air 1 day	2.5±0.1
	Ringer's 60 days	2.4±0.2
CMW Smartset GHV	Air 1 day	2.2±0.1
	Ringer's 60 days	1.8±0.1

8.3.6 Fatigue testing

Figure 8.7 shows the fatigue results obtained for antibiotic-loaded and unloaded cements after ageing in air. The crack growth rates were found to be higher for cements with gentamicin sulphate when compared to cements without gentamicin sulphate.

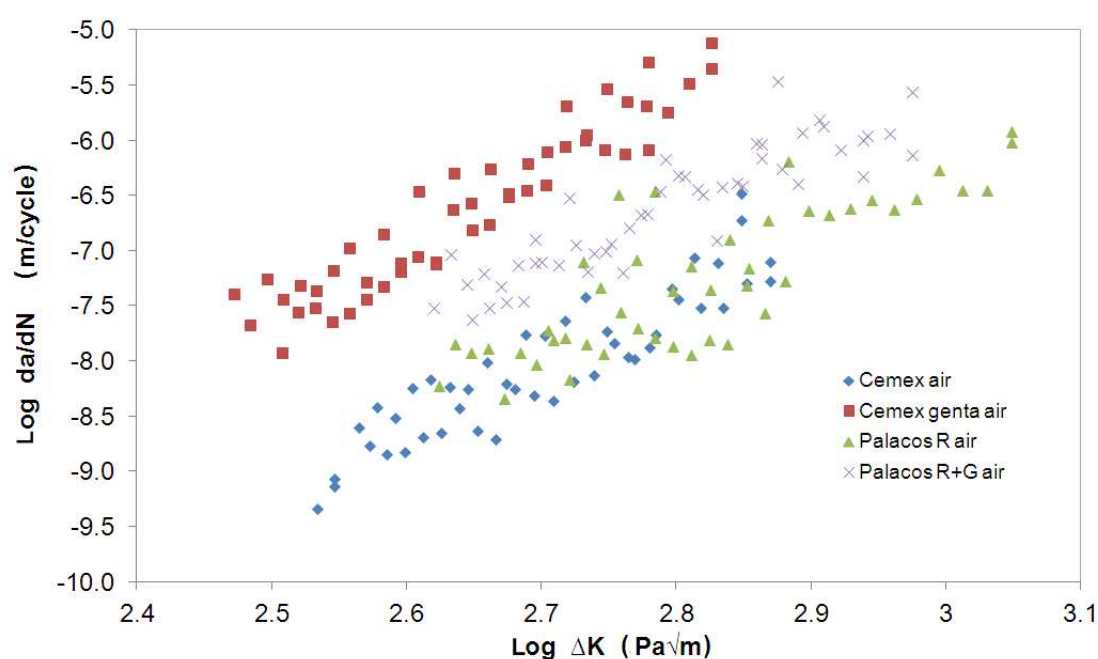


Figure 8.7: Fatigue results from commercially available antibiotic-loaded and unloaded bone cements

The fatigue results obtained for antibiotic-loaded cements after ageing in Ringer's solution for a minimum of 60 days are shown in Figure 8.8. No distinguishable differences were observed in terms of crack growth rates as a result of ageing in Ringer's solution for 60 days.

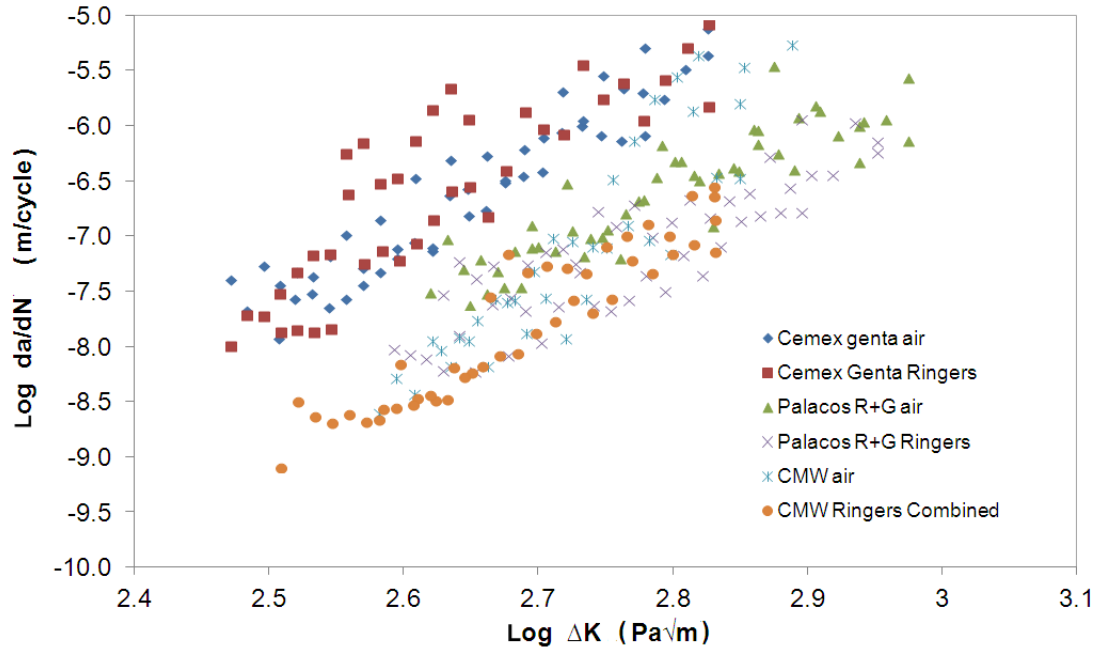


Figure 8.8: Fatigue results from commercially available antibiotic-loaded bone cements before and after ageing in Ringer's at 37°C in Ringer's solution

Table 8.6 shows the fatigue constants obtained when the Paris Law was applied to the experimental data. CMW Smartset GHV aged in air for 24 hours performed the poorest with very high crack growth rates at high stress intensities, whilst Palacos R+G was found to perform the best in terms of fatigue crack propagation. In terms of crack growth rate at $\Delta K=1\text{MPam}^{1/2}$, the 'A' coefficient, there was a reduction for Cemex, Cemex Genta and Palacos R as a result of ageing in Ringer's solution, whilst there was an increase for Palacos R+G and CMW. The addition of gentamicin sulphate to Cemex and Palacos R cements was found to increase the 'A' coefficient at both 24 hours in air and 60 days in Ringer's solution.

The slope of the plot ('m' coefficient), which represents the change in crack growth rate as stress intensity increases, was found to increase for all the cements (except CMW) as a

Table 8.6: Fatigue test constants of commercially available cements before and after ageing in Ringer's for 60 days. 'A' is the crack growth at $\Delta K=1\text{MPam}^{1/2}$ and 'm' is the slope of the data

	A		m		Correlation coefficient	
	1 day air	60 days Ringer's	1 day air	60 days Ringer's	1 day air	60 days Ringer's
Cemex	5.39×10^{-07}	1.29×10^{-05}	5.92	6.20	0.82	0.86
Cemex Genta	7.17×10^{-05}	1.64×10^{-04}	6.99	7.42	0.89	0.79
Palacos R	3.73×10^{-07}	7.34×10^{-07}	4.65	7.33	0.67	0.66
Palacos R+G	2.62×10^{-06}	1.13×10^{-06}	5.01	5.18	0.81	0.74
CMW Smartset GHV	1.39×10^{-04}	2.49×10^{-06}	11.71	6.95	0.86	0.88

result of ageing in Ringer's solution. Furthermore, the 'm' coefficient was found to increase as a consequence of using gentamicin sulphate in Cemex and Palacos R after 24 hours in air. Similarly, after 60 days in Ringer's solution, the addition of gentamicin sulphate to Cemex cement resulted in an increase in the 'm' coefficient. The correlation coefficient for all cements was acceptable (≥ 0.66), demonstrating a moderate correlation between the experimental datum and the applied Paris Law. It was observed however, that the correlation coefficient for Cemex Genta and Palacos R+G was reduced after ageing in Ringer's solution, demonstrating high variability in crack growth rates for stress intensities tested.

8.3.7 SEM images

Figures 8.9 to 8.11 show the SEM images of the fatigue fracture surfaces. All cements were found to have pores due to entrapped air during the mixing process. As discussed in Chapter 7, all cements were found to have a rougher fracture surface as a result of ageing in Ringer's solution. Samples with gentamicin sulphate were found to have significantly more pores than samples without and the pores were found to be irregular in shape and

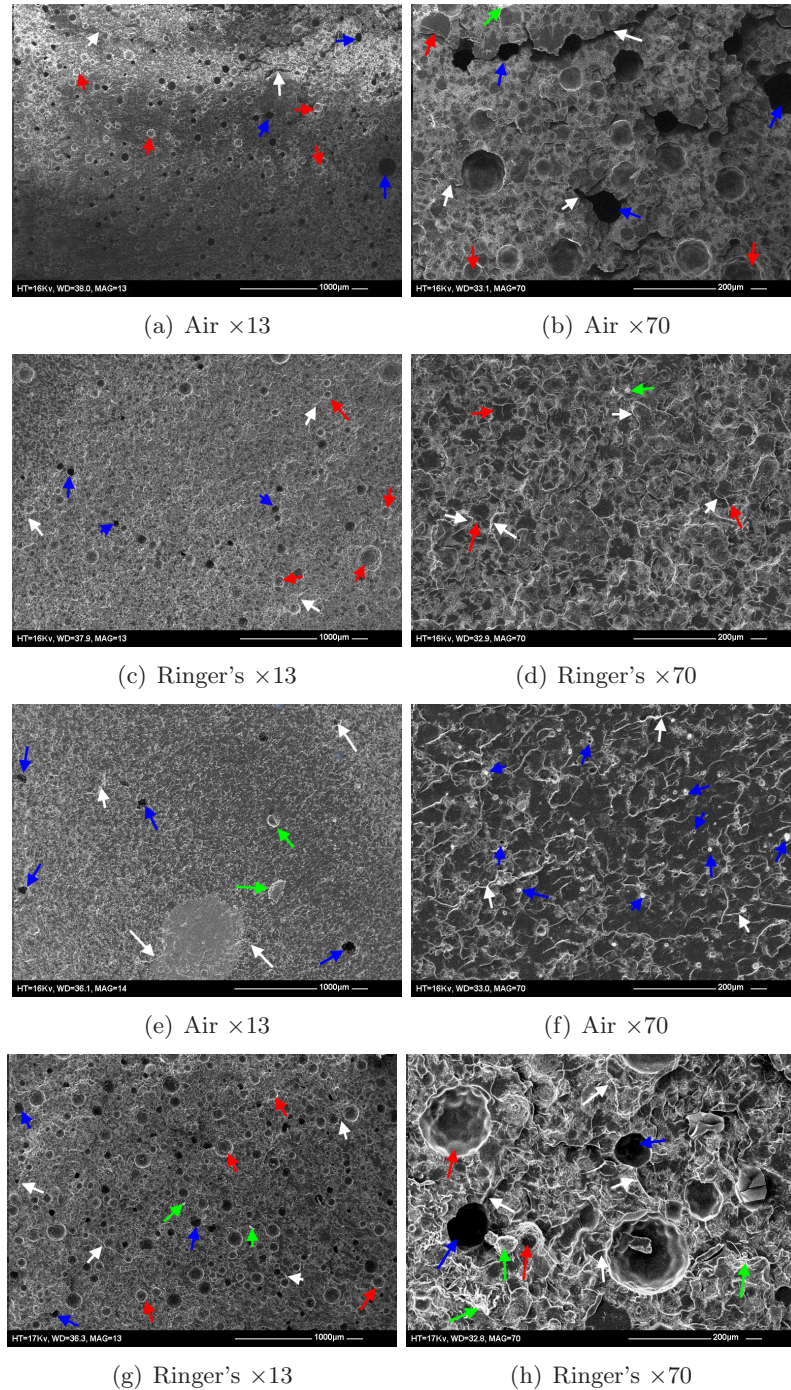


Figure 8.9: Fracture surfaces of fatigue samples aged in air and Ringer's solution for (a-d) Cemex and (e-h) Cemex Genta - Red arrows indicate the location of PMMA beads, green arrows indicate radiopacifier particles, blue arrows indicate pores and white arrows indicate microcracks. Magnification at $\times 13$ and $\times 70$.

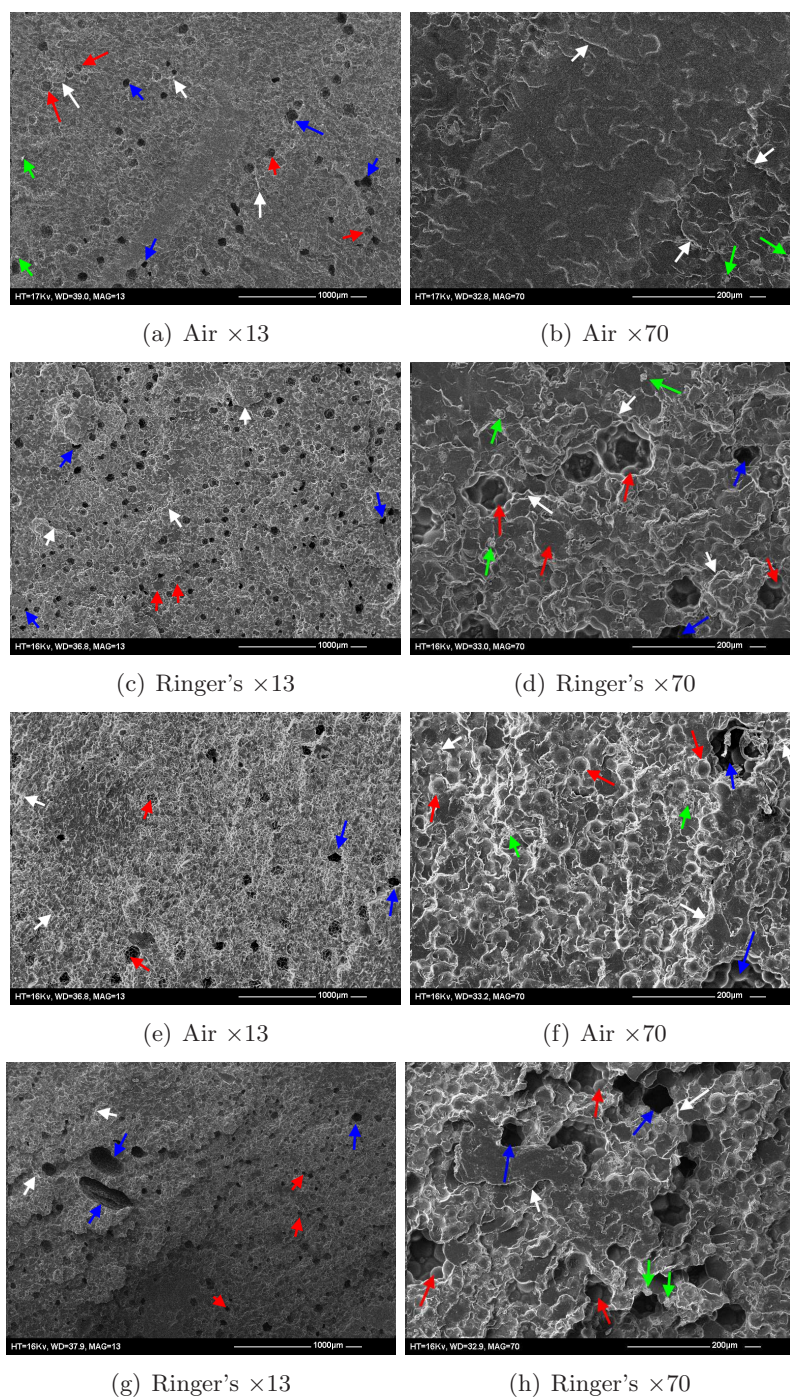


Figure 8.10: Fracture surfaces of fatigue samples aged in air and Ringer's solution for (a-d) Palacos R and (e-h) Palacos R+G - Red arrows indicate the location of PMMA beads, green arrows indicate radiopacifier particles, blue arrows indicate pores and white arrows indicate microcracks. Magnification at $\times 13$ and $\times 70$.

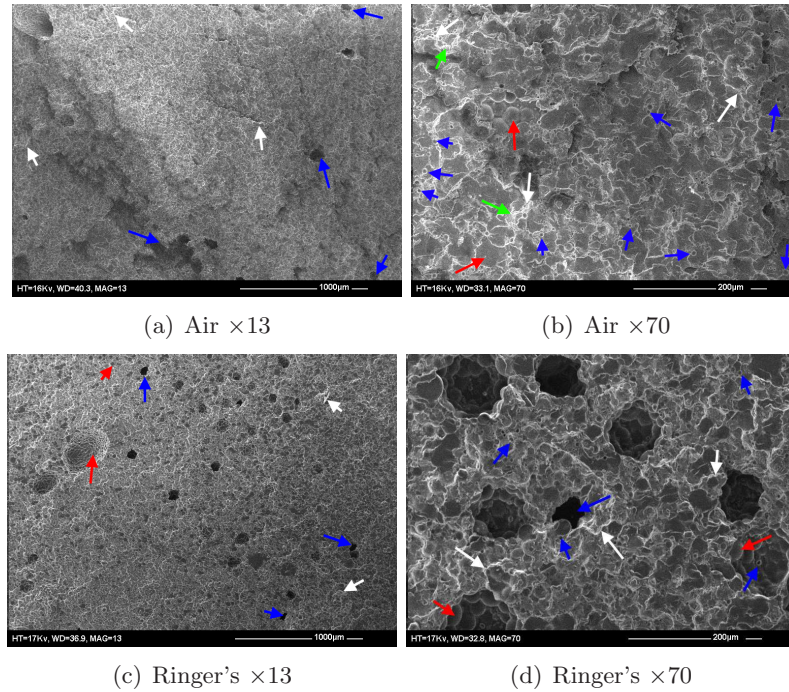


Figure 8.11: Fracture surfaces of fatigue samples aged in air and Ringer's solution for (a-d) CMW Smartset GHV - Red arrows indicate the location of PMMA beads, green arrows indicate radiopacifier particles, blue arrows indicate pores and white arrows indicate microcracks. Magnification at $\times 13$ and $\times 70$.

size, ranging from 10-200µm in length. Closer examination of the fracture surfaces of Cemex Genta and CMW Smartset GHV cements prior to ageing in Ringer's solution found very small (10µm) round beads of gentamicin sulphate. After ageing, in Ringer's solution, a high number of 10µm pores were found on the fracture surfaces of Cemex Genta and CMW Smartset GHV cements.

The SEM images of the antibiotic release assay samples are shown in Figures 8.12 to 8.14. The surface roughness of all samples were similar due to polishing with the same grade silicon carbide paper. All cements prior to incubation were found to have few to no pores on the surface of the sample. Similarly, after 1440 hours incubation, the samples without gentamicin sulphate were found to have few to no pores. Samples with gentamicin sulphate however, had significantly higher levels of porosity on the surface of the cement

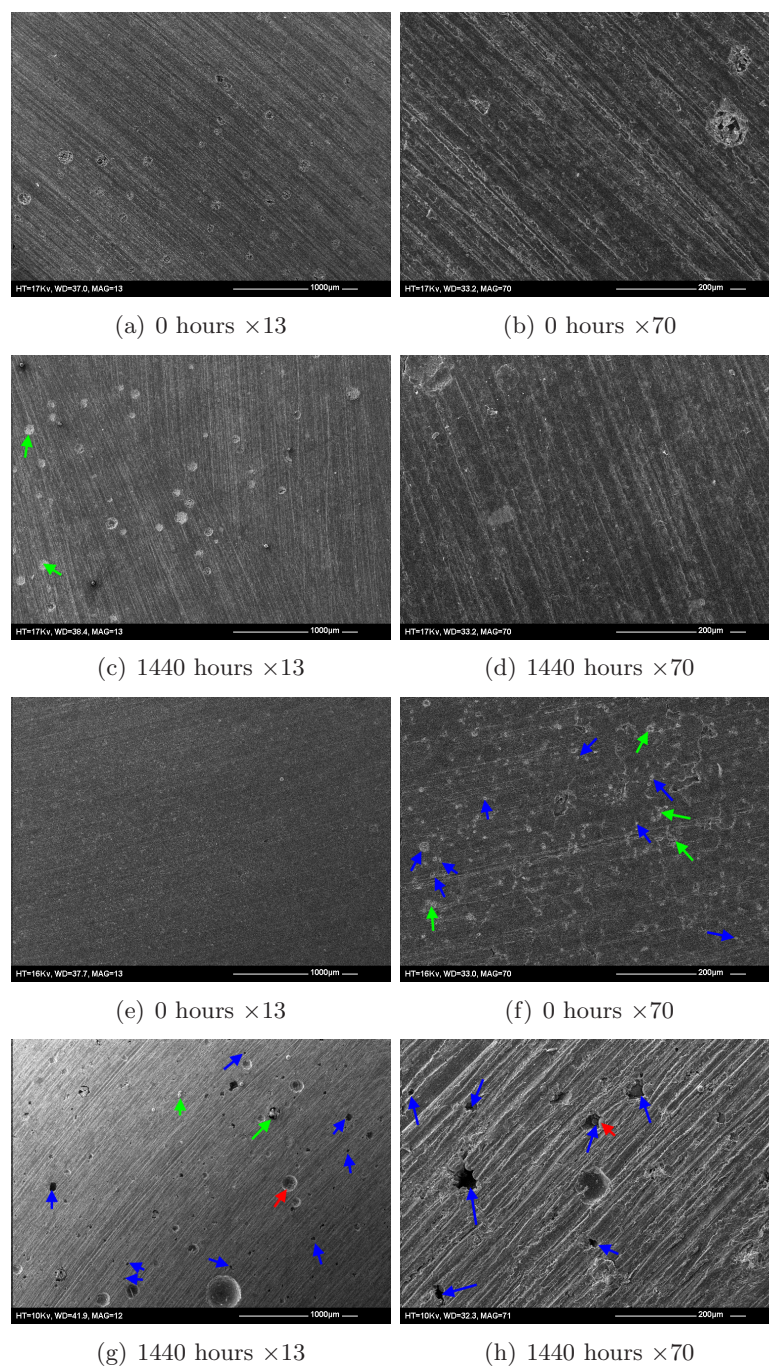


Figure 8.12: Surfaces of antibiotic release samples at 0 hours and after 1440 hours (60 days) in Ringer's solution for (a-d) Cemex and (e-h) Cemex Genta - Red arrows indicate PMMA beads, green arrows indicate radiopaque particles and blue arrows indicate gentamicin sulphate particles or pores created by the release of gentamicin sulphate. Magnification at $\times 13$ and $\times 70$.

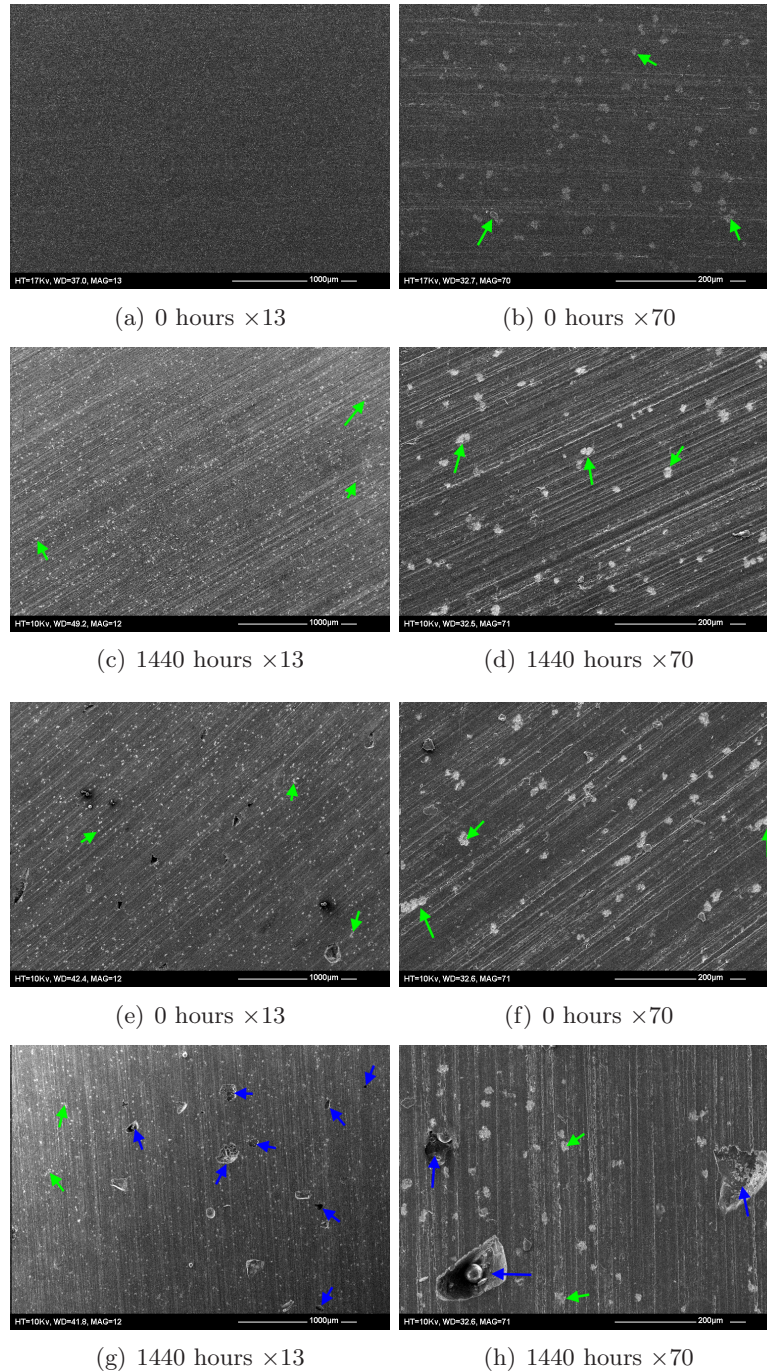


Figure 8.13: Surfaces of antibiotic release samples at 0 hours and after 1440 hours (60 days) in Ringer's solution for (a-d) Palacos R and (e-h) Palacos R+G - Green arrows indicate radiopaque particles, blue arrows indicate gentamicin sulphate particles or pores created by the release of gentamicin sulphate. Magnification at $\times 13$ and $\times 70$.

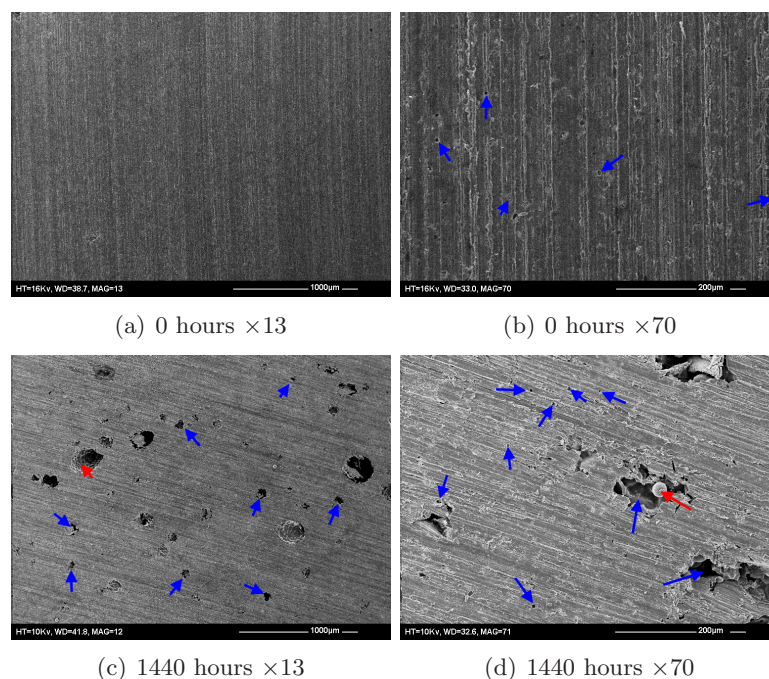


Figure 8.14: Surfaces of antibiotic release samples at (a-b) 0 hours and (c-d) after 1440 hours (60 days) in Ringer’s solution for CMW Smartset GHV - Red arrows indicate PMMA beads and blue arrows indicate gentamicin sulphate particles or pores created by the release of gentamicin sulphate. Magnification at $\times 13$ and $\times 70$.

after incubation. Furthermore, the pores were found to be irregular in shape and ranging from 50-200 μm in length. The increased porosity was not caused by entrapped air during mixing or the removal of PMMA beads.

The powder component of the cements tested is illustrated in Figure 8.15. Cemex cements were found to have a more fused powder morphology, whilst Palacos and CMW cements had clear individual PMMA beads with sizes ranging from 10 μm to 100 μm . The remainder of the powder component consisted of smaller radiopacifier particles and gentamicin sulphate particles. Cemex Genta and CMW were found to have similar gentamicin sulphate morphologies in the form of small ($\approx 10\mu\text{m}$) beads. Palacos R+G was found to have irregular shaped crystalline (5-20 μm) gentamicin sulphate particles.

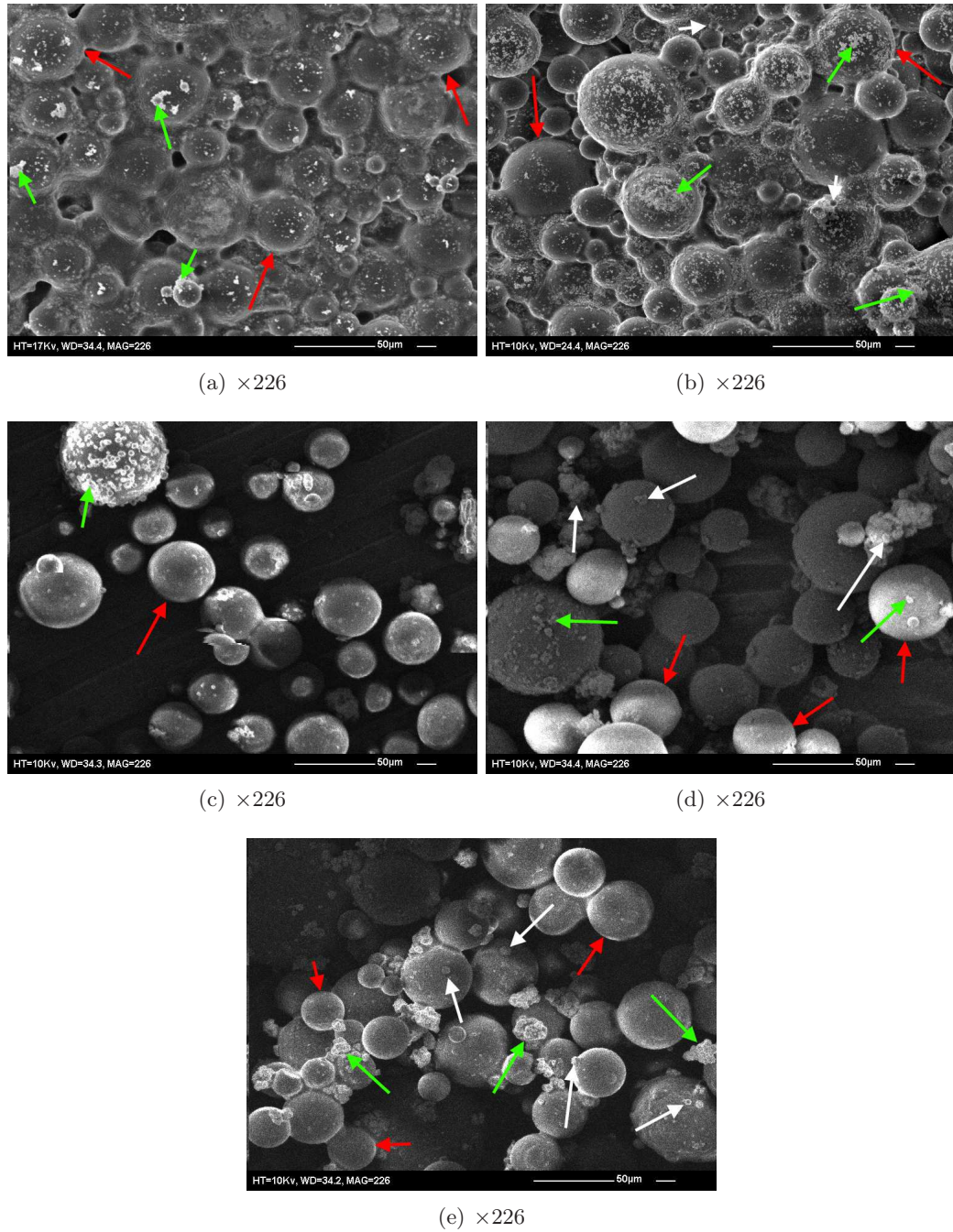


Figure 8.15: SEM images of the powder component of (a) Cemex, (b) Cemex Genta, (c) Palacos R, (d) Palacos R+G and (e) (c) CMW Smartset GHV - Red arrows indicate PMMA beads, green arrows indicate radiopacifier particles and white arrows indicate gentamicin sulphate particles

8.3.8 Vickers hardness

All samples were found to have a reduced hardness value after ageing in Ringer's solution for 60 days (Table 8.7). The reduction was found to be significant for Cemex, Palacos R and Palacos R+G ($p=5.53 \times 10^{-06}$, $p=0.03$ and $p=9.21 \times 10^{-04}$ respectively). There was no significant difference in hardness as a result of adding gentamicin sulphate to Cemex cement ($p=0.92$ after ageing in air and $p=0.08$ after ageing in Ringer's solution for 60 days). Similarly, the hardness of Palacos cement was not affected by gentamicin sulphate when tested after ageing in air ($p=0.23$), however after ageing in Ringer's solution, the hardness of Palacos was significantly reduced by the addition of gentamicin sulphate ($p=0.02$).

Table 8.7: Vickers hardness of commercially available cements before and after ageing in Ringer's for 60 days

		Hardness (HV30/10) / MPa
Cemex	Air 1 day	24.8±2.0
	Ringer's 60 days	19.1±2.0
Cemex Genta	Air 1 day	24.6±5.0
	Ringer's 60 days	21.3±3.3
Palacos R	Air 1 day	19.8±1.8
	Ringer's 60 days	17.5±2.6
Palacos R+G	Air 1 day	18.7±1.8
	Ringer's 60 days	14.4±3.0
CMW Smartset	Air 1 day	21.7±0.9
	Ringer's 60 days	20.2±2.2

8.3.9 Glass transition temperature

All samples, with the exception of Palacos R+G were found to have a significantly lower glass transition temperatures as a result of incubation in Ringer's solution for 60 days, as shown in Table 8.8 ($p < 0.05$). The addition of gentamicin sulphate to Palacos R was found to significantly reduce the glass transition temperature of the cement when tested after 24 hours in air ($p = 1.18 \times 10^{-04}$).

Table 8.8: T_g of commercially available cements before and after ageing in Ringer's for 60 days

		Glass transition temperature (T_g) / °C
Cemex	Air 1 day	127.3±1.6
	Ringer's 60 days	121.6±1.4
Cemex Genta	Air 1 day	128.5±3.8
	Ringer's 60 days	121.1±1.9
Palacos R	Air 1 day	126.2±3.3
	Ringer's 60 days	117.9±1.2
Palacos R+G	Air 1 day	115.4±1.2
	Ringer's 60 days	117.6±1.5
CMW Smartset GHV	Air 1 day	121.9±7.3
	Ringer's 60 days	109.9±0.8

8.4 Discussion

The use of gentamicin sulphate in PMMA bone cement as a local drug delivery system is growing in popularity due to its success in preventing post-operative infections. It is disputed however, whether the use of powdered gentamicin sulphate has a detrimental effect on the performance of PMMA. Furthermore, concern has been raised with regards to the growing number of antibiotic resistant bacteria present in patients with antibiotic-loaded

cements. The work in this chapter has investigated the antibiotic release, the antimicrobial activity and the mechanical and fatigue properties of three commercially available cements.

The PHT assay used in this study was found to be an accurate and useful measure for establishing release profiles of antibiotic-loaded cements, allowing for multiple samples to be tested quickly and easily. This method was not affected by materials leached from the cement. A static release test was performed, as used by Dunne et al.¹⁹⁴; this was unlike the dynamic elution tests used by other authors^{197,356}, which involves continuous mixing. The advantage of the static method was that it allowed for multiple samples from each test group to be tested over extended periods of time, however, this method does not replicate the continuous circulation of blood as occurs *in vivo* and concentration barriers affecting the release of the antibiotic are known to occur in static release tests. In this experiment however, the replacement of Ringer's solution reduced the long-term build up of concentration barriers. Furthermore, immersion of samples in 5mL of fluid ensured sink conditions were maintained, as the antibiotic concentrations obtained can be considered negligible in comparison to the maximum solubility of gentamicin sulphate (50mg/mL).

The standard deviations for the first time points of the release assay were found to be large due to the uncontrolled release of gentamicin sulphate from the surface of the cement. This result agrees with previous publications, whereby a burst of antibiotic release from the surface layers of the cement samples was experienced within the first 6 hours^{194,218,356,357}. This poses significant problems *in vivo* as any bacteria unaffected by the initial release of antibiotic may cause infections at a later time. Palacos R+G was found to release significantly more gentamicin sulphate than the other cements, even though the formulation contains half the amount of gentamicin sulphate. The enhanced release may be attributed to the composition of the cement encouraging certain release mechanisms or the morphology of the gentamicin sulphate used.

A maximum of 10% of the total amount of gentamicin sulphate incorporated was released over 60 days, leaving the majority of the antibiotic entrapped in the bulk of the cement. A maximum of 50mg of gentamicin sulphate was released over the 60 day incubation period. This dosage is locally administered and is a much more efficient treatment method as systemic treatment requires significantly higher doses due to poor uptake (3-6mg/kg body weight for children, adolescents and adults with normal renal function). Although local delivery is more effective in preventing implant infection, a greater and more prolonged release of antibiotic would reduce the likelihood of bacterial activity.

The *in vitro* release concentrations obtained are expected to differ from concentrations found *in vivo*. Nevertheless, the experiment has highlighted key information on the type of release expected to occur *in vivo*. A recent study has shown that the minimum inhibitory concentration (MIC) of gentamicin for *S. aureus* strains isolated from orthopaedic implants was 16-32 μ g/mL³⁶⁶. Although the initial release of antibiotics from the commercial cements tested were found to be above the MIC, low sub-inhibitory levels were found to occur over prolonged periods of time after the initial burst of antibiotic. Subjecting bacteria to levels of antibiotic below the MIC has been shown to contribute to the development of resistant strains^{366,367}. Furthermore, studies have found gentamicin resistant bacteria to be present post-operatively when gentamicin-loaded cements were used^{368,369}. There is therefore a need for prolonged release of antibiotics from bone cement, maintained above minimum inhibitory levels in order to prevent infections and the formation of resistant bacteria.

Results from the mathematical models demonstrated that antibiotic release from bone cements was not governed by diffusion alone. Previous studies have postulated that water cannot diffuse into glassy polymers such as PMMA below the T_g , rather, water penetrates the cement through voids and cracks on the surface^{370,371}. The results from Chapter 7

however, have shown that a certain degree of diffusion takes place. The additional burst coefficient improved the accuracy of all the models as it accounts for the initial release of antibiotics from the surface of the cement. After the initial surface release, water may penetrate the cement via pores and to a certain extent diffusion through the polymer chains, releasing more gentamicin from layers below the surface, but at a slower rate. This finding agrees with other authors who have hypothesised that initial water penetration may create channels by which gentamicin may elute out towards the surface of the cement¹⁹⁷. These theories also provide an explanation for the goodness of fit of the Noyes-Whitney dissolution model. The expanded Korsmeyer-Peppas model developed by Lindner et al.³⁶⁴, which states that antibiotic release is governed by release from the surface of the cement and is exponentially related to time, was found to most accurately model the antibiotic release for all the cements. Other studies have shown that the Khun and Wilson model³⁷², which combines all three factors discussed (surface release, dissolution and diffusion), provides a good fit for antibiotic release from bone cements. An extensive review has been conducted by Lewis et al.³⁷³ highlighting the different release models proposed in the literature.

Recent studies have shown that the rate of drug release from bone cement is affected by the mixing technique employed due to the varying porosities obtained^{203,204}. The samples tested were all prepared in a similar manner with the same surface roughness and few surface pores was detected prior to the release assay. Furthermore, cements without gentamicin were found to have no pores after incubation. Therefore, it is hypothesised that the antibiotic release from the surface of the cement creates pores, which allows water to diffuse further into the cement through subsequent pore generation.

From the antimicrobial assays, it was found that the strain of *S. aureus* used was susceptible to gentamicin sulphate. The 10µg control discs produced consistent zones of inhi-

bition, demonstrating the validity of the assay. Cements without antibiotics were found to have no antimicrobial properties, highlighting the need for a therapeutic delivery system in PMMA bone cement. The use of 1g of powdered gentamicin sulphate per 40g of cement for Cemex Genta and CMW and 0.5g per 40g of cement for Palacos R+G produced moderate antimicrobial activity. Cemex Genta and Palacos R+G samples were found to produce irregular shaped zones and a high level of variation between samples. This is likely due to the poor dispersion of gentamicin sulphate on the surface of the cement, which results in an uneven diffusion of antibiotic through the agar, creating irregular shaped zones. Similar studies have also shown gentamicin sulphate to agglomerate in PMMA bone cement¹⁹⁴. This is due to incompatibilities in terms of hydrophobicity/hydrophilicity between PMMA and gentamicin sulphate resulting in an heterogeneous system with multiple phases.

Although Palacos R+G was found to achieve the best antibiotic release in Ringer's solution, it did not consistently perform as well on agar against bacteria. In agar diffusion tests, the gentamicin diffuses from surface layers of the cement into the agar and creates a zone in which bacterial growth is inhibited. This is an effective test as it demonstrates the efficacy of the delivery system against bacteria commonly found in orthopaedic infections. *In vivo* the cement is assumed to be in direct contact with bone tissue and the diffusion test has shown that poor dispersion of antibiotics on the surface of the cement may not fully inhibit bacteria dispersed around the implant. As zone size is a function of the diffusion rate through the agar, the potency of the antibiotic and the growth of the bacteria, smaller inhibition zones do not always imply less inhibitory action. This technique therefore, can only be used for qualitative purposes. Similar techniques have been used in other studies to assess the antimicrobial activity of different antibiotics in bone cement^{216,374}. The ability of the antibiotic-loaded cements to prevent biofilm formation is another index of its efficacy. Previous studies have shown that using powdered gentamicin sulphate in PMMA bone cement does not prevent the formation of biofilms^{194,198,214,216}.

In terms of mechanical properties and glass transition temperature, the use of powdered gentamicin sulphate did not affect Cemex bone cement, however a reduction was observed when antibiotic was employed in Palacos cement. When testing hardness and fracture toughness, both cements were not affected by the addition of gentamicin sulphate powder. Therefore, the impact of using gentamicin sulphate powder is thought to be dependent upon the cement composition and the type of test performed. The lack of conclusive results from static tests accords with the view of Dunne et al.¹⁹⁴ who stated “antibiotic does not play an active role in the mechanical performance of the cement when it is being statically loaded within its elastic region”.

Ageing in Ringer’s solution for 60 days resulted in the elution of powdered gentamicin sulphate from the commercial cements and as a consequence of this, a reduction was observed in the majority of the properties tested. What is known from studies reported in Chapter 7, however, is that aged cements experience a change in static properties regardless of the presence of gentamicin sulphate. Nevertheless, increased porosity due to antibiotic elution can contribute to reductions in mechanical properties. In similar studies, the addition of supplementary amounts of gentamicin was found to decrease the mechanical and fatigue properties of PMMA bone cements^{194,196,202,375-377}. This was linked to agglomerations of gentamicin sulphate when more than 0.5g of gentamicin sulphate per 40g of cement was used, which resulted in large pores after elution.

When testing fatigue crack propagation, the results demonstrated that the addition of gentamicin sulphate powder increased the crack growth rates for all the cement brands tested. After antibiotic elution, the fatigue crack propagation was not significantly different most probably because the greatest proportion of the antibiotic had not been released. Nevertheless increased porosity was observed in cements with powdered gentamicin sulphate, and this may ultimately have a detrimental effect on the performance of the cement.

A higher number of pores were found on the surfaces of gentamicin sulphate containing samples used in the release assay. This agrees with the hypothesis that initial antibiotic release creates porosity on the surface of samples, which then allows further penetration of water into the cement. The porosity observed is also thought to create stress concentrations upon loading, which weakens the cement.

The morphology of the gentamicin sulphate powder in the cements tested was found to be different. The gentamicin sulphate in Palacos R+G was seen to have a more crystalline and irregular shape whilst CMW and Cemex Genta had smaller rounded particles of gentamicin sulphate. The shape and size of the antibiotic particle has been known to play a vital role on the dose and duration of the release³⁷⁸. Antibiotics in the form of crystalline particles have been shown to dissolve more readily from the surface of the cement and obtain better release profiles than fine powders³⁷⁹. It is likely that the gentamicin sulphate powder selected for use in Palacos R+G along with the porosity of the cement contributed to the overall enhanced antibiotic release when compared to CMW and Cemex Genta.

8.5 Conclusions

The majority of the gentamicin sulphate release was found to occur within the first 6 hours and only a low percentage (<10%) of the total antibiotic was released. This may lead to resistant bacteria forming as sub-inhibitory levels become established after this early phase. Mathematical modelling of the cement demonstrated that release occurred as a result of gentamicin sulphate release from the surface of the cement, followed by porosity driven mechanisms, as confirmed by SEM images. Poor dispersion of antibiotic at the surface of the cement possibly resulted in poor uniformity of antimicrobial activity. Furthermore, the properties of the cements were found to be altered by the use of powdered gentamicin sulphate, particularly in terms of fatigue crack propagation.

Although the use of powdered gentamicin sulphate in PMMA bone cements has been successful in reducing the rate of infections in joint replacement surgery, post-operative infections are still known to occur. Different antibiotics such as ciprofloxacin and vancomycin may be used, which have been shown to be more active against bacteria³⁶⁶, however the limitations of using powdered antibiotics in bone cement, such as poor dispersion and altered mechanical and fatigue properties, are still expected to be present regardless of the therapeutic agent used. Therefore, there is a need for a novel delivery system in PMMA bone cements, which will not affect the mechanical and fatigue properties and will ensure a prolonged release of antibiotic at inhibitory levels. In addition, improved dispersion of the antibiotic is required to ensure adequate distribution of activity at the surface of the implant. Having established these requirements, the subsequent chapters focus on the development and testing of a novel drug delivery system for PMMA bone cements.

Chapter 9

Incorporating a liposomal drug delivery system

9.1 Introduction

Commercially available bone cements with powdered gentamicin sulphate have limitations associated with antimicrobial efficacy, the release of antibiotics, mechanical performance and fatigue properties. Attempts to overcome these problems include the use of gentamicin solution^{206–209}, alternative therapeutic agents^{210–218} and silver nanoparticles^{219–221}. Some of these attempts have met with moderate success, however poor mechanical and antimicrobial properties still limit these novel formulations. To overcome these limitations, a novel approach to drug delivery in bone cement was considered. In this delivery system, liposomes encapsulating a therapeutic agent, were dispersed in PMMA bone cement in an attempt to improve the pharmacokinetic, mechanical and fatigue properties of antibiotic-loaded bone cements. This chapter describes the development of this novel approach and how the stability and dispersion of the system was tested.

9.1.1 Liposomes

Liposomes are vesicles consisting of a bilayer of lipid molecules which usually enclose an aqueous solution (Figure 9.1)³⁸⁰. Although an hydrophobic preparation can also be entrapped. These vesicles, usually composed of phospholipids, were discovered in 1965 when it was found that lipids dispersed in water spontaneously to form large multilamellar vesi-

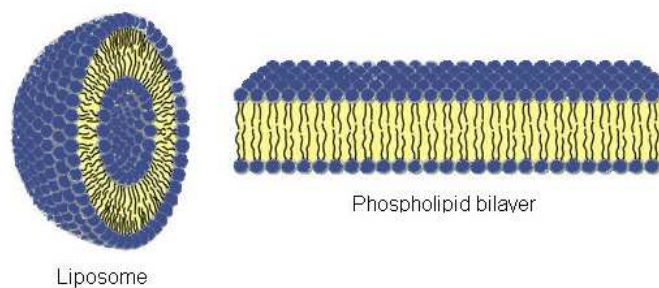


Figure 9.1: Liposome vesicle

cles³⁸¹. Depending on the preparation technique, liposome vesicles can range from tens of nanometres to tens of microns in diameter. The lamellarity of the liposomes can also vary, as can the quantity of material entrapped within the aqueous compartment and lipid bilayer. Liposomes were originally used as models for the lipid bilayer portion of cell membranes³⁸¹. Liposomes can thus be designed to mimic the behaviour of natural membranes, whilst also being degradable in a similar manner, making them an ideal vehicle for medical applications.

The most frequent use of liposome formulations has been to improve the solubility of therapeutic agents. Pharmacologically active agents used in liposomes include antineoplastic and antimicrobial drugs, chelating agents, steroids, vaccines and genetic materials³⁸². Liposomes are able to remain within the circulatory system for increased lengths of time and have been known to accumulate at sites of disease or inflammation, increasing the bioavailability of the therapeutic agents^{383–386}. The lipid bilayer encapsulating the therapeutic agent protects active compounds from biological degradation, leading to an enhancement in therapeutic potency and also reduce the cytotoxicity of certain drugs³⁸⁷. As the lipid vesicle can encapsulate both an aqueous and an hydrophobic solution, a combination of different therapeutic agents can be employed for specific treatments. These advantages along with the proven safety and efficacy of liposomes have made them an attractive candidate for a drug delivery system in the medical field, particularly in the areas of drug targeting and immune modulation.

Phospholipids

Phospholipids are molecules which form the major structural components of cell membranes³⁸⁰. They are naturally occurring, biodegradable, non-toxic and generally consist of two hydrophobic fatty acid chains connected to a hydrophilic polar headgroup as shown in Figure 9.2^{388,389}. The hydrophilic polar headgroup is linked to two hydrophobic acyl hydrocarbon chains by a glycerol molecule, resulting in an amphiphatic molecule. Phospholipids are generally not soluble in aqueous environments as they tend to aggregate and migrate to surfaces. This arises as a result of the hydrophobic fatty acid chains orientating away from water, creating a bilayer sheet with the hydrophilic heads in the aqueous solution and the fatty acid chains protruding into a hydrophobic region, often air. This minimises the interaction between the aqueous solution and the long fatty acid chains. This capability can be exploited however and when the bilayer sheets fold onto themselves, they may create liposome vesicles. Figure 9.3 shows the variety of lamellar structures created when phospholipid bilayers create liposome vesicles.

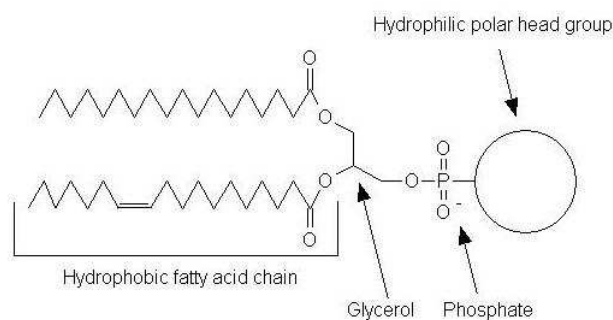


Figure 9.2: Phospholipid structure

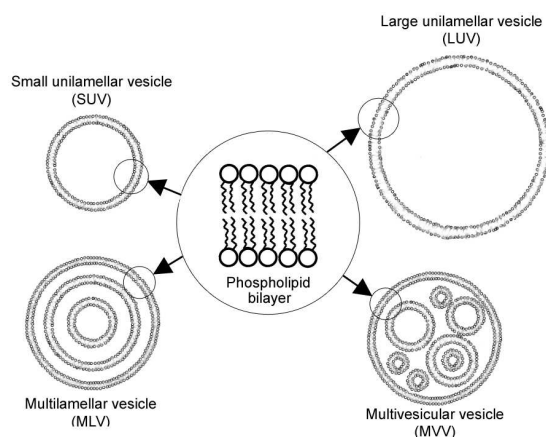


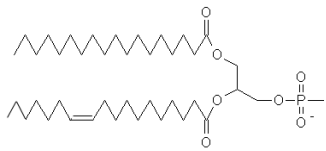
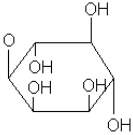
Figure 9.3: Lamellar structures

Liposome charge

A commonly used phospholipid is phosphatidyl choline (PC, also known as lecithin), which can be derived from both natural and synthetic sources. PC can be extracted from egg yolk, soya beans and less readily from bovine heart and spinal cord tissue. PC is frequently employed in formulations due to its low cost relative to other phospholipids, its neutral charge and its chemical inertness. Although the headgroup of PC is positively charged, the negative charge of the phosphate molecule at the phosphatidyl moiety neutralizes the overall charge. This overall neutrality is also seen with phosphatidylethanolamine (Table 9.1). More generally however, and as a result of the phosphate molecule in phospholipids, the majority of phospholipids with neutral and negatively charged headgroups are considered negatively charged overall (e.g. phosphatidylserine, phosphatidylglycerol, phosphatidic acid and phosphatidylinositol).

By altering the polar headgroup of the phospholipid (as shown in Table 9.1), different surface charges thus can be adopted, which may be advantageous to applications such as drug targeting or inducing mineralisation. Recent studies have used phospholipids as a coating material for implants and have shown that phosphatidyl serine (PS) is an effective lipid for promoting calcification both *in vitro* and *in vivo*^{247,254,257}. The surface charge

Table 9.1: Naturally occurring phospholipids

Fatty acid chain	Headgroup	Common Name (Phosphatidyl-)	Abbreviation
	$\text{O}-\text{CH}_2-\text{CH}_2-\overset{\text{CH}_3}{\underset{\text{CH}_3}{\text{N}^+}}-\text{CH}_3$	choline	PC
	$\text{O}-\text{CH}_2-\text{CH}_2-\text{NH}_3^+$	ethanolamine	PE
	$\text{O}-\text{CH}-\overset{\text{NH}_3^+}{\text{C}}-\overset{\text{COO}^-}{\text{C}}$	serine	PS
	$\text{O}-\text{CH}_2-\underset{\text{OH}}{\text{CH}}-\underset{\text{OH}}{\text{CH}_2}$	glycerol	PG
	$\text{O}-\text{H}$	acid	PA
		inositol	PI

of the liposome also affects its stability as lack of surface charge can increase aggregation³⁹⁰. *In vivo* however, neutral and positively charged liposomes and those containing phosphatidylcholine were found to be most stable; whilst negatively charged liposomes were less so, binding to higher amounts of protein in the blood³⁹¹.

Liposomes can be created from a mixture of phospholipids. For example, Santin et al.²⁴⁷ used phosphatidylcholine, phosphatidylserine and cholesterol liposomes at a molar ratio of 7:2:1 to test the calcium-binding potential of phospholipids for implant coatings. Phosphatidylinositol was also tested by replacing phosphatidylserine in the same study. Certain lipids exist which do not have phosphatidyl moieties and can also be employed

in liposome mixtures. The overall charge of these molecules is governed mainly by the charge on the hydrophilic head group. This has allowed for the manufacture of synthetic cationic (positively charged) liposomes, which have gained recent interest in gene delivery due to the negatively charged genetic material binding with the positively charged liposome by electrostatic interactions. Examples of cationic liposomes include DOTAP (1,2-dioleoyloxy-3-(trimethylammonio) propane), DOTMA (N-(2,3- (dioleoyloxy)propyl-N,N,N-trimethyl ammonium), DODAc (dioctadecyldimethylammonium chloride), DM-RIE (1,2-dimyristoyloxypropyl-3-dimethyl-hydroxyethyl ammonium), DOSPA (2,3-dioleoyloxy-N-(2 (sperminecarboxamide) ethyl) -N,N-dimethyl-1-propanaminium) and DOGS (dioctadecylamidoglycylspermine).

Phase transition temperature

The phase transition temperature (T_c), the temperature at which the phospholipid changes from a gel phase to a liquid phase, is important as high T_c liposomes result in a less fluid bilayer at physiological temperatures, which is less likely to leak the encapsulated content. Furthermore, high T_c lipids have been shown to have a lower level of uptake by phagocytic cells³⁸⁶. The use of sterol lipids, such as cholesterol, in liposomes has been shown to increase the T_c and in higher concentrations, completely eliminate the phase transition, resulting in a decrease in membrane fluidity, increased stability and less likelihood of leakage. Heating above the T_c of the phospholipids during manufacture of liposomes is required in order to form vesicles.

Liposome size

Liposomes vary in size ranging from 0.025 to 2.5 μm ³⁸⁷; such liposomes can vary in the number of bilayers. In general, liposomes are classified into one of four categories: small unilamellar vesicles (SUV, <100nm), large unilamellar vesicles (LUV, >100nm), multilamellar vesicles (MLV, >100nm) and multivesicular vesicles (MVV, >100nm)³⁸⁷.

SUVs consist of a single bilayer and are homogeneous in size. Due to their small dimensions, there tends to be excessively high stresses on the bilayer of SUVs which makes them thermodynamically unstable and susceptible to aggregation and fusion³⁹². Furthermore, the low aqueous volume to lipid ratio (0.2-1.5 l/mole lipid) results in limited encapsulation of material, particularly macromolecules. SUVs do, however, have a long circulation half-life³⁸⁷.

LUVs also consist of a single bilayer, however due to its larger size and high aqueous volume to lipid ratio (7 l/mole lipid), they have a much higher encapsulation efficiency and high capture rate of macromolecules. The single bilayer allows for high volumes of hydrophilic drugs to be encapsulated³⁸⁷. The larger size also results in increased stability due to lower stresses associated with the longer curvature of the vesicle.

MLVs consist of more than one bilayer and tend to be larger in size than SUVs and LUVs. The multiple bilayers tend to favour encapsulation of hydrophobic materials. MLVs have a moderate aqueous volume to lipid ratio (1-4 l/mole of lipid)³⁸⁷. The larger size results in a more stable liposome with a long shelf-life, but this size does make MLVs more susceptible to phagocytic uptake. MVVs are similar to MLVs, however consist of a large vesicle encapsulating several smaller vesicles as shown in Figure 9.3. This type of vesicle usually forms in the initial stages of liposome preparation prior to forming SUVs, as discussed later in this chapter.

In order to maximise the accumulation of liposomal drugs at disease sites, homogeneous vesicles with diameters between 70-150nm are usually employed³⁹³. Vesicles of this size are small enough to circulate without becoming trapped in tissue microvasculature, but also small enough to penetrate through pores and gaps in the vascular endothelium associated with areas of inflammation^{394, 395}. This size range has good therapeutic carrying capabili-

ties, with acceptable encapsulation efficiencies and the liposomes are small enough to pass through sterilizing filters without damage or loss of contents. Furthermore, liposomes of this size range are generally considered to be stable in suspension. Although larger liposomes are also considered stable, sedimentation of the suspension has been known to occur over time, resulting in a shorter usable shelf-life.

9.1.2 Preparation of liposomes

The preparation method largely dictates the size, structure, dispersity and shelf-life of liposomal systems. Therefore, the following factors must be taken into account when establishing a method for liposome manufacture:

- The physical chemistry of the material being encapsulated and the lipid composition.
- The toxicity and concentration of the encapsulated material.
- The medium in which the liposome vesicles are being dispersed.
- The size, stability, dispersion and shelf-life requirements.
- The target area, required dosage and release rate.
- Reproducibility and clinical applicability.

Liposomes created by low shear sonication tend to produce MLVs, whilst high shear sonication tends to produce SUVs. Sonicated liposomes have a wide size distribution and as sonication can be detrimental to the structure of certain therapeutic agents, they are less preferred in delivery systems³⁸⁰. For more uniformly sized liposomes that can encapsulate therapeutic agents, extrusion or the Mozafari method is generally used, however this usually results in unilamellar vesicles being formed. A simplified classification of preparation methods is shown in Figure 9.4.

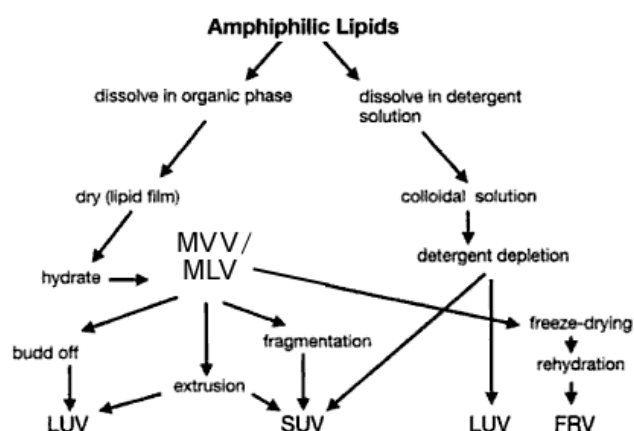


Figure 9.4: Classification of liposome preparation methods (FRV - Freeze/rehydrated vesicles)³⁸⁰.

The method of preparation has a significant effect on the encapsulation efficiency of the liposome. Preparation methods can be classified into two categories according to the method of loading therapeutic agents: these are known as passive and active loading methods. Passive loading involves introducing the drugs before or during the manufacturing process of the liposome, whilst active loading involves loading therapeutic agents into pre-formed liposomes.

Passive loading can be classified further into mechanical dispersion methods (i.e. sonication, membrane extrusion), solvent dispersion methods (i.e. ethanol injection, reverse phase evaporation) and detergent removal methods (i.e. dialysis, column chromatography)³⁸⁰. Although passive loading methods, such as the thin-film hydration technique, are simple, they are associated with a relatively poor encapsulation efficiency (5-15%). Other techniques, such as freeze drying, have been shown to improve encapsulation efficiency, however these methods can also alter the size distribution of the suspension³⁹⁶.

Active loading creates a concentration gradient to force materials through the bilayer and into preformed liposomes. This method is associated with higher encapsulation efficiencies (up to 90%) and usually involves the use of pH gradients to encapsulate materials³⁹⁷.

9.1.3 Liposomes in PMMA bone cements

Despite their long availability, liposomal drug delivery systems are still being developed and optimised for a variety of medical applications. A recent literature search has found little mention of using liposomes in polymeric materials for medical application. The main anticipated issues with using liposomes in bone cements include: incompatibilities with the hydrophobic and aqueous systems comprising the cement ingredients; the high setting temperature of bone cements; the dispersion of the liposomes in the cement; the release of the liposome vesicles from the cement; the bioavailability of any entrapped agents; and the effect of included liposomes on the mechanical and fatigue properties of bone cement. The work in the next two chapters is designed to investigate the stability and dispersion of liposomes in PMMA bone cement, the delivery of an antibiotic from bone cement using liposomes, and their effect on mechanical, fatigue and structural properties.

9.1.4 Surfactants

Liposomes intended to encapsulate a water-soluble antibiotic are generally formed in an aqueous suspension, which is incompatible with the hydrophobic MMA and PMMA that makes up bone cement. Freeze drying or lyophilizing methods can be used to turn liposomes into a powder which might more readily be incorporated into the powder component of bone cements. Lyophilizing however, is a complex, time consuming and costly process and although the process improves encapsulation efficiency, the liposome bilayer is broken and reformed, altering the size of the liposomes. This results in less control over the size distribution of the final suspension. A more favourable option, and certainly one which in principle offers enhanced dispersion, is to incorporate liposomes into the non-polar liquid component of bone cement (MMA). This difference in polarity between the two liquids, however, will result in phase separation and loss of stability.

When mixing an aqueous liposomal suspension with MMA, a water-in-oil mixture is created, whereby charged water molecules attract each other and MMA molecules with no charge attract each other creating two separate phases. This was found to occur when gentamicin sulphate solution was added to bone cement and resulted in poor mechanical properties^{206,207}. The use of emulsifiers to prevent phase separation has been tested with gentamicin sulphate solution in bone cement, however a reduction in mechanical properties was still found to occur²⁰⁸. Therefore, it is proposed that liposomes will be formulated in the presence of a surfactant, whilst also minimising the aqueous volume by pelleting the liposomes.

When selecting an appropriate surfactant for use in a bone cement, two main considerations must be borne in mind; the surfactant must be non-toxic and it must be able to overcome the forces separating the two phases in order to create a stable emulsion. Surfactants tend to be amphiphilic, like liposomes, and usually consist of a solubilizing hydrophilic “head” group and a hydrophobic “tail” group as shown in Figure 9.5. Surfactants are classified by the charge contained within the hydrophilic head group. The four basic classifications are shown in Table 9.2.

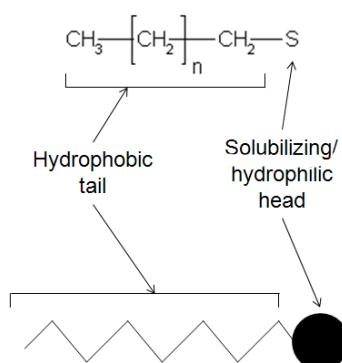
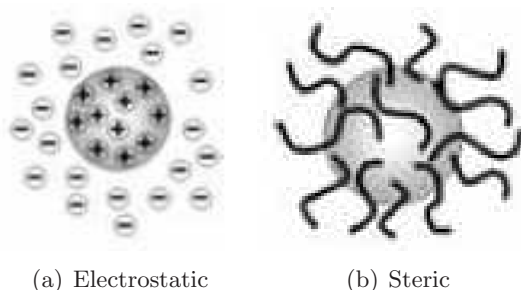


Figure 9.5: Surfactant structure

Table 9.2: Classification of surfactants

Classification	Head group charge	Example head groups
Anionic	Negatively charged	Carboxyl ($\text{RCOO}^- \text{M}^+$), sulphonate ($\text{RSO}_3^- \text{M}^+$), sulphate ($\text{ROSO}_3^- \text{M}^+$) or phosphate ($\text{ROPO}_3^- \text{M}^+$)
Cationic	Positively charged	Quaternary ammonium halides ($\text{R}_4\text{N}^+ \text{X}^-$), pH dependent primary, secondary or tertiary amines
Nonionic	No charge (but contains highly polar groups)	Polyethylene ($\text{R-OCH}_2\text{CH}_2\text{O}$), aliphatic alcohols ($-\text{OH}$)
Amphoteric	Contains positively and negatively charged groups	Amino acids ($\text{NH}_3^+ \text{CHR} \text{COO}^-$), sulphobetaines ($\text{RN}^+ (\text{CH}_3)_2 \text{CH}_2 \text{CH}_2 \text{SO}_3^-$)

Nonionic surfactants generally tend to be less toxic and more biocompatible than other surfactants. As a result of this, nonionic block copolymers are extensively used in therapeutic delivery systems. Another advantage of nonionic block copolymers is that they work via steric repulsion instead of electrostatic stabilization as most surfactants do. With electrostatic stabilization (Figure 9.6(a)), components are added to the solution which change the overall charge of the system and allows for a stable and well dispersed colloid. This method may affect the structure and stability of the liposome as surfactant ions have been known to react with lipid molecules and therefore electrostatic stabilization may not be suitable for this application. Steric repulsion occurs when polymers are added to a system and adsorb on the surface of particles (Figure 9.6(b)). These polymer chains increase the distance between those particles and render van der Waals forces too weak to cause agglomeration.

Figure 9.6: Different stabilization systems³⁹⁸

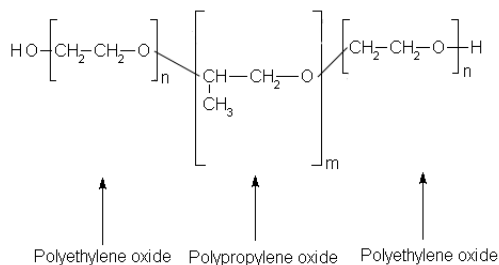


Figure 9.7: Pluronic structure

A particular nonionic surfactant group of interest is the range of polyethylene oxide-polypropylene oxide-polyethylene oxide triblock copolymers (PEO-PPO-PEO), otherwise known under the trade names of Poloxamer and Pluronic. These surfactants are composed of two hydrophilic polyethylene oxide (PEO) chains joined together by a hydrophobic polypropylene oxide (PPO) chain (Figure 9.7). The differences in chemical structure and polarity between the two chains creates an hydrophobic/hydrophilic balance which can be used to address the polarity differences between water and methyl methacrylate (MMA).

For the Pluronics the nomenclature used can be a useful shorthand for the structure: the first letter provides information on its physical form at room temperature (L is liquid, P is paste and F is flake or solid), the first digit (or first two digits if the number is three digits long) multiplied by 300 gives the approximate molecular weight of the PPO component and the last digit multiplied by ten gives the percentage of PEO content. For example, Pluronic L31 is a liquid at room temperature, its PPO component has a molecular weight of 900g/mol and a PEO content of 10%. From this information and knowing the molecular weight of one chain of PPO is 58g/mol and one chain of PEO is 44g/mol, with the OH and O portions having a combined molecular weight of 18g/mol, the number of PEO and PPO chains can be calculated and the structure of the Pluronic deduced. Table 9.3 shows different Pluronic products and their calculated structures.

Table 9.3: Structure of different Pluronics

Pluronic	M_w of PPO / g/mol	% PEO content	M_w of PEO / g/mol	Average M_w / g/mol	Number of PPO chains	Number of PEO chains	HLB	HLB group
L31	900	10	110	1100	15	2	4.5	3 to 6
L43	1200	30	555	1850	21	12	12	8 to 12
L44	1200	40	880	2200	21	20	16	15 to 18
L61	1800	10	200	2000	31	4	3	3 to 6
L62	1800	20	472	2360	31	10	7	7 to 9
L64	1800	40	1160	2900	31	26	15*	13 to 15
P65	1800	50	1700	3400	31	38	17*	15 to 18
F68	1800	80	6720	8400	31	152	29*	n/a
P84	3200	40	1680	4200	55	38	14*	13 to 15
P104	3000	40	2360	5900	52	53	12 to 18*	15 to 18
P123	3600	30	1725	5750	62	39	7 to 12*	8 to 12
F127	3600	70	8820	12600	62	200	22*	n/a

Note: n/a - not applicable as calculated HLB outside of HLB group ranges * - HLB values obtained experimentally

To narrow the selection for this particular application, Pluronics with a working temperature range between 0°C and 100°C were selected as they are capable of withstanding the high exothermic curing temperatures of bone cement and long term use *in vivo*. A semi-empirical scale for selecting an appropriate surfactant can also be used. The scale was originally developed by Griffin et al.^{399,400} and is known as the hydrophilic-lipophilic balance (HLB). The HLB is based on the relative percentage of hydrophilic to hydrophobic components in the surfactant molecule. Table 9.4 shows HLB ranges and their specific applications. Griffin's technique to calculate the HLB value was quite laborious and required several trial and error steps, therefore the process was altered by Davies et al.⁴⁰¹, allowing a surfactant's HLB number to be calculated directly from its chemical formula. The improved method uses Equation 9.1 and empirically determined values for organic groups. Studies have shown HLB values calculated using this method agree with values obtained experimentally^{398,402}.

Table 9.4: HLB values and their application

HLB Range	Application
3-6	water-in-oil emulsifier
7-9	wetting agent
8-12	oil-in-water emulsifier
13-15	detergent
15-18	solubilizer

$$\text{HLB} = 7 + \Sigma(\text{Hydrophilic group no.}) - \Sigma(\text{Hydrophobic group no.}) \quad (9.1)$$

By using Table 9.5, each ethylene oxide (EO) unit has a calculated HLB of 0.33 and each propylene oxide (PO) unit has an HLB of -0.15. Using the estimated number of units in each chain, as shown in Table 9.3, the calculated HLB values for EO and PO and Equation 9.1, the HLB values for the Pluronics were determined. Pluronic L31 and L61 have HLB values of 5 and 4 respectively, making them suitable for oil-in-water emulsions such as incorporating an aqueous liposome solution into MMA. Furthermore, these values

Table 9.5: HLB values for component groups

Group	HLB Number	Group	HLB Number
Hydrophilic		Hydrophobic	
-SO ₄ Na ⁺	38.7	-CH-	0.475
-COO ⁻	21.2	-CH ₂ -	0.475
-COOK	21.1	-CH ₃	0.475
-COONa	19.1	=CH-	0.475
-N (tertiary amine)	9.4	-CF ₂ -	0.87
Ester (sorbitan ring)	6.8	-CF ₃	0.87
Ester (free)	2.4	Derived	
-COOH	2.1	-CH ₂ -CH ₂ -O	0.33
-OH (free)	1.9	-CH ₂ -CH ₂ -CH ₂ -O-	0.15
-O-	1.3		
OH- (sorbitan ring)	0.5		

agree with experimental data (HLB of 1-7 for both)^{398,402}. These calculations however, as described by Davies et al.⁴⁰¹, are not accurate for large molecules with more than 20 PEO units as the different parts of the same molecule act virtually independently. Therefore, for Pluronic with more than 20 PEO units, experimental methods are required.

The precise mechanism by which the Pluronic and the liposome vesicles interact is unknown and the literature on this subject is limited. It can be speculated however, that the hydrophilic PEO chains will orientate themselves to the outer hydrophilic polar heads of the liposome vesicle, leaving the hydrophobic PPO chains free to interact with the hydrophobic non-polar MMA. This structure is shown in Figure 9.8. Due to the limitations

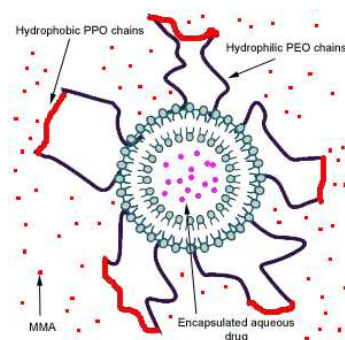


Figure 9.8: Liposome-Pluronic structure

of the available imaging techniques, the structural integrity of the liposome-Pluronic arrangement will be difficult to observe as Pluronic chains tend to be smaller than 5nm. Therefore, the functional stability of the liposome-Pluronic structures in MMA was investigated instead, in terms of sedimentation rate, dispersion and ability to withstand high temperatures.

9.2 Methods

9.2.1 Materials

Phosphatidyl choline (PC) from egg yolk ($\geq 99.0\%$), cholesterol (C, $\geq 99.0\%$), uranyl acetate ($\geq 98.0\%$) and Pluronics L31, L61, F68 and F127 were purchased from Sigma Aldrich (Gillingham, UK). Chloroform (HPLC grade) was purchased from Fisher Scientific (Fisher Scientific UK Ltd, Loughborough, UK). Pluronics L43, L44, L62, L64, P65, P84, P104, P123 were provided by BASF (BASF Corporation, Connecticut, USA). TopFluor cholesterol was purchased from INstruChemie (INstruChemie BV, Delfzijl, Netherlands)

9.2.2 Liposome preparation

Liposomes containing phosphatidyl serine (PS) were to be used due to that lipid's calcu-logenic potential as described in the literature^{247,254,257}, however charge incompatibilities between PS and gentamicin sulphate used in the next chapter, resulted in an unstable li-posome bilayer. Thus, a neutral liposome (phosphatidylcholine (PC) and cholesterol (C)) was used.

PC and C were weighed and combined in a ratio of 7:1 respectively and added to a 50mL round-bottom flask. 5mL of chloroform was added to the flask and the suspension was vor-texed until the lipids dissolved. The flask was attached to a rotary evaporator with a water bath set at 60°C (above T_c of PC) with a vacuum pump and rotation set to 1 revolution

per second. Once all the chloroform had evaporated and a thin film of lipids had formed, deionised water heated to 60°C was added and the flask vortex mixed to create a suspension of liposome vesicles at a concentration of 5mg/mL. The lipid suspension was held at 60°C for 30 minutes for the liposomes to form. The suspension was extruded 10 times under nitrogen pressure (8 bars maximum) using a Lipex extruder (Northern Lipids Inc., British Columbia, Canada) vertically through a 400nm polycarbonate membrane (Whatman, UK) followed by further extrusion 10 times using a 100nm polycarbonate membrane.

The average liposome diameter was measured by laser diffraction using a Beckman Coulter N4 PLUS particle size analyzer (Beckman Coulter Ltd, High Wycombe, UK) to ensure an average 100nm diameter liposome suspension was obtained. 2%w/w of Pluronic (L31, L43, L44, L61, L62, L64, P65, F68, P84, P104, P123 or F127) was added to the liposome suspension after extrusion. This concentration was selected as this is below the critical micelle concentration (CMC) of the Pluronics, which is the concentration above which surfactant micelles form. The liposome-Pluronic suspension was centrifuged at 100,000g (25,000 RPM) for 1 hour at 4°C using a Beckman Optima LE-80K centrifuge (Beckman Coulter Ltd., High Wycombe, UK) with a SW28 rotor to create a pellet in order to minimize the amount of water in the final cement mixture.

9.2.3 Liposome diameter

PC:C liposomes without Pluronics were prepared as described and centrifuged to produce a 10mg pellet. The pellet was resuspended in 10mL of deionised water and vortexed. The liposome diameters were measured by laser diffraction using a Beckman Coulter N4 PLUS particle size analyzer (Beckman Coulter Ltd, High Wycombe, UK), to ensure the liposomes were not damaged or altered during the centrifugation process.

10mg PC:C liposome pellets with and without Pluronics were prepared as described and resuspended in 10mL of MMA by the process of titration, followed by vortexing. The liposome diameters in MMA were measured by laser diffraction.

9.2.4 Sedimentation rate

The sedimentation rate was established by measuring the absorption at 420nm of the liposome-Pluronic suspension in MMA over time using an Hitachi U-1900 spectrophotometer (Hitachi High-Technologies Europe GmbH, Mannheim, Germany) against a MMA blank. The suspensions were agitated initially and placed in the spectrophotometer, where the suspension was allowed to stand undisturbed over a period of one hour whilst absorption readings were taken.

9.2.5 Transmission electron microscopy

Transmission electron microscopy (TEM) was used to image the dispersion of liposomes in MMA and water. PC:C liposomes and PC:C liposomes with L61 Pluronic were prepared as described and mixed at a volumetric ratio of 1:1 with 4%w/v aqueous uranyl acetate and left for 60 minutes. The liposomes were then pelleted as described and resuspended in 10mL of water or MMA. The suspension was further diluted at a 10%v/v concentration and a 10 μ L droplet of the dilute suspension was added to a Formvar carbon film on a 400 mesh Nickel grid (EM Systems Support Ltd., Macclesfield, UK) and allowed to dry in air. MMA alone was also dried on a grid as a control. The grids were observed using a Philips CM12 TEM (Philips Research, Eindhoven, Netherlands) operating at 80kV. Images were recorded using an SIS MegaView III digital camera (Olympus Soft Imaging Solutions GmbH, Münster, Germany).

9.2.6 Temperature stability tests

To ensure the liposome-Pluronic systems are capable of withstanding the high setting temperatures of PMMA bone cements, samples were heated in water and in a dry state at 80°C for 10 minutes. The liposome-Pluronic system was not tested in MMA since this would polymerise under these conditions making characterisation difficult. This particular temperature and time period was selected as a likely worst case scenario for setting temperature and time for bone cements in order to test the robustness of the liposome-Pluronic system.

5mg/mL liposome suspensions with and without Pluronics (L31, L43 or L61) were prepared as described and diluted to 1mg/mL. A small hole was drilled through the top of a 1.5mL Eppendorf tube. 1mL of the 1mg/mL liposome suspension was pipetted into the Eppendorf. A K-wire thermocouple was cleaned and sterilized by washing with 70% ethanol and air dried. The thermocouple was placed into the liposome suspension through the hole in the Eppendorf and connected to a temperature monitor. The Eppendorf was placed in an oven at 80°C and the temperature was monitored. Once the temperature reached 80°C, the Eppendorf was left in the oven for 10 minutes then removed and allowed to cool. The average diameter of the liposome suspension was measured by laser diffraction. The experiment was repeated in triplicate.

For the dry state, 0.1mL of the 1mg/mL liposome suspension with and without Pluronics (L31, L43 or L61) was allowed to dry at room temperature in a 96-well plate. The plate was placed in a oven at 80°C, with the temperature monitored using a sterile K-wire thermocouple within the well. Once the temperature inside the well reached 80°C, the plate was left in the oven for 10 minutes then removed and allowed to cool. Each dry sample was resuspended in 0.1mL of freshly deionised water and the diameter of the liposomes was measured by laser diffraction. The experiment was repeated in triplicate.

9.2.7 Fluorescence microscopy

To assess the dispersion of the liposomes in a commercial cement, 100mg of liposomal material was suspended in water at a concentration of 5mg/mL, as described. Fluorescent TopFluor Cholesterol (FC, 23-(dipyrometheneboron difluoride)-24-norcholesterol, INstru-chemie BV, Delfzijl, Netherlands) was used to substitute for a portion of the cholesterol component to give a ratio of 7:0.9:0.1 of PC:C:FC. The fluorescent liposome suspension was sized using laser diffraction to ensure 100nm liposomes were formed. 1mL of the suspension was diluted in 4mL of distilled deionised water to obtain a concentration of 1mg/mL and fluorescent images were taken for observation. The remaining 5mg/mL liposomal suspension was divided into four aliquots of 4mL. 2%w/w of Pluronic L31, L43 or L61 was added to three of the aliquots and the suspension was pelleted as previously described. Similarly, the remaining 4mL aliquot of 5mg/mL liposomal suspension alone was pelleted. The four pellets were individually resuspended in 2mL of the liquid component of Palacos R (MMA). This was mixed with 4g of the Palacos R powder as described in Section 2.1. The cement was compressed between two glass slides to create a thin sample capable of transmitting light. All cement samples were inspected under a light microscope for pores and transparency and stored in the dark until observed using an Olympus IX50 fluorescent microscope. A green filter (495-570nm) was used to excite the fluorescent lipids and images of the emitted red fluorescence were taken.

9.3 Results

9.3.1 Liposome diameter

The average diameter of the PC:C liposomes in water prior to extrusion was 588.4 ± 242.9 nm. After sequential extrusion through a 400nm and then 100nm polycarbonate membrane, the average diameter reduced to 100.3 ± 18.50 nm. The addition of the Pluronics after extrusion did not significantly alter the average diameters of the liposomes

(L31=107.9±27.8nm, L43=105.6±20.5nm and L61=100.9±29.5nm). The centrifugation process did not to affect the liposome size as the average diameter of the PC:C liposomes after centrifugation and resuspension in water was 110.5±16.33nm.

Table 9.6 shows the average liposome size after centrifugation and resuspension in MMA for suspensions with and without Pluronic. The diameters of all liposome suspensions in MMA were larger when compared to measurements in water. The accuracy of the laser diffraction technique was also found to be reduced when taking measurements in MMA. This may be due to liposomes aggregating or reforming in the MMA or due to laser diffraction being an unsuitable technique for particle size measurements in MMA. Regardless of this, liposomes with L31, L43 and L61 were found to produce the smallest liposomes with the narrowest size distributions.

Table 9.6: Particle size of liposomes with Pluronic in MMA

	Size / nm
PC:C	870±400
PC:C L31	380±180
PC:C L43	390±150
PC:C L44	1580±120
PC:C L61	450±200
PC:C L62	2000±860
PC:C L64	1080±520
PC:C F68	1100±490
PC:C P84	840±370
PC:C P104	920±440
PC:C P123	750±250
PC:C F127	6160±2860

9.3.2 Sedimentation rate

Figure 9.9 shows the absorbance at 420nm over one hour for liposome pellets resuspended in MMA with and without Pluronic. All suspensions had an initial absorbance value between 1.8 and 2.5. All samples were stable for up to 120 seconds, after which period the liposomes, with exception of L31, L43 and L61, aggregated and sedimented rapidly. After 2400 seconds, only three liposome-Pluronic combinations remained fully suspended (L31, L43 and L61), whilst the remainder of the suspensions were unstable. Sedimented samples were characterised by a white solid at the bottom of the cuvette, whilst suspended samples were found to range from visually clear to slightly cloudy in appearance.

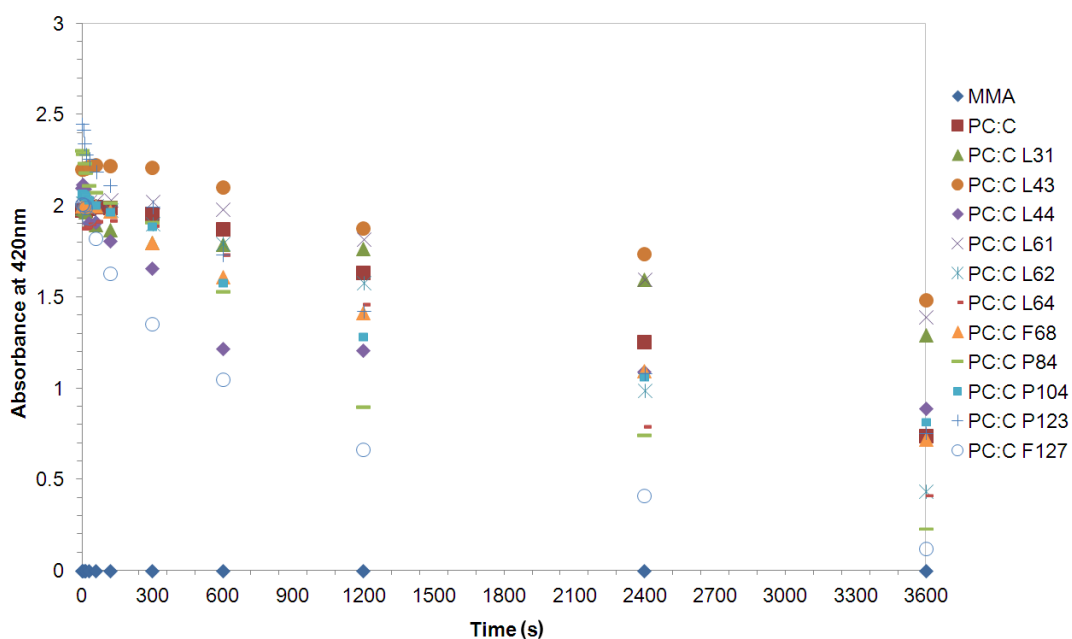


Figure 9.9: Sedimentation rate of liposomes with different Pluronic in MMA

9.3.3 Transmission electron microscopy

Figure 9.10 shows TEM images of pelleted PC:C liposome suspensions in water and MMA with and without L61 Pluronic. In all images, Pluronic micelles, which are usually 2-10nm in diameter, were not observed⁴⁰³. Pelleted PC:C liposomes resuspended in water had some aggregations present with sizes ranging from 400nm up to 2 μ m, however the majority of the liposomes dispersed were between 80 and 200nm in diameter. When PC:C liposomes with L61 Pluronic were pelleted and resuspended in water, the liposomes aggregated, forming large agglomerations of liposomes ranging from 200nm to several microns.

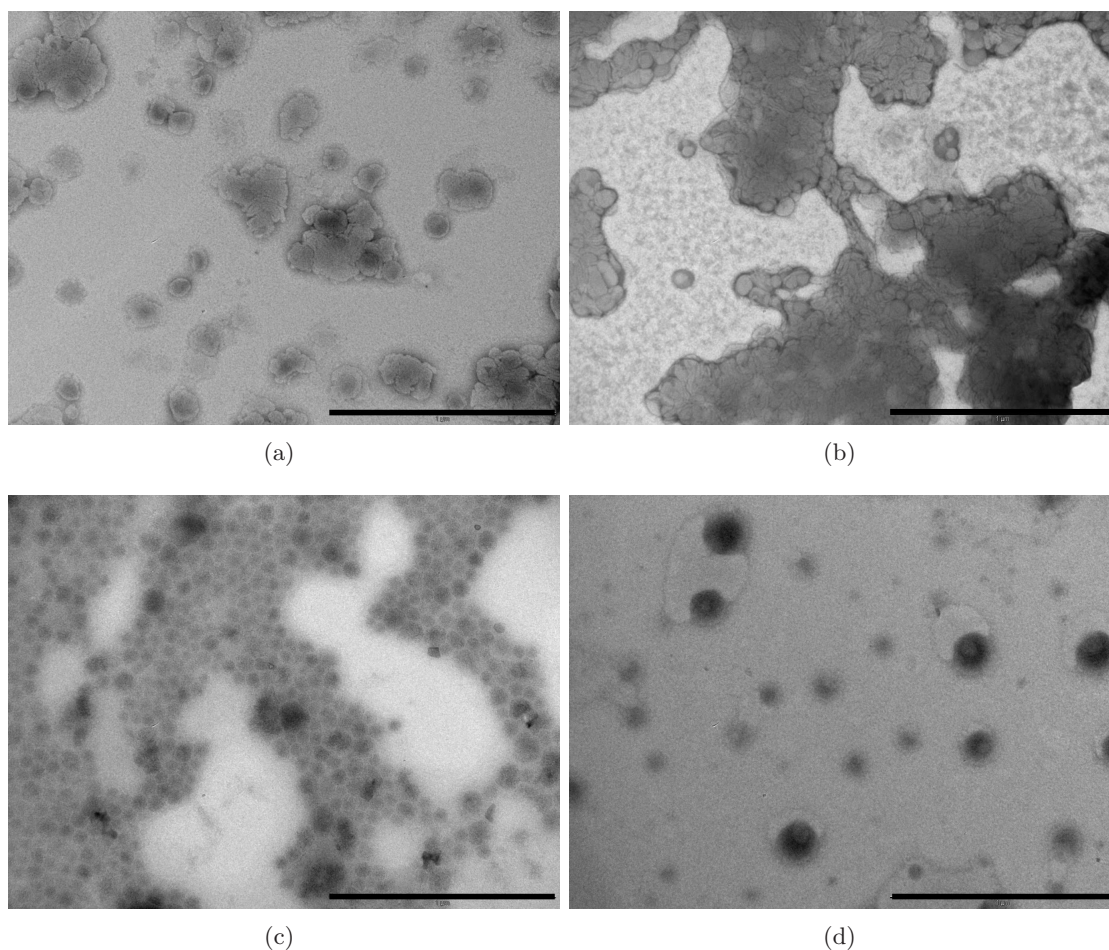


Figure 9.10: TEM images of PC:C liposomes in (a) water, (b) water with L61, (c) MMA and (d) MMA with L61 (Bar=1 μ m)

Similarly, pelleted PC:C liposomes resuspended in MMA agglomerated, however within the agglomerations, the individual liposomes were intact, with diameters ranging from 60 to 200nm. When PC:C liposomes with L61 Pluronic were pelleted and resuspended in MMA, the liposomes were well dispersed, with intact bilayers and diameters ranging from 50 to 200nm.

Figure 9.11 shows pelleted PC:C liposomes with L61 Pluronic that have been resuspended in MMA. Few agglomerations are observed and the liposomes are well dispersed with diameters ranging from 50 to 200nm.

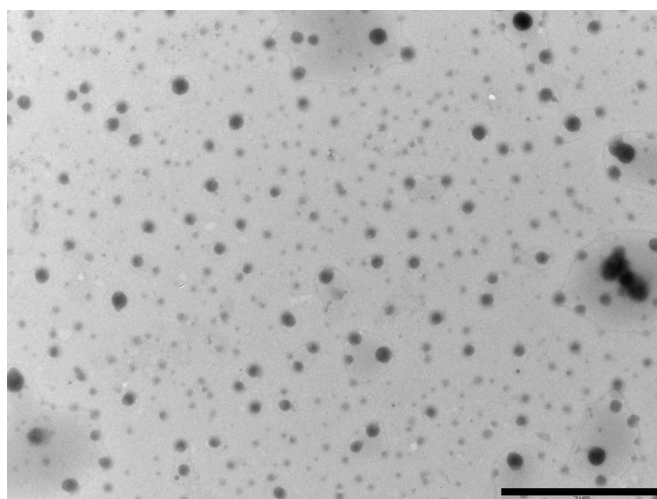


Figure 9.11: TEM of dispersed liposomes with L61 in MMA (Bar=2 μ m)

9.3.4 Temperature stability tests

Table 9.7 shows the average liposomal diameters for liposome suspensions with and without Pluronics heated to 80°C in a wet and dry state. Initially all liposomes were approximately 100nm in diameter when suspended at 23°C in water. When heated to 80°C for 10 minutes, the changes were not significant (ANOVA, $p < 0.05$). When dried at room temperature, heated to 80°C for 10 minutes and resuspended, all suspensions increased significantly in size with large standard deviations and size distributions.

Table 9.7: Particle size of liposomes before and after heating in a wet and dry state

		Size /nm
PC:C	23°C	100.3±18.5
	80°C wet	101.6±16.5
	80°C dry	540.8±241.8
PC:C L31	23°C	107.9±27.8
	80°C wet	113.5±27.6
	80°C dry	706.1±328.2
PC:C L43	23°C	105.6±20.5
	80°C wet	111.0±23.9
	80°C dry	597.4±270.9
PC:C L61	23°C	100.9±29.5
	80°C wet	95.8±15.6
	80°C dry	979.9±455.3

9.3.5 Fluorescence microscopy

Figure 9.12 shows the fluorescence microscopy images of fluorescent PC:C:FC liposomes in water and pelleted fluorescent PC:C:FC liposomes with and without Pluronics in Palacos R cement. The liposomes with fluorescent TopFluor cholesterol emitted detectable

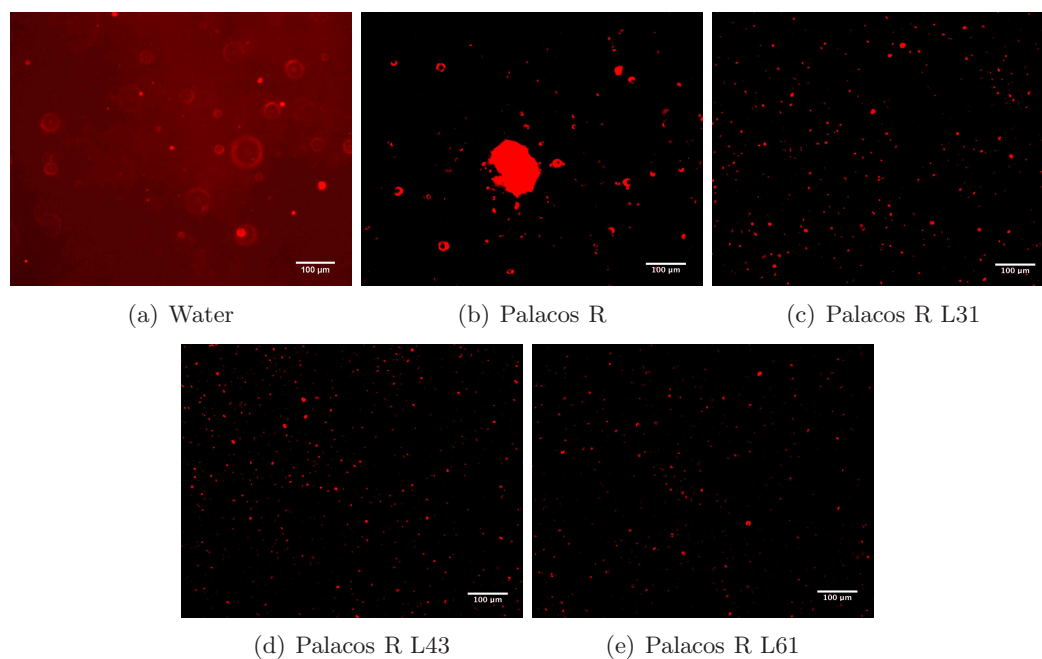


Figure 9.12: Fluorescent microscopy images of liposomes (a) in water, (b) in Palacos R, (c) in Palacos R with L31, (d) in Palacos R with L43 and (e) in Palacos R with L61

levels of fluorescence. Although well dispersed in water, the red fluorescent liposomes were significantly larger when compared to measurements obtained using laser diffraction methods. Fluorescence was observed for all fluorescent liposomes in Palacos R samples; although all appeared greater than 100nm in size. For liposomes in Palacos R without Pluronic, large agglomerations were observed up to 100 μ m in size. In contrast, for liposomes with Pluronic L31, L43 and L61 in Palacos R, the fluorescent images were found to be significantly smaller and well dispersed throughout the cement sample.

9.4 Discussion

Liposomes have been extensively used as pharmaceutical carriers in recent years due to their unique ability to encapsulate both hydrophobic and hydrophilic therapeutic agents. Liposomes can: protect these drugs from external conditions; reduce the cytotoxicity of therapeutic agents; be functionalized with ligands to target specific cells and tissues; and, be coated with inert biocompatible polymers such as PEO to stabilize and prolong the circulation half-life *in vivo*. Liposomes can also be manufactured to desired formulations in terms of composition, size, surface charge, combination of encapsulated therapeutic agents and other properties³⁸³⁻³⁸⁵.

Prior to extrusion, the liposomes formed by the thin-film hydration technique were large with a wide size distribution. After extrusion through a 100nm polycarbonate membrane, a uniform suspension of 100nm liposomes with a small size distribution was obtained. By using the extrusion technique, liposome size can be controlled according to the membrane pore size, making it an ideal technique for consistent delivery of therapeutic agents.

The addition of Pluronic to the surface of the liposomes did not affect the bilayer as liposomes were intact and roughly 100nm in size. If disruption of the bilayer had occurred, the liposomes would have been likely to reform to the state prior to extrusion,

with diameters of several hundred nanometres. These findings agree with studies using liposomes and Pluronics in an aqueous solution^{404–406}. Although, small changes to the liposome diameter occurred as a result of using Pluronics, these changes were not significant and Pluronic chains are too small ($\leq 5\text{nm}$) to be detected by laser diffraction methods.

When a high centrifugal force was applied to the liposomes to obtain a pellet, the bilayer was still found to remain intact and the diameters and distributions were found to be unchanged from the original suspension, as established by laser diffraction and TEM. Furthermore, the pelleted liposomes were easily resuspended in water by agitation or vortexing. Centrifugation of liposomes does however, reduce the final yield of liposomal material after resuspension. Smaller liposomes ($\leq 50\text{nm}$) may remain suspended after centrifugation and are therefore lost when the supernatant is discarded. The final concentration of the pelleted liposomes cannot therefore be accurately deduced.

When resuspending the liposome pellets in MMA, not all combinations of Pluronic produced stable suspensions. Visually, the unstable suspensions in MMA were characterised by a cloudy appearance with large lipid agglomerations, which were found to rapidly sediment. The stability of these suspensions was not improved by increased agitation or vortexing. As a consequence of this, sizing using laser diffraction was difficult and the applicability of the technique was significantly reduced, particularly as measurement in non-polar, polymeric liquids, such as MMA, are not usually conducted. Furthermore, laser diffraction measurements assume the particles being measured are spherical and the technique cannot provide information on the shape and morphology of the measured particle. Laser diffraction however, was able to demonstrate that Pluronic L31, L43 and L61 treatment created the smallest ($< 500\text{nm}$) liposome diameters, whilst the other Pluronics produced much larger sizes with wide size distributions. As the stability of liposomes in MMA has not been previously studied, two possible explanations for these results are presented.

Firstly, the liposome bilayer may be disrupted in MMA due to the hydrophobic nature of the liquid, causing the liposomes to reorientate themselves to minimise hydrophilic-hydrophobic interactions. This would result in the formation of larger liposomes such as those experienced prior to extrusion and the hydrophobic fatty acid chains would be orientated outwards, resulting in the encapsulated therapeutic agents being released. The second possible explanation for the increase in liposome diameters in MMA is as a result of agglomeration through hydrophile-hydrophile attraction in the hydrophobic MMA. L31, L43 and L61 were found to reduce agglomeration supposedly by creating a hydrophobic layer of PPO chains around the liposomes with consequential steric repulsion. This combined with the low resolution, sensitivity and accuracy of laser diffraction measurements in MMA resulted in much larger diameters being estimated.

The sedimentation measurements agree with the agglomeration hypothesis as all liposome-Pluronic combinations were found to sediment over time, with the exception of Pluronics L31, L43, L61, which produced a stable suspension. All initial absorbance values were found to be around 2.0, demonstrating at the start of the experiment around 99% of the light at 420nm was absorbed by the sample due to the presence of suspended lipid material in the MMA. Although the majority of the Pluronic treated liposomes did not sediment in the first few minutes, the stability of the system over extended periods of time is important as it will dictate the shelf-life of the product. For the majority of the suspensions with Pluronics, agitation was sufficient to temporarily resuspend the sedimented lipid material. This is important as agitation of the suspension can be carried out by the surgeon prior to mixing the cement. Ultimately, the most important parameter is the dispersion of the liposomes in the MMA as this will govern the release and the uniformity of mechanical and the fatigue properties of the cement.

To investigate the structure and morphology of the liposomes, TEM imaging was used.

The method developed to image the liposomes using TEM was successful. Negative staining of the liposomes by adding uranyl acetate prior to centrifugation proved to be the most effective method; staining after centrifugation did not produce clear images.

The TEM images show that the liposome structure is intact after centrifugation and re-suspension in water, again demonstrating that the high centrifugal forces did not disrupt the lipid bilayer. No Pluronic micelles were observed as the Pluronic was used below its CMC.

Pluronic L61 was detrimental to the dispersion of the liposome pellet in water most probably due to Pluronic L61 being predominantly hydrophobic (longer PPO chains than PEO chains). Furthermore, the proposed arrangement between the liposome and the Pluronic would result in the hydrophobic PPO chains facing outwards. This would result in a more hydrophobic liposome surface, which in an aqueous solution would cause the liposomes to aggregate. Agglomerations were also observed when the pelleted liposomes were suspended in MMA without Pluronics. This is likely due to the orientation of the liposome hydrophilic outer layer causing aggregation in the non-polar, hydrophobic MMA. From the TEM images however, it was clear that the liposomes remained intact, with average diameters of roughly 100nm, when suspended in MMA. This supports the agglomeration hypothesis as opposed to the disruption, reorientation and formation of larger liposomes. Furthermore, this demonstrates that laser diffraction in MMA measured the size of the agglomerations and not the diameter of the individual liposomes. When using Pluronic L61, the liposomes were well dispersed in MMA. Therefore, the TEM images demonstrated that Pluronics can be used to effectively disperse liposomes in MMA. It is proposed that the Pluronics increase the surface hydrophobicity of the liposomes by adsorbing on the outermost surface of the phospholipid head groups.

In terms of stability at high temperatures, the liposome formulation used was found to be stable at 80°C for 10 minutes when in an aqueous suspension. When dried and heated however, the bilayer may have disassociated and the liposomes were then found to reform into multilamellar vesicles. Studies on lyophilizing and drying liposomes have found that the use of cryopreservatives, such as sugar molecules, to replace the water molecules at the bilayer during drying, maintains the bilayer structure and therefore, the liposome size and entrapped contents³⁸⁰. The use of sucrose to preserve the liposomes during drying provides an additional method for reducing the water content in the final cement mixture. Lyophilizing liposomes could not be undertaken in this study. Nevertheless, as the results have shown, pelleting of liposomes by centrifugation has maintained the liposomal structure and when incorporated within the setting cement, the liposome structure is assumed to remain intact due to the surrounding cement matrix.

Sizing by fluorescence microscopy differed from the measurements obtained by TEM and laser diffraction. This is attributed to the distortion of the emitted fluorescent light source as it travels through the medium (water or PMMA) before it is detected by the microscope. Furthermore, as a large number of liposomes are present throughout the cross-section of a sample, the focal plane cannot detect all the fluorescent sources. As the focal plane is moved away from a fluorescent source, a “halo” is formed, which becomes larger and more diffuse, as observed for fluorescent liposomes in water. Therefore, the fluorescent images only provide qualitative results and TEM images have confirmed the size of the liposomes in MMA. Nevertheless, fluorescence microscopy was found to be an effective technique to demonstrate the dispersion of liposomes in PMMA.

In the absence of Pluronic, the fluorescent liposomes were found to aggregate in the cement, resulting in large fluorescent patches. Fluorescent liposomes with Pluronic L31, L43 and L61 were found to produce much smaller foci of fluorescence, which were well

dispersed, demonstrating the effectiveness of these Pluronics in dispersing the liposomes throughout the cement.

Generally Pluronic block copolymers were found effective in dispersing liposomes in non-aqueous environments. Not all Pluronics were found to be suitable for dispersing liposomes in MMA. Pluronics L31, L43, L61 were found to produce the most favourable results. This agrees with the HLB scale for Pluronics L31 and L61, which have HLB values between 3 and 6 and are therefore suitable as water-in-oil emulsifiers. Pluronic L43 however, which is considered an oil-in-water emulsifier, with an HLB value of 12, was also found to perform well for this application. This demonstrates that the HLB scale can only be used as a guide for selecting surfactants. When comparing the properties of Pluronics L31, L43 and L61, they were all found to have molecular weights less than or equal 2000 and be more hydrophobic in nature with higher PPO than PEO content. This agrees with the theory that the Pluronics increase the hydrophobicity of the liposome system in order to improve the dispersion.

Referring back to the proposed liposome-Pluronic structure (Figure 9.8), the presence of long PPO chains may 'block' the attachment sites for additional Pluronics. Similarly, long PEO chains may cause the attached Pluronics to extend farther from the surface of the liposome and shield the surface from the approach of additional Pluronics. It also offers the suggestion that there may be some steric hindrance occurring on the liposome surface when either or both PPO and PEO chains are lengthy.

The use of liposomes with block copolymers has been investigated by several authors^{407,408}. Such an arrangement has been shown to reduce the systemic toxicity of drugs, such as paclitaxel, when used as a hydrogel⁴⁰⁹. Melittin liposomes, surface modified with Pluronics were shown to exhibit enhanced bioavailability, effective anticancer activity and reduced

side effects compared with melittin solution⁴⁰⁶. Furthermore, the use of polymers in conjunction with liposomes is well documented, particularly for cancer treatments^{385,387,410}. Nevertheless, these systems employed polymers in order to enhance liposomal dispersion and circulation characteristics in an aqueous phase and previous thought has not been given to apply such systems to disperse liposomes in non-aqueous environments. The interactions between block copolymers and liposomes are not well understood. Kostarelos et al.^{404,405} proposed a specific orientation of the Pluronic on the surface of the liposome, whereby the hydrophobic PPO chain is in contact with the hydrophilic outer surface of the liposome, leaving the PEO chains to interact with the aqueous solution. Although plausible, this system would not improve the dispersion of the liposomes in MMA. Furthermore, the interactions between PPO and the hydrophilic head groups of lipids are unfavourable. Kostarelos et al.⁴⁰⁵ also proposed incorporating the Pluronics into the bilayer structure during the preparation process. This would result in the PPO chains located inside the lipid bilayer and the PEO chains in either the aqueous compartment of the liposome or outside of the liposome. This proposed structure would not alter the hydrophobicity on the surface of the liposome and therefore, would not alter the dispersion of liposomes in MMA. Furthermore, Pluronic molecules not incorporated in the bilayer would be free to attach on the surface of the liposome, resulting in both systems being present, with little control over the liposome-Pluronic arrangement. This method was attempted in the early stages of this study, however due to the above reasons was not felt sufficiently controlled to pursue further.

The proposed attachment between the PEO chains of the Pluronic molecule and the surface of the liposome is not a covalent bond but is considered to be a weak physical adsorption, governed mainly by van der Waals forces. Therefore, the attachment itself is not permanent, however data in this thesis has shown that interactions between certain Pluronic molecules and liposomes is sustained sufficiently to improve dispersion proper-

ties. The use of Pluronics adsorbed on the surface of liposomes provides a convenient and cost-effective method for altering surface characteristics in order to improve dispersion properties.

Although, the stability of liposomes in MMA with specific Pluronics has been shown to be acceptable in the short term, further studies are required to assess long-term stability. This is vital as it will establish the shelf-life of the potential product and its viability as a drug delivery system for PMMA bone cements.

9.5 Conclusions

A uniform suspension of 100nm liposomes with a small size distribution was obtained by the method of thin-film hydration and extrusion. The size and morphology of the liposomes were not altered by the addition of Pluronics or by centrifugation. Furthermore, the liposomes were found to withstand the high setting temperature of PMMA bone cement unless previously dried. Pluronics are required to ensure stable suspensions of liposomes in MMA; without the addition of Pluronics, liposomes were found to agglomerate and sediment. Optimal activity was obtained from Pluronics with a molecular weight of less than 2000 and a larger hydrophobic portion (e.g. such as L31, L43 and L61); other Pluronics could not produce the required stability and dispersion of liposomes in MMA. It is hypothesised that the PEO chains of the Pluronic adsorb onto the surface of the liposome and the PPO chains are left on the outermost layer to interact with the medium. This results in a hydrophobic outer layer, which allows the liposomes to be dispersed in non-polar, hydrophobic liquids, such as MMA.

In conclusion, a novel method for incorporating liposomes in bone cement, using Pluronic block copolymers, has been developed. Such a combination of liposomes with certain Pluronics was found to achieve good stability and dispersion in a commercially available

cement (Palacos R). Liposomes encapsulating therapeutic agents, such as gentamicin sulphate, can now be incorporated into commercial cements to study the antibiotic release and antimicrobial properties. The results can then be compared with the findings from Chapter 8 for commercially available antibiotic cements, which use powdered gentamicin sulphate. Similarly, the effect of the novel therapeutic delivery system on mechanical and fatigue properties must be investigated to ensure the novel system is suitable for PMMA bone cements.

Chapter 10

Release characteristics of liposomal bone cements and their mechanical, fatigue and structural properties

10.1 Introduction

Liposomes have been successfully incorporated into a commercially available bone cement (Palacos R) as discussed in the previous chapter. Having established the stability and dispersion of the liposomes in PMMA bone cement, this chapter investigates the release, antimicrobial, mechanical, fatigue and structural properties of the novel liposomal system with encapsulated gentamicin sulphate. Furthermore, the results obtained are compared with data from Chapter 8 for commercially available antibiotic-loaded cements.

Previous studies have investigated the use of aminoglycoside antibiotics, such as gentamicin sulphate, encapsulated in liposomes. It was found that liposomes significantly increase the therapeutic index of gentamicin sulphate when administered as free particles directly into the circulation due to improved pharmacokinetics and pharmacodynamics⁴¹¹. The use of liposomes was also found to enhance the accumulation of therapeutic agents at the site of infection^{384,412}. Furthermore, encapsulated gentamicin was found to have a longer circulation half-life than free gentamicin in mouse and rat studies⁴¹³.

As a result of incompatibilities between aqueous liposomes and hydrophobic materials, such as PMMA, little research has been conducted on using liposomes in bone cement. A recent study was published however, which incorporated a powdered form of liposomal amphotericin B (AmBisome) into the powder component of Simplex P bone cement⁴¹⁴. This technique differs from the one developed in Chapter 9 as there is no attempt to overcome the incompatibilities discussed and the results and findings obtained in this thesis remain novel.

10.2 Methods

10.2.1 Materials

Phosphatidyl choline (PC) from egg yolk ($\geq 99\%$), cholesterol (C, $\geq 99\%$) and gentamicin sulphate ($\geq 590\mu\text{g}$ gentamicin base per mg) were purchased from Sigma Aldrich (Sigma-Aldrich Company Ltd., Gillingham, UK). Chloroform (HPLC grade) was purchased from Fisher Scientific (Fisher Scientific UK Ltd, Loughborough, UK). Palacos R cement was provided by Heraeus (Heraeus Medical Ltd., Newbury, UK).

10.2.2 Liposome preparation

A similar method for liposome preparation was undertaken as described in Chapter 9. 175mg of PC and 25mg of C were weighed and added to a 50mL round bottom flask. 5mL of chloroform was added to the flask and the suspension was vortexed until the lipids dissolved.

The flask was attached to a rotary evaporator with a water bath set at 60°C (above T_c of PC) with a vacuum pump and rotation set to 1 revolution per second. Once the chloroform had evaporated and a thin film of lipids had formed, 40mL of 5mg/mL gentamicin sulphate solution, heated to 60°C , was added and the flask vortex mixed to create a

suspension of liposome vesicles with a concentration of 5mg/mL. The liposome suspension was held at 60°C for 30 minutes for the liposomes to form. The suspension was extruded 10 times under nitrogen pressure (8 bars maximum) using a Lipex extruder (Northern Lipids Inc., British Columbia, Canada) vertically through a 400nm polycarbonate membrane (Whatman, UK) followed by further extrusion 10 times through a 100nm polycarbonate membrane. A Beckman Coulter N4 PLUS particle size analyzer was used to ensure 100nm diameter liposomes were produced. 2%w/w of L31 Pluronic was added and the solution was centrifuged at 100,000g (25,000 RPM) for 1 hour at 4°C using a Beckman Optima LE-80K centrifuge with a SW28 rotor to create a pellet. The 200mg pellet was resuspended in 20mL of the liquid component of Palacos R (MMA) by a process of titration using a glass mortar and pestle followed by vortexing. The method was repeated for L43 and L61 Pluronics.

10.2.3 Antibiotic release

Palacos R bone cement containing 200mg of liposomal gentamicin sulphate (with Pluronics L31, L43 or L61) per 40g of cement (herein referred as liposomal Palacos R) was prepared and tested as outlined in Section 8.2.2. The same time points (6 hours, 1, 2, 3, 7, 15, 30 and 60 days) were used to allow for comparison with commercial cements. The amount of gentamicin sulphate used in the liposomal cements was $1/5^{th}$ of the amount that is in Cemex Genta and $2/5^{ths}$ of the amount that is in Palacos R+G (see Table 8.1 in Chapter 8). The results for gentamicin sulphate release from Palacos R+G, Cemex Genta and CMW were taken from previous chapters.

10.2.4 Mathematical modelling

Mathematical models were applied to the antibiotic release data for the liposomal Palacos R cements as described in Section 8.2.3. The Higuchi, Korsmeyer-Peppas and Noyes-Whitney models were applied to the data as were the expanded versions, which use an

additional coefficient to represent the burst of release of gentamicin sulphate from the surface of the cement.

10.2.5 Agar diffusion assay

Liposomal Palacos R cement samples were prepared as described above and tested against *S. aureus* as described in Section 8.2.4. The results for Palacos R+G were taken from previous chapters.

10.2.6 Mechanical testing

Compression and bending samples of liposomal Palacos R were prepared and tested after 24 hours in air at 23°C and 60 days in Ringer's solution at 37°C, with the Ringer's solution changed every 2 weeks, as described in Sections 2.3.1 and 2.3.2. The results for Palacos R and Palacos R+G were taken from previous chapters.

10.2.7 Fracture toughness

Fracture toughness values for the liposomal Palacos R samples were obtained as described in Section 2.4 for samples aged in air for 24 hours at 23°C and Ringer's solution at 37°C for 60 days, with the Ringer's solution changed every 2 weeks. The results for Palacos R and Palacos R+G were taken from previous chapters.

10.2.8 Fatigue testing

Fatigue test samples of liposomal Palacos R cements were prepared and tested as described in Section 2.5 for samples aged in air for 24 hours at 23°C and Ringer's solution at 37°C for 60 days, with the Ringer's solution changed every 2 weeks. The results for Palacos R and Palacos R+G were taken from previous chapters.

10.2.9 SEM images

SEM images of the fracture surface of the fatigue test samples were taken as described in Section 2.8. SEM images of the surfaces of release samples after 0 hours and 60 days in Ringer's solution at 37°C were taken and SEM images for Palacos R and Palacos R+G were taken from previous chapters.

10.2.10 Vickers hardness

Vickers hardness was determined as described in Section 2.6 for liposomal Palacos R samples aged in air for 24 hours at 23°C and Ringer's solution at 37°C for 60 days, with the Ringer's solution changed every 2 weeks. Hardness values for Palacos R and Palacos R+G were taken from previous chapters.

10.2.11 Glass transition temperature

The glass transition temperature of liposomal Palacos R samples were obtained for samples aged in air for 24 hours at 37°C and Ringer's solution at 37°C for 60 days as described in Section 2.7.

10.2.12 Structural changes

The molecular structure of the liposomal Palacos R cement containing Pluronic L61 was studied by Fourier Transform Infrared Spectroscopy (FTIR) using a Perkin Elmer Spectrum One FT-IR Spectrometer with FT-IR Spectrum software (Perkin Elmer, Massachusetts, USA). Attenuated total reflectance (ATR) measurements were taken of Palacos R, Palacos R+G and the liposomal Palacos R with L61 pluronic. Measurements were taken between 4000cm^{-1} and 450cm^{-1} with a resolution of 4cm^{-1} . 30 scans at 6 different sections of each sample were taken to obtain average spectra. Samples were scanned after 24 hours in air at 23°C.

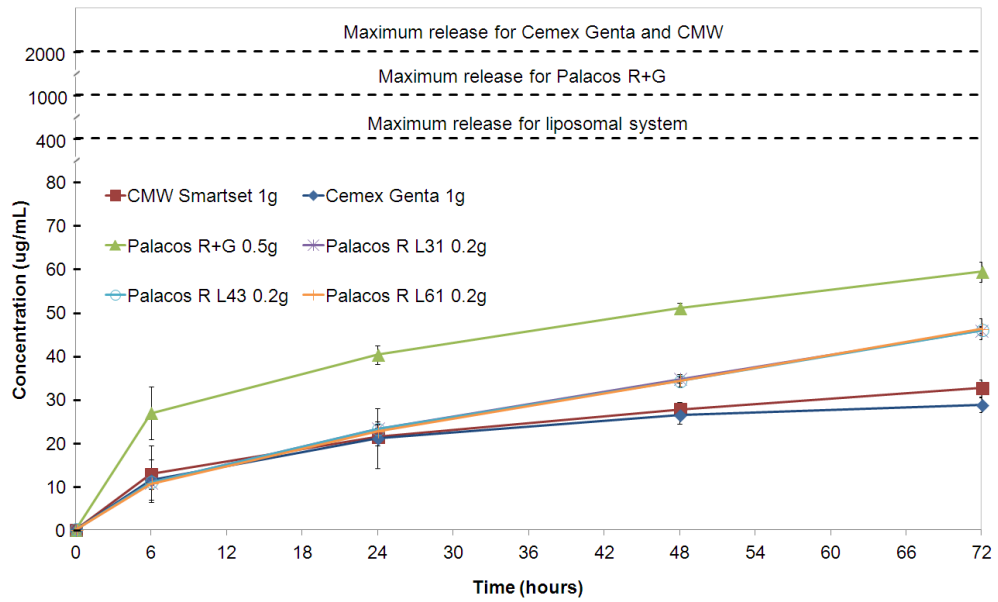
10.3 Results

Liposomal Palacos R cements will be referred to individually as Palacos R L31, Palacos R L43 and Palacos R L61 for the explanation of results.

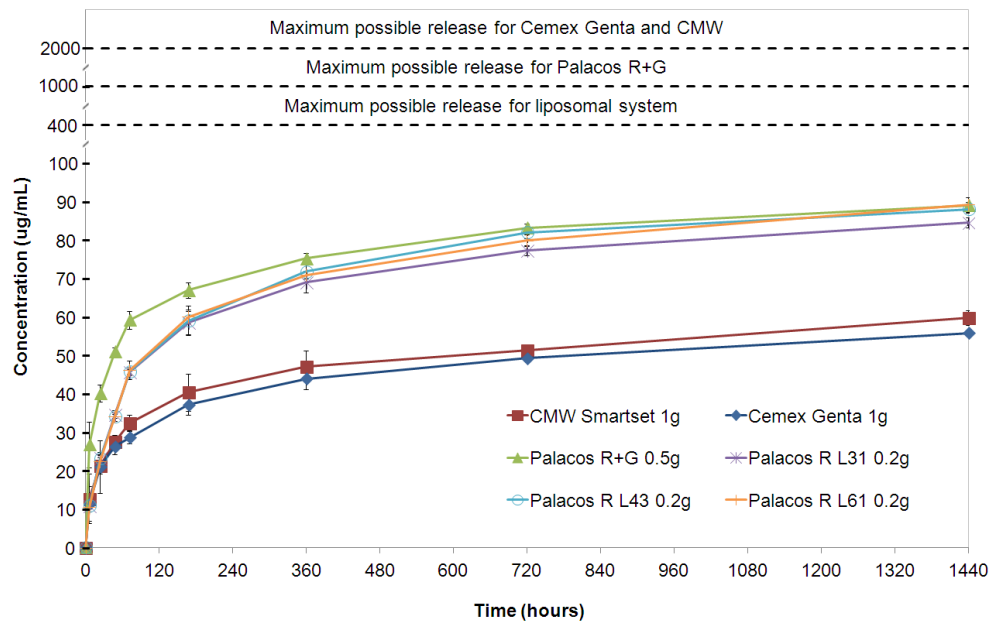
10.3.1 Antibiotic release

Figure 10.1 shows the cumulative release of gentamicin sulphate from Cemex Genta, CMW, Palacos R+G and the liposomal Palacos R cements over 72 and 1440 hours. All three liposomal Palacos R cements released similar amounts of gentamicin sulphate at all time points. At 6 and 24 hours the liposomal Palacos R cements released similar concentrations of gentamicin sulphate as Cemex Genta and CMW (creating concentrations $\simeq 10\mu\text{g}/\text{mL}$), which was much lower than the initial burst of gentamicin sulphate from Palacos R+G (creating concentrations $\simeq 25\mu\text{g}/\text{mL}$). At 72 hours, the liposomal Palacos R cements released gentamicin sulphate, which created concentrations of roughly $45\mu\text{g}/\text{mL}$ in the surrounding Ringer's solution, whilst Palacos R+G achieved a concentration of $59\mu\text{g}/\text{mL}$ and Cemex Genta and CMW a concentration $30\mu\text{g}/\text{mL}$. When assessing the release for the first 72 hours for the liposomal Palacos R cements, a linear release was obtained with a constant release of roughly $10\mu\text{g}/\text{mL}$ at each time point. Furthermore, the standard deviations experienced for all liposomal Palacos R cements within the first 72 hours were smaller than those experienced by the commercial cements with powdered gentamicin. After 360 hours, the cumulative gentamicin sulphate concentration obtained from the liposomal Palacos R cements were similar to Palacos R+G ($85\text{-}90\mu\text{g}/\text{mL}$), which was significantly higher than Cemex Genta and CMW ($55\text{-}60\mu\text{g}/\text{mL}$).

In terms of total percentage release (Figure 10.2), the liposomal Palacos R cements performed significantly better than the commercial cements. At 6 hours, a similar percentage release was experienced by Palacos R+G and the liposomal Palacos R cements ($\simeq 2.7\%$),

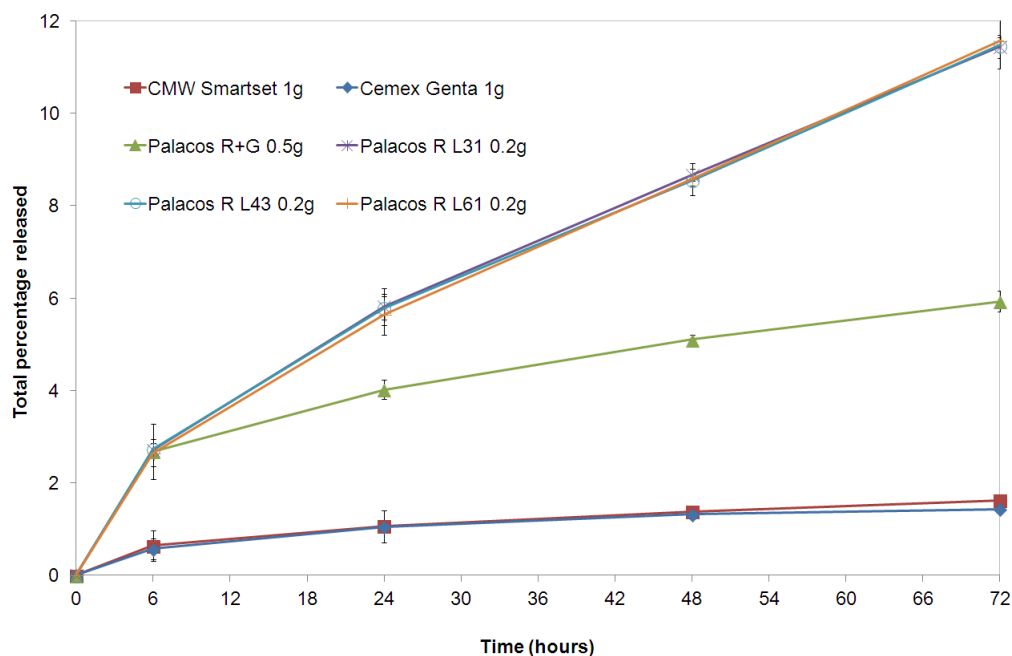


(a) Release after 72 hours

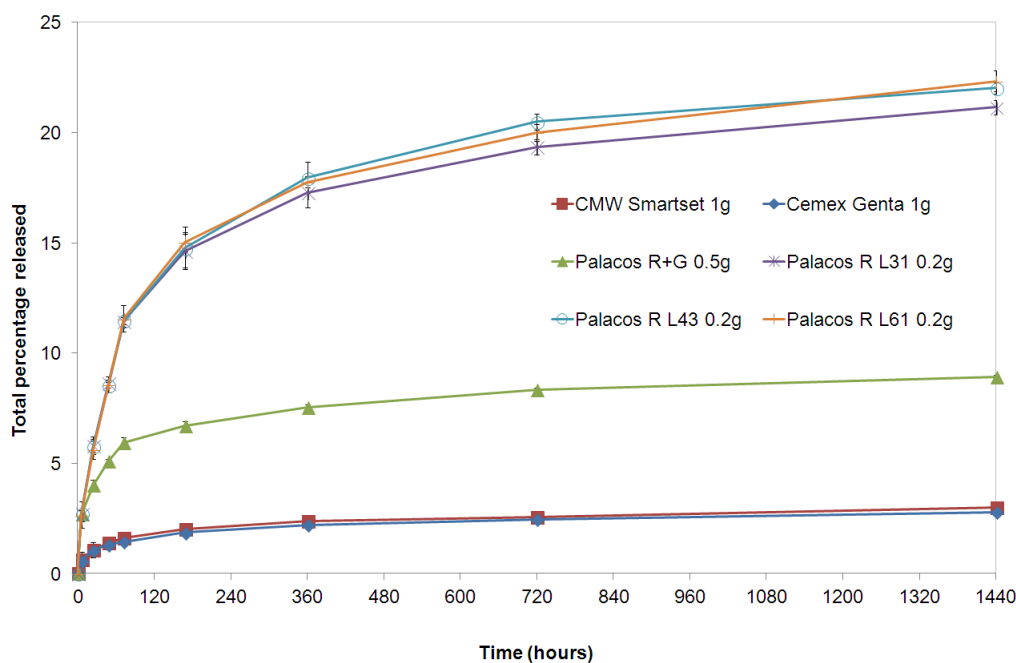


(b) Release after 1440 hours

Figure 10.1: Cumulative gentamicin sulphate release from commercial cements and liposomal Palacos R samples



(a) Percentage release after 72 hours



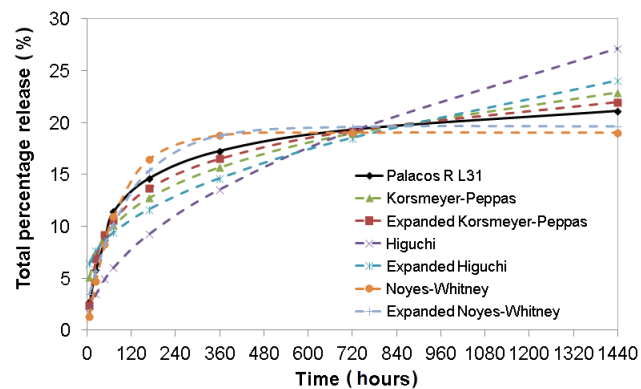
(b) Percentage release after 1440 hours

Figure 10.2: Cumulative percentage release of gentamicin sulphate from commercial cements and liposomal Palacos R samples

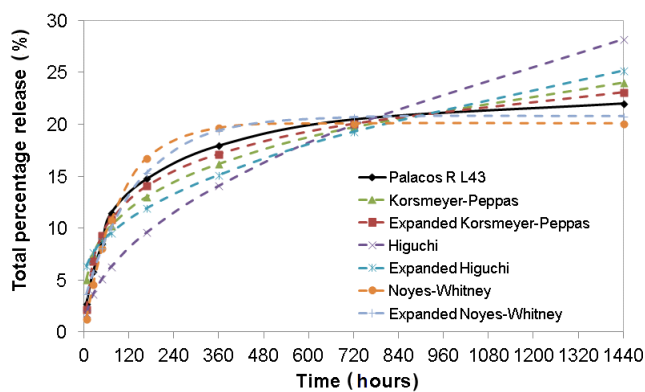
however after this time point the liposomal Palacos R cements achieved much higher percentages. At 72 hours, the liposomal Palacos R released 11-12% of the total gentamicin sulphate used, whilst Palacos R+G released roughly 6% and Cemex Genta and CMW released 1.4-1.7%. This would result in roughly 24mg of antibiotic being released per 40g of cement for the liposomal Palacos R cements compared to 30mg for Palacos R+G and 15mg for Cemex Genta and CMW. After 1440 hours, the liposomal Palacos R cements released 21-22%, whilst Palacos R+G, Cemex Genta and CMW released 8.9%, 2.8% and 3.0%. This would result in 44mg for the liposomal Palacos R cements, 45mg for Palacos R+G and 30mg for Cemex Genta and CMW per 40g of PMMA bone cement, which is equivalent to one dose of cement, over the course of 1440 hours.

10.3.2 Mathematical modelling

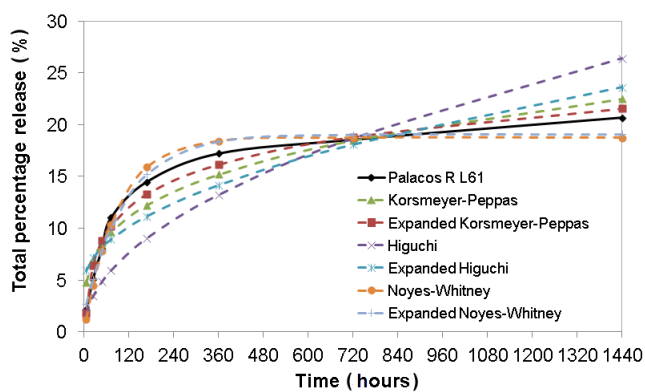
Figure 10.3 shows the goodness of fit for the mathematical models compared to the experimental data obtained from liposomal Palacos R cements with Pluronic L31, L43 and L61. The expanded Noyes-Whitney and the expanded Korsmeyer-Peppas models were found to most accurately model the gentamicin sulphate release from the liposomal Palacos R cements, whilst the Higuchi and the expanded Higuchi equations modelled the release least accurately.



(a) L31



(b) L43



(c) L61

Figure 10.3: Antibiotic release models for liposomal Palacos R with (a) L31, (b) L43 and (c) L61

The results from the mathematical modelling of the gentamicin sulphate release from liposomal Palacos R is shown in Table 10.1. The Noyes-Whitney dissolution model fits the experimental release data for the liposomal Palacos R cements the best. This is contrary to the results obtained when modelling the commercial antibiotic cements, where the Korsmeyer-Peppas model produced the most accurate model. The exponential (n) and the diffusion (k) coefficients obtained for the Korsmeyer-Peppas models on the liposomal Palacos R cements were similar to the coefficients obtained from the commercial antibiotic cements. Although the Higuchi equation poorly modelled the data for the liposomal Palacos R cements, the goodness of fit (R-values) was greater than when the model was applied to the commercial antibiotic cements. The coefficient and goodness of fit values were similar for all liposomal Palacos R cements.

Table 10.1: Mathematical modelling of antibiotic release for liposomal Palacos R

		Korsmeyer	Higuchi	Noyes-Whitney
		$R_t = kt^n$	$R_t = kt^{1/2}$	$R_t = k[1 - \exp(-nt)]$
Palacos R L31	k	3.142	0.716	19.070
	n	0.273	0.500	0.012
	R-value	0.9345	0.5828	0.9555
Palacos R L43	k	3.039	0.743	20.072
	n	0.284	0.500	0.011
	R-value	0.9396	0.6420	0.9559
Palacos R L61	k	2.861	0.6959	18.746
	n	0.284	0.500	0.011
	R-value	0.9187	0.6242	0.9716

Table 10.2 shows the results from the mathematical modelling of the liposomal Palacos R when using the additional coefficient with the Korsmeyer-Peppas, Higuchi and Noyes-Whitney models. The additional coefficient improved the goodness of fit for all the models. The additional coefficient also resulted in the expanded Korsmeyer-Peppas and the expanded Noyes-Whitney models having similar R-values. The ‘b’ coefficient was found to be positive for the expanded Noyes-Whitney and Higuchi models and negative for the

expanded Korsmeyer-Peppas models, as occurred with the commercial antibiotic cements. The coefficient and goodness of fit values were similar for all three liposomal Palacos R cements.

Table 10.2: Mathematical modelling of antibiotic release for liposomal Palacos R samples using the additional coefficient

		Expanded Korsmeyer	Expanded Higuchi	Expanded Noyes-Whitney
		$R_t = b + kt^n$	$R_t = b + kt^{1/2}$	$R_t =$ $b + k[1 - \exp(-nt)]$
Palacos R L31	k	56.050	0.496	16.930
	n	0.051	0.500	0.008
	b	-58.930	5.224	2.698
	R-value	0.9855	0.8483	0.9761
Palacos R L43	k	48.389	0.531	17.830
	n	0.060	0.500	0.007
	b	-51.675	5.045	2.938
	R-value	0.9857	0.8612	0.9796
Palacos R L61	k	74.105	0.498	17.324
	n	0.040	0.500	0.009
	b	-77.852	4.700	1.736
	R-value	0.9797	0.8334	0.9803

10.3.3 Agar diffusion

Figures 10.4 and 10.5 show the zones of inhibition obtained for the 10µg gentamicin discs, Palacos R+G and the liposomal Palacos R cements with Pluronic L31, L43 and L61. As described in Chapter 8, Palacos R+G had poorly consistent antimicrobial properties, with irregular shaped zones and significant differences between samples. The liposomal Palacos cement samples however produced regular, circular zones of similar sizes. Furthermore, the standard deviations were found to be small, as were the differences between samples in each group. The use of different Pluronic did not significantly affect the size and shape of the zone of inhibition produced. The zones obtained for the 10µg gentamicin control disc were also consistent, with similar sizes and shapes obtained for all three discs.

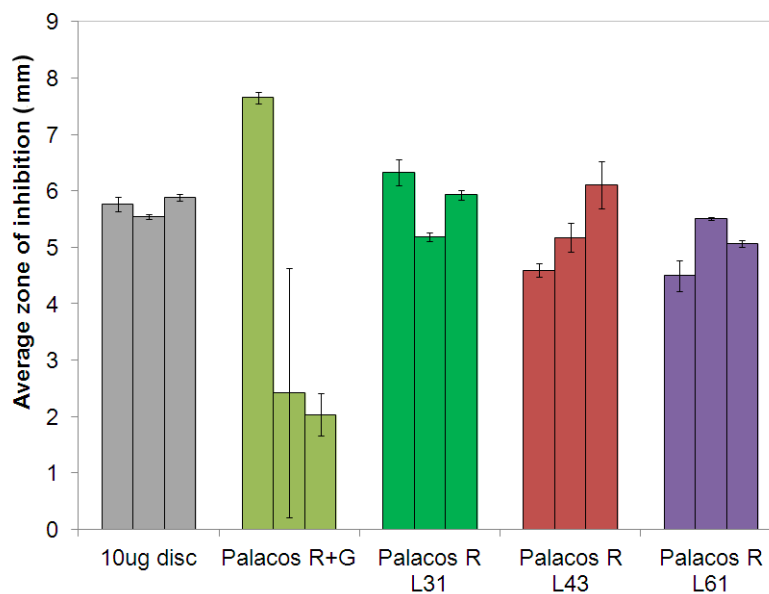


Figure 10.4: Average zones of inhibition for Palacos R+G and the liposomal Palacos R cements

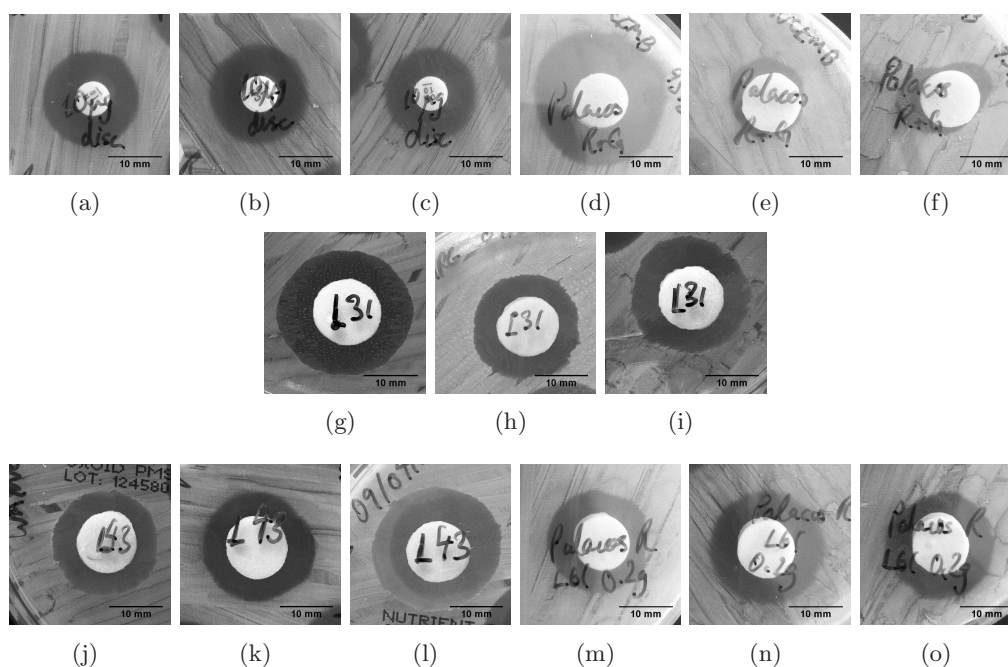


Figure 10.5: Zones of inhibition for the (a-c) 10 μ g discs, (d-f) Palacos R+G and the liposomal Palacos R cements with L31 (g-i), L43 (j-l) and L61 (m-o) Pluronic

10.3.4 Mechanical properties

The mechanical properties of Palacos R, Palacos R+G and the liposomal Palacos R bone cements with Pluronic L31, L43 and L61 are shown in Table 10.3. At 24 hours in air, all liposomal Palacos R samples were significantly worse in compression than Palacos R and Palacos R+G (ANOVA, $p < 0.05$). There were no significant differences between the different Pluronic in terms of compressive strength for the liposomal Palacos R cements after 1 day ($p > 0.05$). After 60 days in Ringer's solution, Palacos R L31 and L43 were significantly stronger than Palacos R ($p = 1.09 \times 10^{-04}$ for Palacos R L31 and $p = 0.01$ for Palacos R L43) and Palacos R+G ($p = 2.13 \times 10^{-05}$ for Palacos R L31 and $p = 0.03$ for Palacos R L43). There was no significant difference between Palacos R L61 and Palacos R/R+G ($p = 0.16$ and $p = 1.00$ respectively). After 60 days in Ringer's solution, there were significant differences in terms of compressive strength between all three liposomal Palacos R cements ($p = 8.35 \times 10^{-07}$), with L31 being the strongest, followed by L43 and L61 cements. The liposomal Palacos R cements increased in compressive strength after storage for 60 days in Ringer's solution (L31 and L43 significantly - $p = 2.90 \times 10^{-05}$ and $p = 8.14 \times 10^{-04}$

Table 10.3: Mechanical properties of commercial and liposomal Palacos R bone cements before and after storage in Ringer's solution for 60 days

		Compressive strength (σ_c) / MPa	Bending modulus (E_b) / MPa	Bending strength (B) / MPa
Palacos R	Air 1 day	104.6±2.6	3460±97	73.4±2.9
	Ringer's 60 days	75.5±5.7	3180±80	69.4±0.6
Palacos R+G	Air 1 day	95.7±3.3	3110±110	66.6±2.4
	Ringer's 60 days	80.3±3.3	2790±155	50.4±7.0
Palacos R L31	Air 1 day	80.8±3.4	3200±61	79.0±3.9
	Ringer's 60 days	99.6±3.6	2640±212	68.7±6.4
Palacos R L43	Air 1 day	77.4±2.4	3330±181	73.0±4.3
	Ringer's 60 days	84.7±1.5	2590±214	65.3±7.0
Palacos R L61	Air 1 day	78.2±1.5	3270±137	74.1±3.4
	Ringer's 60 days	80.3±3.5	2780±87	70.3±6.8

respectively), whilst Palacos R and Palacos R+G were found to decrease significantly in compressive strength ($p=2.19\times 10^{-05}$ and $p=1.18\times 10^{-04}$ respectively).

In terms of bending modulus, at 24 hours in air and 60 days in Ringer's solution, there were no significant differences between the different Pluronic of the liposomal Palacos R cements ($p=0.79$ for air and $p=0.97$ for Ringer's solution). The bending modulus of Palacos R L31 was significantly lower than Palacos R ($p=1.70\times 10^{-03}$), whilst there were no significant differences between Palacos R and Palacos R L43 ($p=0.23$) and L61 ($p=0.05$) at 24 hours. There were no significant differences in bending modulus at 24 hours and 60 days in Ringer's solution between the liposomal Palacos cements and Palacos R+G ($p=0.11$ for air and $p=0.27$ for Ringer's solution). After 60 days in Ringer's solution however, all the liposomal Palacos R cements were found to have significantly lower bending modulus than Palacos R ($p<0.05$). All the cements experienced a significant reduction in bending modulus as result of storage in Ringer's solution for 60 days ($p<0.05$).

After 24 hours in air and 60 days in Ringer's solution, there were no significant differences in bending strength between Palacos R and the liposomal Palacos R cements ($p=0.09$ for air and $p=0.68$ for Ringer's solution). When compared to Palacos R+G however, the liposomal Palacos R cements were found to have significantly higher bending strengths at both 24 hours ($p<0.05$) and 60 days ($p<0.05$). There were no significant differences between the three liposomal Palacos R cements under both storage conditions ($p=0.08$ for air and $p=0.66$ for Ringer's solution). Storage in Ringer's solution was found to significantly decrease the bending strength of all cements, except Palacos L43 ($p=0.09$) and L61 ($p=0.30$). It was observed that not all liposomal Palacos R bending samples fractured. Some samples were loaded past the elastic limit of the material and brittle fracture did not occur. The sample plastically deformed to a point where insufficient contact with the rollers did not allow further loading.

All liposomal Palacos R cements were above the ISO5833 minimum requirements for compressive strength (70MPa), bending modulus (1800MPa) and bending strength (50MPa).

10.3.5 Fracture toughness

Table 10.4 shows the fracture toughness of Palacos R, Palacos R+G and the liposomal Palacos R bone cements with Pluronic L31, L43 and L61. The liposomal Palacos R cements were found to be significantly higher (by approximately 20%) than Palacos R and Palacos R+G at 24 hours in air and 60 days in Ringer's solution ($p < 0.05$). Palacos R was found to be significantly reduced in toughness as a result of ageing in Ringer's solution ($p = 3.87 \times 10^{-04}$), whilst Palacos R+G and the liposomal Palacos R cements were not significantly different ($p > 0.05$).

Table 10.4: Fracture toughness of commercial and liposomal bone cements before and after storage in Ringer's solution for 60 days

		Critical stress intensity factor (K_{IC}) / MPam ^{1/2}
Palacos R	Air 1 day	2.46±0.19
	Ringer's 60 days	1.50±0.31
Palacos R+G	Air 1 day	2.49±0.13
	Ringer's 60 days	2.35±0.19
Palacos R L31	Air 1 day	3.04±0.27
	Ringer's 60 days	2.94±0.21
Palacos R L43	Air 1 day	2.86±0.18
	Ringer's 60 days	2.85±0.35
Palacos R L61	Air 1 day	2.92±0.24
	Ringer's 60 days	2.83±0.09

10.3.6 Fatigue testing

Figure 10.6 shows the fatigue results for commercial Palacos R, Palacos R+G and the liposomal Palacos R cements after storage in air. All three liposomal Palacos R cements performed similarly in terms of crack growth rates. Lower crack growth rates were ob-

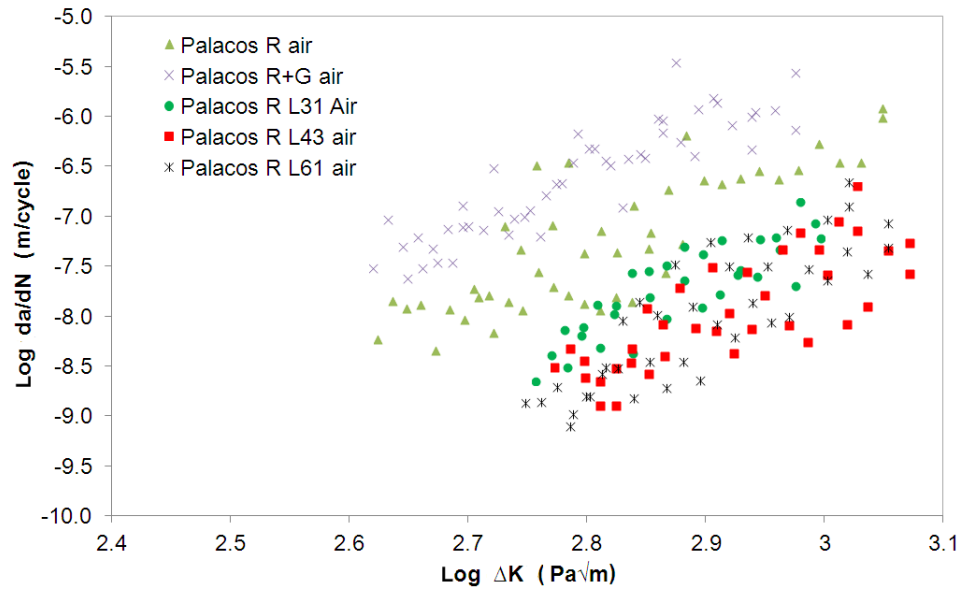


Figure 10.6: Fatigue results from commercial and liposomal Palacos R bone cement after storage in air

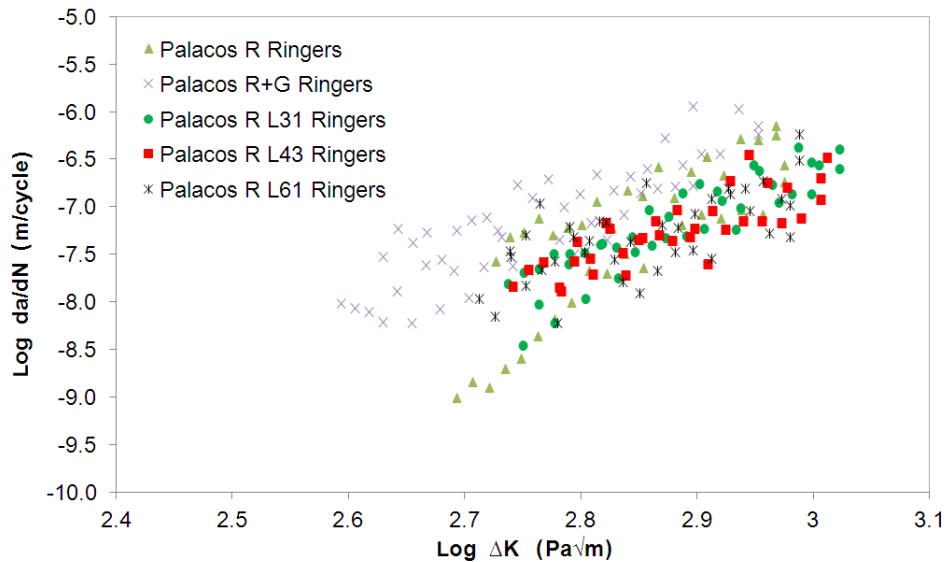


Figure 10.7: Fatigue results from commercial and liposomal bone cement after storage in Ringer's solution at 37°C in Ringer's solution

tained for the liposomal Palacos R cements when compared to both Palacos R and Palacos R+G. Furthermore, low crack growth rates could not be achieved under low stress intensities with the liposomal Palacos R cements.

Figure 10.7 shows the fatigue results for commercial Palacos R, Palacos R+G and the liposomal Palacos R cements after storage in Ringer's solution at 37°C for a minimum of 60 days. The crack growth rates for the liposomal Palacos R bone cements were increased as a result of storage in Ringer's solution for 60 days. The crack growth rates for the liposomal Palacos R cements were similar to Palacos R and lower than Palacos R+G. The three liposomal Palacos R cements obtained similar crack growth rates for the stress intensities tested.

The constants obtained when the Paris Law was applied to the fatigue data is shown in Table 10.5 for Palacos R, Palacos R+G and the liposomal Palacos R cements with Pluronics L31, L43 and L61. As previously described, the crack growth rates at $1\text{MPam}^{1/2}$ ('A'

Table 10.5: Fatigue test constants of commercial and liposomal Palacos R bone cement before and after storage in Ringer's solution for 60 days

	A		m		Correlation coefficient	
	1 day air	60 days Ringer's	1 day air	60 days Ringer's	1 day air	60 days Ringer's
Palacos R	3.73×10^{-07}	7.34×10^{-07}	4.65	7.33	0.67	0.66
Palacos R+G	2.62×10^{-06}	1.13×10^{-06}	5.01	5.18	0.81	0.74
Palacos R L31	8.50×10^{-08}	2.75×10^{-07}	5.39	5.30	0.72	0.80
Palacos R L43	2.68×10^{-08}	1.64×10^{-07}	4.85	3.90	0.61	0.75
Palacos R L61	4.45×10^{-08}	1.63×10^{-07}	6.47	2.94	0.72	0.75

coefficient) for the liposomal Palacos R cements were lower than the other cements. This is demonstrated for samples aged for 1 day in air and 60 days in Ringer's solution. Storage in Ringer's solution increased the crack growth rates for all cements, except Palacos R+G, which remained unchanged.

The slope of the plots ('m' coefficient) for the liposomal Palacos R cements were greater than the slope for Palacos R after 1 day in air. Similarly for Palacos R L31 and L61, the slopes were greater than Palacos R+G. After 60 days in Ringer's solution, the slopes of Palacos R L43 and L61 were significantly lower than those obtained by Palacos R and Palacos R+G, whilst the slope for Palacos R L31 remained unchanged. Furthermore, the 'm' coefficient of the liposomal Palacos R cements were not worsened by storage in Ringer's solution for 60 days, as experienced with the other cements.

10.3.7 SEM images

SEM images of the fracture surfaces of the fatigue samples are shown in Figures 10.8 to 10.10. All cements were found to have pores present after storage in air for 1 day and Ringer's solution for 60 days. Air entrapped during mixing and removal of PMMA beads during fracture may have caused the porosity of the fracture surface. When tested in air, the liposomal Palacos R cements were found to have smaller sized pores (20-50 μm), whilst Palacos R and Palacos R+G had larger pores (50-100 μm). After storage in Ringer's solution for 60 days, all fracture surfaces were found to have large 50-100 μm pores. Closer inspection of the liposomal Palacos R cements found small well-dispersed pores (<10 μm) throughout the fracture surface. Rough fracture surfaces were also observed for the liposomal Palacos R cements aged in air and Ringer's solution, indicating a non-brittle fracture.

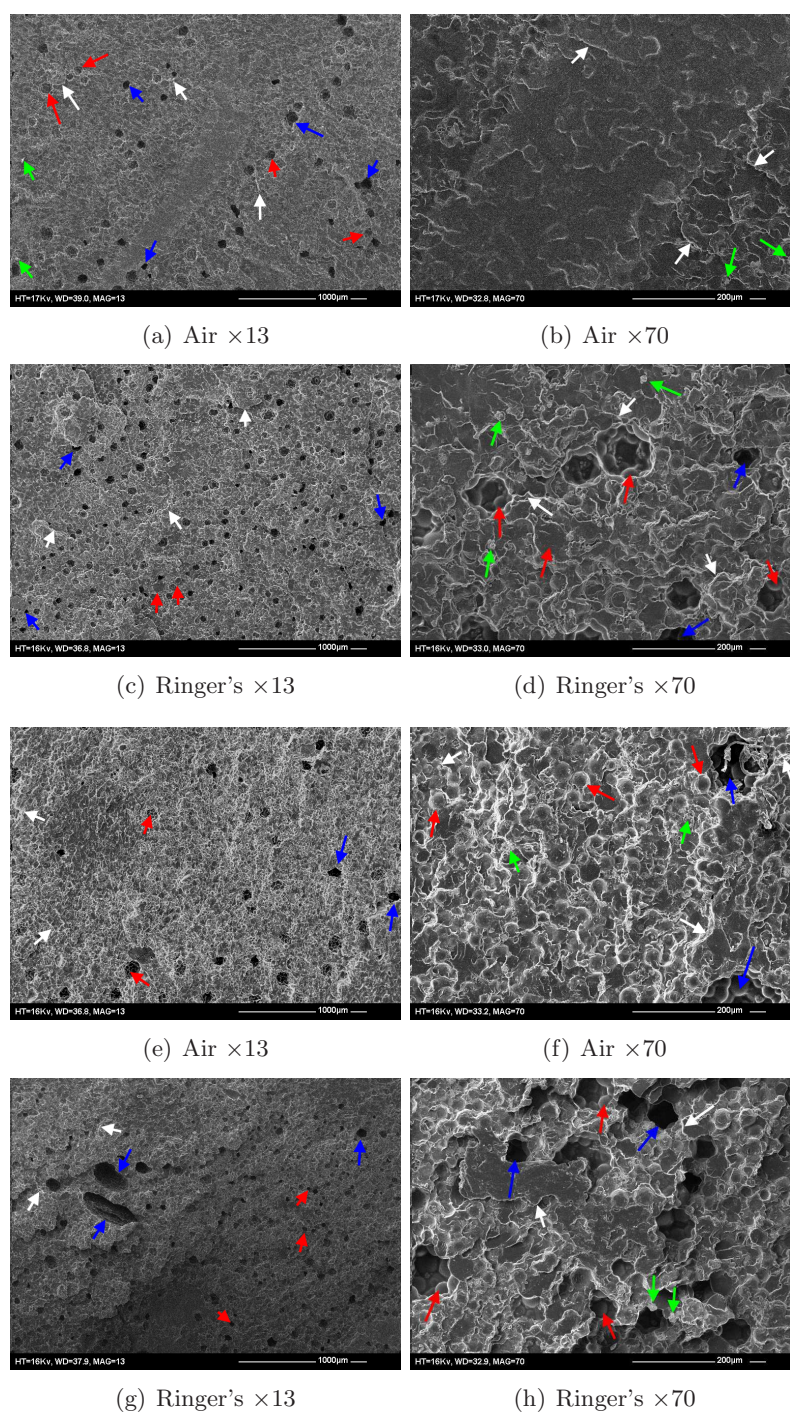


Figure 10.8: Fracture surfaces of fatigue samples aged in air and Ringer's solution for (a-d) Palacos R and (e-h) Palacos R+G - Red arrows indicate the location of PMMA beads, green arrows indicate radiopaque particles, blue arrows indicate pores and white arrows indicate microcracks.

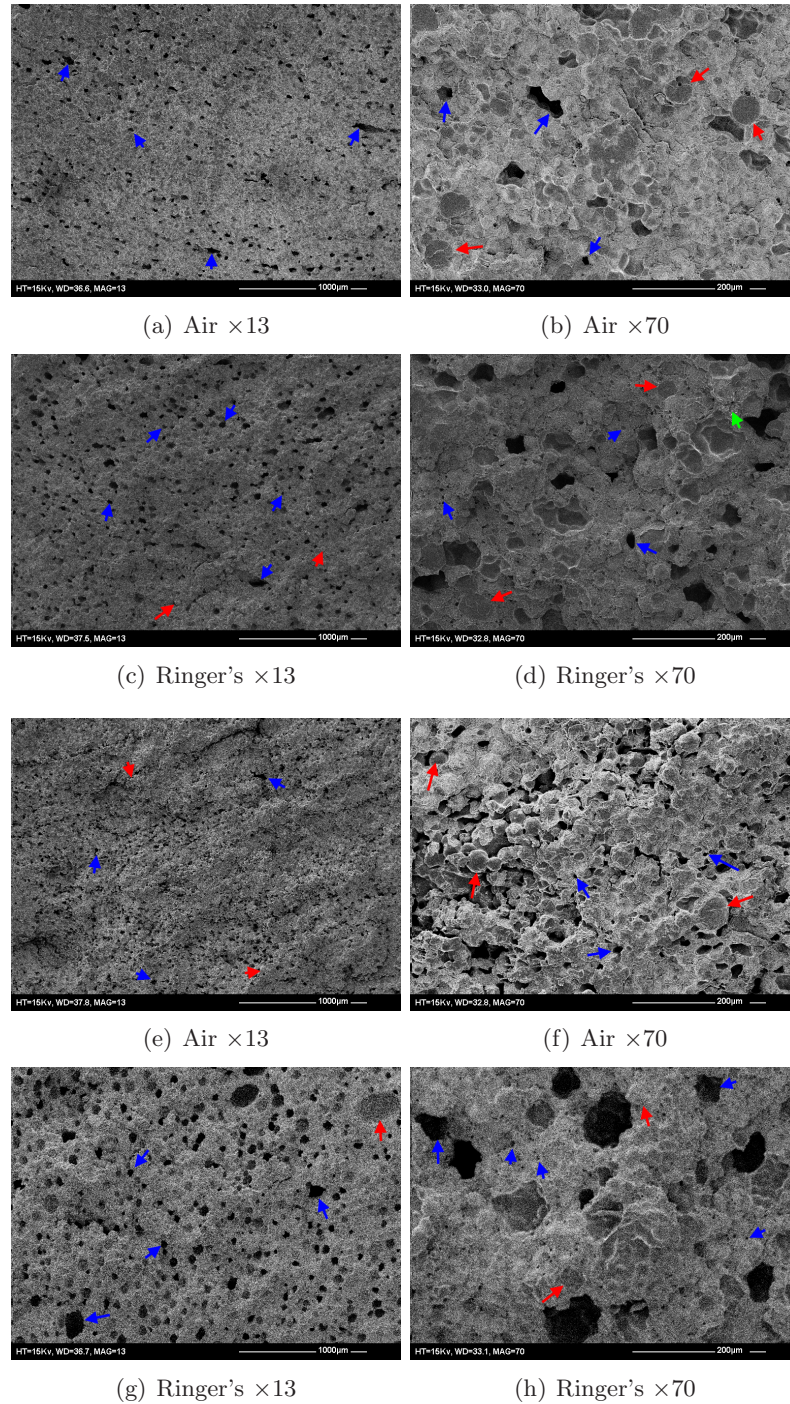


Figure 10.9: Fracture surfaces of fatigue samples aged in air and Ringer's solution for (a-d) liposomal Palacos R with L31 and (e-h) L43 - Red arrows indicate the location of PMMA beads, green arrows indicate radiopaque particles and blue arrows indicate pores.

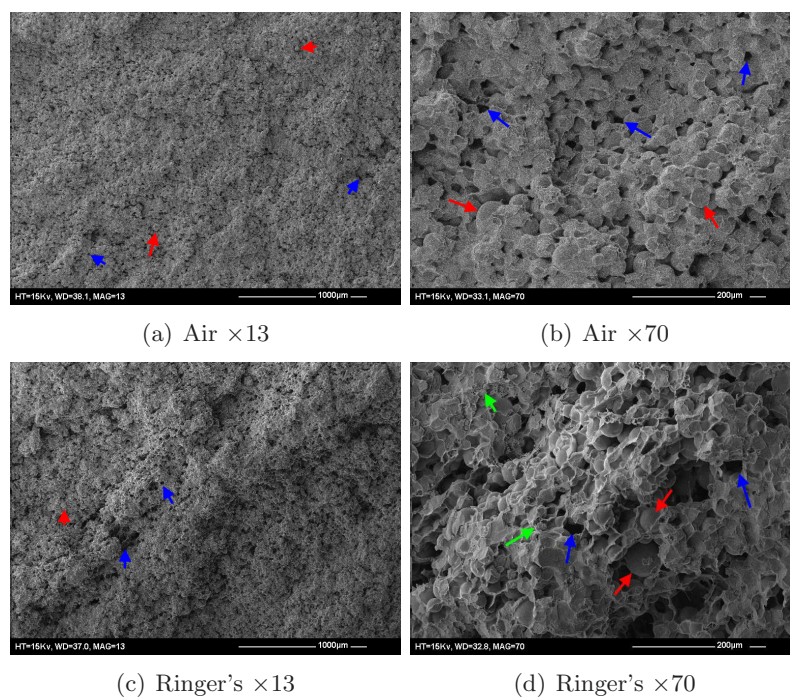


Figure 10.10: Fracture surfaces of fatigue samples aged in (a-b) air and (c-d) Ringer's solution for liposomal Palacos R with L61 - Red arrows indicate the location of PMMA beads, green arrows indicate radiopacifier particles and blue arrows indicate pores.

SEM images of the surface of the antibiotic release samples (Figures 10.11 to 10.13) demonstrated that the liposomal Palacos R cements did not have large pores both before or after storage in Ringer's solution for 60 days, whilst Palacos R+G had 50-200µm pores on the surface of the cement. Closer examination of the surface of the liposomal Palacos R cements found small well-dispersed pores ($<10\mu\text{m}$) as found in the fracture surfaces.

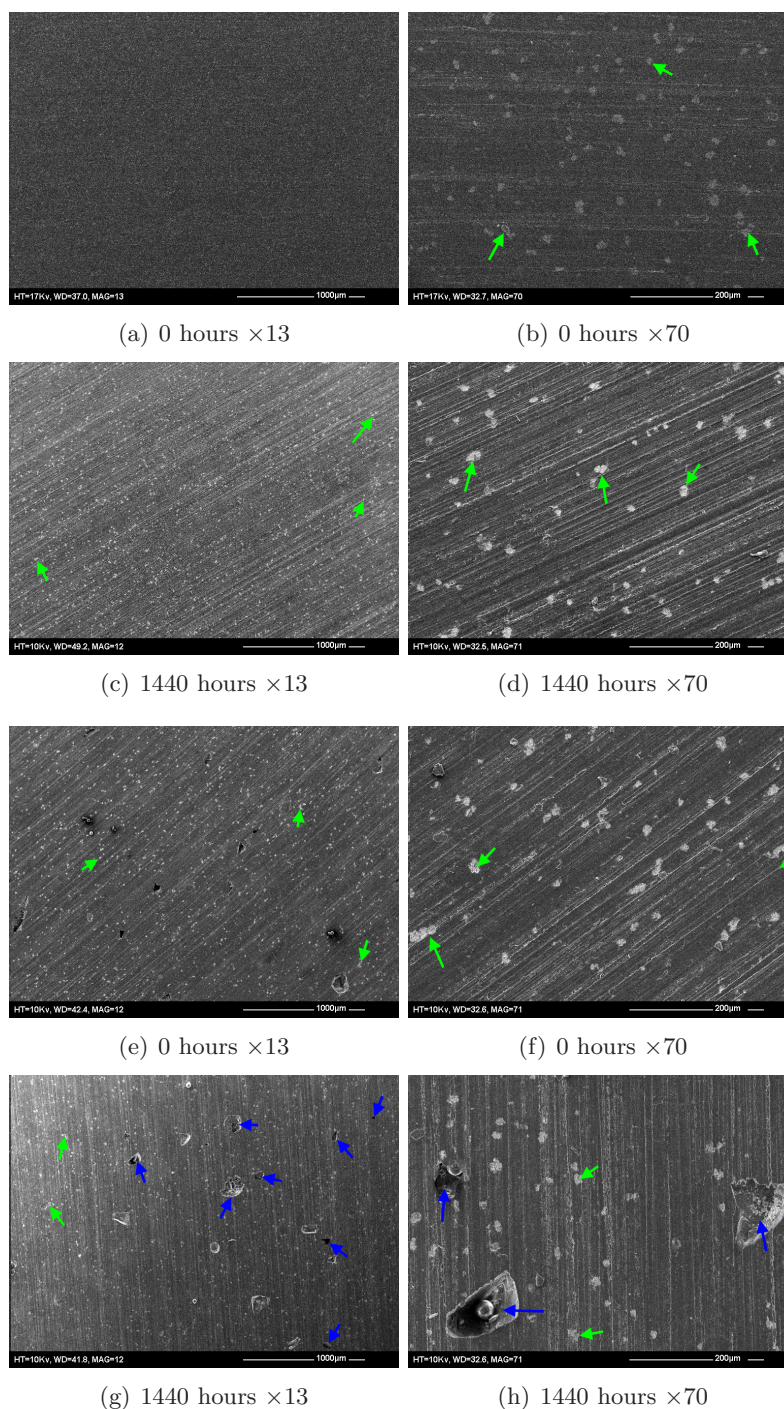


Figure 10.11: Surfaces of antibiotic release samples after 0 and 1440 hours (60 days) in Ringer's solution for (a-d) Palacos R and (e-h) Palacos R+G - Green arrows indicate radiopacifier particles and blue arrows indicate gentamicin sulphate particles or pores created by the release of gentamicin sulphate.

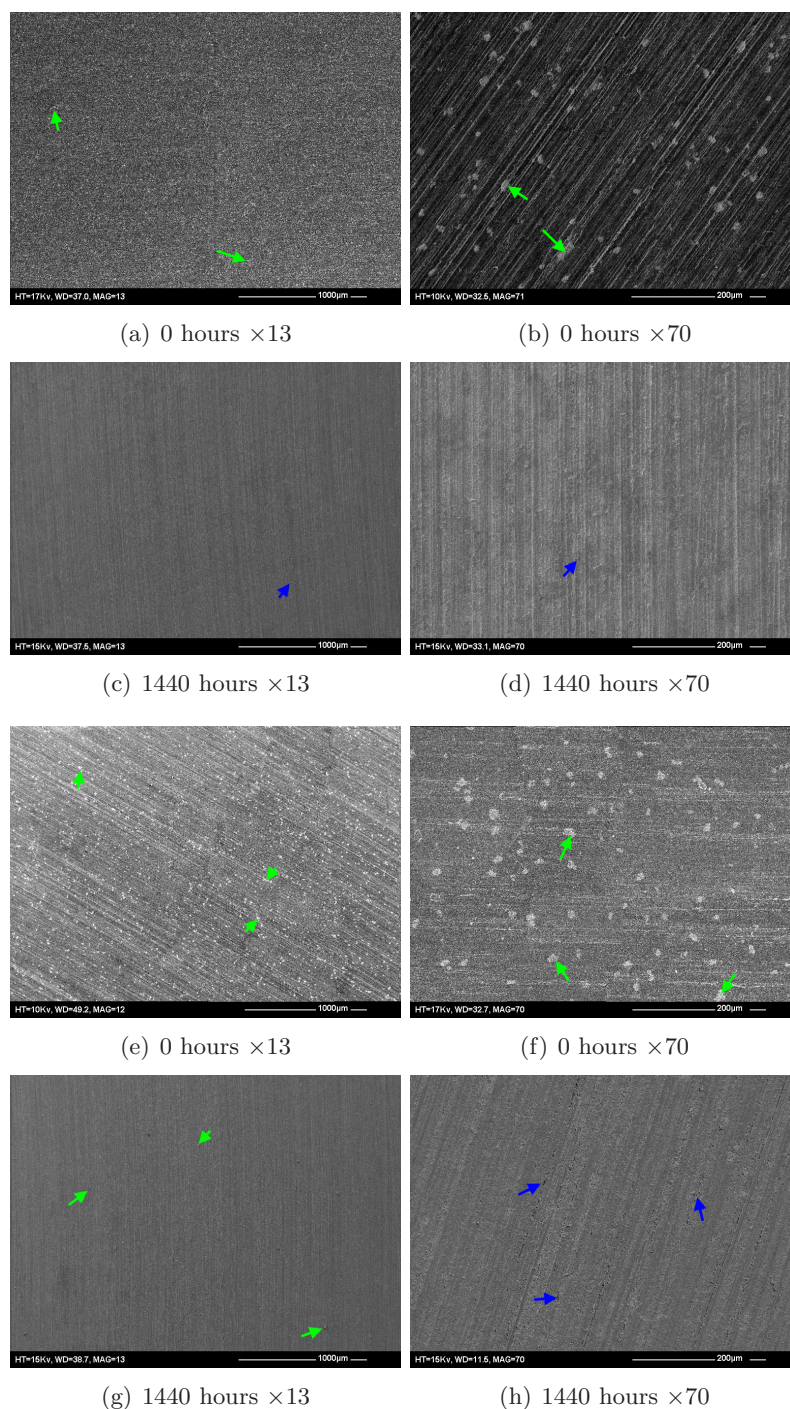


Figure 10.12: Surfaces of antibiotic release samples after 0 and 1440 hours (60 days) in Ringer's solution for (a-d) liposomal Palacos R with L31 and (e-h) L43 - Green arrows indicate radiopaque particles and blue arrows indicate gentamicin sulphate particles or pores created by the release of gentamicin sulphate.

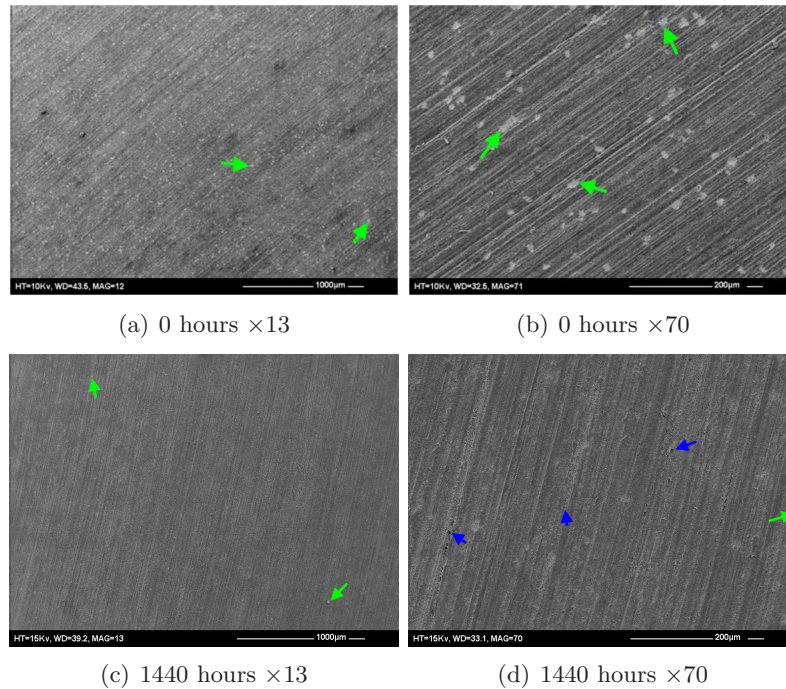


Figure 10.13: Surfaces of antibiotic release samples after (a-b) 0 hours and (c-d) 1440 hours (60 days) in Ringer's solution for liposomal Palacos R with L61 - Green arrows indicate radiopaque particles and blue arrows indicate gentamicin sulphate particles or pores created by the release of gentamicin sulphate.

10.3.8 Vickers hardness

The hardness values for Palacos R, Palacos R+G and the liposomal Palacos R cements before and after storage in Ringer's solution for 60 days are shown in Table 10.6. All three liposomal Palacos R cements had significantly (ANOVA, $p < 0.05$) higher hardness values than Palacos R and Palacos R+G after storage in air and Ringer's solution ($p < 0.05$). Ageing in Ringer's solution for 60 days did not significantly reduce the hardness of the liposomal Palacos R cements ($p > 0.05$). All three liposomal Palacos R cements had similar hardness values (not significantly different, $p = 0.28$ for air and $p = 0.28$ for Ringer's solution).

Table 10.6: Vickers hardness of commercially available antibiotic-loaded cements and liposomal Palacos R before and after storage in Ringer's solution for 60 days

		Hardness (HV30/10) / MPa
Palacos R	Air 1 day	19.76±1.84
	Ringer's 60 days	17.47±2.58
Palacos R+G	Air 1 day	18.74±1.80
	Ringer's 60 days	14.35±3.01
Palacos R L31	Air 1 day	26.55±3.22
	Ringer's 60 days	23.77±2.77
Palacos R L43	Air 1 day	25.92±1.93
	Ringer's 60 days	23.54±3.39
Palacos R L61	Air 1 day	28.10±3.76
	Ringer's 60 days	25.41±2.06

10.3.9 Glass transition temperature

Table 10.7 shows the T_g values for Palacos R, Palacos R+G and the liposomal Palacos R cements before and after storage in Ringer's solution for 60 days. After 1 day in air and 60 days in Ringer's solution, all three liposomal Palacos R cements had similar T_g values (not significantly different, $p=0.52$ for air and $p=0.13$ for Ringer's solution). After 1 day in air, Palacos R had significantly higher T_g value than Palacos R L43 ($p=0.03$), but not significantly higher than L31 ($p=0.08$) and L61 ($p=0.10$). After 60 days in Ringer's solution, Palacos R L31 and L43 had significantly higher T_g values than Palacos R ($p=0.03$ and $p=2.49 \times 10^{-03}$ respectively), whilst L61 was not significantly different ($p=0.09$). The liposomal Palacos R samples at 1 day in air had significantly higher T_g values than Palacos R+G ($p<0.05$). Similarly, at 60 days in Ringer's solution, Palacos L31 and L43 had significantly higher T_g values than Palacos R+G ($p=0.03$ and $p=2.63 \times 10^{-03}$ respectively). All the cements, with the exception of Palacos R L43, experienced a drop in T_g as a result of storage in Ringer's solution for 60 days.

Table 10.7: T_g of commercially available antibiotic-loaded cements and liposomal Palacos R before and after storage in Ringer's solution for 60 days

		Glass transition temperature (T_g) / °C
Palacos R	Air 1 day	126.17±3.25
	Ringer's 60 days	117.90±1.23
Palacos R+G	Air 1 day	115.44±1.16
	Ringer's 60 days	117.58±1.50
Palacos R L31	Air 1 day	122.68±2.24
	Ringer's 60 days	119.86±1.18
Palacos R L43	Air 1 day	121.78±2.10
	Ringer's 60 days	121.52±1.40
Palacos R L61	Air 1 day	123.20±1.36
	Ringer's 60 days	119.74±1.69

10.3.10 Structural changes

Figure 10.14 shows the FTIR spectra obtained by ATR measurements for Palacos R, Palacos R+G and Palacos R L61. Peaks, from PMMA molecules were found for all samples. These include methylene (CH_2) and methyl (CH_3) peaks between 2850cm^{-1} and 2950cm^{-1} , at 1400cm^{-1} and at 1450cm^{-1} ; the C=O stretch at 1730cm^{-1} ; the C-C-O stretch at 1250cm^{-1} ; the O-C-C stretch at 1150cm^{-1} and C-O stretches between 1300cm^{-1} and 900cm^{-1} . For Palacos R+G, the peaks around 2900cm^{-1} were different, with the primary peak at 2850cm^{-1} being suppressed, when compared to Palacos R L61 and Palacos R. Small peaks were present in both Palacos R+G and the liposomal Palacos R cements, which represent gentamicin sulphate, however peaks for liposomal and Pluronic materials were not detected potentially due to very small concentrations being present in the cement. The gentamicin sulphate peaks were located at roughly 1050cm^{-1} , 1540cm^{-1} , 3000cm^{-1} and as broad peaks around 3400cm^{-1} . The strongest peaks for gentamicin sulphate located at 2340cm^{-1} and 2360cm^{-1} however, were not detected. This may

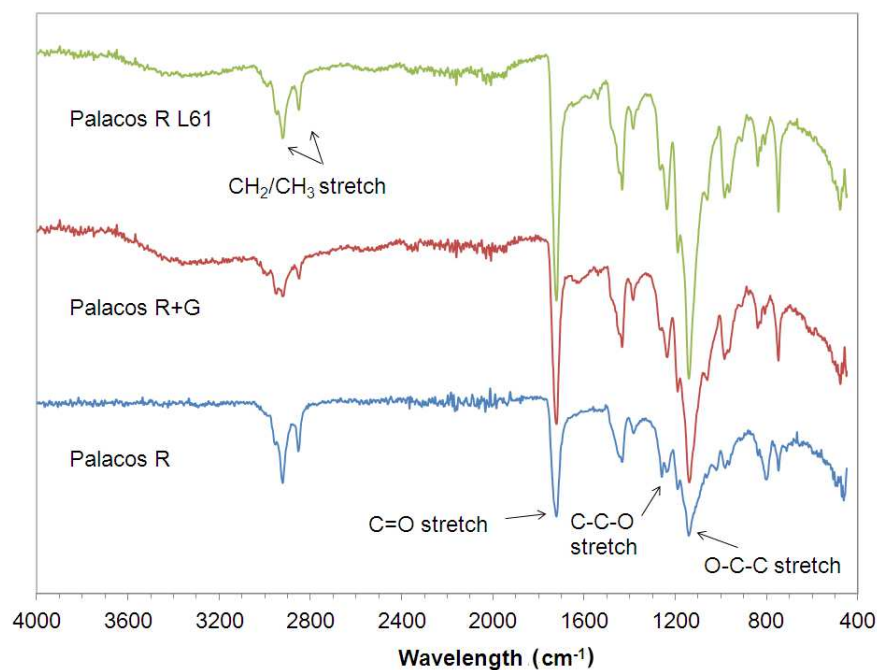


Figure 10.14: FTIR spectrum of Palacos R, Palacos R+G and liposomal Palacos R using ATR

be due to the infra-red signals obtained from PMMA being much stronger than those obtained from gentamicin sulphate. Overall, few differences were detected between the cements, demonstrating similar molecular structures.

10.4 Discussion

Commercially available antibiotic-loaded cements, such as Palacos R+G, employ large amounts of gentamicin sulphate powder to achieve therapeutic levels of release (from 0.5-1g per 40g of cement). Although these cements have reduced infection rates in cemented joint replacements, there are several limitations associated with this delivery system. A large dose of the antibiotic is released in an uncontrolled manner from the surface of the cement within the first 6 hours, after which, lower, possibly sub-inhibitory levels, are released over prolonged periods of time. This may enable the formation of resistant bacteria.

Although large amounts of gentamicin sulphate are incorporated in commercial cements, only a small percentage of this is released, leaving the majority of the antibiotic unused in the bulk of the cement. Large amounts of powdered gentamicin in bone cements has been shown to affect mechanical and fatigue properties in previous studies^{194–196,200}, with no beneficial influence on the formation of biofilms^{198,199}. Furthermore, the results from Chapter 8 has shown poor dispersion of gentamicin sulphate in bone cement to result in poor antimicrobial activity. With this in mind, there is an opportunity to improve antibiotic-loaded cements.

Liposomes have been extensively used in medicine as drug delivery devices for the treatment of infections and cancers. Liposomes have also been used in ophthalmology, pain management and vaccinations^{385,387,410}. Various therapeutic agents have been employed within liposomes, including antimicrobial and antineoplastic therapeutic agents, chelating agents, steroids, vaccines and genetic materials³⁸². The majority of these liposomal systems are administered as an aqueous suspension and there is little evidence of use in polymers or non-aqueous environments. Nevertheless, the results from this chapter and Chapter 9 demonstrate that liposomes with an encapsulated antibiotic can be effectively dispersed in PMMA bone cement using certain Pluronics (L31, L43 and L61). All three Pluronics gave similar results in terms of antibiotic release, antimicrobial efficacy and mechanical, fatigue and material properties as a result of good dispersion throughout the cement.

For the liposomal Palacos R cements, there was a small initial burst of gentamicin sulphate released from the surface of the cement as these surface liposomes came into contact with water. The initial burst of gentamicin sulphate was lower than the commercial cements however, as significantly less gentamicin sulphate was employed and fewer agglomerations were present on the surface. This resulted in a more linear, gradual and prolonged release

of antibiotic. The SEM images of the release samples confirm this as the commercial cements had randomly located large pores caused by the release of surface agglomerations of gentamicin sulphate, whilst the liposomal Palacos R cements had much smaller well-dispersed pores. The presence of small well-dispersed pores would allow for the controlled diffusion of water through the outer layers of the cement. This in turn would allow water to penetrate the antibiotic below the surface of the cement, resulting in a more gradual and controlled release. Large random pores caused by agglomerations of gentamicin sulphate powder would result in a less controlled release as water penetration into the cement would be less uniform. The standard deviations for the liposomal Palacos R cements were also smaller, demonstrating consistency between the samples tested over the early time points. Commercial cements on the other hand demonstrated large standard deviations due to different levels of antibiotic being released from each sample.

After 360 hours, the release from the liposomal Palacos R cements was equal to that of Palacos R+G, despite there being 60% less gentamicin sulphate in the liposomal Palacos R cements. This resulted in a much higher percentage release (11-12% at 72 hours and 21-22% at 1440 hours), more than double that of Palacos R+G and 7 times greater than Cemex Genta and CMW cements. The high release from Palacos cements may be attributed to the cement composition and therefore a limitation of this study is that comparisons with Cemex Genta and CMW cements cannot be accurately performed. It is possible that the gentamicin sulphate release from the liposomal system would differ when used in other cement brands, although improvements would be expected.

Similar amounts of gentamicin sulphate were released from the liposomal Palacos R cements and Palacos R+G, however the liposomal system demonstrated much higher efficiency compared to cements with powdered gentamicin sulphate. A recent study using liposomal amphotericin B in Simplex P bone cement obtained similar results, whereby

cement with liposomal amphotericin B achieved higher levels of release than cement with amphotericin B deoxycholate⁴¹⁴. Furthermore, the release was also speculated to be related to diffusion from pores in the cement.

The PHT assay was deemed sufficiently accurate and reproducible for assessing the release of gentamicin sulphate from PMMA bone cements between concentrations of 0 and 100µg/mL, as discussed in Chapter 8. Should a finer resolution and greater sensitivity to detect lower concentrations of release be required, high-performance liquid chromatography (HPLC) can be employed as used by Dunne et al.¹⁹⁴. Static release tests were carried out to compare the release from liposomal Palacos R cements with the release results from Chapter 8 for commercial cements. Although dynamic elution tests would more accurately replicate *in vivo* conditions, the static release test used provides basic information on the release of gentamicin sulphate as a result of water penetration and therefore, mathematical modelling is simplified as fewer parameters need to be considered. Results obtained using dynamic elution techniques however, may be different as the cement is subjected to a continuous circulation of medium, which may encourage degradation of the cement, allowing for increased water penetration and antibiotic release. Although Ringer's solution at 37°C replicated similar temperatures, pH and salt concentrations found *in vivo*, the viscosity of the solution differs from blood, which is increased due to the presence of plasma and particles, such as red blood cells. *In vivo* therefore, the penetration of blood into the cement may differ from that of Ringer's solution, resulting in different release rates. Therefore, this *in vitro* investigation can be used to compare the performance of different therapeutic delivery systems, but cannot be used to quantitatively determine antibiotic tissue and fluid concentrations *in vivo*.

As discussed in Chapter 9, centrifugation of liposomes may not harvest all the lipid material for inclusion in the MMA, but calculations on gentamicin content have assumed

that all the liposomes were incorporated in cement. Furthermore, a high encapsulation efficiency (nearing 100%) of gentamicin sulphate was also assumed, however studies have shown the encapsulation efficiency of gentamicin sulphate in liposomes to range from 5 to 40%^{415,416}. Therefore, the efficiency of gentamicin sulphate release from the liposomal Palacos R cement is thought to be significantly higher than the calculated results.

The high efficiency of delivery from the liposomal system may be attributed to the release mechanisms taking place. Equations for antibiotic release were used in an attempt to establish this mechanism. Although the equations used were simple, it was possible to establish the dominant release mechanism in the cements tested, although it is likely that a combination of mechanisms are occurring during the release of gentamicin sulphate. Therefore, combining the release equations may provide a more accurate model, as demonstrated by Khun and Wilson³⁷². The results from the mathematical models have highlighted differences between the liposomal Palacos R cements and the commercial cements. The Noyes-Whitney equation was found to model the release data for the liposomal cements most effectively, whilst the Korsmeyer-Peppas equation best suited the commercial cements (Chapter 8). Furthermore, the Higuchi model was also more accurate for the liposomal Palacos R cements, demonstrating a closer relationship to Fickian diffusion. The use of an additional coefficient improved the goodness of fit for all the models accommodating the initial burst of gentamicin sulphate released from the surface of the cement. Interestingly, the burst coefficient improved the models for the commercial cements to a greater extent than the liposomal Palacos R cements. Overall, the expanded Korsmeyer-Peppas and expanded Noyes-Whitney models best suited the gentamicin sulphate release from the liposomal Palacos R cements, demonstrating the release was exponentially related to time and governed by concentration and surface area dependent processes.

The agar diffusion test demonstrated good bioavailability of the encapsulated gentamicin

sulphate in the liposomal Palacos R cements as reproducible zones of inhibition against *S. aureus* were obtained, consistent in both size and shape between all the liposomal Palacos R samples. Good dispersion of the liposomes on the surface layers of cement would result in an even diffusion of gentamicin sulphate through the agar, creating consistent zones of inhibition. It can be concluded, therefore, that the liposomal system would most likely inhibit bacteria in all regions of the cement, unlike commercial products which were found to have inconsistent zones of inhibition due to an uneven distribution of gentamicin sulphate. The efficacy of the liposomal system was only tested against one strain of bacteria as a bioindicator. The ability of liposomes to encapsulate a combination of antibiotics could widen the antimicrobial spectrum of the cement without altering the release properties.

Although the liposomal Palacos R cements were found to have good release and antimicrobial properties, a reduction in compressive strength was experienced. It is thought that the liposomes are more easily deformed than rigid gentamicin sulphate particles and the presence of well-dispersed 100nm liposomes would result in a more porous cement, making the liposomal Palacos R cements weak in compression. The reduction in compressive strength may also be attributed to the presence of water. The presence of water has been shown to decrease the polymerisation induction period of methyl methacrylate⁴¹⁷. The induction period for free radical polymerisation reactions is the time required for complete consumption of the inhibitor (hydroquinone in the case of bone cement). Although water did not alter the polymerisation of MMA in the study, a shorter induction period may have implications on the mechanical properties of the cement. A study using lyophilized liposomes in bone cement also demonstrated a reduction in compressive strength⁴¹⁴, therefore, the presence of small quantities of water is unlikely to have caused the reduction. After storage in Ringer's solution, the compressive strength of the liposomal Palacos R cements increased, whilst the compressive strength of Palacos R and Palacos R+G decreased. This may be due to the liposomal Palacos R cements setting slowly over 60 days

or the plasticisation effect of water not affecting the liposomal Palacos R cements. This suggests that the liposomal cements may perform better in terms of compressive strength *in vivo*.

The bending modulus of the liposomal Palacos R cement was not significantly different from Palacos R+G and all the cements experienced a reduction in modulus due to storage in Ringer's solution as a result of plasticisation and hydrolysis of PMMA as discussed in Chapter 7. The bending modulus of the liposomal Palacos R cement was significantly lower than Palacos R after 60 days in Ringer's solution due to the gentamicin sulphate being released, resulting in a more porous cement.

Improvements in bending strength were observed for the liposomal Palacos R cement when compared to Palacos R+G. This is due to the even dispersion of the liposomes which contrasts with the weakening effect of agglomerations of powdered gentamicin sulphate. No improvements in bending strength were observed when compared to Palacos R.

The compression and bending tests were carried out according to the ISO5833 standard, which all cements must undergo prior to approval for medical application. The liposomal Palacos R cements were found to exceed the ISO5833 minimum requirements for compression and bending properties, demonstrating the novel delivery system in Palacos cement is suitable as an acrylic cement for orthopaedics.

After the release of gentamicin sulphate from the liposomal Palacos R cements, small well-dispersed pores were observed in the SEM images. It has been hypothesised that small dispersed pores may be beneficial to mechanical and fatigue properties by dispersing energy ahead of the crack tip, as well as blunting the crack tip⁴¹⁸. Small pores are also thought to reduce polymerisation shrinkage, reducing the likelihood of residual stress-

induced cracks⁶¹. It is postulated that the sub-micron pores and liposomes in the liposomal Palacos R cements behave similar to small rubber particles, inducing toughening mechanisms. Rubber particles have been shown to improve the fracture toughness of bone cement through plastic deformation, crack deviation and craze formation^{166–168}. As discussed in Chapter 3, crazes are considered load bearing cracks with highly drawn fibrils spanning the crack. This provides support against loads and delays failure. Although crazing is usually a precursor to brittle failure, the highly drawn fibrils require considerable plastic deformation and energy to form, therefore enhancing the fracture toughness of the material. Rubber particles used in brittle polymers have been shown to increase fracture toughness by increased craze density^{419–422}. Under high strain rates, shear yielding is induced by cavitation of the rubber particles, whilst at low strain rates, matrix deformation and crack deviation is induced¹⁶⁹. It is hypothesised that the liposomes and pores behave in a similar manner. This theory may offer an explanation for the reduced compressive strength of the liposomal Palacos R cements, as the compression test was conducted at a strain rate of 20mm/min, causing cavitation, whilst bending was conducted at 5mm/min, which induced matrix deformation, crack deviation and crazing. Furthermore, rubber particles have also been shown to reduce the modulus of materials, as experienced with the liposomal Palacos R cements⁴²³.

The theory of rubber-like toughening in the liposomal Palacos R cements is further corroborated by the fact that fracture toughness and fatigue crack propagation were improved by the use of well-dispersed liposomes. The fracture surfaces were found to be rougher in the liposomal Palacos R cements, demonstrating non-brittle fracture. Furthermore, the fracture toughness was not significantly reduced by ageing in Ringer's solution.

Tests on the structure of liposomal Palacos R cements demonstrate that liposomes do not affect the molecular structure of the cement, however the hardness of the cement was

significantly increased by the addition of liposomes. As the yield stress of a material is roughly three times the hardness value, it is expected that the yield stress of the liposomal Palacos R cements would also be significantly higher than Palacos R/R+G. The glass transition temperature was also affected, however at temperatures well below the T_g of the cements (e.g. *in vivo* temperatures of 37°C), it is expected that the slight change will not be detrimental to the mechanical properties as fatigue testing at 37°C was not detrimental to crack growth rates. The ISO5833 standard used for mechanical testing does not specify required testing temperatures. Nevertheless, testing at this temperature would ensure the changes in T_g experienced do not significantly affect the compression and bending properties of the liposomal Palacos R cements. Furthermore, creep testing would provide useful information on the rate of deformation that the novel cement is likely to undergo *in vivo*.

10.5 Conclusions

Liposomes have been successfully incorporated into a commercial PMMA bone cement (Palacos R) and with the exception of compressive strength, the commercial cement properties were not adversely affected. Furthermore, all cement properties were above the ISO5833 minimum requirements for acrylic resin cements and the presence of well-dispersed liposomes throughout the cement improved the bending, fracture toughness, fatigue and hardness properties of the commercial cement. It is speculated that the improvement in crack growth resistance is caused by the dispersed liposomes inducing rubber toughening mechanisms, such as crazing, crack deviation and matrix deformation. The novel drug delivery system demonstrated enhanced dispersion of antibiotics when compared to the current powdered antibiotic system. This resulted in a more controlled, gradual and prolonged release of gentamicin sulphate; enhanced antimicrobial properties and higher efficiency, requiring less gentamicin sulphate to achieve therapeutic levels of release. The mechanism of release was found to be altered as it is speculated that the

dispersed liposomes allowed water to penetrate and diffuse below the surface of cement in a controlled manner.

Although the initial results are promising, it is essential to study the long-term stability of liposomes in MMA to establish the shelf-life of the system. The behaviour and integrity of the liposomes in the cement will have implications on the therapeutic index and circulation times *in vivo* and therefore, must be investigated. The system must also be optimised in terms of the antibiotics used; the size and composition of the liposomes; the encapsulation efficiency and the use of other preparation methods, such as lyophilization, to ensure optimum release, antimicrobial, mechanical and fatigue properties *in vivo*.

In conclusion, the release of liposomal therapeutic agents from PMMA bone cement may play a vital role in reducing infection rates in cemented joint replacements. The ability of liposomes to deliver a diverse range of therapeutic agents combined with the technology to disperse liposomes in methacrylate-based materials and potentially other polymeric materials has a wide range of applications.

Chapter 11

Discussion

The failure rate of recently implanted cemented joint replacements has been shown to be roughly 10% after 15 years⁷⁴. With an ageing population on the increase, implant failure, which requires revision surgery, may have considerable consequences for the health care services. Furthermore, the increase in life expectancy requires better implants, which are more resistant to loading, biological responses and the biological environment in order to preserve the quality of life of patients. Although PMMA bone cement is known to fail predominantly as a result of aseptic loosening²¹, the mechanisms behind this are not fully understood. Understanding cement failure and how it behaves *in vivo* over time is essential for developing future formulations.

Several studies have investigated the ageing of PMMA bone cements. These studies however, were limited to investigating changes in surface properties, molecular weight and chemical structure as a result of ageing^{149,150,348}. The impact of physiological ageing on important parameters, such as moisture uptake and mechanical and fatigue properties were not studied. In this study, two commercial cements with different compositions were aged *in vitro* to investigate changes in these properties that may occur due to body temperature, pH, moisture uptake and physiological salts over time. Storage in Ringer's solution at 37°C had a significant impact on the compression, bending, fracture toughness and fatigue properties of the cement. Changes to these properties were attributed to a 2% increase in weight, caused by moisture uptake as a result of Fickian diffusion of water into the cement. As postulated by Hughes et al.¹⁴⁹ and Bettencourt et al.¹⁵⁰, the penetration

of water into the cement is thought to cause polymeric chain scission by hydrolysis of the ester groups of PMMA. This would increase chain mobility, decrease mechanical properties and cause changes to the molecular structure of the cement, as observed in the results. High variability in the results were observed however, due to variation in the preparation techniques creating inhomogeneities in the samples. Preparation techniques that are capable of producing homogeneous samples in a controlled and reproducible manner are required to improve the precision of the results. X-ray imaging or porosimetry measurements may also be employed to determine the presence of pores or agglomerations, which may affect results, prior to ageing and testing. Furthermore, *in vivo* conditions could be more accurately replicated, for example, by using blood as opposed to Ringer's solution. Therefore, the results obtained cannot quantitatively predict the changes that will occur *in vivo*. Nevertheless, qualitative data has been obtained and demonstrates that physiological ageing of PMMA bone cement is a potential contributor to *in vivo* failure. This study also highlights the limitations of using ISO standards to establish the suitability of cement formulations. The ISO5833 standard for acrylic resin cement does not consider the implications of cement ageing, which may influence the clinical success of the cemented implant. An example of this is Boneloc cement (Biomet Inc., Indiana, USA), which met the minimum requirements set by the standard, however resulted in unacceptably high levels of clinical failure due to *in vivo* temperatures inducing changes in mechanical properties¹⁵¹. Therefore, testing of novel cement formulations after ageing is recommended to prevent undesirable clinical outcomes.

A review of the literature has highlighted limitations of the current cement formulations and other potential contributors to failure. A widely disputed contributor is the radiopacifier employed in PMMA bone cement. Previous studies have demonstrated that radiopacifiers influence the mechanical and fatigue properties of commercial cements^{35,66,82,91–95}. The majority of studies testing novel radiopacifiers however, had a different composition

from the commercial cements being used for comparison^{180,188}. Therefore, an accurate comparison between the novel cements and the commercial cements could not be made. With this in mind, a model cement was developed to investigate the effect of using different radiopacifier materials, on the properties of bone cement. Two cement brands, Cemex (Tecres, Sommacampagna, Italy) and Palacos R (Heraeus, Newbury, UK), were used as a baseline due to their distinctly different properties and compositions. The model cement was designed to have intermediate properties between the two commercial cements in an attempt to represent a generic PMMA bone cement. Thus, changes in the properties of the model cement when formulated with different radiopacifiers could be compared with the model cement and would be as a direct result of changes in the radiopacifier. This method was also considered to be more effective than attempting to replace the radiopacifier in commercial cements, as removing the radiopacifier from a pre-blended cement would be difficult to achieve. The complete removal of the radiopacifier material cannot be guaranteed and the method of removal may affect some cement properties.

Anatase TiO_2 and yttria-stabilised ZrO_2 are materials commonly employed to improve the properties of composites. Although similar materials have been tested in PMMA bone cement, the development of a model cement has allowed the effect of using anatase TiO_2 and yttria-stabilised ZrO_2 over conventional radiopacifiers to be determined. All radiopacifiers were found to be suitable for PMMA bone cement, however, there were no significant improvements in using anatase TiO_2 or yttria-stabilised ZrO_2 over BaSO_4 . All the radiopacifiers tested demonstrated a similar problem in that the radiopacifier particles were found to agglomerate in the cement due to the hydrophilic nature of the material when surrounded by hydrophobic PMMA. These results agree with previous studies, which have demonstrated that the agglomerating nature of radiopacifiers is detrimental to the performance of PMMA bone cements^{35,91,92,95}.

To overcome the incompatibilities between PMMA and the radiopacifier particles, a methacrylate based silane was used to alter the surface characteristics to improve the dispersion and adhesion of the radiopacifiers to the polymer matrix. The silane treatment proved to be successful for anatase TiO_2 , which demonstrated significant improvements in mechanical properties. Furthermore, the unique surface properties of anatase TiO_2 and the silane were found to improve the bone growth properties of PMMA bone cement. The biocompatibility of the silane was questioned however, as cell proliferation was adversely influenced by the presence of the coating. Further tests would be required to fully establish the viability of this technology for PMMA bone cement. Tests using bone chips on the surface of the cement, as employed by Schuler et al.³³⁹, would more accurately replicate the conditions found at the cement-bone interface and provide vital information on the performance *in vivo*. Furthermore, changes in surface properties of the cement as a result of using the novel radiopacifiers may have implications on the moisture uptake and ageing of the cement. Therefore, a limitation of this study is that the long-term performance of the cement was not assessed. Nevertheless, silane-treated anatase TiO_2 has been shown to be a suitable radiopacifier for PMMA bone cement, demonstrating improvements in mechanical and bone growth properties. As PMMA is generally considered bioinert in terms of bone growth, improvements in the osseointegrative properties of PMMA bone cement may play a vital role in reducing loosening at the cement-bone interface.

Infected joint replacements account for only a small percentage of failed implants. Nevertheless, post-surgical infections are difficult to treat and are therefore a serious problem with severe implications for patient outcomes and survival rates. Bacteria on the surface of the implant are not easily eliminated and may act as a reservoir for recurring infections. Furthermore, systemic antibiotics are not effective in reaching and treating the affected area due to limited blood flow. The use of bone cement as a local delivery system for antibiotics is a popular solution to this problem, with the number of surgeons opting to

use commercially available antibiotic-loaded cements increasing. The current system however, which utilises powdered gentamicin sulphate, was found to have several limitations. Poor dispersion and agglomerations of the powdered gentamicin sulphate resulted in poor release profiles, with a burst of antibiotic release occurring from surface agglomerations in an uncontrolled manner. This results in large, irregular, randomly located pores on the surface of the cement, which altered the mechanical and fatigue properties of the cement. Furthermore, the majority of the antibiotic release occurs within the first 6 hours, after which sub-inhibitory levels are maintained, which may encourage the formation of resistant bacteria. Although large quantities of gentamicin sulphate are incorporated into the cement (0.5-1g of gentamicin sulphate per 40g of cement), only a small percentage of this is released. These findings strongly agree with the results from other studies and show that the limitations are related to the type of system, as opposed to the antibiotic used^{194–197,200}.

Given these shortcomings, a delivery system, using liposomes as a therapeutic carrier, was developed for PMMA bone cements. A novel method for dispersing hydrophilic liposomes in a hydrophobic liquid using biocompatible block copolymers was developed to overcome incompatibilities between the two systems. The dispersion of sub-micron liposomes improved the bending, fracture toughness, fatigue and hardness properties of the commercial cement and maintained other properties meeting the ISO standard requirements both before and after ageing. Improved antimicrobial performance was observed and the release of gentamicin sulphate from the liposomal cement was more controlled, gradual and prolonged when compared to the powdered antibiotic system.

Overall, the results for the liposomal cement are encouraging and have demonstrated that the liposomal delivery system performs well in a methacrylate-based polymer. A benefit of this technology, is that it does not alter the surgical procedure and therefore, additional

training is not required to mix and apply the liposomal cement. A cost analysis however, is necessary to determine the economical viability of implementing and manufacturing this technology on an industrial scale. Other methacrylate-based medical devices, which may benefit from this technology include: dental materials; screw fixation in bone; bone cavity and skull defect fillers; and materials used for vertebral stabilisation⁴²⁴.

The advantages associated with liposomes, such as the ability to incorporate a combination of therapeutic agents, improved delivery control and the ability to regulate the size and composition, may allow optimisation of the system and further enhance the performance of liposomal bone cements. This flexibility increases the range of applications for this technology. For example, triclosan may be encapsulated in liposomes and incorporated into dental cements. Bone growth factors or strontium may be encapsulated in liposomes to enhance the bone growth of orthopaedic cements or spacers. Bone growth properties may be further enhanced as liposomes composed of certain phospholipids (e.g. phosphatidylserine and phosphatidylinositol) have demonstrated calciotropic properties^{247, 254, 257}.

The use of liposomes outside of methacrylate-based materials would further widen the applicability of the technology. If liposomes can be dispersed in other hydrophobic polymeric materials using Pluronic, then the technology can be applied to other medical devices, such as catheters or biodegradable implants, to deliver therapeutic agents and prevent infections. Furthermore, the release of liposomes from polymeric systems may allow for the local delivery of therapeutic agents, such as cytotoxic antineoplastic drugs used in cancer treatments, closer to the site requiring treatment. For a comprehensive list of the liposome-therapeutic combinations, which have been clinically approved and are currently undergoing clinical trials, refer to Tables 11.1 and 11.2^{385, 387, 410}. Light-sensitive liposomes may also be incorporated into polymeric systems to control the release of encapsulated materials by light activation, closer to the disease site. Radiopaque liquids,

such as iodine-based liquids, may be encapsulated in liposomes and dispersed in polymers to provide radiopacity limiting the potentially toxic effects of using liquid radiopacifiers. Similarly, metal particles, such as those used in magnetic liposomes for magnetic resonance imaging (MRI), may be encapsulated in liposomes to produce radiopacity without the undesirable effects associated with using powdered radiopacifiers.

Table 11.1: Clinically approved liposomal-based therapeutics

Trade Name	Company	Liposome Composition	Liposome Charge	Therapeutic	Therapeutic Type	Form/Shelf-life	Indication
Abelcet	Enzon, Cephalon	DMPC and DMPG (7:3 molar ratio)	Negative	Amphoterecin B	Polyene antimycotics	Suspension/24 months	Fungal infections
AmBisome	Gilead Sciences, NeXstar	HSPC, DSPG and cholesterol (2:0.8:1 molar ratio)	Negative	Amphoterecin B	Polyene antimycotics	Powder/36 months	Fungal and protozoal infections
Amphotec	Sequus	Cholesteryl sulfate	Negative	Amphotericin B	Polyene antimycotics	Powder/24 months	Fungal infections
DepoCyt	SkyePharma, Napp	DOPC, DPPG, Cholesterol and Triolein (7:1:11:1 molar ratio)	Negative	Cytarabine	Antineoplastics	Suspension/18 months	Malignant lymphomatous meningitis
DaunoXome	Gilead Sciences, NeXstar, Galen	DSPC and cholesterol (2:1 molar ratio)	Neutral	Daunorubicin citrate	Antineoplastics	Emulsion/12 months	HIV-related Kaposi sarcoma
Myocet	Zeneus, Cephalon	EPC and cholesterol (55:45 molar ratio)	Neutral	Doxorubicin hydrochloride	Antineoplastics	Powder/18 months	Combination therapy with cyclophosphamide in metastatic breast cancer
Epaxal	Berna Biotech, Janssen-Cilag	DOPC and DOPE	Neutral	Inactivated hepatitis A virus (haemagglutinin)	Vaccine	Suspension/36 months	Hepatitis A
Inflexal V	Berna Biotech, Janssen-Cilag	DOPC and DOPE	Neutral	Influenza virus surface antigens (haemagglutinin and neuraminidase)	Vaccine	Suspension/12 months	Influenza
DepoDur	SkyePharma, Endo	DOPC, DPPG, cholesterol, Triolein (7:1:11:1 molar ratio)	Negative	Morphine sulphate pentahydrate	Analgesic	Suspension/24 months	Postsurgical analgesia
Visudyne	QLT, Novartis	EPG and DMPC (3:5 molar ratio)	Neutral	Verteporfin	Photosensitizing agent	Powder/48 months	Age-related macular degeneration, pathologic myopia, ocular histoplasmosis
Doxil/Caelyx	Ortho Biotech, Schering-Plough, Seqqus, Janssen-Cilag	HSPC, cholesterol and PEG 200-DSPE (56:39:5 molar ratio)	Neutral	Doxorubicin hydrochloride	Antineoplastics	Suspension/20 months	HIV-related Kaposi sarcoma, metastatic breast cancer, metastatic ovarian cancer and prostate cancer
Estrasorb	Novavax	HSPC	Neutral	Estradiol hemihydrate	Hormone	Emulsion/36 months	Menopausal therapy

Table 11.2: Liposomal-based therapeutics in clinical trials

Trade Name	Company	Liposome Composition	Liposome Charge	Therapeutic	Therapeutic Type	Indication
LEP-ETU	NeoPharm	DOPC, cholesterol and cariolipin (90:5:5 molar ratio)	Negative	Paclitaxel	Mitotic inhibitor	Ovarian, breast, lung cancer
LEM-ETU	NeoPharm	DOPC, cholesterol and cariolipin (90:5:5 molar ratio)	Negative	Mitoxantrone	Antineoplastics	Leukemia, breast, stomach, liver, ovarian cancers
EndoTAG-1	Medigene	DOTAP, DOPC and paclitaxel (50:43:3 molar ratio)	Positive	Paclitaxel	Mitotic inhibitor	Anti-angiogenic properties, breast cancer, pancreatic cancer
Arikace	Insmed	DPPC and cholesterol	Neutral	Amikacin	Aminoglycoside antibiotic	Lung infection
Marqibo	Talon therapeutics	Egg sphingomyelin and cholesterol (55:45 molar ratio)	Negative	Vincristine	Mitotic inhibitor	Metastatic malignant uveal melanoma
ThermoDox	Celsion	DPPC, MSPC and PEG 200-DSPE (90:10:4 molar ratio)	Neutral	Doxorubicin hydrochloride	Antineoplastics	Non-resectable hepatocellular carcinoma
Atragen	Aronex	DMPC and soybean oil	Neutral	Tretinoin	Antineoplastics	Acute promyelocytic leukemia, hormone-refractory prostate cancer
T4N5 liposome lotion	AGI Dermatics	Unknown	-	Bacteriophage T4 endonuclease 5	Bacteriophage/Enzyme	Xeroderma pigmentosum
Liposomal Grb-2	Bio-Path	Unknown	-	Grb2 antisense, oligodeoxynucleotide	Synthetic DNA	Acute myeloid leukemia, chronic myelogenous leukemia, acute lymphoblastic leukemia
Nyotran	Aronex	DMPC, DMPG and cholesterol	Negative	Nystatin	Polyene antimycotics	Systemic fungal infections
LE-SN38	NeoPharm, Insys Therapeutics	DOPC, cholesterol and cardiolipin	Negative	SN-38	Metabolite	Metastatic colorectal cancer
Aroplatin	Antigenics	DMPC and DMPG	Negative	Cisplatin	Antineoplastics	Metastatic colorectal cancer
Liprostin	Endovasc	Unknown	-	Prostaglandin E1	Antiulcerative	Peripheral vascular disease

Stimuvax	Merck KGaA	Monophosphoryl lipid A, cholesterol, DMPG and DPPC	Negative	BLP25 lipopeptide	Vaccine	Cancer vaccine for multiple myeloma developed encephalitis
SPI-077	Sequus	SHPC, cholesterol, DSPE-PEG	Neutral	Cisplatin	Antineoplastics	Head and neck cancer, lung cancer
Lipoplatin	Regulon	SPC, DPPG, cholesterol and mPEG 2000-DSPE	Negative	Cisplatin	Antineoplastics	Pancreatic cancer, head and neck cancer, mesothelioma, breast and gastric cancer, non-squamous non-small-cell lung cancer
S-CKD602	Alza	DPSC and DSPE-PEG (95:5 molar ratio)	Neutral	Camptothecin	Drug intermediate	Recurrent and progressive carcinoma of the uterine cervix
OSI-211	OSI Pharmaceuticals	HSPC, cholesterol (2:1 molar ratio)	Neutral	Lurtotecan	Anti-histamine	Ovarian cancer, head and neck cancer
INX-0125	Inex	Egg sphingomyelin and cholesterol (55:45 molar ratio)	Neutral	Vinorelbine	Mitotic inhibitor	Advanced solid tumors
INX-0076	Inex	Egg sphingomyelin and cholesterol (55:45 molar ratio)	Neutral	Topotecan	Antineoplastics	Advanced solid tumors
Liposome-Annamycin	Callisto	DSPC and DSPG	Negative	Annamycin	Anthracycline antibiotic	Acute lymphocytic leukemia
SLIT Cisplatin	Transave	DPPC and cholesterol	Neutral	Cisplatin	Antineoplastics	Cancer treatments
AeroLEF	Delex Therapeutics	EPC/SPC, cholesterol	Neutral	Fentanyl	Analgesic	Pain treatment
Onco TCS	Inex, Enzon	DSPC, cholesterol	Neutral	Vincristine sulfate	Antineoplastic Agents	Cancer treatments
Allovectin-7	Vical	DMRIE and DOPE	Positive	HLA-B7 plasmid	Gene	Gene therapy of metastatic cancers
Annamycin	Aronex	DMPC, DPPC, DMPG, Sterylamine (SA), cholesterol	Negative	Annamycin	Anthracycline antibiotic	Breast cancer

Chapter 12

Conclusions and further work

12.1 Conclusions

The recent evolution of biomaterials has resulted in biological sciences representing an equally important contribution to that of materials science and engineering in laying the foundations for effective medical devices. Furthermore, advances in technology have increased the sophistication with which biomaterials are designed and have permitted the development of materials with increasingly complex functions. In spite of this, PMMA bone cements have experienced few improvements since first being introduced into orthopaedics in the late 1950s. Failure of cemented implants still remains an issue and with an ageing demographic, there is a clear need to improve current cement formulations in an attempt to reduce failure rates. Nevertheless, PMMA bone cement remains one of the most reliable methods for implant fixation and plays a vital role in the treatment of severe joint conditions, such as osteoarthritis.

The main purpose of this research programme was to develop novel formulations of PMMA bone cement, which may contribute to preventing failure. In order to achieve this, it was necessary to gain an understanding of the properties and characteristics of PMMA bone cement, why it fails and what has been done in an attempt to prevent failure. A good understanding of the different test methods used to determine the properties of PMMA was also required and knowledge of the principles behind the test methods allowed for a critical assessment of the results.

Previous studies have demonstrated clear changes in chemical and molecular properties as a result of ageing, however little is known about the moisture uptake of PMMA bone cement and the effect this may have on mechanical and fatigue properties. This study found that significant changes to the mechanical and fatigue properties were experienced when cement was aged *in vitro*, in partially simulated *in vivo* conditions. The reduction in properties was found to coincide with the time when maximum moisture uptake was achieved. The mechanism by which water diffuses into the cement was hypothesised and the structural ageing and degradation of bone cement was found to agree with those postulated by other authors. This study has highlighted the need for more accurate standards of testing, which fully address the effects of physiological ageing over extended periods of time. Furthermore, this study has significant implications on how bone cement is thought to behave *in vivo* over time and provides insight into a potential cause of failure.

Another contributor to the early failure of PMMA bone cement has been linked to the radiopacifier material used. In order to study the effect of different radiopacifier materials on the properties of PMMA bone cement, a different approach was required. A model cement was developed with intermediate properties between two distinctly different commercial cements. This allowed novel radiopacifier materials to be tested and the direct impact of those materials to be deduced. Silane-treated anatase TiO_2 was found to be a suitable radiopacifier material, demonstrating good mechanical and fatigue properties and improved bone growth properties. The improvement in bone growth may help prevent loosening at the cement-bone interface and therefore, reduce the number of failed implants.

Powdered antibiotic in PMMA bone cement is currently used in an attempt to reduce surgical infections and is a technique that is growing in popularity. Nevertheless, previous studies have hypothesized that powdered antibiotic is detrimental to the performance of PMMA bone cement and performs poorly in terms of antibiotic release and in prevent-

ing bacterial growth. This study has established suitable test methods for determining the release and antimicrobial properties of antibiotic-loaded bone cements. Furthermore, these methods have highlighted the limitations of using powdered antibiotic in PMMA bone cements.

Having established the inability of the current delivery system to achieve acceptable release and antimicrobial activity without adversely affecting mechanical and fatigue properties, a novel delivery system was developed. The system combined two materials widely employed in drug delivery systems: block copolymers and lipids. The specific combination and arrangement of the two materials allowed for the dispersal of hydrophilic liposomes in a hydrophobic environment in a completely novel way. Sub-micron liposomes were dispersed in PMMA bone cement, which in turn improved the release, antimicrobial, mechanical and fatigue properties of the commercial cement. This novel system achieved controlled delivery of gentamicin from PMMA bone cement without adversely affecting mechanical performance. This in turn will not only contribute to reducing infection rates, but has broader implications since the technology has the potential to be incorporated in a variety of materials and therefore, may find applicability in a wide range of medical devices.

In conclusion, this study set out to develop novel techniques to help prevent the failure of cemented joint replacements. In doing so, an understanding of the science behind PMMA bone cement, the potential causes of failure, methods of testing the different properties of PMMA bone cement, and techniques to prevent failure have been established. There was a contribution to the existing knowledge on cement failure and two novel techniques were developed, which may aid in preventing cement failure *in vivo*. Recent advances in technology have highlighted the need for cross-disciplinary collaborations, such as this one, and have created opportunities to improve biomaterials using novel approaches. Advancing knowledge in this particular field of science is of paramount importance as improvements

will not only lessen the burden on health care services, but will also contribute to improving patient outcomes and a higher quality of life.

12.2 Further work

The work carried out in this study has produced novel techniques and has contributed to the existing body of knowledge and as a result, a series of further questions have emerged from this. The following experiments have been deemed outside the scope and time frame of this study, but they may form the basis for potential future research.

Although silane treated anatase TiO₂ demonstrated encouraging mechanical, fatigue and bone growth properties, the biocompatibility of the particular silane employed has been questioned. A series of *in vitro* experiments investigating the toxicity of the silane on tissues and cells would clarify the clinical applicability of the technology. Should the outcome of such experiments be favourable, animal trials may then be justifiable to assess the extent of osseointegration.

The ageing experiments have provided useful information on the nature of PMMA and showed the moisture uptake was sufficient for the release of therapeutic agents. The experiment however, did not establish the depth of penetration of water, an important parameter, which will dictate the release characteristics of therapeutic agents from bone cement. Additionally, such an experiment may offer further information on the extent of degradation expected to occur *in vivo* over time. A potential method of studying fluid penetration in PMMA bone cement may involve the use of dyes, such a methylene blue, or spectroscopic and optical measurement techniques.

The development of the liposomal delivery system has created exciting possibilities for the delivery of therapeutic agents from bone cement. The delivery system however, still

requires development to ensure optimum drug release, and further improvements to mechanical and fatigue properties. Further, the composition of the liposome vesicles may play a significant role in cellular and tissue interactions *in vivo*. For example, the use of phosphatidylserine and phosphatidylinositol lipids have demonstrated calciotropic properties when employed as coatings for metallic implants^{247, 254, 257}. The use of these phospholipids may encourage osseointegration of bone cement and advanced experiments may involve studying gene expression in osteoblast and osteoblast precursor cells in the presence of the phospholipids. Similarly, the delivery of osteogenic materials, such bone growth factors, using the liposomal delivery system may offer a unique and novel approach to enhance the bone growth properties of PMMA bone cement.

Another promising and exciting aspect of the liposomal delivery system is its potential to deliver a combination of antibiotics to achieve a synergistic effect. Agar diffusion tests, double-disk synergy tests or the checkerboard method would be simple, yet effective methods to evaluate synergy between antibiotics against known bacterial strains. Synergistic combinations could then be employed in bone cement using the liposomal delivery system and the release and inhibition of bacterial strains could be studied. Furthermore, there is the possibility of performing these tests against clinical isolates from infected joint replacements, obtained through clinical collaborators. Investigating the efficacy of the novel delivery system in preventing biofilms is also of great interest as a solution to this problem in joint replacements is yet to be discovered.

Successful implementation of the liposomal delivery system would require industrial scale production methods. Batch production methods to obtain large quantities of materials may alter the properties of the final product and therefore careful consideration and investigation of the processes are required. Similarly, the method of mixing the bone cement, as previously discussed, alters the porosity of the polymerised product. This in turn may

affect the release characteristics of the liposomal cement and therefore, further work in this area is necessary.

The final experimental work that is of great interest is the wider applicability of the liposomal delivery system in various biomaterials. Having enhanced the properties of PMMA bone cement, the use of such a technology may be advantageous to other biomaterials, such as restorative dental materials or catheters. Although this is merely speculative, it is worthwhile investigating and may create further opportunities for future research and collaborations.

References

- [1] R. Cracknell. The ageing population. London, UK. http://www.parliament.uk/documents/commons/lib/research/key_issues/Key%20Issues%20The%20ageing%20population2007.pdf, 2010. [Online; accessed 10th March 2012].
- [2] K.L. Minaker. Common clinical sequelae of ageing. In L. Goldman and A.I. Schafer, editors, *Cecil Medicine*. Saunders Elsevier, Philadelphia, 24th edition, 2011.
- [3] National Joint Registry, UK. National Joint Registry for England and Wales, 6th Annual Report 2009. Technical report, National Joint Registry UK, 2009.
- [4] American Accreditation Health Care Commission. Osteoarthritis. Harvard, MA, USA. <https://ssl.adam.com/content.aspx?productId=10&pid=10&gid=000035&site=morehead2.adam.com&login=MORE6662>, 2012. [Online; accessed 15th January 2011].
- [5] N. Arden and M.C. Nevitt. Osteoarthritis. Epidemiology. *Best Pract Res Clin Rheumatol*, 20(1):3–25, 2006.
- [6] V. Majithia and S.A. Geraci. Rheumatoid arthritis: Diagnosis and management. *Am J Med*, 120(11):936–9, 2007.
- [7] J.Y. Wong, J.D. Bronzino, and D.R. Peterson. *Biomaterials: Principles and Practices*. CRC Press, Simsbury, 2012.
- [8] G. Lemperle, N. Hazan-Gathier, and M. Lemperle. PMMA Microspheres (Artecoll) for skin and soft-tissue augmentation. Part II: Clinical investigations. *Plast Reconstr Surg*, 96(3):627–34, 1995.
- [9] J. Charnley. Anchorage of the femoral head prostheses of the shaft of the femur. *J Bone Joint Surg (Am)*, 42:28–30, 1960.
- [10] Q. Cui, W.M. Mihalko, J.S. Shields, M. Ries, and K.J. Saleh. Antibiotic-impregnated cement spacers for the treatment of infection associated with total hip or knee arthroplasty. *J Bone Joint Surg (Am)*, 89(4):871–82, 2007.

References

- [11] M.R. Whitehouse and S.L. Evans. Bone cement: An overview. *Int J Nano Biomat*, 3(1):4–19, 2010.
- [12] G. Garellick, J. Karrholm, C. Rogmark, and P. Herberts. Swedish hip arthroplasty register: Annual report 2010. Technical report, Swedish Hip Arthroplasty Register, 2010.
- [13] M. Nordin and V.H. Frankel. *Basic biomechanics of the musculoskeletal system*. Lippincott Williams and Wilkins, Philadelphia, 2001.
- [14] H. Malchau, P. Herberts, T. Eisler, G. Garellick, and P. Soderman. The swedish total hip replacement register. *J Bone Joint Surg (Am)*, 84:2–20, 2002.
- [15] K.J. Bozic, P. Katz, M. Cisternas, L. Ono, M.D. Ries, and J. Showstack. Hospital resource utilization for primary and revision total hip arthroplasty. *J Bone Joint Surg (Am)*, 87(3):570–6, 2005.
- [16] R. Iorio, W.L. Healy, and J.A. Richards. Comparison of the hospital cost of primary and revision total knee arthroplasty after cost containment. *Orthopedics*, 22(2):195–9, 1999.
- [17] P.D. Patel, A.K. Klika, T.G. Murray, K.A. Elsharkawy, V.E. Krebs, and W.K. Barsoum. Influence of technique with distally fixed modular stems in revision total hip arthroplasty. *J Arthroplasty*, 25(6):926–31, 2010.
- [18] I.S. Vanhegan, A.K. Malik, P. Jayakumar, S. Ul Islam, and F.S. Haddad. A financial analysis of revision hip arthroplasty. The economic burden in relation to the national tariff. *J Bone Joint Surg (Br)*, 94B(5):619–23, 2012.
- [19] T. Dixon, M. Shaw, S. Ebrahim, and P. Dieppe. Trends in hip and knee joint replacement: socioeconomic inequalities and projections of need. *Ann Rheum Dis*, 63(7):825–30, 2004.
- [20] Department of Health. Payment by results: tariff information 2007/8. http://webarchive.nationalarchives.gov.uk/+www.dh.gov.uk/en/Publicationsandstatistics/Publications/PublicationsPolicyAndGuidance/DH_4140197, 2006. [Online; accessed 8th March 2012].
- [21] National Joint Registry, UK. National Joint Registry for England and Wales, 7th Annual Report 2010. Technical report, National Joint Registry UK, 2010.

- [22] J.G.E. Hendriks, J.R. van Horn, H.C. van der Mei, and H.J. Busscher. Backgrounds of antibiotic-loaded bone cement and prosthesis related infection. *Biomaterials*, 25(3):545–56, 2004.
- [23] K. Markatos, E. Brilakis, and N. Efstathopoulos. The evolution in reconstructive orthopaedic surgery - Arthroplasty and its implants after World War II. *Acta Orthop Traumatol Hel*, 61(4):203–7, 2010.
- [24] S.J. Breusch and H. Malchau. *The well-cemented total hip arthroplasty: theory and practice*. Springer, Berlin, 2005.
- [25] K.D. Kuhn. *Bone Cements*. Springer, Berlin, 2000.
- [26] O. Kleinschmitt. Plexiglas zur deckung von schdelcken. *Chirurg*, 13:273, 1941.
- [27] J. Judet and R. Judet. The use of an artificial femoral head for arthroplasty of the hip joint. *J Bone Surg*, 32B:166, 1956.
- [28] E.J. Haboush. A new operation for arthroplasty of the hip based on biomechanics, photoelasticity, fast-setting dental acrylic and other considerations. *Bull Hops Joint Dis*, 14:242–77, 1953.
- [29] J. Charnley. *Clinical experiences with self-curing acrylic cement*. Acrylic cement in orthopaedic surgery. Churchill Livingstone, Edinburgh, 1970.
- [30] H.W. Buchholz and H. Engelbrecht. Uber die depotwirkung einiger antibiotica bei vermischung mit dem kunstharz Palacos. *Chirurg*, 41(11):511–5, 1970.
- [31] K.D. Kuhn, W. Ege, and U. Gopp. Acrylic bone cements: composition and properties. *Orthop Clin North Am*, 36(1):17–28, 2005.
- [32] G. Lewis. Fatigue testing and performance of acrylic bone-cement materials: State-of-the-art review. *J Biomed Mater Res, Part B*, 66B(1):457–86, 2003.
- [33] S. Evans. Effects of intermittent overloads on fatigue of PMMA bone cement. *Int J Nano Biomat*, 3(1):65–77, 2010.
- [34] D. Hoey and D. Taylor. Fatigue in porous PMMA: The effect of stress concentrations. *Int J Fatigue*, 30(6):989–95, 2008.
- [35] P.E. Sinnett-Jones, M. Browne, A.J. Moffat, J.R.T. Jeffers, N. Saffari, J.-Y. Buffire, and I. Sinclair. Crack initiation processes in acrylic bone cement. *J Biomed Mater Res, Part A*, 89A(4):1088–97, 2009.

References

- [36] A. Bettencourt, A. Calado, J. Amaral, F.M. Vale, J.M.T. Rico, J. Monteiro, and M. Castro. The influence of vacuum mixing on methylmethacrylate liberation from acrylic cement powder. *Int J Pharm*, 219(1-2):89–93, 2001.
- [37] Tecres S.P.A. Cemex bone cement. Sommacampagna, Italy. <http://www.tecres.it/en/products/orthopaedics/bone-cement>, 2012. [Online; accessed 23rd March 2012].
- [38] J. Charnley. *Acrylic Cement in Orthopaedic Surgery*. Williams and Wilkins Company, Baltimore, 1970.
- [39] P.M. Frost. Cardiac arrest and bone cement. *Br Med J*, 3:524, 1970.
- [40] D.J. Peebles, R.H. Ellis, S.D. Stride, and B.R. Simpson. Cardiovascular effects of methylmethacrylate cement. *Br Med J*, 1(5796):349–51, 1972.
- [41] D.S. Bright, H.G. Clark, and D.E. McCollum. Serum analysis and toxic effects of methylmethacrylate. *Surg Forum*, 23:4557, 1972.
- [42] C.A. Homsy, H.S. Tullos, M.S. Anderson, N.M. Diferrante, and J.W. King. Some physiological aspects of prosthesis stabilization with acrylic polymer. *Clin Orthop*, 83:317–28, 1972.
- [43] G. Schlag, H.J. Schliep, E. Dingeldein, A. Grieben, and W. Ringsdorf. Does methylmethacrylate induce cardiovascular complications during alloarthroplastic surgery of the hip joint? *Anaesthetist*, 25:60–7, 1976.
- [44] J. Christie, R. Burnett, H.R. Potts, and A.C. Pell. Echocardiography of transatrial embolism during cemented and uncemented hemiarthroplasty of the hip. *J Bone Joint Surg (Br)*, 76:409–12, 1994.
- [45] J. Parvizi, A.D. Holiday, M.H. Ereth, and D.G. Lewallen. Sudden death during primary total hip arthroplasty. *Clin Orthop*, 369:39–48, 1999.
- [46] W. Leidinger, G. Hoffmann, J.N. Meierhofer, and R. Wolfel. Reduction of severe cardiac complications during implantation of cemented total hip endoprostheses in femoral neck fractures. *Unfallchirurg*, 105:675–9, 2002.
- [47] A.J. Donaldson, H.E. Thomson, N.J. Harper, and N.W. Kenny. Bone cement implantation syndrome. *Br J Anaesth*, 102(1):12–22, 2009.

- [48] H. Gray, P. L. Williams, and L. H. Bannister. *Gray's Anatomy: The Anatomical Basis of Medicine and Surgery*. Churchill Livingstone, Philadelphia, 38th edition, 1995.
- [49] J. Hill, J. Orr, and N. Dunne. In vitro study investigating the mechanical properties of acrylic bone cement containing calcium carbonate nanoparticles. *J Mater Sci Mater Med*, 19(11):3327–33, 2008.
- [50] M. Nottrott. Acrylic bone cements. *Acta Orthop*, 81(S341):1–27, 2010.
- [51] D.E. Font-Rodriguez, G.R. Scuderi, and J.N. Insall. Survivorship of cemented total knee arthroplasty. *Clin Orthop Relat Res*, (345):79–86, 1997.
- [52] L.D. Topoleski, P. Ducheyne, and J.M. Cuckler. A fractography analysis of in vivo poly(methyl methacrylate) bone cement failure mechanisms. *J Biomed Mater Res*, 24:135–42, 1990.
- [53] P. Culleton, P.J. Prendergast, and D. Taylor. Fatigue failure in the cement mantle of an artificial hip joint. *Clin Mater*, 12(2):95–102, 1993.
- [54] M. Jasty, D.O. OConnor, W.J. Maloney, C.R. Bragdon, T. Haire, and W.H. Harris. The initiation of failure in cemented femoral components of hip arthroplasties. *J Bone Jt Surg Br*, 73(4):551–8, 1991.
- [55] G. Bergmann, G. Deuretzbacher, M. Heller, F. Graichen, A. Rohlmann, J. Strauss, and G.N. Duda. Hip contact forces and gait patterns from routine activities. *J Biomech*, 34(7):859–71, 2001.
- [56] G.C. Pulos and W.G. Knauss. Nonsteady crack and craze behavior in PMMA under cyclical loading - II. effect of load history on growth rate and fracture morphology. *Int J Fract*, 93(1-4):161–85, 1998.
- [57] B.K.C. Yuen and F. Taheri. The effects of frequency, tensile overload and compressive underload on the fatigue crack propagation behaviour of polymethylmethacrylate. *Polym Test*, 23(5):491–500, 2004.
- [58] S. Evans. Fatigue crack propagation under variable amplitude loading in PMMA and bone cement. *J Mater Sci Mater Med*, 18(9):1711–7, 2007.
- [59] J.R.T. Jeffers, M. Browne, and M. Taylor. Damage accumulation, fatigue and creep behaviour of vacuum mixed bone cement. *Biomaterials*, 26(27):5532–41, 2005.

- [60] S. Evans. Effects of porosity on the fatigue performance of polymethyl methacrylate bone cement: an analytical investigation. *Proc Inst Mech Eng H*, 220(1):1–10, 2005.
- [61] D. Hoey and D. Taylor. Statistical distribution of the fatigue strength of porous bone cement. *Biomaterials*, 30(31):6309–17, 2009.
- [62] M. Mavrogordato, M. Taylor, A. Taylor, and M. Browne. Acoustic emission monitoring and 3D visualization of polymerization-induced damage of acrylic polymer materials. *J Biomed Mater Res, Part B*, 90B(1):223–8, 2009.
- [63] D. Hoey and D. Taylor. Quantitative analysis of the effect of porosity on the fatigue strength of bone cement. *Acta Biomater*, 5(2):719–26, 2009.
- [64] L.D. Topoleski, P. Ducheyne, and J.M. Cuckler. Microstructural pathway of fracture in poly(methyl methacrylate) bone cement. *Biomaterials*, 14(15):1165–72, 1993.
- [65] K.E. Tanner, J.-S. Wang, F. Kjellson, and L. Lidgren. Comparison of two methods of fatigue testing bone cement. *Acta Biomater*, 6(3):943–52, 2009.
- [66] O.J. Coultrup, M. Browne, C. Hunt, and M. Taylor. Accounting for inclusions and voids allows the prediction of tensile fatigue life of bone cement. *J Biomech Eng*, 131(5):1–8, 2009.
- [67] J.R. Lieberman. Cemented femoral revision: Lest we forget. *J Arthroplasty*, 20(2):72–4, 2005.
- [68] J. Graham, L. Pruitt, M. Ries, and N. Gundiah. Fracture and fatigue properties of acrylic bone cement: the effects of mixing method, sterilization treatment, and molecular weight. *J Arthroplasty*, 15(8):1028–35, 2000.
- [69] D. Hansen and J.S. Jensen. Pre-chilling and vacuum mixing not suitable for all bone cements. *J Arthroplasty*, 5(4):287–90, 1990.
- [70] B. Pascual, B. Vazquez, M. Gurrachaga, I. Goni, M.P. Ginebra, F.J. Gil, J.A. Planell, B. Levenfeld, and J.S. Roman. New aspects of the effect of size and size distribution on the setting parameters and mechanical properties of acrylic bone cements. *Biomaterials*, 17(5):509–16, 1996.
- [71] N. Dunne, J.F. Orr, M.T. Mushipe, and R.J. Eveleigh. The relationship between porosity and fatigue characteristics of bone cements. *Biomaterials*, 24(2):239–45, 2003.

- [72] E.T. Ng and G. Qi. Material fatigue behavior characterization using the wavelet-based AE technique - a case study of acrylic bone cement. *Eng Fract Mech*, 68(13):1477–92, 2001.
- [73] U. Linden. Fatigue properties of bone cement: Comparison of mixing techniques. *Acta Orthop*, 60(4):431–3, 1989.
- [74] G. Lewis. Properties of acrylic bone cement: state of the art review. *J Biomed Mater Res*, 38(2):155–82, 1997.
- [75] B.P. Murphy and P.J. Prendergast. On the magnitude and variability of the fatigue strength of acrylic bone cement. *Int J Fatigue*, 22(10):855–64, 2000.
- [76] K.J. Messick, M.A. Miller, L.A. Damron, A. Race, M.T. Clarke, and K.A. Mann. Vacuum-mixing cement does not decrease overall porosity in cemented femoral stems: an in vitro laboratory investigation. *J Bone Joint Surg (Br)*, 89(8):1115–21, 2007.
- [77] N. Dunne and J.F. Orr. Influence of mixing techniques on the physical properties of acrylic bone cement. *Biomaterials*, 22(13):1819–26, 2001.
- [78] D. Janssen, J. Stolk, and N. Verdonschot. Why would cement porosity reduction be clinically irrelevant, while experimental data show the contrary. *J Orthop Res*, 23(4):691–7, 2005.
- [79] M.H. Pelletier, A.C. Lau, P.J. Smitham, G. Nielsen, and W.R. Walsh. Pore distribution and material properties of bone cement cured at different temperatures. *Acta Biomater*, 6(3):886–91, 2010.
- [80] G.M. Walker, C. Daly, N.J. Dunne, and J.F. Orr. Liquid monomer-powder particle interaction in acrylic bone cement. *Chem Eng J*, 139(3):489–94, 2008.
- [81] C. Li, S. Schmid, and J. Mason. Effects of pre-cooling and pre-heating procedures on cement polymerization and thermal osteonecrosis in cemented hip replacements. *Med Eng Phys*, 25(7):559–64, 2003.
- [82] M.P. Ginebra, L. Albuixech, E. Fernandez-Barragen, C. Aparicio, F.J. Gil, J. San Roman, B. Vazquez, and J.A. Planell. Mechanical performance of acrylic bone cements containing different radiopacifying agents. *Biomaterials*, 23(8):1873–82, 2002.

- [83] M. Baleani and M. Viceconti. The effect of adding 10 percent of barium sulphate radiopacifier on the mechanical behaviour of acrylic bone cement. *Fatigue Fract Eng Mater Struct*, 34(5):374–82, 2011.
- [84] G. Lewis and M. Carroll. Rheological properties of acrylic bone cement during curing and the role of the size of the powder particles. *J Biomed Mater Res*, 63(2):191–9, 2002.
- [85] T.A. Freitag and S.L. Cannon. Fracture and fatigue characteristics of bone cements II. fatigue. *J Biomed Mater Res*, 11:609–24, 1977.
- [86] H.W. Demian, A.C. Wey, and S.W. Shalaby. Bone cement with exceptionally uniform dispersion of radiopacifier. In *Trans 21st Ann Mtg, Soc Biomater*, page 368, San Francisco, CA, 1995.
- [87] L.H. Koole, M.B. Kruft, J.M. Colnot, R. Kuijter, and S.K. Bulstra. Studies on a new, all-polymeric radiopaque orthopaedic bone cement. In *Trans 25th Ann Mtg, Soc Biomater*, page 316, Providence, RI, 1999.
- [88] C. Minari, L. Cristofolini, F. Baruffaldi, and L. Pierotti. Radiopacity and fatigue characterization of a novel acrylic bone cement with sodium fluoride. *Artif Organs*, 24:751–7, 2000.
- [89] A. Bellare, A. Gomoll, W. Fitz, D. Baker, L. Pruitt, R. Scott, and T. Thornhill. Using nanotechnology to improve the fatigue performance of acrylic bone cement. In *Trans 47th Ann Mtg, Orthop Res Soc*, page 182, San Francisco, CA, 2001.
- [90] A. Bellare, M. Turell, P. Ganesam, A. Gomoll, W. Fitz, D. Baker, L. Pruitt, R. Scott, and T. Thornhill. Mechanisms of crack propagation in a conventional and nanocomposite bone cement. In *Trans 48th Ann Mtg, Orthop Res Soc*, page 1067, Dallas, TX, 2002.
- [91] N. Shearwood-Porter, M. Browne, and I. Sinclair. Micromechanical characterisation of failure in acrylic bone cement: The effect of barium sulphate agglomerates. *J Mech Behav Biomed Mater*, 13:85–92, 2012.
- [92] C. Liu, S.M. Green, N.D. Watkins, P.J. Gregg, and A.W. McCaskie. Some failure modes of four clinical bone cements. *Proc Inst Mech Eng H*, 215(4):359–66, 2001.
- [93] P.E. Sinnott-Jones, M. Browne, W. Ludwig, J.Y. Buffiere, and I. Sinclair. Microtomography assessment of failure in acrylic bone cement. *Biomaterials*, 26:6460–6, 2005.

- [94] S.K. Bhambri and L.N. Gilbertson. Micromechanism of fatigue crack initiation and propagation in bone cements. *J Biomed Mater Res*, 29:233–7, 1995.
- [95] P.W. Beaumont. Fracture processes in acrylic bone cement containing barium sulphate dispersions. *J Biomed Eng*, 1(3):147–52, 1979.
- [96] G.H. Isaac, J.R. Atkinson, D. Dowson, P.D. Kennedy, and M.R. Smith. The causes of femoral head roughening in explanted charnley hip prostheses. *Eng Med*, 16:167–73, 1987.
- [97] L. Caravia, D. Dowson, J. Fisher, and B. Jobbins. The influence of bone and bone cement debris on counterface roughness in sliding wear tests of ultra-high molecular weight polyethylene on stainless steel. *Proc Inst Mech Eng H*, 204:65–70, 1990.
- [98] J.R. Cooper, D. Dowson, J. Fisher, and B. Jobbins. Ceramic bearing surfaces in total artificial joints: resistance to third body wear damage from bone cement particles. *J Med Eng Technol*, 15:63–7, 1991.
- [99] A. Sabokbar, Y. Fujikawa, D.W. Murray, and N.A. Athanasou. Radioopaque agents in bone cement increase bone resorption. *J Bone Jt Surg*, 79B:129–34, 1997.
- [100] R. Huiskes. Some fundamental aspects of human joint replacement: analysis of stresses and heat conduction in bone-prosthesis structures. *Acta Orthop Scand Suppl*, 185:1–208, 1980.
- [101] B. Mjoberg. Loosening of the cemented hip prosthesis: the importance of heat injury. *Acta Orthop Scand Suppl*, 221:1–40, 1986.
- [102] J.A. DiPisa, G.S. Sih, and A.T. Berman. The temperature problem at the bone-acrylic cement interface of the total hip replacement. *Clin Orthop Relat Res*, (121):95–8, 1976.
- [103] P.R. Meyer, E.P. Lautenschlager, and B.K. Moore. On the setting properties of acrylic bone cement. *J Bone Joint Surg (Am)*, 55(1):149–56, 1973.
- [104] S. Madigan, M. Towler, and G. Lewis. Optimisation of the composition of an acrylic bone cement: application to relative amounts of the initiator and the activator/co-initiator in surgical Simplex P. *J Mater Sci Mater Med*, 17(4):307–11, 2006.
- [105] E. Hansen. Modelling heat transfer in a bone-cement-prosthesis system. *J Biomech*, 36(6):787–95, 2003.

References

- [106] F.W. Reckling and W.L. Dillon. The bone-cement interface temperature during total joint replacement. *J Bone Joint Surg (Am)*, 59(1):80–2, 1977.
- [107] S. Harving, K. Soballe, and C. Bunger. A method for bone-cement interface thermometry. An in vitro comparison between low temperature curing cement Palavit, and surgical Simplex P. *Acta Orthop Scand*, 62(6):546–8, 1991.
- [108] S. Toksvig-Larsen, H. Franzen, and L. Ryd. Cement interface temperature in hip arthroplasty. *Acta Orthop Scand*, 62(2):102–5, 1991.
- [109] A.R. Moritz and F.C. Henriques. Studies of thermal injury II. *Am J Path*, 23:695–720, 1947.
- [110] J. Lundskog. Heat and bone tissue: an experimental investigation of the thermal properties of bone and threshold levels for thermal injury. *Scand J Plast Reconstr Surg*, 9:1–80, 1972.
- [111] R.A. Eriksson, T. Albrektsson, and B. Magnusson. Assessment of bone viability after heat trauma: a histological, histochemical and vital microscopic study in the rabbit. *Scand J Plast Reconstr Surg*, 18(3):261–8, 1984.
- [112] L. Linder. Reaction of bone to the acute chemical trauma of bone cement. *J Bone Joint Surg*, 59(A):82–7, 1977.
- [113] J.W. Stachiewkz, J. Miller, and D.L. Burke. Hoop stress generated by shrinkage of PMMA as a source of prosthetic loosening, 1976.
- [114] J.F. Orr, N.J. Dunne, and J.C. Quinn. Shrinkage stresses in bone cement. *Biomaterials*, 24(17):2933–40, 2003.
- [115] A. Roques, M. Browne, A. Taylor, A. New, and D. Baker. Quantitative measurement of the stresses induced during polymerisation of bone cement. *Biomaterials*, 25(18):4415–24, 2004.
- [116] A.B. Lennon and P.J. Prendergast. Residual stress due to curing can initiate damage in porous bone cement: experimental and theoretical evidence. *J Biomech*, 35(3):311–21, 2002.
- [117] G. Lewis and S. Mladi. Effect of sterilization method on properties of Palacos R acrylic bone cement. *Biomaterials*, 19(1-3):117–24, 1998.

- [118] L. Morejon, J.A. Delgado, L. Agüero, M. Rapado, M.P. Ginebra, F.J. Gil, and E. Mendizabal. Effect of the sterilization process on physical and mechanical properties of the Bonacryl bone cement. *Latin Am Appl Res*, 38:201–4, 2008.
- [119] E.J. Harper, M. Braden, W. Bonfield, E. Dingeldein, and H. Wahlig. Influence of sterilization upon a range of properties of experimental bone cements. *J Mater Sci Mater Med*, 8(12):849–53, 1997.
- [120] Heraeus. Palacos product line. Newbury, UK. www.heraeus-medical.com/media/webmedia_local/dc/dc_en/PALACOS_product_line_UK.pdf, 2012. [Online; accessed 23rd March 2012].
- [121] J.C. Webb and R.F. Spencer. The role of polymethylmethacrylate bone cement in modern orthopaedic surgery. *J Bone Joint Surg (Br)*, 89B(7):851–7, 2007.
- [122] M.J. Provenzano, K.P. Murphy, and L.H. Riley. Bone cements: Review of their physiochemical and biochemical properties in percutaneous vertebroplasty. *Am J Neuroradiol*, 25:1286–90, 2004.
- [123] S.S. Haas, G.M. Brauer, and G. Dickson. A characterization of polymethylmethacrylate bone cement. *J Bone Joint Surg (Am)*, 57(3):380–91, 1975.
- [124] R.C. Turner, P.E. Atkins, M.A. Ackley, and J.B. Park. Molecular and macroscopic properties of PMMA bone cement: Free-radical generation and temperature change versus mixing ratio. *J Biomed Mater Res*, 15(3):425–32, 1980.
- [125] B. Vazquez, S. Deb, and W. Bonfield. Optimization of benzoyl peroxide concentration in an experimental bone cement based on poly(methyl methacrylate). *J Mater Sci Mater Med*, 8(7):455–60, 1997.
- [126] R. Milner. The development of theoretical relationships between some handling parameters (setting time and setting temperature), composition (relative amounts of initiator and activator) and ambient temperature for acrylic bone cement. *J Biomed Mater Res B Appl Biomater*, 68(2):180–5, 2004.
- [127] P.C. Noble. Selection of acrylic bone cements for use in joint replacement. *Biomaterials*, 4(2):94–100, 1983.
- [128] L.E. Jasper, H. Deramond, J.M. Mathis, and S.M. Belkoff. The effect of monomer-to-powder ratio on the material properties of cranio-plastic. *Bone*, 25(2):27–9, 1999.

- [129] S.M. Belkoff, J.C. Sanders, and L.E. Jasper. The effect of the monomer-to-powder ratio on the material properties of acrylic bone cement. *J Biomed Mater Res, Part B*, 63(4):396–9, 2002.
- [130] A. Dawoodi. The effect of monomer/polymer and initiator/activator ratios on thermal and mechanical properties of acrylic bone cement. Technical report, Cardiff University, 2009.
- [131] T. Mumme, R. Marx, R. Muller-Rath, C. Siebert, and D. Wirtz. Surface coating to improve the metal-cement bonding in cemented femur stems. *Arch Orthop Trauma Surg*, 128(8):773–81, 2008.
- [132] A.M. Ahmed, S. Raab, and J.E. Miller. Metal/cement interface strength in cemented stem fixation. *J Orthop Res*, 2(2):105–18, 1984.
- [133] J.P. Davies, M.K. Tse, and W.H. Harris. Monitoring the integrity of the cement-metal interface of total joint components in vitro using acoustic emission and ultrasound. *J Arthroplasty*, 11(5):594–601, 1996.
- [134] S.A. Yerby, A.F. Paal, P.M. Young, G.S. Beaupre, K.L. Ohashi, and S.B. Goodman. The effect of a silane coupling agent on the bond strength of bone cement and cobalt-chrome alloy. *J Biomed Mater Res*, 49(1):127–33, 2000.
- [135] R.C. Gardiner and W.J. Hozack. Failure of the cement-bone interface. A consequence of strengthening the cement-prosthesis interface? *J Bone Joint Surg (Br)*, 76(1):49–52, 1994.
- [136] S.Y. Leung, A.M. New, and M. Browne. The use of complementary non-destructive evaluation methods to evaluate the integrity of the cement-bone interface. *Proc Inst Mech Eng H*, 223(1):75–86, 2009.
- [137] A. Terrier, P. Buchler, and A. Farron. Bone-cement interface of the glenoid component: stress analysis for varying cement thickness. *Clin Biomech*, 20(7):710–7, 2005.
- [138] E.L. Radin, C.T. Rubin, E.L. Thrasher, L.E. Lanyon, A.M. Crugnola, A.S. Schiller, I.L. Paul, and R.M. Rose. Changes in the bone-cement interface after total hip replacement. An in vivo animal study. *J Bone Joint Surg (Am)*, 64(8):1188–200, 1982.

- [139] S.R. Goldring, A.L. Schiller, M. Roelke, C.M. Rourke, D.A. O'Neil, and W.H. Harris. The synovial-like membrane at the bone-cement interface in loose total hip replacements and its proposed role in bone lysis. *J Bone Joint Surg (Am)*, 65(5):575–84, 1983.
- [140] L. Savarino, S. Stea, G. Ciapetti, G. Paganetto, M.E. Donati, P. Alvergnia, and A. Pizzoferrato. Microstructural investigation of bone-cement interface. *J Biomed Mater Res*, 29(6):701–5, 1995.
- [141] N.A. Johanson, P.G. Bullough, P.D. Wilson Jr, E.A. Salvati, and C.S. Ranawat. The microscopic anatomy of the bone-cement interface in failed total hip arthroplasties. *Clin Orthop Relat Res*, (218):123–35, 1987.
- [142] U.E. Pazzaglia. Pathology of the bone-cement interface in loosening of total hip replacement. *Arch Orthop Trauma Surg*, 109(2):83–8, 1990.
- [143] G. Lewis and S.I. Janna. Effect of fabrication pressure on the fatigue performance of Cemex XL acrylic bone cement. *Biomaterials*, 25(7-8):1415–20, 2003.
- [144] M. Kopec, J. Milbrandt, T. Duellman, D. Mangan, and D.G. Allan. Effect of hand packing versus cement gun pressurization on cement mantle in total knee arthroplasty. *Can J Surg*, 52(6):490–4, 2009.
- [145] R.W. Klein, C.P. Scott, and P.A. Higham. The strength of acrylic bone cement cured under thumb pressure. *Biomaterials*, 25(5):943–7, 2004.
- [146] M.J. Askew, J.W. Steege, J.L. Lewis, J.R. Ranieri, and R.L. Wixson. Effect of cement pressure and bone strength on polymethylmethacrylate fixation. *J Orthop Res*, 1(4):412–20, 1984.
- [147] M. Nottrott, A.O. Molster, and N.R. Gjerdet. Time dependent mechanical properties of bone cement. An in vitro study over one year. *J Biomed Mater Res, Part B*, 83B(2):416–21, 2007.
- [148] J.C. Arnold and N.P. Venditti. Effects of environment on the creep properties of a poly(ethylmethacrylate) based bone cement. *J Mater Sci Mater Med*, 12(8):707–17, 2001.
- [149] K.F. Hughes, M.D. Ries, and L.A. Pruitt. Structural degradation of acrylic bone cements due to in vivo and simulated ageing. *J Biomed Mater Res, Part A*, 65A(2):126–35, 2003.

- [150] A. Bettencourt, A. Calado, J. Amaral, A. Alfaia, F.M. Vale, J. Monteiro, M.F. Montemor, M.G. Ferreira, and M. Castro. Surface studies on acrylic bone cement. *Int J Pharm*, 278(1):181–6, 2004.
- [151] T. Kindt-Larsen, D.B. Smith, and J.S. Jensen. Innovations in acrylic bone cement and applications equipment. *J Appl Biomater*, 6:75–83, 1995.
- [152] K.F. Abdel-Kader, S. Allcock, D.I. Walker, and S.B. Chaudhry. Boneloc bone-cement: experience in hip arthroplasty during a 3-year period. *J Arthroplasty*, 16(7):811–9, 2001.
- [153] J.M. Hasenwinkel, E.P. Lautenschlager, R.L. Wixson, and J.L. Gilbert. A novel high-viscosity, two-solution acrylic bone cement: Effect of chemical composition on properties. *J Biomed Mater Res*, 47(1):36–45, 1999.
- [154] J.M. Hasenwinkel, E.P. Lautenschlager, R.L. Wixson, and J.L. Gilbert. Effect of initiation chemistry on the fracture toughness, fatigue strength, and residual monomer content of a novel high-viscosity, two-solution acrylic bone cement. *J Biomed Mater Res*, 59(3):411–21, 2002.
- [155] D.C. Rodrigues, J.L. Gilbert, and J.M. Hasenwinkel. Two-solution bone cements with cross-linked micro and nano-particles for vertebral fracture applications: Effects of zirconium dioxide content on the material and setting properties. *J Biomed Mater Res, Part B*, 92B(1):13–23, 2010.
- [156] J.B. Shim, S.J. Warner, J.M. Hasenwinkel, and J.L. Gilbert. Analysis of the shelf life of a two-solution bone cement. *Biomaterials*, 26(19):4181–7, 2005.
- [157] C.R. Jacobs. Bone cement compositions. PCT/US99/05497(09/042,067), 1999.
- [158] S. Deb, B. Vazquez, and W. Bonfield. Effect of crosslinking agents on acrylic bone cements based on poly(methylmethacrylate). *J Biomed Mater Res*, 37(4):465–73, 1997.
- [159] S. Deb and B. Vazquez. The effect of cross-linking agents on acrylic bone cements containing radiopacifiers. *Biomaterials*, 22(15):2177–81, 2001.
- [160] Y. Nien, S. Chen, and J. Chen. Preparation and characterization of crosslinked poly(methylmethacrylate-acrylic acid sodium salt)-modified bone cement. *J Appl Polym Sci*, 117(5):2839–46, 2010.

- [161] M.A. Puska, L.V. Lassila, T.O. Nrhi, A.U.O. Yli-Urpo, and P.K. Vallittu. Improvement of mechanical properties of oligomer-modified acrylic bone cement with glass-fibers. *Appl Compos Mater*, 11(1):17–31, 2004.
- [162] M.A. Puska, T.O. Nrhi, A.J. Aho, A.i. Yli-Urpo, and P.K. Vallittu. Flexural properties of crosslinked and oligomer-modified glass-fibre reinforced acrylic bone cement. *J Mater Sci Mater Med*, 15(9):1037–43, 2004.
- [163] M.H. Gutierrez-Villarreal and J. Rodriguez-Velazquez. The effect of citrate esters as plasticizers on the thermal and mechanical properties of poly(methyl methacrylate). *J Appl Polym Sci*, 105(4):2370–5, 2007.
- [164] A. Lopez, A. Hoess, T. Thersleff, M. Ott, H. Engqvist, and C. Persson. Low-modulus PMMA bone cement modified with castor oil. *Biomed Mater Eng*, 21(5-6):323–32, 2011.
- [165] W.M. Lam, H.B. Pan, M.K. Fong, W.S. Cheung, K.L. Wong, Z.Y. Li, K.D. Luk, W.K. Chan, C.T. Wong, C. Yang, and W.W. Lu. In vitro characterization of low modulus linoleic acid coated strontium-substituted hydroxyapatite containing PMMA bone cement. *J Biomed Mater Res B Appl Biomater*, 96(1):76–83, 2011.
- [166] K. Cho, Y. JaeHo, and C.E. Park. The effect of interfacial adhesion on toughening behaviour of rubber modified poly(methyl methacrylate). *Polymer*, 38(20):5161–7, 1997.
- [167] A.D. Puckett, B. Roberts, L. Bu, and J.W. Mays. Improved orthopaedic bone cement formulations based on rubber toughening. *Crit Rev Biomed Eng*, 28(3 - 4):457–61, 2000.
- [168] L. Lalande, C.J.G. Plummer, J.E. Manson, and P. Gerard. Microdeformation mechanisms in rubber toughened PMMA and PMMA-based copolymers. *Eng Fract Mech*, 73(16):2413–26, 2006.
- [169] K. Cho, Y. JaeHo, and C.E. Park. The effect of rubber particle size on toughening behaviour of rubber-modified poly(methyl methacrylate) with different test methods. *Polymer*, 39(14):3073–81, 1998.
- [170] A. Artola, I. Goni, J. Gil, P. Ginebra, J.M. Manero, and M. Gurruchaga. A radiopaque polymeric matrix for acrylic bone cements. *J Biomed Mater Res, Part B*, 64B(1):44–55, 2003.

- [171] A. Artola, M. Gurruchaga, B. Vazquez, J. San Romn, and I. Goni. Elimination of barium sulphate from acrylic bone cements. Use of two iodine-containing monomers. *Biomaterials*, 24(22):4071–80, 2003.
- [172] G. Lewis, C.S.J. van Hooy-Corstjens, A. Bhattaram, and L.H. Koole. Influence of the radiopacifier in an acrylic bone cement on its mechanical, thermal, and physical properties: Barium sulfate-containing cement versus iodine-containing cement. *J Biomed Mater Res, Part B*, 73B(1):77–87, 2005.
- [173] J.M. Manero, M.P. Ginebra, F.J. Gil, J.A. Planell, J.A. Delgado, L. Morejon, A. Artola, M. Gurruchaga, and I. Goni. Propagation of fatigue cracks in acrylic bone cements containing different radiopaque agents. *Proc Inst Mech Eng H*, 218(3):167–72, 2004.
- [174] S. Kotha, C. Li, S. Schmid, and J. Mason. Reinforcement of bone cement using zirconia fibers with and without acrylic coating. *J Biomed Mater Res, Part A*, 88A(4):898–906, 2009.
- [175] J.L. Gilbert, D.S. Ney, and E.P. Lautenschlager. Self-reinforced composite poly(methyl methacrylate): static and fatigue properties. *Biomaterials*, 16(14):1043–55, 1995.
- [176] G. Lewis, J. Xu, S. Madigan, and M.R. Towler. Influence of strontia on various properties of surgical Simplex P acrylic bone cement and experimental variants. *Acta Biomater*, 3(6):970–9, 2007.
- [177] T.G. Tihan, M.D. Ionita, R.G. Popescu, and D. Iordachescu. Effect of hydrophilic-hydrophobic balance on biocompatibility of poly(methyl methacrylate) (PMMA)-hydroxyapatite (HA) composites. *Mater Chem Phys*, 118(2-3):265–9, 2009.
- [178] P.M. Chou and M. Mariatti. The properties of polymethyl methacrylate (PMMA) bone cement filled with titania and hydroxyapatite fillers. *Polym-Plast Technol*, 49(12):1163 – 71, 2010.
- [179] S.M. Zebarjad, S.A. Sajjadi, T. Ebrahimi Sdrabadi, A. Yaghmaei, and B. Naderi. A study on mechanical properties of PMMA/Hydroxyapatite nanocomposite. *Engineering*, 3(8):795–801, 2011.
- [180] C. Fukuda, K. Goto, M. Imamura, and T. Nakamura. Bioactive bone cement with a low content of titania particles without postsilanization: Effect of filler content

- on osteoconductivity, mechanical properties, and handling characteristics. *J Biomed Mater Res, Part B*, 95B(2):407–13, 2010.
- [181] R. Gillani, B. Ercan, A. Qiao, and T.J. Webster. Nanofunctionalized zirconia and barium sulfate particles as bone cement additives. *Int J Nanomedicine*, 5:1–11, 2009.
- [182] U. Gbureck, S. Grbel, R. Thull, and J.E. Barralet. Modified PMMA cements for a hydrolysis resistant metal-polymer interface in orthopaedic applications. *Acta Biomater*, 1(6):671–6, 2005.
- [183] T. Miyazaki, C. Ohtsuki, M. Kyomoto, M. Tanihara, A. Mori, and K. Kuramoto. Bioactive PMMA bone cement prepared by modification with methacryloxypropyltrimethoxysilane and calcium chloride. *J Biomed Mater Res, Part A*, 67A(4):1417–23, 2003.
- [184] F. Li, D. Zhao, Q. Luo, R. Liu, and R. Yin. Research on surface-modification of nano-TiO₂ by span 60. *J Ceram Process Res*, 9(4):398–400, 2008.
- [185] Gelest Inc. Silane coupling agents: Connecting across boundaries. Morrisville, PA, USA. <http://www.gelest.com/goods/pdf/couplingagents.pdf>, 2006. [Online; accessed 15th January 2011].
- [186] A.H. Gomoll, W. Fitz, R.D. Scott, T.S. Thornhill, and A. Bellare. Nanoparticulate fillers improve the mechanical strength of bone cement. *Acta Orthop*, 79(3):421–7, 2008.
- [187] A. Bellare, W. Fitz, A. Gomoll, M.B. Turell, R.D. Scott, and T.S. Thornhill. Using nanotechnology to improve the performance of acrylic bone cements. *Orthop J Harvard Med School*, 11, 2009.
- [188] A. Ricker, P. Liu-Snyder, and T.J. Webster. The influence of nano MgO and BaSO₄ particle size additives on properties of PMMA bone cement. *Int J Nanomedicine*, 3(1):125–32, 2008.
- [189] Y. Nien and C. Huang. The mechanical study of acrylic bone cement reinforced with carbon nanotube. *Mater Sci Eng, B*, 169(1-3):134–7, 2010.
- [190] B. Marrs, R. Andrews, T. Rantell, and D. Pienkowski. Augmentation of acrylic bone cement with multiwall carbon nanotubes. *J Biomed Mater Res, Part A*, 77A(2):269–76, 2006.

- [191] R. Ormsby, T. McNally, C. Mitchell, and N. Dunne. Incorporation of multiwalled carbon nanotubes to acrylic based bone cements: Effects on mechanical and thermal properties. *J Mech Behav Biomed Mater*, 3(2):136–45, 2009.
- [192] R. Ormsby, T. McNally, C. Mitchell, P. Halley, D. Martin, T. Nicholson, and N. Dunne. Effect of MWCNT addition on the thermal and rheological properties of polymethyl methacrylate bone cement. *Carbon*, 49(9):2893–904, 2011.
- [193] Y. Usui, K. Aoki, N. Narita, N. Murakami, I. Nakamura, K. Nakamura, N. Ishigaki, H. Yamazaki, H. Horiuchi, H. Kato, S. Taruta, Y.A. Kim, M. Endo, and N. Saito. Carbon nanotubes with high bone-tissue compatibility and bone-formation acceleration effects. *Small*, 4(2):240–6, 2008.
- [194] N. Dunne, J. Hill, P. McAfee, K. Todd, R. Kirkpatrick, M. Tunney, and S. Patrick. In vitro study of the efficacy of acrylic bone cement loaded with supplementary amounts of gentamicin: Effect on mechanical properties, antibiotic release, and biofilm formation. *Acta Orthop*, 78(6):774 – 85, 2007.
- [195] N. Dunne, J. Hill, P. McAfee, R. Kirkpatrick, S. Patrick, and M. Tunney. Incorporation of large amounts of gentamicin sulphate into acrylic bone cement: effect on handling and mechanical properties, antibiotic release, and biofilm formation. *Proc Inst Mech Eng H*, 222(3):355–65, 2008.
- [196] E.P. Lautenschlager, J.J. Jacobs, G.W. Marshall, and P.R. Meyer. Mechanical properties of bone cements containing large doses of antibiotic powders. *J Biomed Mater Res*, 10(6):929–38, 1976.
- [197] E. Diez-Pena, G. Frutos, P. Frutos, and J.M. Barrales-Rienda. Gentamicin sulphate release from a modified commercial acrylic surgical radiopaque bone cement. I. Influence of the gentamicin concentration on the release process mechanism. *Chem Pharm Bull*, 50(9):1201–8, 2002.
- [198] H. van de Belt, D. Neut, W. Schenk, J.R. van Horn, H.C. van der Mei, and H.J. Busscher. Gentamicin release from polymethylmethacrylate bone cements and staphylococcus aureus biofilm formation. *Acta Orthop Scand*, 71(6):625–9, 2000.
- [199] K.A. Poelstra, H.J. Busscher, W. Schenk, J.R. van Horn, and H.C. van der Mei. Effect of gentamicin loaded PMMA bone cement on Staphylococcus aureus biofilm formation. *Biofouling*, 14(3):249–54, 1999.

- [200] P.D. Postak and A.S. Greenwald. The influence of antibiotics on the fatigue life of acrylic bone cement. *J Bone Joint Surg (Am)*, 88(4):148–55, 2006.
- [201] M. Baleani, L. Cristofolini, C. Minari, and A. Toni. Fatigue strength of PMMA bone cement mixed with gentamicin and barium sulphate vs pure PMMA. *Proc Inst Mech Eng [H]*, 217(1):9–12, 2003.
- [202] J.P. Davies, D.O. O’Connor, D.W. Burke, and W.H. Harris. Influence of antibiotic impregnation on the fatigue life of Simplex P and Palacos R acrylic bone cements, with and without centrifugation. *J Biomed Mater Res*, 23(4):379–97, 1989.
- [203] J. Meyer, G. Piller, C.A. Spiegel, S. Hetzel, and M. Squire. Vacuum-mixing significantly changes antibiotic elution characteristics of commercially available antibiotic-impregnated bone cements. *J Bone Joint Surg (Am)*, 93(22):2049–56, 2011.
- [204] D. Neut, H. van de Belt, J.R. van Horn, H.C. van der Mei, and H.J. Busscher. The effect of mixing on gentamicin release from polymethylmethacrylate bone cements. *Acta Orthop Scand*, 74(6):670–6, 2003.
- [205] A.C. McLaren, M. Nugent, K. Economopoulos, H. Kaul, B.L. Vernon, and R. McLemore. Hand-mixed and premixed antibiotic-loaded bone cement have similar homogeneity. *Clin Orthop*, 467(7):1693–8, 2009.
- [206] R.M. Seldes, R. Winiarsky, L.C. Jordan, T. Baldini, B. Brause, F. Zodda, and T.P. Sculco. Liquid gentamicin in bone cement: a laboratory study of a potentially more cost-effective cement spacer. *J Bone Joint Surg (Am)*, 87(2):268–72, 2005.
- [207] P.H. Hsieh, K.C. Huang, and C.L. Tai. Liquid gentamicin in bone cement spacers: in vivo antibiotic release and systemic safety in two-stage revision of infected hip arthroplasty. *J Trauma*, 66(3):804–8, 2009.
- [208] R.B. Miller, A.C. McLaren, C.M. Leon, B.L. Vernon, and R. McLemore. Surfactant-stabilized emulsion increases gentamicin elution from bone cement. *Clinical Orthopaedics and Related Research*, 469(11):2995–3001, 2010.
- [209] P. Hsieh, C. Tai, P. Lee, and Y. Chang. Liquid gentamicin and vancomycin in bone cement: A potentially more cost-effective regimen. *J Arthroplasty*, 24(1):125–30, 2009.
- [210] J.C. Laine, T.Q. Nguyen, J.M. Buckley, and H.T. Kim. Effects of mixing techniques on vancomycin-impregnated polymethylmethacrylate. *J Arthroplasty*, 26(8):1562–6, 2011.

- [211] J. Gallo, M. Kolar, A.V. Florschütz, R. Novotný, R. Pantucek, and M. Kesselová. In vitro testing of gentamicin-vancomycin loaded bone cement to prevent prosthetic joint infection. *Biomed Pap Med Fac Univ Palacky Olomouc Czech Repub*, 149(1):153–8, 2005.
- [212] E. Bertazzoni Minelli, T. Della Bora, and A. Benini. Different microbial biofilm formation on polymethylmethacrylate (PMMA) bone cement loaded with gentamicin and vancomycin. *Anaerobe*, 17(6):380–3, 2011.
- [213] N. Dunne, F. Buchanan, J. Hill, C. Newe, M. Tunney, A. Brady, and G. Walker. In vitro testing of chitosan in gentamicin-loaded bone cement: No antimicrobial effect and reduced mechanical performance. *Acta Orthop*, 79(6):851–60, 2008.
- [214] M. Tunney, A. Brady, F. Buchanan, C. Newe, and N. Dunne. Incorporation of chitosan in acrylic bone cement: Effect on antibiotic release, bacterial biofilm formation and mechanical properties. *J Mater Sci Mater Med*, 19(4):1609–15, 2008.
- [215] K. Padois and F. Rodriguez. Effects of chitosan addition to self-setting bone cement. *Biomed Mater Eng*, 17(5):309–20, 2007.
- [216] D. Neut, J.G.E. Hendriks, J.R. van Horn, R.S.Z. Kowalski, H.C. van der Mei, and H.J. Busscher. Antimicrobial efficacy of gentamicin-loaded acrylic bone cements with fusidic acid or clindamycin added. *J Orthop Res*, 24(2):291–9, 2006.
- [217] M.R. Virto, P. Frutos, S. Torrado, and G. Frutos. Gentamicin release from modified acrylic bone cements with lactose and hydroxypropylmethylcellulose. *Biomaterials*, 24(1):79–87, 2003.
- [218] G. Frutos, J.Y. Pastor, N. Martnez, M.R. Virto, and S. Torrado. Influence of lactose addition to gentamicin-loaded acrylic bone cement on the kinetics of release of the antibiotic and the cement properties. *Acta Biomater*, 6(3):804–11, 2010.
- [219] H. Kong and J. Jang. Antibacterial properties of novel poly(methyl methacrylate) nanofiber containing silver nanoparticles. *Langmuir*, 24(5):2051–6, 2008.
- [220] V. Alt, T. Bechert, P. Steinrcke, M. Wagener, P. Seidel, E. Dingeldein, E. Domann, and R. Schnettler. An in vitro assessment of the antibacterial properties and cytotoxicity of nanoparticulate silver bone cement. *Biomaterials*, 25(18):4383–91, 2004.
- [221] D.J.F. Moojen, H.C. Vogely, A. Fleer, A.J. Verbout, R.M. Castelein, and W.J.A. Dhert. No efficacy of silver bone cement in the prevention of methicillin-sensitive

- Staphylococcal infections in a rabbit contaminated implant bed model. *J Orthop Res*, 27(8):1002–7, 2009.
- [222] S. Saha and S. Pal. Mechanical properties of bone cement: a review. *J Biomed Mater Res*, 18(4):435–62, 1984.
- [223] British Standards Institution. *ISO5833:2002 Implants for surgery: Acrylic resin cements*. BSI, London. 2002.
- [224] ASTM International. *ASTM F451 - 08 Standard Specification for Acrylic Bone Cement*. ASTM International, 2008.
- [225] K. Sunnegardh-Gronberg, A. Peutzfeldt, and J.W. van Dijken. Hardness and in vitro wear of a novel ceramic restorative cement. *Eur J Oral Sci*, 110(2):175–8, 2002.
- [226] N.C. Nguyen, W.J. Maloney, and R.H. Dauskardt. Reliability of PMMA bone cement fixation: fracture and fatigue crack-growth behaviour. *J Mater Sci Mater Med*, 8(8):473–83, 1997.
- [227] A. Roques, M. Browne, J. Thompson, C. Rowland, and A. Taylor. Investigation of fatigue crack growth in acrylic bone cement using the acoustic emission technique. *Biomaterials*, 25(5):769–78, 2004.
- [228] British Standards Institution. *ISO13586:2000 Plastics: Determination of fracture toughness (G_{ic} and K_{ic}). Linear elastic fracture mechanics (LEFM) approach*. BSI, London. 2000.
- [229] ASTM International. *D5045 - 99(2007)e1 Standard Test Methods for Plane-Strain Fracture Toughness and Strain Energy Release Rate of Plastic Materials*. ASTM International, 2007.
- [230] T.L. Norman, V. Kish, J.D. Blaha, T.A. Gruen, and K. Hustosky. Creep characteristics of hand- and vacuum-mixed acrylic bone cement at elevated stress levels. *J Biomed Mater Res*, 29(4):495–501, 1995.
- [231] D.J. Chwirut. Long-term compressive creep deformation and damage in acrylic bone cements. *J Biomed Mater Res*, 18(1):25–37, 1984.
- [232] R.W. Treharne and N. Brown. Factors influencing the creep behavior of poly(methyl methacrylate) cements. *J Biomed Mater Res*, 9(4):81–8, 1975.

- [233] N. Verdonschot and R. Huiskes. Creep behavior of hand-mixed Simplex P bone cement under cyclic tensile loading. *J Appl Biomater*, 5(3):235–43, 1994.
- [234] N. Verdonschot and R. Huiskes. Dynamic creep behavior of acrylic bone cement. *J Biomed Mater Res*, 29(5):575–81, 1995.
- [235] O.R. Eden, A.J. Lee, and R.M. Hooper. Stress relaxation modelling of polymethylmethacrylate bone cement. *Proc Inst Mech Eng H*, 216(3):195–9, 2002.
- [236] A.J.C. Lee. The time-dependent properties of polymethylmethacrylate bone cement: the interaction of shape of femoral stems, surface finish and bone cement. In *Interfaces in total hip arthroplasty*, pages 11–9. Springer, Berlin, 2000.
- [237] N.J. Holm. The relaxation of some acrylic bone cements. *Acta Orthop Scand*, 51(5):727–31, 1980.
- [238] S. Pal and S. Saha. Stress relaxation and creep behaviour of normal and carbon fibre reinforced acrylic bone cement. *Biomaterials*, 3(2):93–6, 1982.
- [239] W.R. Krause, J. Miller, and P. Ng. The viscosity of acrylic bone cements. *J Biomed Mater Res*, 16(3):219–43, 1982.
- [240] S.C. Weber and W.L. Bargar. A comparison of the mechanical properties of Simplex, Zimmer, and Zimmer low viscosity bone cements. *Biomater Med Devices Artif Organs*, 11(1):3–12, 1983.
- [241] N. Dunne and J.F. Orr. Flow characteristics of curing polymethyl methacrylate bone cement. *Proc Inst Mech Eng H*, 212(3):199–207, 1998.
- [242] H.A. Barnes, J.F. Hutton, and K. Walters. *An introduction to rheology*. Elsevier, Amsterdam, 1989.
- [243] J. Ferguson and Z. Kemplowski. *Applied fluid rheology*. Elsevier, London, 1991.
- [244] D.F. Farrar and J. Rose. Rheological properties of PMMA bone cements during curing. *Biomaterials*, 22(22):3005–13, 2001.
- [245] J. Yang, H. Li, M. Yang, and C. Shih. Characterization of acrylic bone cement using dynamic mechanical analysis. *J Biomed Mater Res*, 48(1):52–60, 1999.
- [246] F. Kjellson, T. Almn, K.E. Tanner, I.D. McCarthy, and L. Lidgren. Bone cement X-ray contrast media: A clinically relevant method of measuring their efficacy. *J Biomed Mater Res, Part B*, 70B(2):354–61, 2004.

- [247] M. Santin, W. Rhys-Williams, J. O'Reilly, M.C. Davies, K. Shakesheff, W.G. Love, A.W. Lloyd, and S.P. Denyer. Calcium-binding phospholipids as a coating material for implant osteointegration. *J R Soc Interface*, 3(7):277–81, 2006.
- [248] I. Rehman, J.C. Knowles, and W. Bonfield. Analysis of in vitro reaction layers formed on bioglass using thin-film X-ray diffraction and ATR-FTIR microspectroscopy. *J Biomed Mater Res*, 41(1):162–6, 1998.
- [249] S. Rhee and J. Choi. Preparation of a bioactive poly(methyl methacrylate)/silica nanocomposite. *J Am Ceram Soc*, 85(5):1318–20, 2002.
- [250] W. Xia, C. Lindahl, J. Lausmaa, and H. Engqvist. Biomimetic hydroxyapatite deposition on titanium oxide surfaces for biomedical application. In A. George, editor, *Advances in Biomimetics*. InTech, 2011.
- [251] T. Kokubo, F. Miyaji, H. Kim, and T. Nakamura. Spontaneous formation of bonelike apatite layer on chemically treated titanium metals. *J Am Ceram Soc*, 79(4):1127–9, 1996.
- [252] T. Kokubo. Formation of biologically active bone-like apatite on metals and polymers by a biomimetic process. *Thermochim Acta*, 280-281(0):479–90, 1996.
- [253] T. Kokubo, H. Kim, and M. Kawashita. Novel bioactive materials with different mechanical properties. *Biomaterials*, 24(13):2161–75, 2003.
- [254] M. Bosetti, A.W. Lloyd, M. Santin, S.P. Denyer, and M. Cannas. Effects of phosphatidylserine coatings on titanium on inflammatory cells and cell-induced mineralisation in vitro. *Biomaterials*, 26(36):7572–8, 2005.
- [255] I.O. Smith, L.R. McCabe, and M.J. Baumann. MC3T3-E1 osteoblast attachment and proliferation on porous hydroxyapatite scaffolds fabricated with nanophase powder. *Int J Nanomedicine*, 1(2):189–94, 2006.
- [256] L. Cerroni, R. Filocamo, M. Fabbri, C. Piconi, S. Caropreso, and S.G. Cond. Growth of osteoblast-like cells on porous hydroxyapatite ceramics: an in vitro study. *Biomol Eng*, 19(2-6):119–24, 2002.
- [257] A. Merolli, M. Bosetti, L. Giannotta, A. Lloyd, S. Denyer, W. Rhys-Williams, W. Love, C. Gabbi, A. Cacchioli, P. Leali, M. Cannas, and M. Santin. In vivo assessment of the osteointegrative potential of phosphatidylserine-based coatings. *J Mater Sci Mater Med*, 17(9):789–94, 2006.

- [258] A.J. Timperley, I. Nusem, K. Wilson, S.L. Whitehouse, P. Buma, and R.W. Crawford. A modified cementing technique using bonesource to augment fixation of the acetabulum in a sheep model. *Acta Orthop*, 81(4):503–7, 2010.
- [259] P. Frutos, E. Diez-Pena, G. Frutos, and J.M. Barrales-Rienda. Release of gentamicin sulphate from a modified commercial bone cement. Effect of (2-hydroxyethyl methacrylate) comonomer and poly(N-vinyl-2-pyrrolidone) additive on release mechanism and kinetics. *Biomaterials*, 23(18):3787–97, 2002.
- [260] British Standards Institution. *ISO15850:2002 Plastics: Determination of tension-tension fatigue crack propagation. Linear elastic fracture mechanics (LEFM) approach*. BSI, London. 2002.
- [261] ASTM International. *ASTM E399 - 09e2 Standard Test Method for Linear-Elastic Plane-Strain Fracture Toughness of Metallic Materials*. ASTM International, 2009.
- [262] A.G. Atkins and Y.W. Mai. *Elastic and Plastic Fracture. Metals, Polymers, Ceramics, Composites, Biological Materials*. Ellis Horwood Limited, 1st edition, 1985.
- [263] British Standards Institution. *ISO6507:2005 Metallic materials - Vickers hardness test - Part 1: Test method*. BSI, London. 2005.
- [264] A.J. Kinloch and R.J. Young. *Fracture Behaviour of Polymers*. Elsevier Applied Science Publishers, Essex, 1st edition, 1985.
- [265] R. W. Hertzberg, R. P. Vinci, and J. L. Hertzberg. *Deformation and Fracture Mechanics of Engineering Materials*. John Wiley and Sons, New Jersey, 5th edition, 1996.
- [266] A. Zandiatashbar, C. R. Picu, and N. Koratkar. Nanocomposite creep: Control of epoxy creep using graphene. *Small*, 8(11):1675–1675, 2012.
- [267] B. P. Kanungo, S. C. Glade, P. Asoka-Kumar, and K. M. Flores. Characterization of free volume changes associated with shear band formation in zr- and cu-based bulk metallic glasses. *Intermetallics*, 12(1011):1073–1080, 2004.
- [268] N. Segre, C. Ostertag, and P. J. M. Monteiro. Effect of tire rubber particles on crack propagation in cement paste. *Materials Research*, 9:311–320, 2006.
- [269] A.M. Donald and E.J. Kramer. Craze initiation and growth in high-impact polystyrene. *J Appl Polym Sci*, 27(10):3729–41, 1982.

- [270] E. Kramer and L. Berger. Fundamental processes of craze growth and fracture crazing in polymers. In H. Kausch, editor, *Advances in Polymer Science*, volume 91, pages 1–68. Springer, Berlin, 1990.
- [271] C.E. Inglis. Stresses in a plate due to the presence of cracks and sharp corners. *Transactions of the Institute of Naval Architects*, 55:219–41, 1913.
- [272] A.A. Griffith. The phenomena of rupture and flow in solids. *Philosophical Transactions of the Royal Society of London Series A, Containing Papers of a Mathematical or Physical Character*, 221(582-593):163–98, 1921.
- [273] A. Motarjemi and A. Shirzadi. Structural integrity assessment of engineering components. <http://www.msm.cam.ac.uk/phase-trans/2006/SI/SI.html>, 2006. [Online; accessed 7th January 2011].
- [274] G.R. Irwin. Analysis of stresses and strains near the end of a crack traversing a plate. *J Appl Mech*, 24:361–4, 1957.
- [275] K. Lee and S. Rhee. The mechanical properties and bioactivity of poly(methyl methacrylate)/SiO₂-CaO nanocomposite. *Biomaterials*, 30(20):3444–9, 2009.
- [276] E.J. Davis and ASM International. *Handbook of Materials for Medical Devices*. ASM International, 2003.
- [277] X. Yang, Y. Chen, F. Yang, F. He, and S. Zhao. Enhanced initial adhesion of osteoblast-like cells on an anatase-structured titania surface formed by H₂O₂/HCl solution and heat treatment. *Dent Mater*, 25(4):473–80, 2009.
- [278] J. He, W. Zhou, X. Zhou, X. Zhong, X. Zhang, P. Wan, B. Zhu, and W. Chen. The anatase phase of nanotopography titania plays an important role on osteoblast cell morphology and proliferation. *J Mater Sci Mater Med*, 19(11):3465–72, 2008.
- [279] V. Sollazzo, F. Pezzetti, A. Scarano, A. Piattelli, L. Massari, G. Brunelli, and F. Carinci. Anatase coating improves implant osseointegration in vivo. *J Craniofac Surg*, 18(4):806–10, 2007.
- [280] Z. Bartczak, A.S. Argon, R.E. Cohen, and T. Kowalewski. The morphology and orientation of polyethylene in films of sub-micron thickness crystallized in contact with calcite and rubber substrates. *Polymer*, 40(9):2367–80, 1999.

- [281] J. Beutel, H.L. Kundel, and R.L. van Metter. *Handbook of Medical Imaging: Physics and Psychophysics*, volume 1. The International Society for Optical Instrumentation, Bellington, Washington, 2000.
- [282] R.P. Schram. X-ray attenuation: Application of X-ray imaging for density analysis. Technical report, The Nuclear Research and consultancy Group, 2001.
- [283] J.E. Mark. *Physical Properties of Polymers Handbook*. Springer, New York, 2007.
- [284] S. Ebnesajjad. *Handbook of Adhesives and Surface Preparation - Technology, Applications and Manufacturing*. Elsevier, Oxford, 2011.
- [285] B. Weidenfeller, M. Hfer, and F.R. Schilling. Thermal and electrical properties of magnetite filled polymers. *Compos Part A*, 33(8):1041–53, 2002.
- [286] B. Weidenfeller, M. Hfer, and F.R. Schilling. Thermal conductivity, thermal diffusivity, and specific heat capacity of particle filled polypropylene. *Compos Part A*, 35(4):423–9, 2004.
- [287] ASTM International. *Characterization and Failure Analysis of Plastics*. ASTM International, 2003.
- [288] G.M. Kline. *Modern Plastics Encyclopedia*. McGraw-Hill, 1992.
- [289] E. Ebramzadeh, A. Sarmiento, H.A. McKellop, A. Llinas, and W. Gogan. The cement mantle in total hip arthroplasty. Analysis of long-term radiographic results. *J Bone Joint Surg (Am)*, 76(1):77–87, 1994.
- [290] C. Fukuda, K. Goto, M. Imamura, M. Neo, and T. Nakamura. Bone bonding ability and handling properties of titania-polymethylmethacrylate (PMMA) composite bioactive bone cement modified with unique PMMA powder. *Acta Biomater*, 7(10):3595–600, 2011.
- [291] K.B. May, J. Fox, M.E. Razzoog, and B.R. Lang. Silane to enhance the bond between polymethyl methacrylate and titanium. *J Prosthet Dent*, 73(5):428–31, 1995.
- [292] H. Garoff and W. Ansorge. Improvements of DNA sequencing gels. *Anal Biochem*, 115(2):450–7, 1981.
- [293] J.P. Matinlinna, M. Ozcan, L.V.J. Lassila, and P.K. Vallittu. The effect of a 3-methacryloxypropyltrimethoxysilane and vinyltriisopropoxysilane blend and tris(3-trimethoxysilylpropyl)isocyanurate on the shear bond strength of composite resin to titanium metal. *Dent Mater*, 20(9):804–13, 2004.

- [294] J.P. Matinlinna and L.V. Lassila. Enhanced resin-composite bonding to zirconia framework after pretreatment with selected silane monomers. *Dent Mater*, 27(3):273–80, 2010.
- [295] C.Y. Lung, E. Kukk, and J.P. Matinlinna. Shear bond strength between resin and zirconia with two different silane blends. *Acta Odontol Scand*, 70(5):405–13, 2012.
- [296] G.S. Solnit. The effect of methyl methacrylate reinforcement with silane-treated and untreated glass fibers. *J Prosthet Dent*, 66(3):310–4, 1991.
- [297] W.L. Tham, W.S. Chow, and Z.A.M. Ishak. The effect of 3-(trimethoxysilyl) propyl methacrylate on the mechanical, thermal, and morphological properties of poly(methyl methacrylate)/hydroxyapatite composites. *J Appl Polym Sci*, 118(1):218–28, 2010.
- [298] P. Yadav, R. Mittal, V.K. Sood, and R. Garg. Effect of incorporation of silane-treated silver and aluminum microparticles on strength and thermal conductivity of PMMA. *J Prosthodont*, 21(7):546–51, 2012.
- [299] T. Kanie, K. Fujii, H. Arikawa, and K. Inoue. Adding silanes to MMA: the effects on the water absorption, adhesive strength and mechanical properties of acrylic denture base resins. *Dent Mater J*, 19(4):329–37, 2000.
- [300] S. Park and J. Jin. Effect of silane coupling agent on mechanical interfacial properties of glass fiber-reinforced unsaturated polyester composites. *J Polym Sci, Part B: Polym Phys*, 41(1):55–62, 2003.
- [301] Y.M. Bian, X.Y. Zhang, British Standards Zhu, W.Q. Yu, D.P. Ruan, and M. Min. Influence of different amount of silane coupling agent on the flexural strength of PMMA/nanometer ZrO₂ composites. *Shanghai Kou Qiang Yi Xue*, 16(3):319–23, 2007.
- [302] W.F. Mousa, M. Kobayashi, S. Shinzato, M. Kamimura, M. Neo, S. Yoshihara, and T. Nakamura. Biological and mechanical properties of PMMA-based bioactive bone cements. *Biomaterials*, 21(21):2137–46, 2000.
- [303] M.N. Aboushelib, C.J. Kleverlaan, and A.J. Feilzer. Selective infiltration-etching technique for a strong and durable bond of resin cements to zirconia-based materials. *J Prosthet Dent*, 98(5):379–88, 2007.
- [304] M.N. Aboushelib, J.P. Matinlinna, Z. Salameh, and H. Ounsi. Innovations in bonding to zirconia-based materials: Part I. *Dent Mater*, 24(9):1268–72, 2008.

- [305] J.H. Phark, S. Duarte Jr, M. Blatz, and A. Sadan. An in vitro evaluation of the long-term resin bond to a new densely sintered high-purity zirconium-oxide ceramic surface. *J Prosthet Dent*, 101(1):29–38, 2009.
- [306] E.J. Harper. Bioactive bone cements. *Proc Inst Mech Eng [H]*, 212(2):113–20, 1998.
- [307] H. Oonishi. Orthopaedic applications of hydroxyapatite. *Biomaterials*, 12(2):171–8, 1991.
- [308] L. Morejon, A.E. Mendizabal, J.A. Garcia-Menocal, M.P. Ginebra, C. Aparicio, F.J. Mur, M. Marsal, N. Davidenko, M.E. Ballesteros, and J.A. Planell. Static mechanical properties of hydroxyapatite (HA) powder-filled acrylic bone cements: Effect of type of HA powder. *J Biomed Mater Res, Part B*, 72B(2):345–52, 2005.
- [309] S. Deb, M. Braden, and W. Bonfield. Water absorption characteristics of modified hydroxyapatite bone cements. *Biomaterials*, 16(14):1095–100, 1995.
- [310] D.D. Deligianni, N.D. Katsala, P.G. Koutsoukos, and Y.F. Missirlis. Effect of surface roughness of hydroxyapatite on human bone marrow cell adhesion, proliferation, differentiation and detachment strength. *Biomaterials*, 22(1):87–96, 2000.
- [311] D. Liu. Hydroxyapatite formed on titanium via a self-assembled monolayer and its in vitro behaviour. Technical report, University of Adelaide, 2005.
- [312] G. Ciobanu, G. Carja, O. Ciobanu, I. Sandu, and A. Sandu. SEM and EDX studies of bioactive hydroxyapatite coatings on titanium implants. *Micron*, 40(1):143–6, 2009.
- [313] C.E. Wen, W. Xu, W.Y. Hu, and P.D. Hodgson. Hydroxyapatite/titania sol gel coatings on titanium zirconium alloy for biomedical applications. *Acta Biomater*, 3(3):403–10, 2007.
- [314] C. Loty, J. Sautier, H. Boulekbache, T. Kokubo, H. Kim, and N. Forest. In vitro bone formation on a bone-like apatite layer prepared by a biomimetic process on a bioactive glassceramic. *J Biomed Mater Res*, 49(4):423–34, 2000.
- [315] K. Anselme. Osteoblast adhesion on biomaterials. *Biomaterials*, 22:667–81, 2000.
- [316] C.H. Thomas, C.D. McFarland, M.L. Jenkins, A. Rezanian, J.G. Steele, and K.E. Healy. The role of vitronectin in the attachment and spatial distribution of bone-derived cells on materials with patterned surface chemistry. *J Biomed Mater Res*, 37(1):81–93, 1997.

- [317] T.J. Webster. Nanophase ceramics: The future orthopedic and dental implant material. In *Advances in Chemical Engineering*, volume 27, pages 125–66. Academic Press, 2001.
- [318] L. Hao and J. Lawrence. The adsorption of human serum albumin (HSA) on CO₂ laser modified magnesia partially stabilised zirconia (MgO-PSZ). *Colloids Surf B Biointerfaces*, 34(2):87–94, 2004.
- [319] S.B. Kennedy, N.R. Washburn, C.G. Simon Jr, and E.J. Amis. Combinatorial screen of the effect of surface energy on fibronectin-mediated osteoblast adhesion, spreading and proliferation. *Biomaterials*, 27(20):3817–24, 2006.
- [320] G. Zhao, Z. Schwartz, M. Wieland, F. Rupp, J. Geis-Gerstorfer, D.L. Cochran, and B.D. Boyan. High surface energy enhances cell response to titanium substrate microstructure. *J Biomed Mater Res A*, 74(1):49–58, 2005.
- [321] P. Li, C. Ohtsuki, T. Kokubo, K. Nakanishi, N. Soga, and K. de Groot. The role of hydrated silica, titania, and alumina in inducing apatite on implants. *J Biomed Mater Res*, 28(1):7–15, 1994.
- [322] J.E. Ellingsen and S.P. Lyngstadaas. *Bio-implant interface: improving biomaterials and tissue reactions*. CRC Press, USA, 2003.
- [323] S. Zhou, G. Garnweitner, M. Niederberger, and M. Antonietti. Dispersion behavior of zirconia nanocrystals and their surface functionalization with vinyl group-containing ligands. *Langmuir*, 23(18):9178–87, 2007.
- [324] J. Lausmaa. Surface spectroscopic characterization of titanium implant materials. *J Electron Spectr Related Phenom*, 81:343–61, 1996.
- [325] J. Ellingsen. A study on the mechanism of protein adsorption to TiO₂. *Biomaterials*, 12:593–6, 1991.
- [326] M. Svetina, L. Colombi, O. Sbaizero, and S. Meriani. Deposition of calcium ions on rutile (110): A first-principles investigation. *Acta Mater*, 49:2169–77, 2001.
- [327] C. Ozcan and N. Hasirci. Evaluation of surface free energy for PMMA films. *J Appl Polym Sci*, 108(1):438–46, 2008.
- [328] J.F. Pinto, G. Buckton, and J.M. Newton. A relationship between surface free energy and polarity data and some physical properties of spheroids. *Int J Pharm*, 118(1):95–101, 1995.

- [329] M.L. Gonzalezmartin, L. Labajos-Broncano, B. Janczuk, and J.M. Bruque. Wettability and surface free energy of zirconia ceramics and their constituents. *J Mater Sci*, 34(23):5923–6, 1999.
- [330] H.J. Busscher, H.P. de Jong, and J. Arends. Surface free energies of hydroxyapatite, fluorapatite and calcium fluoride. *Mater Chem Phys*, 17(6):553–8, 1987.
- [331] K. Webb, V. Hlady, and P.A. Tresco. Relationships among cell attachment, spreading, cytoskeletal organization, and migration rate for anchorage-dependent cells on model surfaces. *J Biomed Mater Res*, 49(3):362–8, 2000.
- [332] British Standards Institution. *BS EN 828:2013 Adhesives. Wettability. Determination by measurement of contact angle and surface free energy of solid surface*. BSI, London. 1998.
- [333] British Standards Institution. *ISO23317:2007 Implants for surgery - In vitro evaluation for apatite-forming ability of implant materials*. BSI, London. 2007.
- [334] T. Kokubo, H. Kushitani, S. Sakka, T. Kitsugi, and T. Yamamuro. Solutions able to reproduce in vivo surface-structure changes in bioactive glass-ceramic A-W. *J Biomed Mater Res*, 24(6):721–34, 1990.
- [335] C. Ohtsuki, T. Miyazaki, M. Kyomoto, M. Tanihara, and A. Osaka. Development of bioactive PMMA-based cement by modification with alkoxysilane and calcium salt. *J Mater Sci Mater Med*, 12(10-12):895–9, 2001.
- [336] C. Shaoqiang, Z. Ziqiang, Z. Jianzhong, Z. Jian, S. Yanling, Y. Ke, W. Weiming, W. Xiaohua, F. Xiao, L. Laiqiang, and S. Li. Hydroxyapatite coating on porous silicon substrate obtained by precipitation process. *Appl Surf Sci*, 230(14):418–24, 2004.
- [337] A. Mitsionis, T. Vaimakis, C. Trapalis, N. Todorova, D. Bahnemann, and R. Dillert. Hydroxyapatite/titanium dioxide nanocomposites for controlled photocatalytic: No oxidation. *Appl Catal B: Environ*, 106(34):398–404, 2011.
- [338] A. Ochsner and W. Ahmed. *Biomechanics of Hard Tissues*. Wiley-VCH, Weinheim, 2010.
- [339] M. Schuler, D.W. Hamilton, T.P. Kunzler, C.M. Sprecher, M. de Wild, D.M. Brunette, M. Textor, and S.G.P. Tosatti. Comparison of the response of cultured osteoblasts and osteoblasts outgrown from rat calvarial bone chips to nonfouling

- KRSR and FHRRIKA-peptide modified rough titanium surfaces. *J Biomed Mater Res, Part B*, 91B(2):517–27, 2009.
- [340] N.G. McCrum, C.P. Buckley, and C.B. Bucknall. *Principles of Polymer Engineering*. Oxford University Press, Oxford, 2nd edition, 1997.
- [341] T. Alfrey, E.F. Gurnee, and W.G. Lloyd. Diffusion in glassy polymers. *J Polym Sci, Part C: Polym Sym*, 12(1):249–61, 1966.
- [342] L. Masaro and X.X. Zhu. Physical models of diffusion for polymer solutions, gels and solids. *Prog Polym Sci*, 24(5):731–75, 1999.
- [343] M.F. Ashby and D.R.H. Jones. *Engineering materials 1: an introduction to properties, applications and design*. Elsevier, Oxford, 2007.
- [344] R.A. Grinstead, L. Clark, and J.L. Koenig. Study of cyclic sorption-desorption into poly(methyl methacrylate) rods using NMR imaging. *Macromolecules*, 25(4):1235–41, 1992.
- [345] P. Neogi. *Diffusion in Polymers*. CRC Press, New York, 1996.
- [346] V. Bellenger and J. Verdu. Structure-properties relationship for densely crosslinked epoxyamine systems based on epoxide or amine mixtures. *J Mater Sci*, 24:63–8, 1989.
- [347] C.K. Yiu, N.M. King, D.H. Pashley, B.I. Suh, R.M. Carvalho, M.R. Carrilho, and F.R. Tay. Effect of resin hydrophilicity and water storage on resin strength. *Biomaterials*, 25(26):5789–96, 2004.
- [348] H. Oonishi, H. Akiyama, M. Takemoto, T. Kawai, K. Yamamoto, T. Yamamuro, H. Oonishi, and T. Nakamura. The long-term in vivo behavior of polymethyl methacrylate bone cement in total hip arthroplasty. *Acta Orthop*, 82(5):553–8, 2011.
- [349] S. Schmitt, D.J. Krzypow, and C.M. Rimnac. The effect of moisture absorption on the fatigue crack propagation resistance of acrylic bone cement. *Biomed Tech (Berl)*, 49(3):61–5, 2004.
- [350] R.P. Kusy, J.Q. Whitley, and S. Kalachandra. Mechanical properties and interrelationships of poly(methyl methacrylate) following hydration over saturated salts. *Polymer*, 42(6):2585–95, 2001.

- [351] J.F. McCabe and S. Rusby. Water absorption, dimensional change and radial pressure in resin matrix dental restorative materials. *Biomaterials*, 25(18):4001–7, 2004.
- [352] K.E. Smith, P. Trusty, B. Wan, and K. Gall. Long-term toughness of photopolymerizable (meth)acrylate networks in aqueous environments. *Acta Biomater*, 7(2):558–67, 2011.
- [353] M. N’Diaye, F. Pascaretti-Grizon, P. Massin, M.F. Basle, and D. Chappard. Water absorption of poly(methyl methacrylate) measured by vertical interference microscopy. *Langmuir*, 28(31):11609–14, 2012.
- [354] M. Stanczyk and B. van Rietbergen. Thermal analysis of bone cement polymerisation at the cement-bone interface. *J Biomech*, 37(12):1803–10, 2004.
- [355] S. Mazzullot, M. Paolini, and C. Verdi. Numerical simulation of thermal bone necrosis during cementation of femoral prostheses. *J Math Biol*, 29(5):475–94, 1991.
- [356] N.M. van Sorge, J.P. Yska, H. Blansjaar, S. Driessen, P. Schepers, S.R. Bovenga, and A.A. van Sorge. Gentamicin containing surgical bone cement: in vitro characteristics of Palacos and Palamed. In *6th Internet World Congress for Biomedical Sciences (INABIS)*, 2000.
- [357] D. Neut, O.S. Kluin, J. Thompson, H.C. van der Mei, and H.J. Busscher. Gentamicin release from commercially-available gentamicin-loaded PMMA bone cements in a prosthesis-related interfacial gap model and their antibacterial efficacy. *BMC Musculoskel Disord*, 11, 2010.
- [358] P.S. McKinnon and S.L. Davis. Pharmacokinetic and pharmacodynamic issues in the treatment of bacterial infectious diseases. *Eur J Clin Microbiol Infect Dis*, 23:271–88, 2004.
- [359] S.S. Sampath and D.H. Robinson. Comparison of new and existing spectrophotometric methods for the analysis of tobramycin and other aminoglycosides. *J Pharm Sci*, 79(5):428–31, 1990.
- [360] X. Zhang, U.P. Wyss, D. Pichora, and M.F.A. Goosen. Biodegradable controlled antibiotic release devices for osteomyelitis: Optimization of release properties. *J Pharm Pharmacol*, 46(9):718–24, 1994.
- [361] R.W. Korsmeyer, R. Gurny, E. Doelker, P. Buri, and N.A. Peppas. Mechanisms of solute release from porous hydrophilic polymers. *Int J Pharm*, 15(1):25–35, 1983.

- [362] T. Higuchi. Rate of release of medicaments from ointment bases containing drugs in suspension. *J Pharm Sci*, 50(10):874–5, 1961.
- [363] A.A. Noyes and W.R. Whitney. The rate of solution of solid substances in their own solutions. *J Am Chem Soc*, 19(12):930–4, 1897.
- [364] W.D. Lindner and B.C. Lippold. Drug release from hydrocolloid embeddings with high or low susceptibility to hydrodynamic stress. *Pharm Res*, 12(11):1781–5, 1995.
- [365] J.F. Acar and F.W. Goldstein. Disk susceptibility test. In *Antibiotics in laboratory medicine*, pages 17–52. Williams and Wilkins, Baltimore, 3rd edition, 1991.
- [366] M.M. Tunney, G. Ramage, S. Patrick, J.R. Nixon, P.G. Murphy, and S.P. Gorman. Antimicrobial susceptibility of bacteria isolated from orthopedic implants following revision hip surgery. *Antimicrob Agents Chemother*, 42(11):3002–5, 1998.
- [367] B. Thomes, P. Murray, and D. Bouchier-Hayes. Development of resistant strains of *Staphylococcus epidermidis* on gentamicin-loaded bone cement in vivo. *J Bone Joint Surg (Br)*, 84(5):758–60, 2002.
- [368] L. Sanzen and M. Walder. Antibiotic resistance of coagulase-negative staphylococci in an orthopaedic department. *J Hosp Infect*, 12(2):103–8, 1988.
- [369] P.G. Hope, K.G. Kristinsson, P. Norman, and R.A. Elson. Deep infection of cemented total hip arthroplasties caused by coagulase-negative staphylococci. *J Bone Joint Surg (Br)*, 71(5):851–5, 1989.
- [370] A.S. Baker and L.W. Greenham. Release of gentamicin from acrylic bone cement. Elution and diffusion studies. *J Bone Joint Surg*, 70(10):1551–7, 1988.
- [371] S. Torrado, P. Frutos, and G. Frutos. Gentamicin bone cements: characterisation and release (in vitro and in vivo assays). *Int J Pharm*, 217(1-2):57–69, 2001.
- [372] A.T. Kuhn and A.D. Wilson. The dissolution mechanisms of silicate and glass-ionomer dental cements. *Biomaterials*, 6(6):378–82, 1985.
- [373] G. Lewis. Properties of antibiotic-loaded acrylic bone cements for use in cemented arthroplasties: a state-of-the-art review. *J Biomed Mater Res B Appl Biomater*, 89(2):558–74, 2009.
- [374] C.P. Scott, P.A. Higham, and J.H. Dumbleton. Effectiveness of bone cement containing tobramycin. An in vitro susceptibility study of 99 organisms found in infected joint arthroplasty. *J Bone Joint Surg (Br)*, 81(3):440–3, 1999.

- [375] R.C. Nelson, R.O. Hoffman, and T.A. Burton. The effect of antibiotic additions on the mechanical properties of acrylic cement. *J Biomed Mater Res*, 12(4):473–90, 1978.
- [376] Y. He, J.P. Trotignon, B. Loty, A. Tcharkhtchi, and J. Verdu. Effect of antibiotics on the properties of poly(methylmethacrylate)-based bone cement. *J Biomed Mater Res*, 63(6):800–6, 2002.
- [377] M. DeLuise and C.P. Scott. Addition of hand-blended generic tobramycin in bone cement: effect on mechanical strength. *Orthopedics*, 27(12):1289–91, 2004.
- [378] J. Park. Orthopedic prosthesis fixation. *Ann Biomed Eng*, 20(6):583–94, 1992.
- [379] S. Downes. Methods for improving drug release from poly(methyl) methacrylate bone cement. *Clin Mater*, 7:227–31, 1991.
- [380] R.R. New. *Liposomes: A practical approach*. Oxford University Press, Oxford, 1990.
- [381] A.D. Bangham, M.M. Standish, and J.C. Watkins. Diffusion of univalent ions across the lamellae of swollen phospholipids. *J Mol Biol*, 13:238, 1965.
- [382] G. Gregoriadis and A.T. Florence. Liposomes in drug delivery. Clinical, diagnostic and ophthalmic potential. *Drugs*, 45(1):15–28, 1993.
- [383] L. Zhang and S. Granick. How to stabilize phospholipid liposomes (using nanoparticles). *Nano Lett*, 6(4):694–8, 2006.
- [384] V.P. Torchilin. Recent advances with liposomes as pharmaceutical carriers. *Nat Rev Drug Discov*, 4(2):145–60, 2005.
- [385] L. Zhang, F.X. Gu, J.M. Chan, A.Z. Wang, R.S. Langer, and O.C. Farokhzad. Nanoparticles in medicine: therapeutic applications and developments. *Clin Pharmacol Ther*, 83(5):761–9, 2008.
- [386] A. Gabizon and D. Papahadjopoulos. Liposome formulations with prolonged circulation time in blood and enhanced uptake by tumors. *Proc Natl Acad Sci USA*, 85(18):6949–53, 1988.
- [387] A. Sharma and U.S. Sharma. Liposomes in drug delivery: Progress and limitations. *Int J Pharm*, 154(2):123–40, 1997.
- [388] P.M. Furneri, M. Fresta, and G. Puglisi. Ofloxacin-loaded liposomes: in vitro activity and drug accumulation in bacteria. *Antimicrob Agents Chemother*, 44:2458–64, 2000.

- [389] R. Schiffelers, G. Storm, and I. Bakker-Woudenberg. Liposome-encapsulated aminoglycosides in pre-clinical and clinical studies. *J Antimicrob Chemother*, 48:333–44, 2001.
- [390] A. Sharma and R.M. Straubinger. Novel taxol formulations: preparation and characterization of taxol-containing liposomes. *Pharm Res*, 11(6):889–96, 1994.
- [391] T. Hernandez-Caselles, J. Villalain, and J.C. Gomez-Fernandez. Influence of liposome charge and composition on their interaction with human blood serum proteins. *Mol Cell Biochem*, 120(2):119–26, 1993.
- [392] J.D. Burgess. Injectable dispersed systems: Formulation, processing, and performance. In *Drugs and the Pharmaceutical Sciences*, page 136. Informa Healthcare, London, 2005.
- [393] T.M. Allen and P.R. Cullis. Drug delivery systems: entering the mainstream. *Science*, 303:1818–22, 2004.
- [394] S.K. Hobbs, W.L. Mosky, and F. Yuan. Regulation of transport pathways in tumor vessels: role of tumor type and microenvironment. *Proc Natl Acad Sci*, 95:4607–12, 1998.
- [395] S.K. Klimuk, S.C. Semple, P. Scherrer, and M.J. Hope. Contact hypersensitivity: a simple model for the characterization of disease-site targeting by liposomes. *Biochim Biophys Acta*, 1417:191–201, 1999.
- [396] T. Ohsawa, H. Miura, and K. Harada. A novel method for preparing liposome with a high capacity to encapsulate proteinous drugs: freeze-drying method. *Chem Pharm Bull (Tokyo)*, 32(6):2442–5, 1984.
- [397] S. Clerc and Y. Barenholz. Loading of amphipathic weak acids into liposomes in response to transmembrane calcium acetate gradients. *Biochim Biophys Acta*, 1240(2):257–65, 1995.
- [398] T.F. Tadros. *Applied Surfactants: Principles and Applications*. Wiley-VCH Verlag GmbH, Weinheim, 2005.
- [399] W.C. Griffin. Classification of surface-active agents by HLB. *J Soc Cosmet Chem*, 1:311, 1949.
- [400] W.C. Griffin. Calculation of HLB values of non-ionic surfactants. *J Soc Cosmet Chem*, 5:249, 1954.

- [401] J.T. Davies. A quantitative kinetic theory of emulsion type I. Physical chemistry of the emulsifying agent. In *2nd International Congress Surface Activity*, London, 1957.
- [402] J.T. Davies and E.K. Rideal. *Interfacial Phenomena*. Academic Press, New York, 1961.
- [403] C.P. Poole, F.J. Jones, and F.J. Owens. *Introduction to Nanotechnology*. John Wiley and Sons, Inc., 2003.
- [404] K. Kostarelos, T.F. Tadros, and P.F. Luckham. Physical conjugation of (tri-) block copolymers to liposomes toward the construction of sterically stabilized vesicle systems. *Langmuir*, 15(2):369–76, 1998.
- [405] K. Kostarelos, P.F. Luckham, and T.F. Tadros. Addition of block copolymers to liposomes prepared using soybean lecithin. Effects on formation, stability and the specific localization of the incorporated surfactants investigated. *J Liposome Res*, 5(1):117–30, 1995.
- [406] J.L. Tian, X. Ke, Z. Chen, C.J. Wang, Y. Zhang, and T.C. Zhong. Melittin liposomes surface modified with Poloxamer 188: in vitro characterization and in vivo evaluation. *Pharmazie*, 66(5):362–7, 2011.
- [407] S.M. Moghimi, C.J.H. Porter, L. Illum, and S.S. Davis. The effect of Poloxamer-407 on liposome stability and targeting to bone marrow: comparison with polystyrene microspheres. *Int J Pharm*, 68(13):121–6, 1991.
- [408] M. Jamshaid, S.J. Farr, P. Kearney, and I.W. Kellaway. Poloxamer sorption on liposomes: comparison with polystyrene latex and influence on solute efflux. *Int J Pharm*, 48(13):125–31, 1988.
- [409] R.S. Dhanikula, A.B. Dhanikula, and R. Panchagnula. Thermoreversible liposomal poloxamer gel for the delivery of paclitaxel: dose proportionality and hematological toxicity studies. *Pharmazie*, 63(6):439–45, 2008.
- [410] H.I. Chang and M.K. Yeh. Clinical development of liposome-based drugs: formulation, characterization, and therapeutic efficacy. *Int J Nanomedicine*, 7:49–60, 2012.
- [411] Y.Q. Xiong, L.I. Kupferwasser, P.M. Zack, and A.S. Bayer. Comparative efficacies of liposomal amikacin (MiKasome) plus oxacillin versus conventional amikacin plus

- oxacillin in experimental endocarditis induced by *Staphylococcus aureus*: microbiological and echocardiographic analyses. *Antimicrob Agents Chemother*, 43:1737–42, 1999.
- [412] D.D. Lasic and D. Papahadjopoulos. *Medical applications of liposomes*. Elsevier Science B. V., Amsterdam, 1998.
- [413] C.E. Swenson, K.A. Stewart, J.L. Hammett, W.E. Fitzsimmons, and R.S. Ginsberd. Pharmacokinetics and in vivo activity of liposome-encapsulated gentamicin. *Antimicrob Agents Chemother*, 34(2):235–40, 1990.
- [414] B. Cunningham, A.C. McLaren, C. Pauken, and R. McLemore. Liposomal formulation increases local delivery of amphotericin from bone cement: a pilot study. *Clin Orthop Relat Res*, 470(10):2671–6, 2012.
- [415] C. Mugabe, A.O. Azghani, and A. Omri. Liposome-mediated gentamicin delivery: development and activity against resistant strains of *Pseudomonas aeruginosa* isolated from cystic fibrosis patients. *J Antimicrob Chemother*, 55(2):269–71, 2005.
- [416] D.L. MacLeod and J.F. Prescott. The use of liposomally-entrapped gentamicin in the treatment of bovine *Staphylococcus aureus* mastitis. *Can J Vet Res*, 52(4):445–50, 1988.
- [417] I.C. Schoonover, G.M. Brauer, and W.T. Sweeney. Effect of water on the induction period of the polymerization of methyl methacrylate. *J Res Bur Stand*, 49(6):359, 1952.
- [418] D. Hoey and D. Taylor. The effect of mixing technique on fatigue of bone cement when stress concentrations are present. *Int J Nano Biomat*, 3(1):36–48, 2010.
- [419] A. Lazzeri and C.B. Bucknall. Dilatational bands in rubber-toughened polymers. *J Mater Sci*, 28(24):6799–808, 1993.
- [420] C.B. Bucknall and A. Lazzeri. Rubber toughening of plastics Part XIII dilatational yielding in PA6.6/EPR blends. *J Mater Sci*, 35(2):427–35, 2000.
- [421] Y. Huang and A.J. Kinloch. Modelling of the toughening mechanisms in rubber-modified epoxy polymers. *J Mater Sci*, 27(10):2763–9, 1992.
- [422] M. Todo, K. Takahashi, P. Ben Jar, and P. Beguelin. Toughening mechanisms of rubber toughened PMMA. *JSME Int Journal Ser A*, 42(4):585–91, 1999.

References

- [423] J.F. Hwang, J.A. Manson, R.W. Hertzberg, G.A. Miller, and L.H. Sperling. Fatigue crack propagation of rubber-toughened epoxies. *Pol Eng Sci*, 29(20):1477–87, 1989.
- [424] R.Q. Frazer, R.T. Byron, P.B. Osborne, and K.P. West. PMMA: an essential material in medicine and dentistry. *J Long Term Eff Med Implants*, 15(6):629–39, 2005.